2014

Tribological behaviour of H- and W-DLC coatings: Effects of environment and temperature on adhesion

Ahmed Abou Gharam
University of Windsor

TRIBOLOGICAL BEHAVIOUR OF H- AND W-DLC COATINGS: EFFECTS OF ENVIRONMENT AND TEMPERATURE ON ADHESION

By

AHMED ABOU GHARAM

A Dissertation

Submitted to the Faculty of Graduate Studies
through Engineering Materials
in Partial Fulfillment of the Requirements for
the Degree of Doctor of Philosophy
at the University of Windsor

Windsor, Ontario, Canada

2013

TRIBOLOGICAL BEHAVIOUR OF H- AND W-DLC COATINGS: EFFECTS OF ENVIRONMENT AND TEMPERATURE ON ADHESION

by

AHMED ABOU GHARAM

APPROVED BY:

_____

Dr. S. Corbin (External Examiner)
Department of Mineral Resource Engineering, Dalhousie University

_____

Dr. S. H. Eichhorn (Outside Department Reader)
Department of Chemistry and Biochemistry

_____

Dr. D. Northwood (Department Reader)
Department of Mechanical, Automotive & Materials Engineering

_____

Dr. A. Edrisy (Department Reader)
Department of Mechanical, Automotive & Materials Engineering

_____

Dr. A. T. Alpas (Advisor)
Department of Mechanical, Automotive & Materials Engineering

_____

Dr. M. J. Lukitsch (Industrial Advisor)
General Motors Research and Development Center

December 12, 2013

DECLARATION OF CO-AUTHORSHIP / PREVIOUS PUBLICATION

This thesis includes 4 original papers that have been previously published in peer reviewed journals and conference proceedings, as follows:

Thesis Chapter	Publication title/full citation	Publication status
Chapter 2	A. Abou Gharam, M.J. Lukitsch, Y. Qi, A.T. Alpas, Wear, V 271, Issue 9-10, 2011, pp. 2157‑2163	Published
Chapter 3	A. Abou Gharam, M.J. Lukitsch, M.P. Balogh, A.T. Alpas, Thin Solid Films, V 519, Issue 5, 2010, pp. 1611‑1617	Published
Chapter 4	A. Abou Gharam, M.J. Lukitsch, M.P. Balogh, N. Irish, A.T. Alpas, Surface Coatings & Technology, V 206, Issue 7, 2011, pp. 1905‑1912	Published
Chapter 5	A. Abou Gharam, M.J. Lukitsch, A.T. Alpas, 55th Annual Technical Conference Proceedings of the Society of Vacuum Coaters, 2012, pp. 623-629	Published

I certify that I have obtained a written permission from the copyright owner(s) to include the above published material(s) in my thesis. I certify that the above material describes work completed during my registration as graduate student at the University of Windsor. I am aware of the University of Windsor Senate Policy on Authorship and I certify that I have properly acknowledged the contribution of other researchers to my thesis, and have obtained written permission from each of the co-authors to include the above materials in my dissertation.

In all four original published papers I was the sole student investigator on the projects reported and had a major role in conducting the wear test, surface analyses and the preparation of the manuscripts. I acknowledge the co-authors as they contributed to the data and results interpretation (wear tests and surface analyses) along with the valuable discussion to reach the main conclusions and also contributed to the final editing of the papers.

I declare that, to the best of my knowledge, my thesis does not infringe upon anyone's copyright nor violate any proprietary rights and that any ideas, techniques, quotations, or any other material from the work of other people included in my thesis, published or otherwise, are fully acknowledged in accordance with the standard referencing practices. Furthermore, to the extent that I have included copyrighted material that surpasses the bounds of fair dealing within the meaning of the Canada Copyright Act, I certify that I have obtained a written permission from the copyright owner(s) to include such material(s) in my thesis.

I declare that this is a true copy of my thesis, including any final revisions, as approved by my thesis committee and the Graduate Studies office, and that this thesis has not been submitted for a higher degree to any other University or Institution.

ABSTRACT

The objective of this study was to gain insight into the friction, aluminum adhesion, and wear mechanisms of diamond-like carbon (DLC) coatings, and to provide guidelines for coating design and development. Mechanisms that control the tribological behaviour of DLC coatings and the effects of dopants (i.e. hydrogen (H-DLC), and tungsten (W-DLC)) against aluminum alloys were investigated under various environments and test temperatures.

The effects of temperature and an oxygen-rich environment on dopant-free DLC, H- DLC, and W- DLC were investigated. Experimental analyses of dopant-free DLC showed that, when it was tested in an atmosphere consisting of 50% oxygen and 45% moisture, a high COF of 0.6 observed during the running-in against aluminum was eliminated compared to environment without moisture. At elevated temperatures, presence of hydrogen reduced the COF of H-DLC (e.g., to 0.06 at 200 ºC). W-DLC coatings provided a low COF of 0.18 and minimized aluminum adhesion at temperatures ranging between 400 ºC and 500 ºC, which was attributed to the formation of a tungsten oxide film. Additionally, DLC coatings were found to generate a low COF at subzero temperatures (-196 ºC), with W-DLC and H-DLC generating a COF of 0.18.

The work of adhesion (W_{ad}) was determined using a nano-indentation pull-off force method. In this way, insight was gained into the nature of atomic interactions contributing to tribological mechanisms at elevated temperatures. The results showed that the adhesion of the diamond tip against all four samples tested (H-DLC, dopant-free

DLC, W-DLC, and aluminum) decreased with temperature. At 25 °C, no aluminum adhesion was observed on the diamond tip, due to OH passivation of the diamond surface in agreement with the low COF of 0.12 for the dopant-free DLC coating. The elimination of meniscus forces due to adsorbed water molecules on the sample surface was identified as an important factor contributing to the adhesion at room temperature. The results also confirmed that the hydrogen in the H-DLC mitigated interatomic interactions at the surface and reduced W_{ad} to as low as 0.01 J/m^2 at 200 ºC. At 25 °C, there was no aluminum adhesion observed on the diamond tip, due to OH passivation of the diamond surface in agreement with the low COF of 0.12 for the dopant-free DLC coating.

DEDICATION

I dedicate this work to my family and close friends.

I could not have done it without their unconditional love and constant support.

ACKNOWLEDGMENTS

I would like to specially thank and acknowledge Dr. Alpas, for giving me the opportunity to do this study under his supervision. Thank you for your support and encouragement throughout my studies at the University of Windsor. In addition, I would like to thank my committee members Dr. Edrisy, Dr. Northwood and Dr. Eichorn for their valuable guidance, discussions and suggestions.

I would also like to acknowledge and thank Dr. Lukitsch of GM Global Research and Development Center for their support and the share of their expertise and knowledge. I am also grateful to Dr. Perry, Dr. Qi, Dr. Sachdev and Dr. Cheng of GM Global Research and Development Center for the valuable discussions and help at various stages of this study. I also would like to thank GM Global Research and Development Center staff for their assistance and support. I thank Bob Kubic and Curtis Wong for their assistance with SEM, Deborah Eckel for conducting infrared analysis, Rick Waldo for conducting electron microprobe analyses and Robert Paluch for his help with the metallography and sample preparation. I also would like to acknowledge the support and assistance of all faculty and staff of the University of Windsor. Thanks to Mrs. Barbara Denomey and Ms. Rosemarie Gignac for their administrative assistance. I also would like to thank all my fellow graduate students of GM industrial research chair research group, especially Dr. Konca, Dr. Akarca, Mr. Dey, Mrs. Das , Mr. Bhowmick, Mr. Shafiei, Mrs. Chen and Dr. Sen for their help and friendship.

TABLE OF CONTENTS

DECLARATION OF CO-AUTHORSHIP / PREVIOUS PUBLICATION iii

ABSTRACT v

DEDICATION vii

ACKNOWLEDGMENTS viii

TABLE OF FIGURES xiv

TABLE OF TABLES xxii

Chapter 1 Review of Relevant Literature 1

1.1 Introduction 1

1.2 Tribology 4

1.3 Friction and adhesion 5

1.4 Solid lubricants 13

1.4.1 Graphite 13

1.4.2 Molybdenum and tungsten disulfides 15

1.4.3 Diamond-like carbon 19

1.4.3.1 Industrial production and application 22

1.4.3.2 Application 26

1.4.3.3 Tribological behaviour of hydrogenated DLC 28

1.4.3.4 Tribological behaviour of dopants free DLC 33

1.4.3.5 Tribological behaviour of metal doped DLC 35

1.5 Organization of dissertation 40

References 41

Chapter 2 Role of Oxygen and Humidity on the Tribo-Chemical Behaviour of Non-Hydrogenated Diamond-Like Carbon Coatings 48
2.1 Introduction 48
2.2 Experimental details 51
2.3 Experimental desults 53
2.3.1 Steady-state COF 53
2.3.2 COF variation during running-in period 56
2.4 Discussion 62
2.5 Conclusions 67
References 68
Chapter 3 High Temperature Tribological Behaviour of Carbon Based (B_4C and DLC) Coatings in Sliding Contact with Aluminum 71
3.1 Introduction 71
3.2 Experimental details 73
3.2.1 Coating deposition and properties 73
3.2.2 Tribological tests and surface characterization 74
3.3 Results 75
3.3.1 Boron carbide coating 75
3.3.2 Diamond-like carbon coating 79
3.4 Discussion 82
3.4.1 Intergranular coating fracture in B_4C 82
3.4.2 Aluminum adhesion mitigation by DLC 84

3.5 Conclusions 85

References 86

Chapter 4 High Temperature Tribological Behaviour of W-DLC against Aluminum 88

4.1 Introduction 88

4.2 Experimental details 91

4.2.1 Coating properties 91

4.2.2 Tribological tests and analyses 92

4.3 Results 93

4.3.1 Pin-on-disk tests 93

4.3.2 Structural analysis 98

4.3.3 Chemical Analysis 101

4.4 Discussion 103

4.5 Summary and conclusions 108

References 109

Chapter 5 Tribological Behaviour of Heat Treated Tungsten Doped Diamond-Like Carbon Coating at Elevated Temperatures 112

5.1 Introduction 112

5.2 Experimental details 113

5.3 Results 114

5.3.1 Structure and composition 114

5.3.2 Tribological behaviour 116

5.3.3 SEM investigations 119
5.4 Discussion 123
5.5 Summary and Conclusions 125
References 126
Chapter 6 Temperature Effect on the Tribological Behaviour of W-DLC and H-DLC 128
6.1 Introduction 128
6.2 Experimental details 129
6.3 Results 130
6.3.1 Friction at elevated temperature 130
6.3.2 Effects of subzero temperatures 132
6.4 Discussion 135
6.5 Conclusions 138
References 139
Chapter 7 Experimental Investigations of Work of Adhesion Between DLC and Single Crystal (111) Aluminum 141
7.1 Introduction 141
7.2 Experimental details 144
7.3 Results 146
7.4 Discussion 152
7.5 Conclusions 157
References 159
Chapter 8 General Discussion and Conclusions 161

8.1 Summary and general discussion 161

8.2 A summary of original conclusions of this work 169

Appendix A 171

Appendix B 177

PUBLICATIONS 181

VITA AUCTORIS 182

TABLE OF FIGURES

Figure 1-1: Mechanical losses in internal combustion engine [3]. 2

Figure 1-2: Schematics of tribological contacts at (a) macro-mechanical, (b) micro-mechanical, and (c) nano-mechanical/atomic level. 5

Figure 1-3: Contact angle β for liquid droplet applied to the surface 7

Figure 1-4: Schematic diagram of force distance curve obtained by AFM adapted from [22]. 8

Figure 1-5: Meniscus bridge due to presence of liquid at the interface [25]. 10

Figure 1-6: Pull-off force as a function of temperature between AFM diamond tip and silica substrate. (♦) Heating of the initial surface (◊) cooling after the initial heating (●) reheating of the surface. 12

Figure 1-7: schematic of Graphite lamellar structure 14

Figure 1-8: Schematic of graphite (a) basal plane stacking sequence of hexagonal and rhombohedral structures (b) projection of the basal plane on the c plane [30]..... 15

Figure 1-9: Metals that form lamellar structures [44]. 16

Figure 1-10: Schematic diagram of MoS_2 layered structure [46]. 17

Figure 1-11: Coefficient of friction as a function of sliding cycles of MoS_2 against steel in HV, UHV and d-nitrogen [45]. 18

Figure 1-12: Coefficient of friction of WS_2 sliding against 52100 Steel at various temperatures [45]. 19

Figure 1-13: Schematic of sp^2 and sp^3 hybridization [52]. 20

Figure 1-14: Schematic of common carbon structures [52]..... 20

Figure 1-15: Schematic phase diagram of DLC after [52]. 21

Figure 1-16: Seven categories of amorphous carbon coatings. a-C (hydrogen-free amorphous carbon), ta-C (tetrahedral-bonded hydrogen-free amorphous carbon), a-C:Me (metal-doped hydrogen-free amorphous carbon (Me = W, Ti)), a-C:H (hydrogen-containing amorphous carbon), ta-C:H (tetrahedral-bonded hydrogen-containing amorphous carbon), a-C:H:Me (metal-doped hydrogen-containing amorphous carbon (Me = W, Ti)), a-C:H:X (modified hydrogen-containing amorphous carbon (X = Si, O, N, F, B)). 21

Figure 1-17: PVD processing techniques: (1a) vacuum evaporation, (1b and 1c) sputter deposition in a plasma environment, (1d) sputter deposition in a vacuum, (1e) ion plating in a plasma environment with a thermal evaporation source, (1f) ion plating with a sputtering source, (1g) ion plating with an arc vaporization source and, (1h) Ion Beam Assisted Deposition (IBAD) with a thermal evaporation source and ion bombardment from an ion gun [8]. 24

Figure 1-18: Coating structure as a function of temperature and Argon pressure [56] 26

Figure 1-19: Coefficient of friction of H-DLC as a function of moisture in the atmosphere [60]. 29

Figure 1-20: Coefficient of friction of DLC as a function of deposition source gas [12]. 30

Figure 1-21: Coefficient of friction of DLC as a function of hydrogen content [64]. 31

Figure 1-22: Schematics of the interface of hydrogen terminated surfaces [13]. 32

Figure 1-23: Coefficient of friction of dopants free DLC sliding against aluminum as a function of hydrogen gas partial pressure in the test chamber [65]. 32

Figure 1-24: Coefficient of frication of W-DLC as a function of carbon content [81]. ... 36

Figure 1-25: Coefficient of friction and hardness as a function of carbon content [82]... 37

Figure 1-26: Coefficient of friction of W-DLC as a function of carbon content of na and nc W-DLC (a) air 50 %RH (b) nitrogen 0.5 %RH [83]..... 38

Figure 2-1: COF of dopants free DLC coating tested against 319 aluminum pins sliding for 1000 sliding cycles under humid Ar, humid and dry (O2 + Ar) at 5 N load and 0.1 m/s sliding speed..... 54

Figure 2-2: Secondary electron images of the material transfer layers observed on the 319 aluminum pins and their corresponding FTIR spectra after sliding in (a, d) humid Ar with 45 % RH; (b, e) humid (O_2 + Ar) atmosphere with 45% RH and; (c, f) dry (O_2 + Ar) atmosphere with 0% RH..... 56

Figure 2-3: Running-in experiments of dopants free DLC coating against 319 aluminum pins sliding for 10 cycles, 40 cycles and 80 cycles under (a, b, c) humid Ar with 45% RH and (d, e, f) humid (O_2 + Ar) with 45% RH at 5 N load and 0.1 m/s sliding speed. Each curve represents a different test on a new sample..... 58

Figure 2-4: Secondary electron images of the 319 aluminum pins after sliding for (a) 10 cycles, (b) 40 cycles and (c) 80 cycles and their back scattered electron micrographs after sliding for (d) 10 cycles, (e) 40 cycles and (f) 80 cycles under a humid Ar atmosphere with 45% RH..... 59

Figure 2-5: Secondary electron images of the dopants free DLC's wear tracks after sliding for (a) 10 cycles, (b) 40 cycles and (c) 80 cycles under a humid Ar atmosphere with 45% RH..... 60

Figure 2-6: Secondary electron images of the 319 aluminum pins after sliding for (a) 10 cycles, (b) 40 cycles and (c) 80 cycles and their back scattered electron

micrographs after sliding for (d) 10 cycles, (e) 40 cycles and (f) 80 cycles under humid (O_2 + Ar) atmosphere with 45% RH. 61

Figure 2-7: Secondary electron micrographs of the dopants free DLC's wear tracks after sliding for (a) 10 cycles, (b) 40 cycles and (c) 80 cycles under humid (O_2 + Ar) atmosphere with 45% RH. 62

Figure 2-8: Schematic representation of the surface termination mechanisms in (a) humid (O_2 + Ar) - 45% RH, (b) humid Ar - 45% RH and (c) dry (O_2 + Ar) - 0% RH. .. 66

Figure 3-1: COF of 319 aluminum pins sliding for 1000 sliding cycles against the B_4C and DLC coating at temperatures ranging from 25 °C to 400 °C at 5 N load and 0.1 m/s sliding speed. 76

Figure 3-2: Percent area covered by aluminum inside the B_4C wear track, calculated from EPMA mapping of aluminum as a function of temperature. 77

Figure 3-3: Micrographs of (a) B_4C wear track cross section produced at 25 °C by the aluminum counterface (b) coating fracture along the columnar grain boundaries 78

Figure 3-4: Micrographs of (a) B_4C wear track cross section wear track produced at 300 °C by the aluminum counterface (b) wear track damage due to sliding along the columnar grain boundaries inducing substrate deformation. 78

Figure 3-5: EDS Maping of (a) Boron and (b) Carbon, Aluminum, Chromium and Iron of the cross sectioned wear track, shown in Figure 4..... 79

Figure 3-6: Wear rates of DLC as a function of temperature with inserts of surface profile images of the wear tracks at 25 °C, 200 °C and 400 °C 80

Figure 3-7: Micrographs of (a) the DLC wear track cross section (b) coating damage and aluminum adhesion inside the wear track at 400 °C. 81

Figure 3-8: FTIR of the material transfer observed on the Al pins as shown in the micrograph inserts at (a) 25 °C and (b) 400 °C 81

Figure 3-9: Raman spectra of the pristine B_4C, wear track after sliding in 25 °C, 200 °C and 300 ° C test conditions along with graphite spectra for reference. 83

Figure 4-1: (a) Cross section of the W-DLC coating deposited on Si substrate and EDS Mapping of (b) Carbon, Chromium and (c) Tungsten and Silicon..... 91

Figure 4-2: (a) COF as a function of sliding cycles at temperatures ranging from 25 °C to 400 °C (b) Steady-state COF as a function of temperature. Error bars are the standard deviations of the steady state values..... 94

Figure 4-3: SEM image of W-DLC wear tracks and aluminum pins wear scar after testing at (a), (b) room temperature (b), (c) 100 °C, (e), (f) 300 °C and (g), (h) 400 °C.. 96

Figure 4-4: Wear rates of W-DLC as a function of temperature ranging from 25 °C to 400 °C. The error bars represent the standard deviation of four separate measurements. 97

Figure 4-5: SEM of (a) the W-DLC wear track FIB cross-section (b) coating damage and aluminum adhesion inside the wear track at 100 °C (c) EDS elemental mapping of W in the DLC coating, Cr interlayer, Fe from the substrate and C deposited by the FIB prior to milling. 99

Figure 4-6: SEM of (a) the W-DLC wear track FIB cross-section (b) higher magnification of the cross section at 400 °C (c) EDS elemental mapping of W in the DLC coating, Cr interlayer, Fe from the substrate and C deposited by the FIB prior to milling. 100

Figure 4-7: TEM images of W-DLC coating (a) columnar structure (b) top surface (c) high resolution of the top surface layer after testing at 400 ºC, with insert of SAED showing the diffraction of an amorphous structure. 101

Figure 4-8: X-ray photoelectron spectroscopy of W-DLC coating (a) as-received (b) after testing at 500 ºC. 102

Figure 4-9: Micro-Raman spectra of material transfer formed on the 319 Al pins after sliding against W-DLC at 25 °C and 400 °C. 103

Figure 4-10: Micro-Raman spectra of W-DLC coating deposited on (100) Si wafer as received and annealed samples at 100, 200, 300, 400, and 500 °C. 106

Figure 5-1: W-DLC heat treated at 500 °C (a) cross sectional TEM and (b) XPS depth profile 115

Figure 5-2: XRD of W-DLC coating deposited on (100) Si wafer as deposited and heat treated at 500 °C and 600 °C. 116

Figure 5-3: Coefficient of friction of W-DLC heat treated at 500 °C tested at (a) 25 °C, 100 °C, 200 °C and (b) 300 °C, 400 °C and W-DLC heat treated at 600 °C tested at (c) 25 °C, 100 °C, 200 °C, (d) 300 °C and 400 °C. 118

Figure 5-4: (a) Average COF of as-deposited and heat treated at 500 °C and 600 °C, (b) Wear rates of W-DLC as a function of temperature ranging from 25 °C to 400 °C. 119

Figure 5-5: SEM image of W-DLC heat treated at 500 °C wear tracks and aluminum pins wear scar after testing at (a), (b) 25 °C, (c), (d) 100 °C, (e), (f) 200 °C, (g), (h) 300 °C and (i), (j) 400 °C. 121

Figure 5-6: SEM image of W-DLC heat treated at 600 °C wear tracks and aluminum pins wear scar after testing at (a), (b) 25 °C, (c), (d) 100 °C, (e), (f) 200 °C, (g), (h) 300 °C and (i), (j) 400 °C. 122

Figure 6-1: COF of W-DLC sliding against 319 Al at 25 °C, 200 °C and 400 °C. 131

Figure 6-2: COF of H-DLC sliding against 319 Al at 25 °C, 200 °C and 400 °C. 132

Figure 6-3: COF of H-DLC, W-DLC and uncoated 52100 steel sliding against 319 Al at below freezing temperature in liquid nitrogen. 133

Figure 6-4: Wear rates of H-DLC, W-DLC, uncoated 52100 steel and 319 Al pins after testing at subzero temperatures. 134

Figure 6-5: SEM of (a) Uncoated 52100 steel, (b) W-DLC, (c) H-DLC wear tracks and 319 aluminum pins wear scar after testing at subzero temperature against (d) Uncoated 52100 steel, (e) W-DLC, (f) H-DLC. 135

Figure 6-6: Average COF of W-DLC and H-DLC coatings as a function of temperatures ranging from -196 °C to 500 °C 137

Figure 7-1: Loading-unloading schematic 146

Figure 7-2: Typical load displacement curve of H-DLC as a function of testing temperature. 147

Figure 7-3: Typical load displacement curve of dopants free DLC as a function of testing temperature. 148

Figure 7-4: Typical load displacement curve of W-DLC as a function of testing temperature. 149

Figure 7-5: Typical load displacement curve of single crystal Aluminum (SC Al) as a function of testing temperature. 150

Figure 7-6: W_{ad} of hydrogen doped DLC (H-DLC), dopants free DLC (DLC) and Tungsten doped DLC (W-DLC) as a function of temperature. 151

Figure 7-7: W_{ad} of SC Al as a function of temperature. 152

Figure 7-8: Schematic of meniscus forces due to presence of water molecules between the nano indenter tip and the specimen surface. 153

Figure 7-9: W_{ad} of H-DLC, dopants free DLC, W-DLC and SC Al as a function of temperature. 154

Figure 7-10: Schematic of the diamond / H-DLC interface 155

Figure 7-11: Schematic of the diamond / dopants free DLC interface and diamond / W-DLC interface..... 156

Figure 7-12: Schematic of the diamond / Al interface..... 157

Figure 8-1: Average COF obtained by pin-on-disc of 319 Al sliding against dopant-free DLC at various environments 163

TABLE OF TABLES

Table 1-1: Work of adhesion between glass surfaces in the presence of the water, glycerine, decane and octane [24] 10

Table 1-2: DLC introduction to diesel injection systems [58] 27

Table 1-3: DLC in engine components [58] 27

Table 7-1: Work of adhesion literature for various interfaces. 143

Table A-8-1: Work of adhesion calculation of H-DLC 173

Table A-8-2: Work of adhesion calculation of W-DLC 174

Table A-8-3: Work of adhesion calculation of dopant free DLC 175

Table A-8-4: Work of adhesion calculation of single crystal Al 176

CHAPTER 1
REVIEW OF RELEVANT LITERATURE

1.1 Introduction

Diamond-like carbon (DLC) coatings have great potential as a low friction (coefficient of friction (COF) < 0.1), while maintaining high wear resistance [1]. These properties are of benefits to many tribological systems, specially found in automobile. However, these novel tribological properties are found to be specific to certain environments and additives in the coating (i.e. H and W). Thus there is a need to fully understand their mechanisms at various environments, especially at elevated temperatures, subzero temperatures and oxygen rich environments to be able to apply DLC in the proper application and fully utilize their full potential. Consequently the aim of this dissertation is to gain insight into the friction, adhesion, and wear mechanisms of DLC coatings, and to provide guidelines for coating design and development.

The friction and wear of materials result from two moving components of the same or different materials in contact with each other. Tribological systems are encountered on a daily basis in activities as simple as sharpening a kitchen knife and shaving to more complex systems such as mine drilling and metal forming, cutting and machining. Because of its wide scope and significance for our daily actions, the study of friction and wear, or tribology, became a scientific discipline in 1967 [2]. For instance, in an internal combustion engine only 12% of the power is used to drive the car, 73% is lost to cooling/exhaust and pumping, and 15% is lost to mechanical losses [3]. The 15% of mechanical losses are attributed to various tribological systems (i.e., piston ring/bore,

tappet/rocker arm, bearings, gears, camshafts and crank shafts), as shown in Figure 1-1. Tribological systems also greatly influence efficiency and gas mileage because they can be a cost burden and cause unpredictable environmental effects of CO and CO_2 emissions [4].

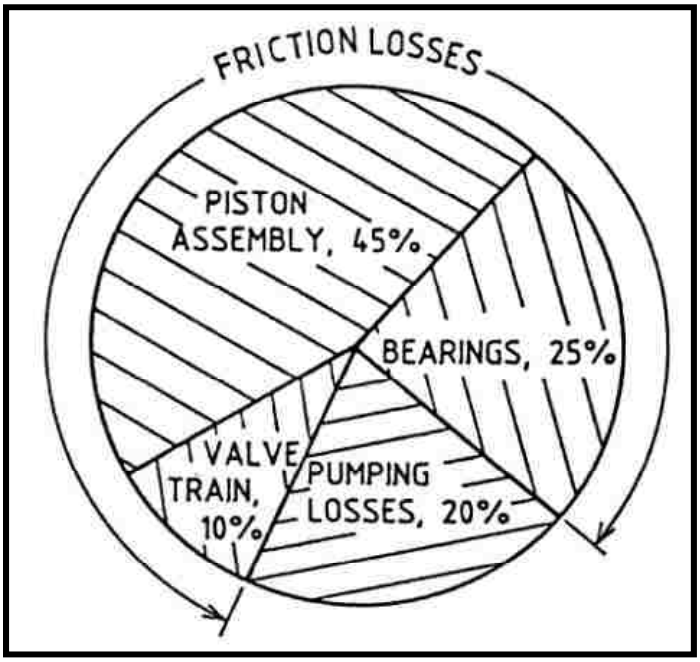

Figure 1-1: Mechanical losses in internal combustion engine [3].

For many years, case hardening treatments, such as carburizing and nitriding, have been introduced to steels commonly used for tools and tribo-surfaces to increase the wear resistance [5]. The friction has been remedied by introducing oils to eliminate metal-to-metal contact. In lubricated tribological systems, three friction regimes exist: hydrodynamic, elasto-hydrodynamic and boundary lubrication regimes [6]. In hydrodynamic and elasto-hydrodynamic lubrication regimes, the lubricant carries most of the applied load, creating an easily sheared medium that separates the sliding surfaces. In the boundary regime, high loads and low speeds result in the formation of a very thin

lubricating film on the mating surfaces. Consequently, a considerable amount of contact occurs between the adjacent asperities, leading to higher COF relative to the values produced by the hydrodynamic and elasto-hydrodynamic lubrication regimes [7].

However, in the past decade, wear resistant and self-lubricious coatings, such as diamond-like carbon (DLC), have been introduced to the working surface to enhance tribological performance and eliminate the various friction and wear regimes (hydrodynamic, elasto-hydrodynamic and boundary lubrication regimes) commonly observed in lubricated systems. Tribological coatings are commonly introduced to the surface using physical vapor deposition (PVD), chemical vapor deposition (CVD) and thermal spray [8]–[10].

This dissertation focuses on the tribological mechanisms of DLC coatings at various environments (oxygen rich, elevated temperatures, and sub-zero temperatures). DLC coatings have been known since the late 1990s for their low COF and high wear resistance in inert environments because of the presence of hydrogen [11]. Hydrogen was found to eliminate interatomic interactions at the sliding interface by terminating the carbon dangling bonds [12], [13]. However, the effects of oxygen and temperature on DLC are not fully understood. The aim of this dissertation is to investigate low friction mechanisms in order to provide guidelines on how to utilize dopants, such as H and W, to mitigate aluminum adhesion and achieve low COF in a wide range of environments.

1.2 Tribology

Tribology is a very complex process with different types of friction and wear mechanisms at various scales, as schematically presented in Figure 1-2. Thus, it is beneficial to study and analyze the mechanical and chemical changes at macro, micro and nano scales to understand fully the tribological mechanism of coatings. At the macro scale (Figure 1-2 a), properties such as coating and substrate hardness, coating thickness and surface roughness greatly influence the tribological mechanism. For instance, softer coatings are applied to hard substrates to achieve low friction and increase conformability [14], [15]. This is common in tribo-electrical contacts, such as conductive bushings for moving components. In contrast relatively harder coatings are applied to softer substrates to increase their life span by providing wear protection and supporting the applied load.

The micro scale (Figure 1-2 b) focuses on single-asperity deformation and on how each asperity is sheared and fractured by sliding. Fracture and defragmentation of asperities form wear particles that can lead to several scenarios. These wear particles can react with the mating surface, forming an abrasive third body that is detrimental to the wear and life span of the part. Depending on the tribo-chemical reaction and the nature of the material, it can also form a protective wear-resistant third body [14], [15].

However, it is more challenging to get a full grasp and understanding of the nano mechanisms that occur during sliding (Figure 1-2 c). However, recent advances in molecular dynamic simulation and atomistic experimental investigations using the atomic force microscope (AFM) and focused ion beam (FIB) have achieved major breakthroughs. For instance, based on hydrogen terminated diamond simulations, we

have a much better understanding of the effects of hydrogen on DLC coatings, showing that the hydrogen-terminated surface reduces friction by minimizing interatomic interactions at the sliding interface [16].

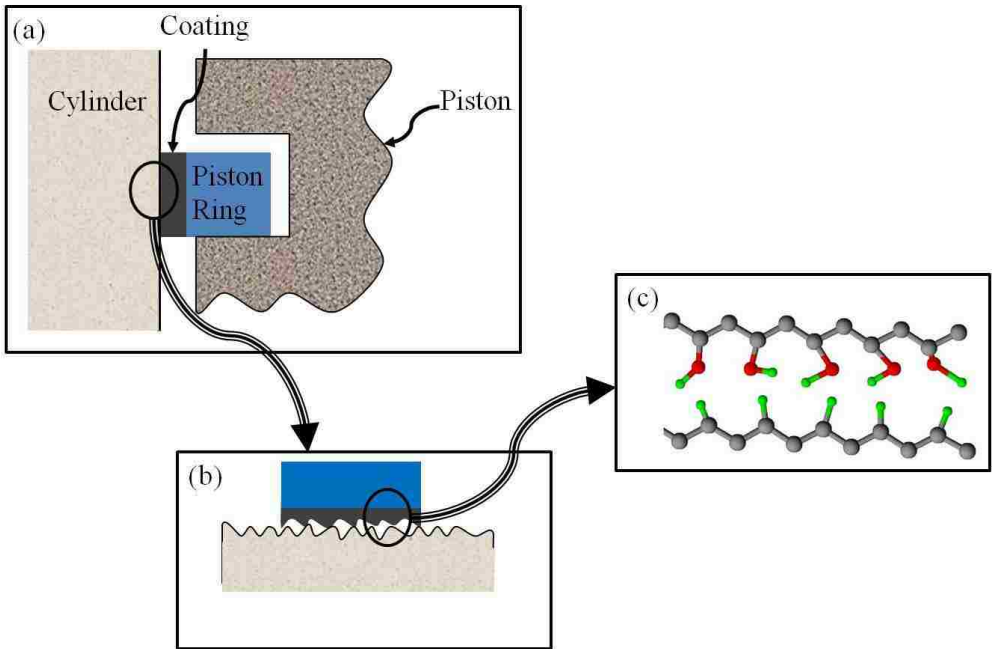

Figure 1-2: Schematics of tribological contacts at (a) macro-mechanical, (b) micro-mechanical, and (c) nano-mechanical/atomic level.

1.3 Friction and adhesion

When two solids are in contact, the contact area is described as the sum of contact spots or metallic junctions at the asperities caused by surface roughness. During sliding, a shear force has to be applied to overcome the friction force, which is attributed to either mechanical interlocking or the adhesive force between the two surfaces caused by interatomic attractions. The surfaces “stick” together at these junctions until the shear force or a pull breaks the junctions and causes a rapid “slip”. This process is repeated

during sliding and is commonly referred to as the stick-slip phenomenon [17]. The sticking portion can be caused by mechanical surface roughness or various types of chemical bonds and interface interactions that may occur at the sliding interface. This phenomenon is commonly observed in aluminum forming and machining applications, as aluminum tends to adhere to metallic and carbide surfaces.

The adhesion forces at the asperity junctions can be studied using the concept of surface-free energy. A cleaved crystalline plane is a highly energetic surface with multiple, highly energetic active bonds: “dangling bonds”. This free surface energy leads to interactions with other surfaces and hence contributes to the friction and wear of sliding materials [18]. To quantify this energy, the work of adhesion (W_{ad}) was defined as the energy required to break interfacial bonding and create a new surface. It can be calculated by the Dupré equation [19]:

$$\mathbf{W_{ad}} = \Delta\boldsymbol{\gamma} = \boldsymbol{\gamma_1} + \boldsymbol{\gamma_2} - \boldsymbol{\gamma_{12}} \qquad \text{Equation 1}$$

where $\Delta\gamma$ is the reduction in surface energy of the system per unit area and is usually described in mJ/m^2 (1 mJ/m^2 = 1 erg/cm^2 = 1 dyn/cm = 1 mN/m). γ_1 and γ_2 are the free surface energies per unit area in air, and γ_{12} is the interfacial surface energy per unit area between surface 1 and surface 2 [20].

The sessile drop technique is one of the most common and easiest ways of determining surface energy. The technique utilizes a liquid droplet on the surface, and the

droplet angle depends on the force of attraction or repulsion between the solid and the liquid. The surface energy (γ_{sv}) is defined by Young's equation [19]:

$$\boldsymbol{\gamma_{SV} = \gamma_{SL} + \gamma_{LV} \cos \beta} \qquad \text{Equation 2}$$

where γ_{SL} is the surface energy of the solid (S) liquid (L) interface or γ_{12} in Equation 1-1. It is understood that as β decreases, γ_{SV} increases. Thus, W_{ad} can be obtained by the combination of Equations 1-1 and 1-2.

$$\boldsymbol{W_{ad} = \Delta\gamma = \gamma_{SV} + \gamma_{LV} - \gamma_{SL} = \gamma_{LV}(1 + \cos \beta)} \qquad \text{Equation 3}$$

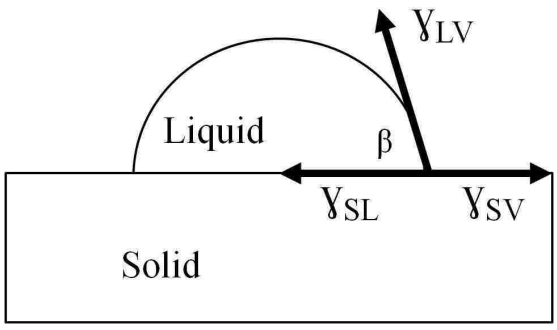

Figure 1-3: Contact angle β for liquid droplet applied to the surface

W_{ad} can be measured at the nano or atomic scale using the atomic force microscope (AFM), which can mimic a single asperity adhesion [21]. AFM measures the pull-off force through the force distance curve of the static AFM tip on the surface, as shown below in Figure 1-4. In regime (i) the AFM tip and the sample are far apart and experience no external forces. As the tip approaches the sample surface, in regime (ii), the tip experiences an attractive negative force towards the sample. The force increases as

the tip approaches the surface, causing the tip to snap on the surface. In regime (iv) during unloading, the tip experiences a repulsive force caused by the electrostatic repulsive forces that develop between surfaces. Adhesion between the AFM tip and sample maintains the contact as the tip separates from the sample, as shown in regime (v). The pull-off force is then defined as the maximum negative force right before the tip leaves the surface or the maximum force that has to be exerted to separate the tip from the surface, as shown in regime (iv) [22].

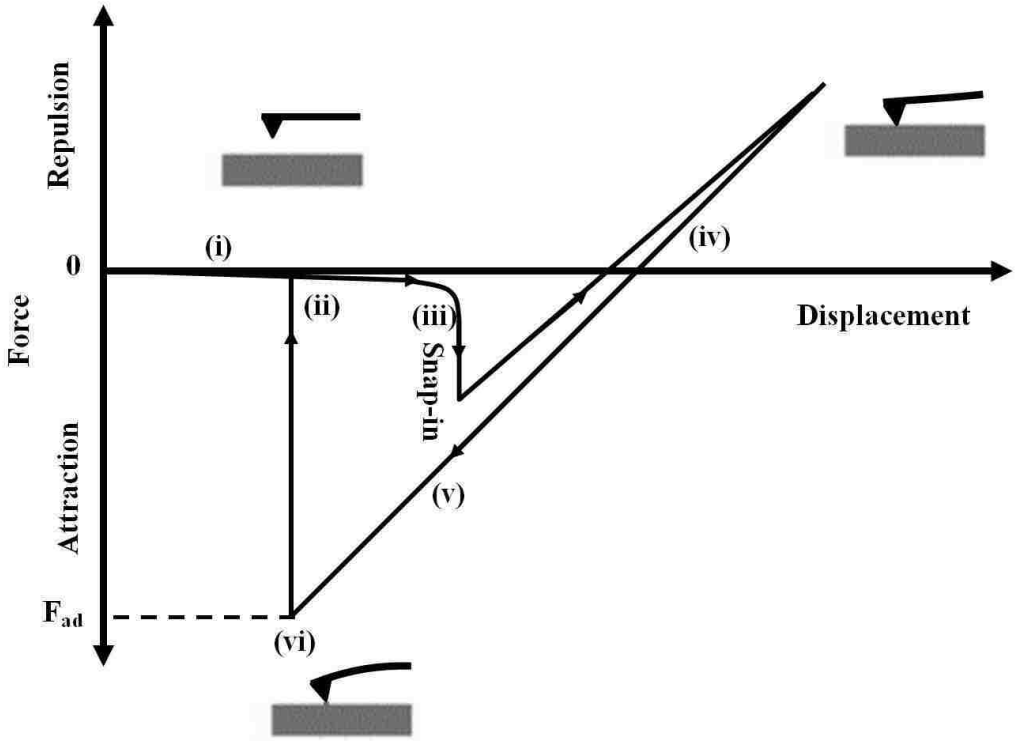

Figure 1-4: Schematic diagram of force distance curve obtained by AFM adapted from [22].

Prior to the sophisticated AFM, MaFarlane and Tabor [23] estimated adhesion through the force required to shear the junctions in contact. They assumed a two-dimensional metallic junction with an interfacial area A with normal load W and normal

pressure P = W/A. During sliding, the tangential stress S was assumed to shear the interface. By applying the von Mises criterion of plasticity,

$$\mathbf{P^2 + 3S^2 = Y^2} \qquad \text{Equation 4}$$

where Y is the elastic limit of the material. Thus, if the metal were plastically deformed because of the normal load, very little tangential stress would be required to break the metallic junction and initiate the tangential motion or sliding. Thus, the adhesion can be estimated from the tensile strength of the junctions, and the friction is the measure of the material's shear strength.

MaFarlane and Tabor [24] also used a pendulum to measure the adhesion between a spherical bead and a flat vertical plate. The bead and the plate were brought into contact, and then the plate was moved back until it separated. The apparatus successfully measured the adhesion between the glass surfaces with the presence of water, glycerine, decane and octane between the glass surfaces, as shown in Table 1-1. Water was found to have the highest W_{ad} at 67.3 mJ/m^2 and octane (C_8H_{18}) had the lowest W_{ad} at 19.9 mJ/m^2 on glass.

Table 1-1: Work of adhesion between glass surfaces in the presence of the water, glycerine, decane and octane [24]

Liquid	**Work of adhesion (mJ/m^2)**
Water	67.3
Glycerine	59.0
Decane	22.4
Octane	19.9

Forces caused by liquid films are commonly referred to as meniscus forces. The surface tension of the liquid results in a pressure difference. Concave meniscus liquids indicate that the pressure inside the liquid is lower than that outside the liquid [25], thus causing a meniscus bridge connecting two surfaces in contact, as shown in Figure 1-5.

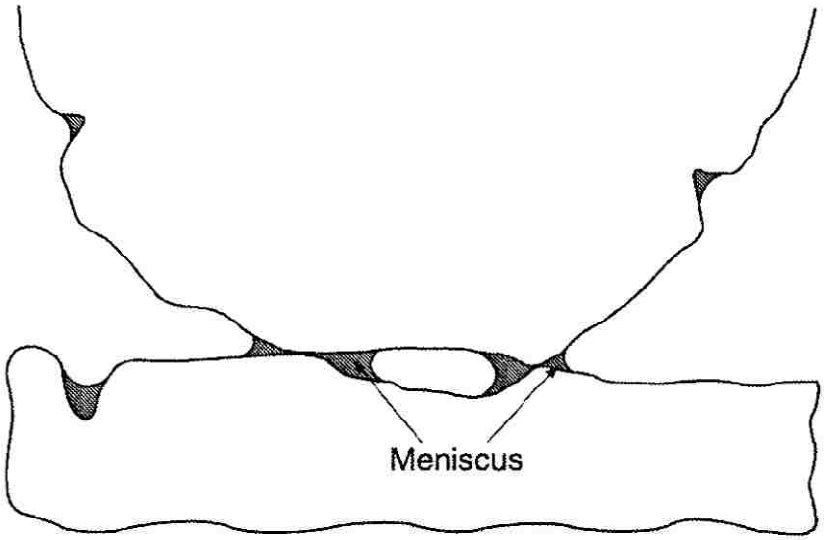

Figure 1-5: Meniscus bridge due to presence of liquid at the interface [25].

These meniscus forces were found to contribute to the adhesion force between solid surfaces. Xiao and Qian [26] investigated the effects of humidity on the adhesion between SiO_2 and Si_3N_4 AFM with a tip radius of 100 nm. The adhesion force, or pull-off

force, was observed to maintain a value of 35 nN up to 25% RH. The adhesion force then increased to 75 nN as the relative humidity increased to 75% RH. As the relative humidity continued to increase, the adhesion force decreased again to 30 nN. This indicated that adhesion force is greatly influenced by the surrounding atmosphere and the amount of moisture present. In a study of AFM pull-off force, Sirghi et al. [27] showed that during surface separation, water bridges stretch until a critical distance is reached separating the two surfaces. Analysis predicted that the breakup distance of the water bridge is almost equal to the cube root of the volume of the water bridge. Another AFM study of adhesion between silica and AFM tip as a function of temperature [28] found that at room temperatures water is always present between silica surfaces. Heating the system to 100 °C and 160 °C was found to result in a decrease in the pull-off force, as shown in Figure 1-6. The pull off force was observed to reach 0.2, a 90% reduction. When the sample was kept in a dry nitrogen atmosphere, the surface maintained its low adhesion properties with a consistent pull-off force of 0.4 during cooling and reheating at temperatures ranging between 25 °C and 160 °C. This decrease was attributed to the evaporation of water and elimination of meniscus forces.

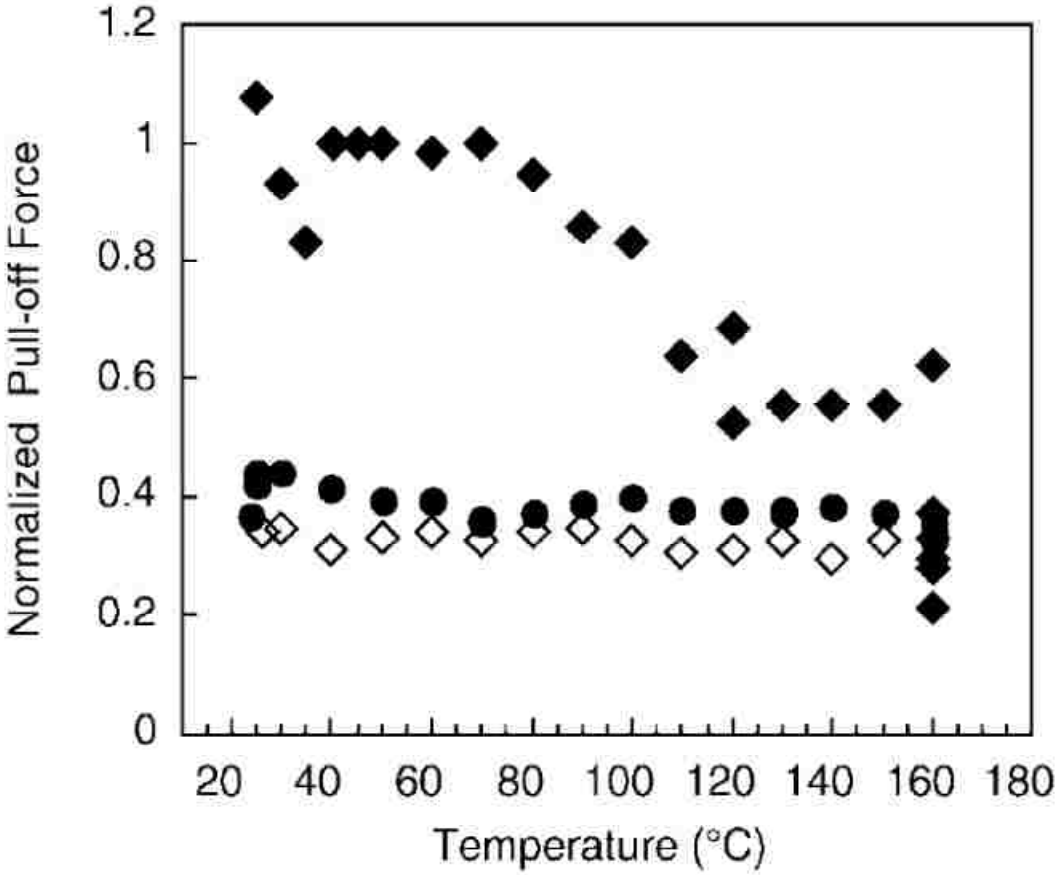

Figure 1-6: Pull-off force as a function of temperature between AFM diamond tip and silica substrate. (♦) Heating of the initial surface (◊) cooling after the initial heating (●) reheating of the surface.

In summary, adhesion is found at the interface between solid-solid contacts, which influences static friction. Thus, the relationship between adhesion and friction can yield insight into how to reduce if not eliminate high friction in tribological systems. This can be achieved by quantifying adhesion by means of measuring the work of separation to identify how much it contributes to friction.

1.4 Solid lubricants

Many tribo-systems require higher performance, which in many cases is limited by the tribological properties of conventional materials, such as steels. However, the introduction of surface coatings has opened up many possibilities. The substrates can be designed for structural rigidity, and the coating can provide low friction and wear resistance at the sliding interface. Another obvious advantage is their ability to function in environments, such as a vacuum, and in food processing applications that may cause contamination [2]. Various surface coatings exhibit the low friction and low wear properties commonly referred to as solid lubricants, such as Graphite, MoS_2, WS_2, and diamond-like carbon (DLC) coatings.

1.4.1 Graphite

Graphite is one of the most well-known solid lubricants. It is commonly used in pencils because of its low COF, which ranges from 0.07 to 0.14 [29]. Natural graphite consists of a hexagonal, closely packed structure with an “aba” stacking sequence that has a 5–15% rhombohedral structure with an “abc” stacking sequence, as illustrated in Figure 1-8 [30]. The rhombohedral structure was observed by TEM in highly oriented pyrolytic graphite (HOPG) in the area between two partial dislocations. The low friction of graphite is attributed to its lamellar structure, which was reported in 1928 by Bragg, using X-ray diffraction [31] (Figure 1-7). This lamellar structure has weakly bonded basal planes that have very low resistance to mechanical shear [32]. The lamellar structure consists of layers of hexagonal rings of carbon, which are referred to as graphene. First-principle density functional theory has shown that the graphene layers have 3.1 Å to 3.2 Å spacing, and their interatomic interactions range from 60 meV to 72

meV which is consistent with van der Waals type of interactions [33]. In 1960, Rowe [34] suggested that vapours enter between the layers in the structure, increasing the interlayer spacing between the graphite basal planes and reducing friction. However, subsequent studies showed no evidence of interlayer spacing between the graphite basal planes, but they confirmed that water vapor is needed to achieve low friction [35], [36]. This was also confirmed by Savage who observed that graphite wore into fine dust with a high COF of 0.8 in vacuum [37]. The poor tribological behaviour in vacuum was attributed to the lack of surface passivants, such as hydrogen or adsorbed water molecules, which dissociated to H+ and OH- ions which terminate active dangling carbon bonds between the graphene layers as they shear, thus minimizing C-C interactions and reducing COF [37]–[39]. The tribological behaviour of graphite [32] at high temperatures showed a COF of 0.5 at 400 ºC - 500 ºC. The high COF at elevated temperatures was attributed to the removal of adsorbed water and carbon oxidation [40], [41].

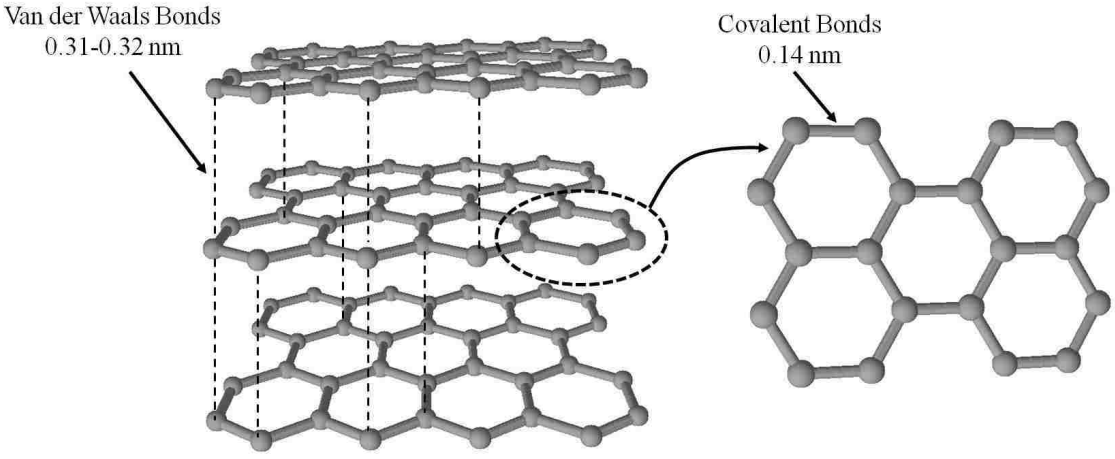

Figure 1-7: schematic of Graphite lamellar structure

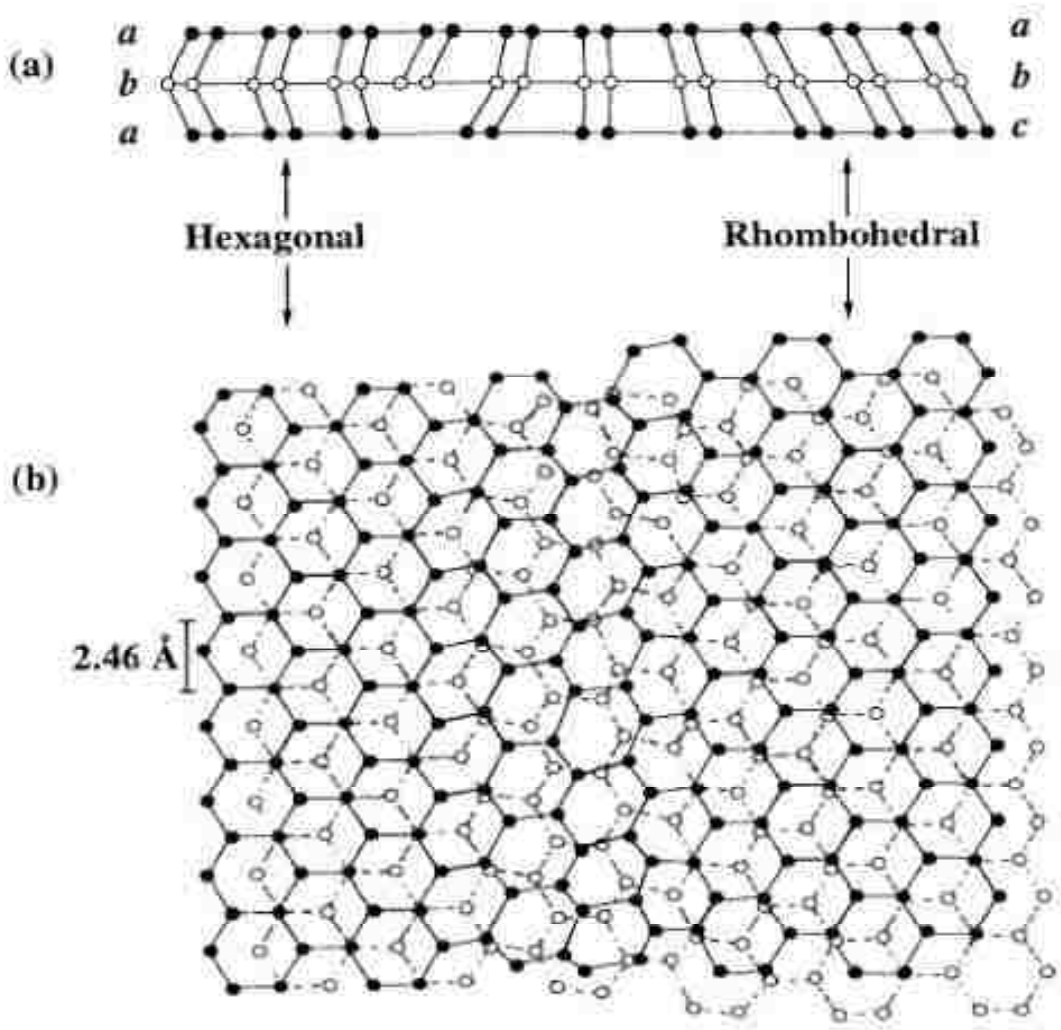

Figure 1-8: Schematic of graphite (a) basal plane stacking sequence of hexagonal and rhombohedral structures (b) projection of the basal plane on the c plane [30].

1.4.2 Molybdenum and tungsten disulfides

Metal dichalcogenides (MoS_2, WS_2) and BN form a lamellar structure and generate low friction. Metal dichalcogenides have the same structure as graphite and possess good tribological properties because of the relatively large interplaner spacing and weak van der Waals interactions between the layers [42]. As shown in Figure 1-9, the metal elements surrounded by dashed lines form lamellar structures when bonded with

sulfur or selenium. However only sulfides and selenides of molybdenum and tungsten have favorable tribological properties (elements surrounded by solid lines in Figure 1-9) with low shear strength ranging from 1–2 MPa [43]. In metal dichalcogenides, their structures consist of six nonbonding electrons that fill a band and are confined in the structure. The electrons create a positive charge on the surface, thus promoting easy shear through electrostatic repulsion [42].

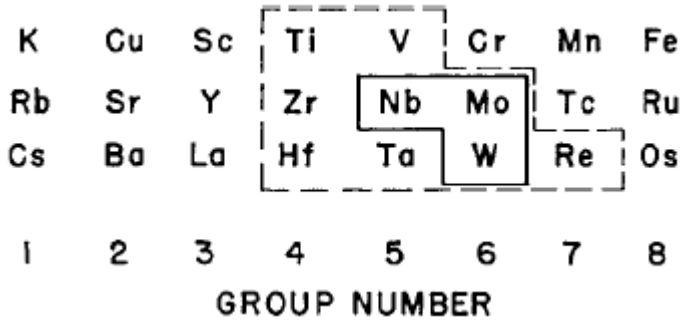

Figure 1-9: Metals that form lamellar structures [44].

MoS_2 exhibits a super-low COF below 0.01 in vacuum. Figure 1-11 illustrates the super-lubricity nature of MoS_2 in high vacuum (HV = 10 uPa), pure dry nitrogen (d-nitrogen) and ultra-high vacuum (UHV = 0.1 uPa). The results showed that oxygen and moisture are detrimental to the super-low friction behaviour of MoS_2 [45]. The super-low friction mechanism was attributed to the S-Mo-S sheets with van der Waals interactions between the sheets, as shown in Figure 1-10 [46].

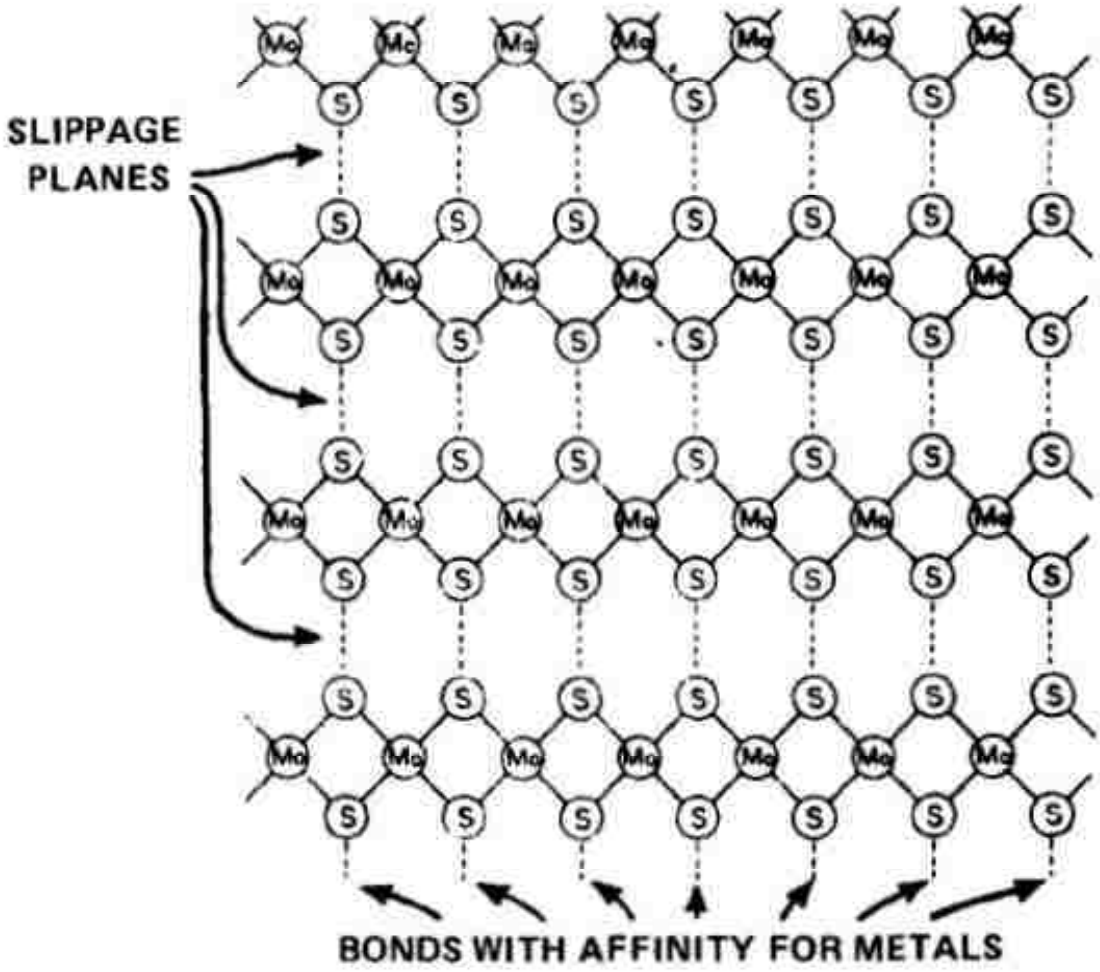

Figure 1-10: Schematic diagram of MoS_2 layered structure [46].

The low COF of 0.14 is also observed in ambient air and similar to graphite, as the temperature increased the COF reached 0.4 at 350 ºC [47], [48]. The increase in COF is attributed to the loss of volatiles through oxidation of the sulphide and formation of $MoS_{2-x}O_x$ [49]. Studies also have shown that the addition of Ti to MoS_2 (MoST) reduces oxygen and moisture sensitivity and generates a COF of 0.03-0.05 against Al and 0.04-0.09 against stainless steel [50]. The addition of Ti also increases thermal stability up to 450 ºC [51].

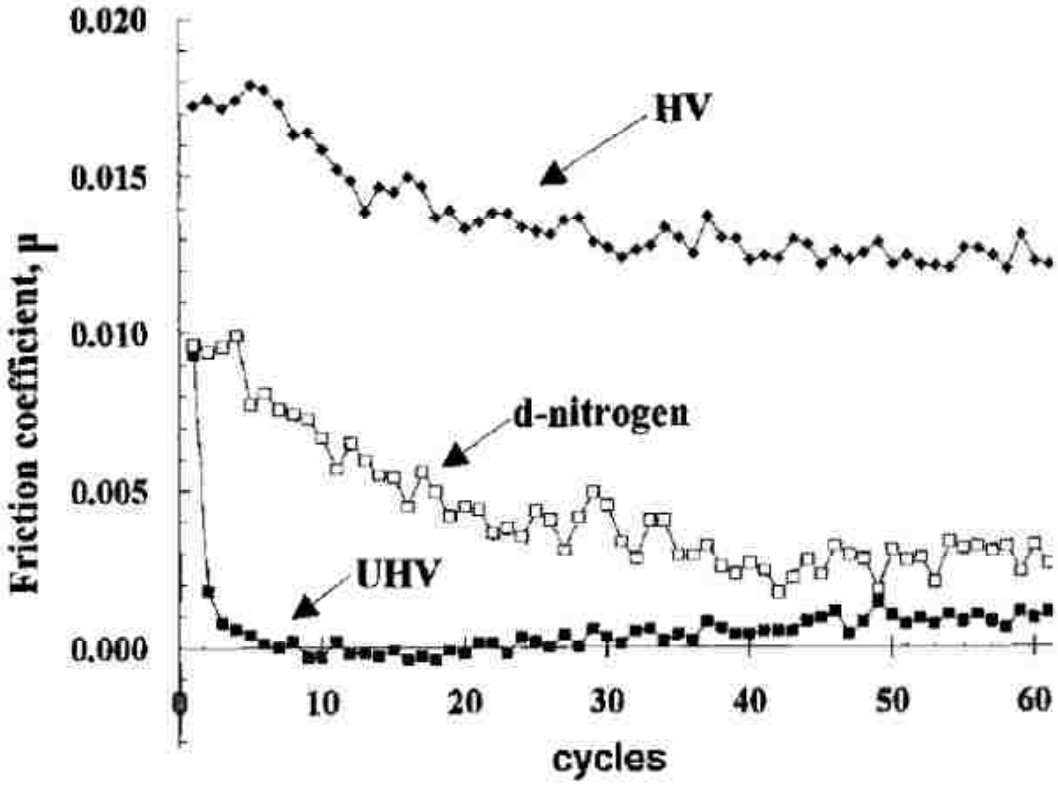

Figure 1-11: Coefficient of friction as a function of sliding cycles of MoS_2 against steel in HV, UHV and d-nitrogen [45].

WS_2 exhibits a super-low COF similar to that of MoS_2 in vacuum and low temperatures, as shown in Figure 1-12. However, WS_2 was observed to be more thermally stable and resistant to oxidation (about 50 to 100 ºC) than MoS_2 was [3]. The slow rate of oxidation of WS_2 can be explained by the formation of tungsten trioxide (WO_3), which is also known to provide a lower COF than MoO_3.

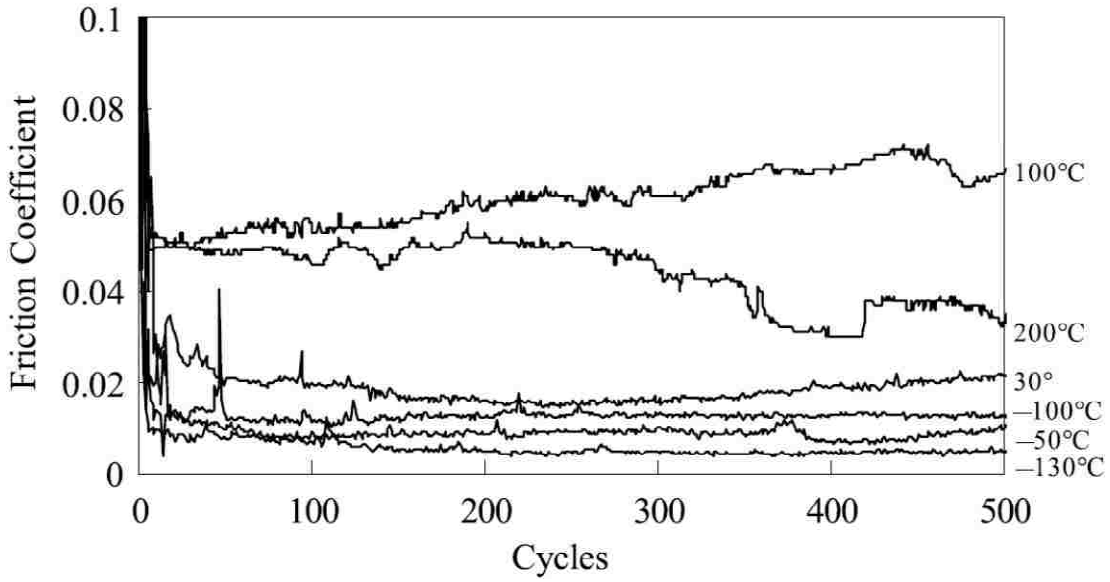

Figure 1-12: Coefficient of friction of WS_2 sliding against 52100 Steel at various temperatures [45].

1.4.3 Diamond-like carbon

Diamond-like carbon (DLC) is part of the carbon family and is classified as amorphous carbon. In the carbon family, the two main phases are graphite (sp^2 hybridization) and diamond (sp^3 hybridization) (Figure 1-13). There are also nano-crystaline graphite (nc-G), amorphous carbon (a-C) and tetrahedral amorphous carbon (ta-C), which are presented in Figure 1-14.

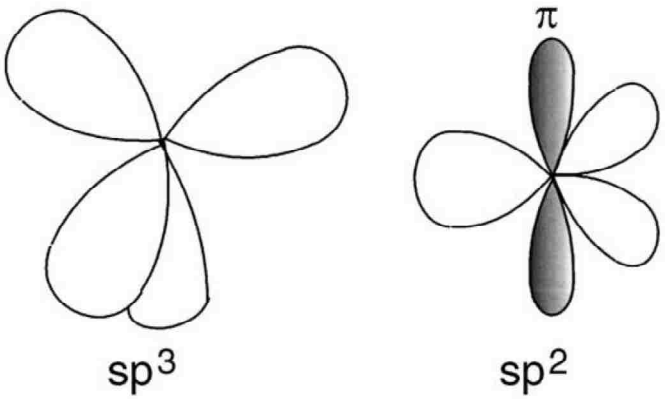

Figure 1-13: Schematic of sp^2 and sp^3 hybridization [52].

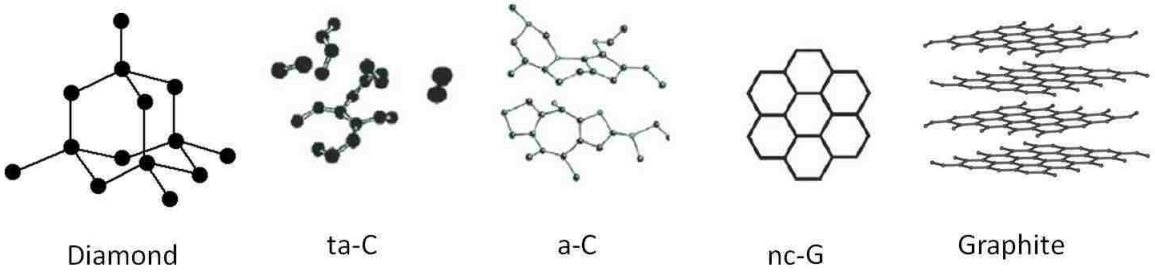

Figure 1-14: Schematic of common carbon structures [52].

Within the carbon family are amorphous carbon sub families that include different types of DLCs. In the DLC family are two of the most common types of DLC, tetrahedral amorphous carbon (ta-C), which consists mainly of the sp^3 bonded carbon network, and amorphous carbon (a-C), with sp^2-structured network. Within these two families of DLCs are two commonly studied types of DLC: hydrogenated DLC (ta-C:H and a-C:H) and dopant-free DLC (ta-C and a-C). A schematic of the ternary phase diagram of the DLC families and their types is presented in Figure 1-15.

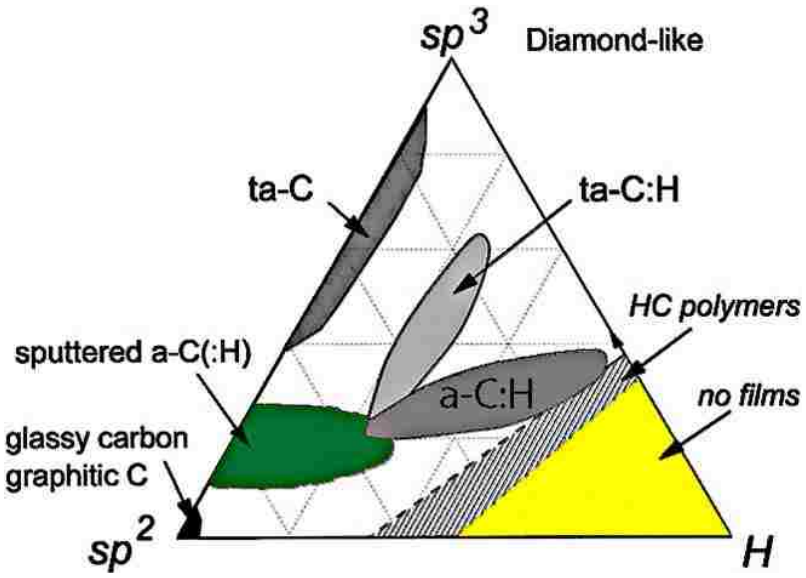

Figure 1-15: Schematic phase diagram of DLC after [52].

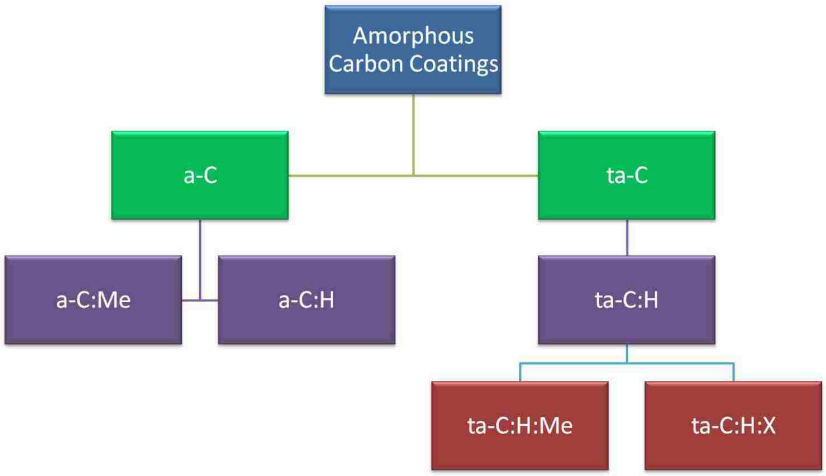

Figure 1-16: Seven categories of amorphous carbon coatings. a-C (hydrogen-free amorphous carbon), ta-C (tetrahedral-bonded hydrogen-free amorphous carbon), a-C:Me (metal-doped hydrogen-free amorphous carbon (Me = W, Ti)), a-C:H (hydrogen-containing amorphous carbon), ta-C:H (tetrahedral-bonded hydrogen-containing amorphous carbon), a-C:H:Me (metal-doped hydrogen-containing amorphous carbon (Me = W, Ti)), a-C:H:X (modified hydrogen-containing amorphous carbon (X = Si, O, N, F, B)).

DLC is a metastable non-crystalline amorphous carbon that consists of partially sp^2- and sp^3-bonded carbon. The deposition of DLC consists of an accelerated C ion toward the substrate with energy ranging from 50-500 eV. The sp^2-bonded carbons are formed by low energy ions that adhere to the surface [53]. The sp^3 fraction is caused by highly energetic ions penetrating the surface; however, the excess energy dissipates in the form of heat, which relaxes the structure. Thus, optimal densification, or the formation of $sp^{3,}$ occurs at ion energy with maximum penetration and minimum relaxation [53].

Although Schmellenmeier [2] developed diamond-like carbon coatings in 1953, the first comprehensive study was reported by Aisenberg and Chabot [3] in 1971. In the 1980s, systematic studies and research were conducted on DLC for production and in-depth chemical characterization [1]. Mechanical and tribological characterization of DLC began in the 1990s. It was not until the late 1990s that DLC films were used extensively in razor blades and the fuel injector systems of diesel engines.

1.4.3.1 Industrial production and application

All the amorphous carbon coatings, i.e., DLC coatings shown in Figure 1-16 can be applied using physical vapour deposition (PVD), plasma assisted chemical vapour deposition (PACVD), or a combination of both techniques.

The main categories of PVD processing are vacuum evaporation, sputter deposition, and ion plating, as shown in Figure 1-17. In these processes, the target/source material is evaporated and deposited on the substrate at rates ranging between 0.5 and 5 μm/h. In the evaporation process, coatings are deposited by the condensation of vapour on the substrate. A cathodic arc or electron beam PVD can be used to deposit DLC.

However, these techniques require high temperatures to evaporate the carbon. Thus, it can be challenging to prevent high substrate temperatures and droplets or macro-particles that can deteriorate the carbon coating. Consequently, magnetron sputtering is more favorable, since it utilizes the discharge of argon glow, in which the plasma is generated in front of the target/source material and ionized argon collides with the target at 100-1000 eV, ejecting atoms from the target. The ejected atoms then accelerate towards the substrate with a kinetic energy ranging from 10 to 40 eV, which is much higher than that of the evaporated atoms (0.2-0.3 eV), forming a stronger adhesion to the surface. In ion plating, the plasma is formed in front of the substrate [8].

In any of these techniques, the coating recipe or coating stages are as follows: the first stage is to pump down and evacuate the chamber to less than 10 mPa (10^{-4} Torr) of any contaminates. This stage is followed by heating to eliminate water vapour and any adsorbed species on the chamber walls. It is then essential to clean the substrate via ion bombardment and or arc-enhanced glow discharge (AEGD) to ensure good interfacial adhesion between the substrate and the coating [54].

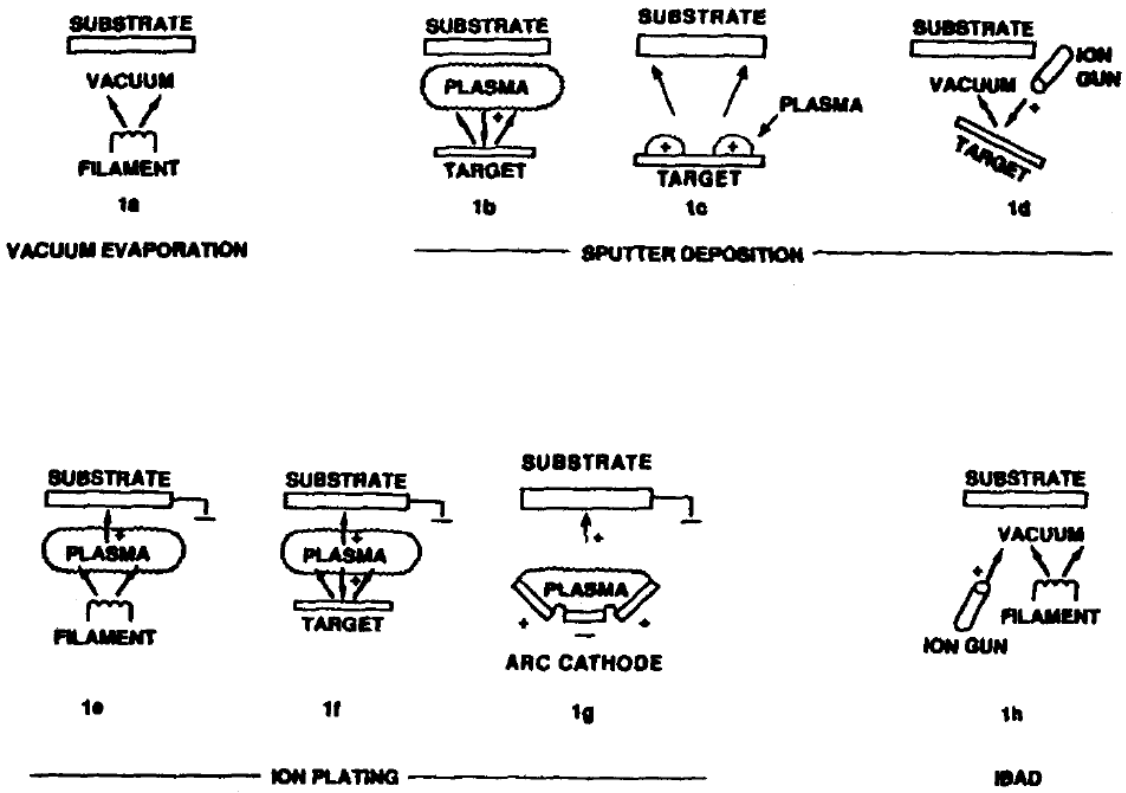

Figure 1-17: PVD processing techniques: (1a) vacuum evaporation, (1b and 1c) sputter deposition in a plasma environment, (1d) sputter deposition in a vacuum, (1e) ion plating in a plasma environment with a thermal evaporation source, (1f) ion plating with a sputtering source, (1g) ion plating with an arc vaporization source and, (1h) Ion Beam Assisted Deposition (IBAD) with a thermal evaporation source and ion bombardment from an ion gun [8].

The cleaning stage is followed by the deposition of an interlayer, which is a mono or gradient layer typically of Cr, Ti, CrN or TiAlN commonly applied prior to the DLC coating to enhance adhesion [55]. Next, the DLC coating stage uses the PVD or PACVD techniques described above with a negative bias applied to the substrate. The coating

chemistry and structure is greatly influenced by the pressure, ion energy and temperature. For instance, sp3 bonded carbon favors low pressures and high ion energy.

Coating structure was investigated by Thornton in 1977 [56], who outlined four different zone structures that resulted from altering the substrate temperature and the argon pressure, as illustrated in Figure 1-18. The first zone is observed at low temperatures (T/T_m <0.3) to consist of a loosely bonded columnar structure with domed tops caused by low adatom mobility. Zone 2 occurs at T/T_m <0.5 with straight columnar stricture and smooth topography, which is attributed to surface diffusion. In Zone 3, the substrate temperature is more than half the substrate melting temperature (T/Tm <0.5), with equiaxed grains caused by bulk diffusion. Finally, the fourth zone was found to occur somewhere between zones 1 and 2. The fourth zone is commonly referred to as zone T, which consists of dense fibrous grains with low internal stress, making it the ideal structure for surface coatings deposited with PVD. In order to achieve these structures, the heating temperature can easily be increased, which, however, can consume time and energy. Thus, the temperature is commonly increased by increasing ion bombardment by increasing the ion current or substrate bias. Nevertheless, the ion current is more favorable because increasing bias can induce coating defects such as loosely bonded nodulars. These nodulars are caused by molten droplets from the targets, which can be entrapped via a filter. The filter consists of a bent path for the ionized evaporated material, which is directed towards the substrate by a magnetic field. However, it is not commonly used in production because it significantly reduces the deposition rate.

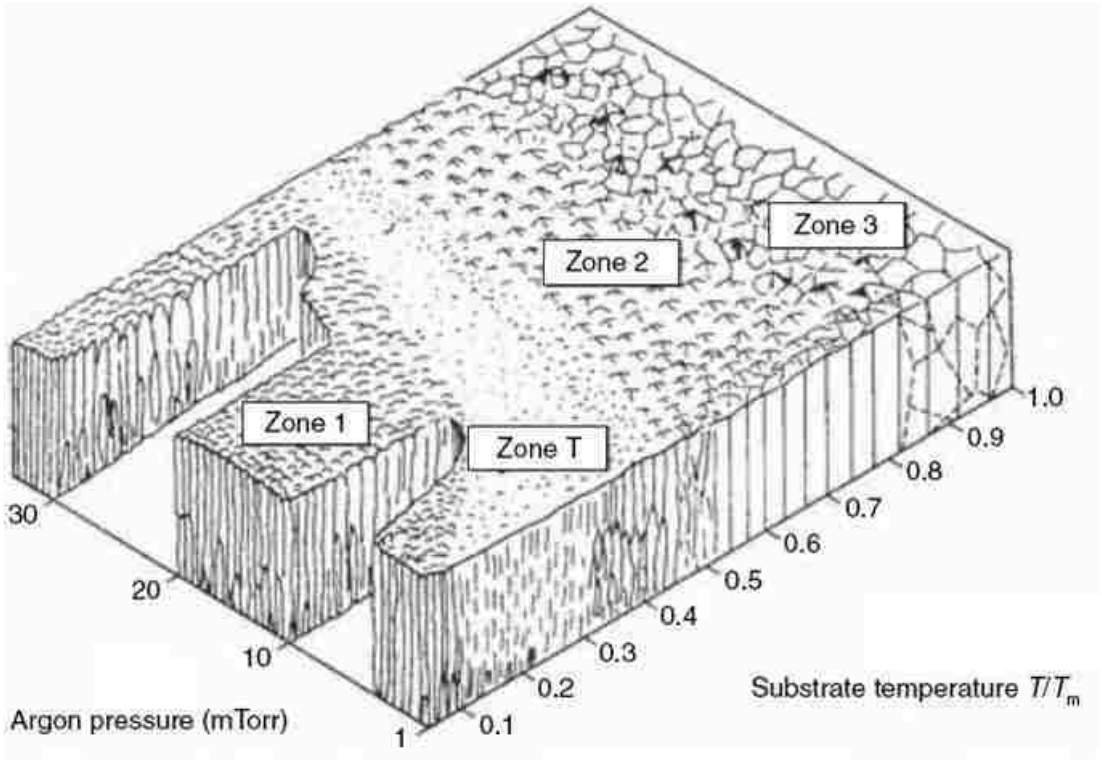

Figure 1-18: Coating structure as a function of temperature and Argon pressure [56]

Finally, the cooling stage in vacuum prevents coating or substrate oxidation, which is commonly achieved by circulating cold water through the chamber walls.

1.4.3.2 Application

The attractive tribological behaviour of DLC coatings caught the attention of many industries, such as the tool industry, automotive industry, aerospace industry, moulding industry and medical industry. In the tool industry, DLC coatings represent 70% of the total amount of coated tools in the market, such as CD moulds, accounting for almost 1400 million Euros. This trend has been increasing since 1980. DLC has also been used in diesel injection; it was observed to increase injection pressure from 1400 to 2000 bar [57]. Japan initially applied CrN in the 1990s, and North America applied TiN in the

same period. However, since 1995, multilayered DLC, specifically a-C:H:W, has been applied to diesel injection, as shown in Table 1-2 below.

Table 1-2: DLC introduction to diesel injection systems [58]

Europe	Patent	1983
initially a-C:H:W	Application development	1993
Now a-C:H:W/a-C:H	Large-volume application	1995 onwards
or CrN/a-C:H	Market penetration > 50%	~1998
Japan	Basic development	Late 1970s
Initially CrN	Application development	1990–1995
	Large-volume application	1995 onwards
	Market penetration >50%	
North America	Basic development	Late 1970s
Initially TiN	Application development	1990–1995
Now a-C:H:W/a-C:H	Large-volume application	1995 onwards
	Market penetration > 50%	

The attractive performance of DLC in diesel injection systems paved the road for other components, such as rocker arm, tappets, piston pins, piston rings and crankshaft bearings. Mass production was initiated around 2002 and is predicted to increase, as illustrated in the table below.

Table 1-3: DLC in engine components [58]

Application	Introduction	Penetration 2006 (%)	Coating
Diesel injection	1994	95	Multilayer a-C:H
Tappet	2002	2	Multilayer a-C:H, Cr_2N
Piston pin	2004	<1	Multilayer a-C:H
CD mould	Early 1990s	~100	a-C:H
Racing	Early 1990s	~100	Multilayer a-C:H
Gears	Early 1990s	~0	

1.4.3.3 Tribological behaviour of hydrogenated DLC

Hydrogenated DLC is well known for its super-low COF (<0.01) in inert and vacuum environments [13]. Super-low COF is commonly attributed to the presence of hydrogen, which eliminates interatomic interactions at the sliding interface because of weak van der Waals interactions with low binding energy (0.08 eV) [13], [59]. In 1979, Enke et al. [60] were the first to investigate the effects of the atmosphere on hydrogenated DLC using acetylene (C_2H_2). The study showed that the COF of the hydrogenated DLC exhibited a COF of 0.01 at 10^{-7} %RH and increased monotonically to 0.2 as the water vapour content increased beyond 50% RH, as shown in Figure 1-19. Several studies confirmed the observation and attributed the increase in COF to capillary forces, particularly at high humidity levels, and to carbon oxidation, which induces attractive forces at the sliding interface leading to increases in COF [61]–[63].

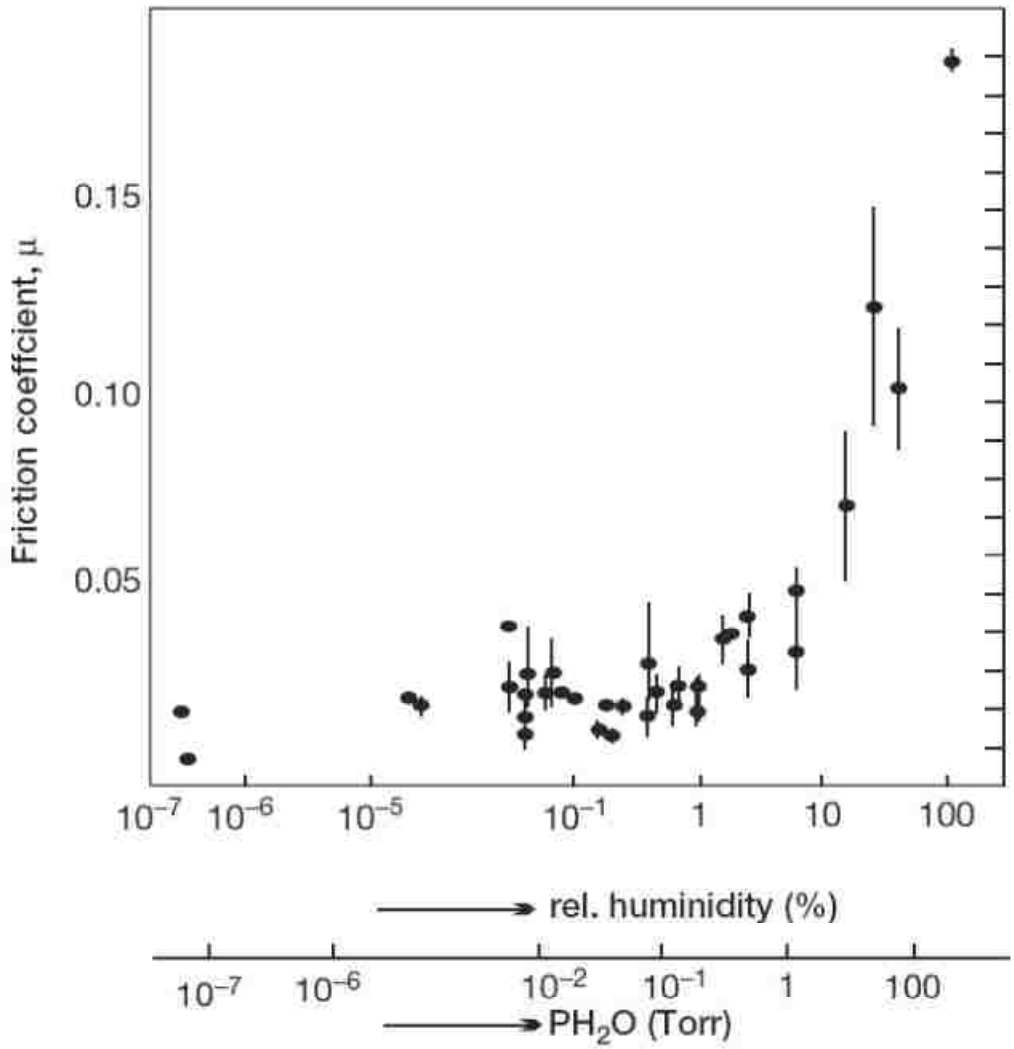

Figure 1-19: Coefficient of friction of H-DLC as a function of moisture in the atmosphere [60].

Further investigations of the hydrogen content in hydrogenated DLC coatings observed its great influence on COF. Tribological investigations of hydrogenated DLC coatings deposited using PECVD and various hydrocarbons (C_2H_2, CH_4, 75%CH_4+25%H_2, 50%CH_4+50%H_2 and 25%CH_4+75%H_2) showed that the COF decreased with increases in hydrogen content in the gas mixture or higher H/C ratios [12]. Consequently, because of the increase in hydrogen content, super-low COF of 0.001

was observed in hydrogenated DLC coatings deposited by 25% CH_4+75%H_2 when tested against itself at 10 N load and 0.5 m/s speed in a dry nitrogen atmosphere (Figure 1-20).

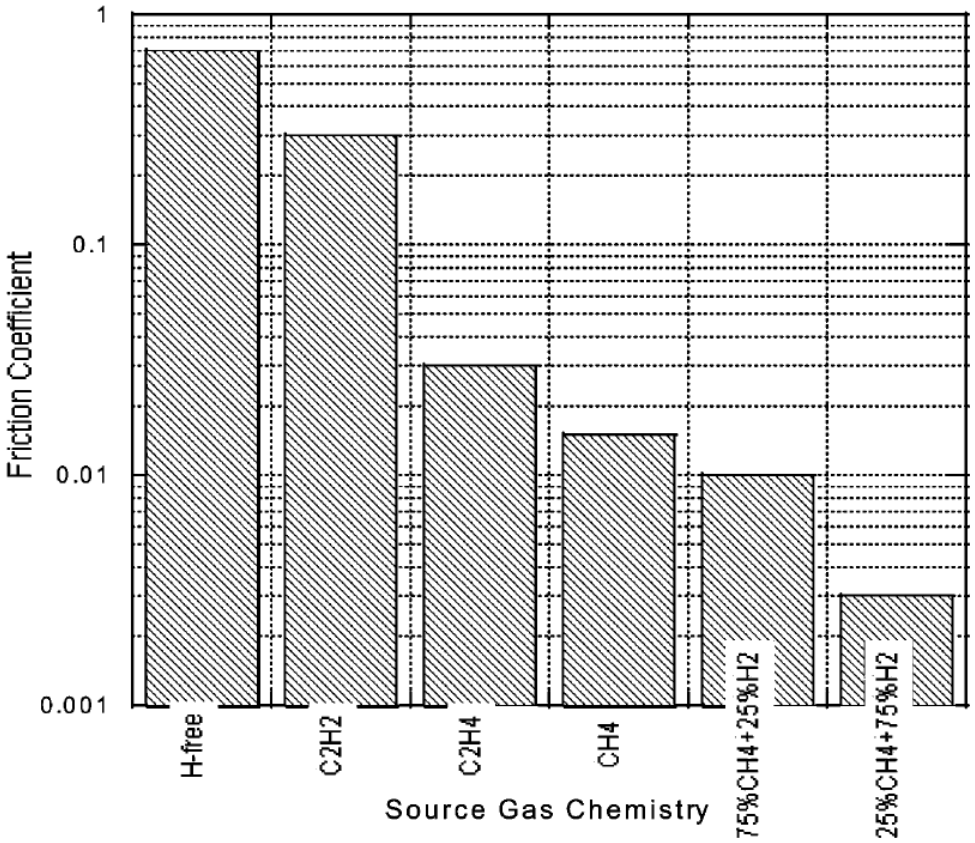

Figure 1-20: Coefficient of friction of DLC as a function of deposition source gas [12].

A study by Donnet and Grill [64] showed that super-low COF of 0.02 in vacuum can be achieved with hydrogen content of 40% or higher. It was also observed that the COF in ambient air does not significantly fluctuate with hydrogen content ranging from 20–40% of hydrogen (Figure 1-21).

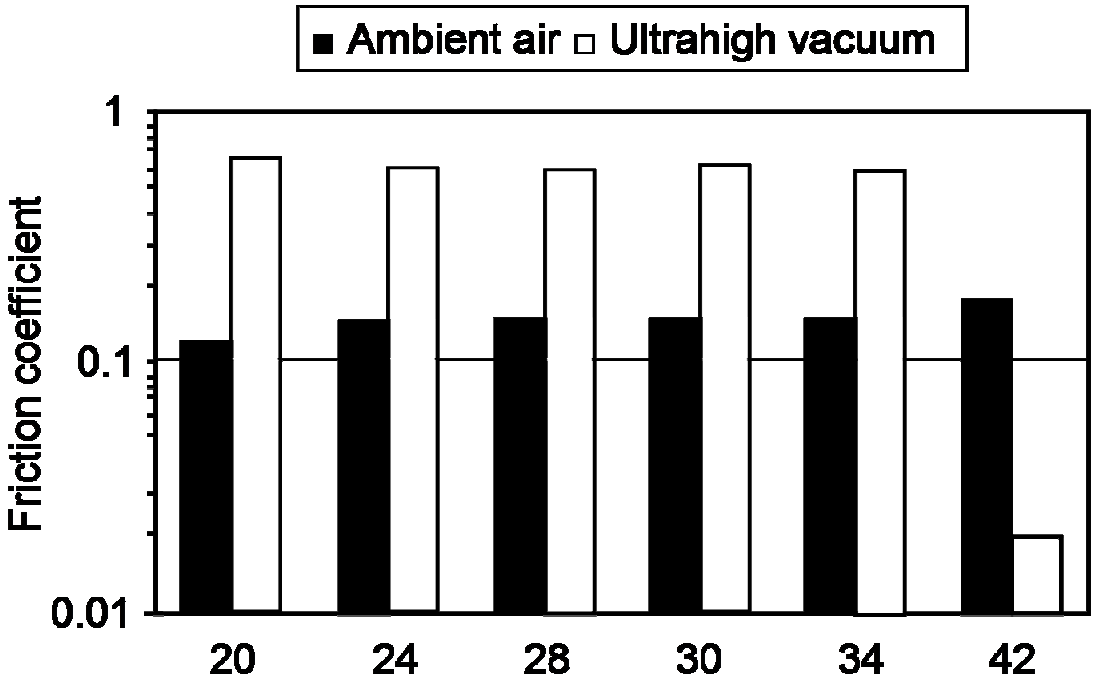

Figure 1-21: Coefficient of friction of DLC as a function of hydrogen content [64].

The super-low COF of hydrogenated DLC coatings is attributed to the hydrogen-terminated surface, which eliminates interatomic interactions at the sliding interface [13]. The hydrogen acts as a passivant to the carbon atoms by mitigating chemical or physical interactions, as shown in Figure 1-22. This mechanism was confirmed by Konca et al. who tested dopant-free DLC in vacuum and a hydrogen rich atmosphere (60% He- 40% H_2) [65]. In vacuum, the dopant-free DLC coating showed a very high COF of 0.6-0.8. When hydrogen gas was introduced to the testing environment, a super-low COF of 0.01 was achieved by hydrogen-surface termination. Figure 1-23 (a) shows a schematic of the sliding contact between two carbon surfaces terminated with hydrogen, and Figure 1-23 (b) shows the schematic of a single atomic contact illustrating the repulsive force induced by hydrogen termination.

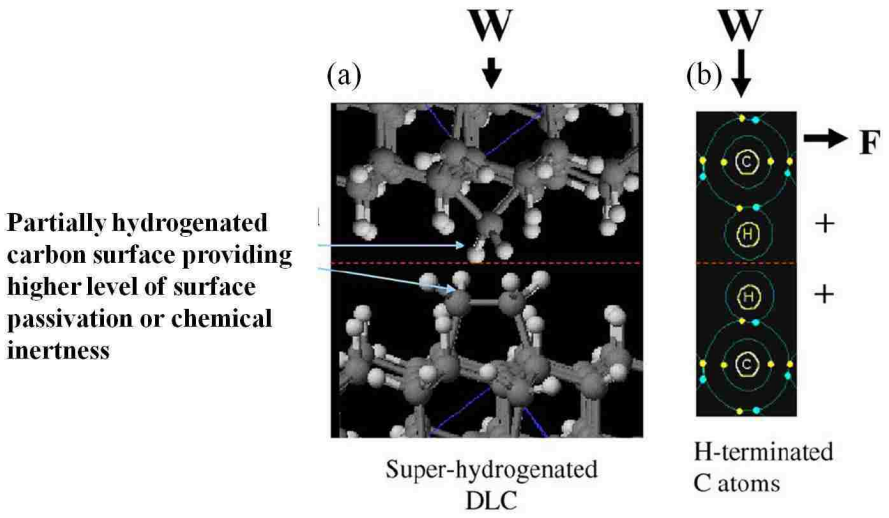

Figure 1-22: Schematics of the interface of hydrogen terminated surfaces [13].

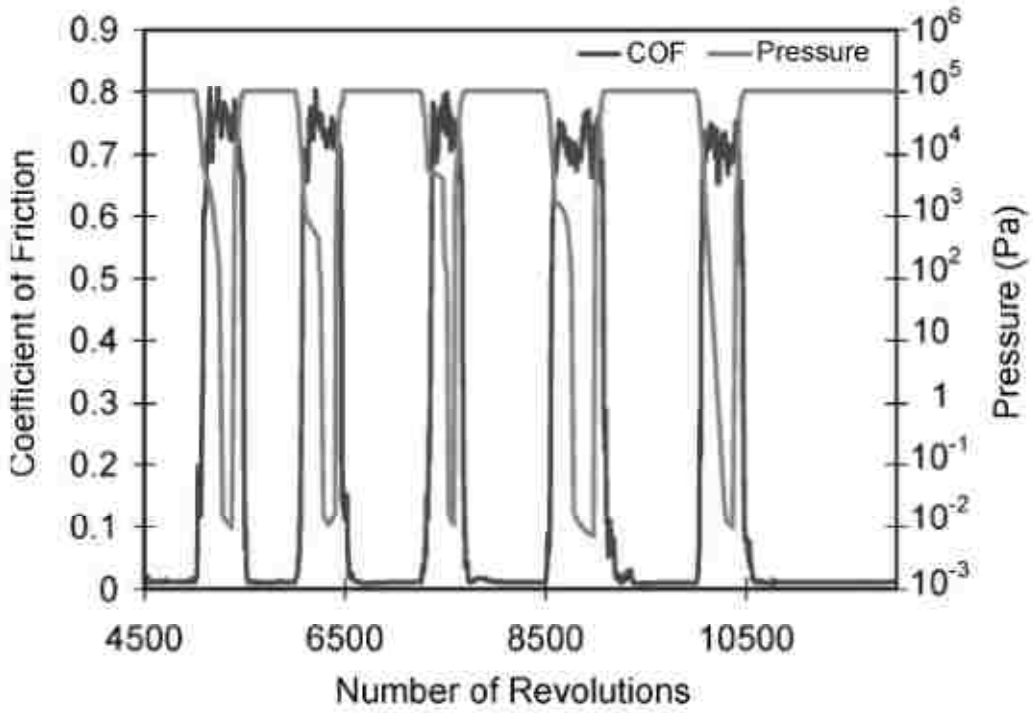

Figure 1-23: Coefficient of friction of dopants free DLC sliding against aluminum as a function of hydrogen gas partial pressure in the test chamber [65].

1.4.3.4 Tribological behaviour of dopants free DLC

The relevant literature shows that the tribological behaviour of DLC coatings is greatly influenced by the testing temperature [66]. Vanhulsel et al. [67] studied the tribological behaviour of H-DLC at elevated temperatures (35 at% H) against corundum balls. The study revealed that the wear scar increased at higher temperatures, but the COF decreased to 0.07 at 300 °C. The results were attributed to structural changes of sp^2 to sp^3 and/or dehydrogenation [67]. Other studies also reported hydrogen loss above 450 ºC, confirming the dehydrogenation theory [68], [69]. Another study by Ni et al. [70] investigated the tribological behaviour of H-DLC (14 at% H) and showed that DLC failed at temperatures higher than 240 °C. Coating failure was attributed to the graphitization of H-DLC for which the positive Raman shift in the G-peak (1580 cm^{-1}) was considered supporting evidence [70].

Dopant-free DLC coatings were observed to behave in an almost completely opposite manner. The COF is very high in vacuum and inert atmospheres, ranging from 0.5 to 0.9. The high friction can be attributed to the presence of highly active unterminated bonds (dangling bonds) on the surface. These dangling bonds react with the mating surface, causing adhesion in the case of materials such as aluminum. *Ab initio* calculations of diamond [16], which is commonly used to simulate DLC, was found to adhere with aluminum in vacuum because the interfacial energy between clean diamond and aluminum was 4.08 J/m^2, which is much higher than the work of de-cohesion of aluminum computed at 1.56 J/m^2. Consequently, the aluminum/aluminum interface breaks before the diamond/aluminum interface because of its lower de-cohesion energy. In addition, the presence of humidity or water vapour was observed to reduce the COF to

0.1 [71]. Konca et al. [72] showed that the COF of WC and 319 Al sliding against dopant-free DLC decreased with increased humidity [72]. The authors attributed the lubricious behaviour in a moisture-rich environment to the formation of a carbonaceous easy-shear tribo-layer on the counterface as well as adsorbed water molecules. Experimental studies revealed that the adsorbed water dissociated and passivated the carbon surface. Strom et al. [73] observed that friction of magnetic disks with carbon overcoat significantly reduced the friction, suggesting that adsorbed water dissociates and passivates dangling carbon bonds in the presence of oxygen. This mechanism was later confirmed by first-principle investigations carried out by Qi et al. [74], who showed that water molecules dissociate to -H and –OH, thus passivating the dangling carbon bonds found on the surface of a hydrogen-free diamond surface.

Temperature has a more significant effect on dopant-free DLC than on H-DLC. Konca et al. [75] explored the effects of temperature on dopant-free DLC against aluminum. The results showed that at 25 ºC, gaseous species, such as H and O, in the air were adsorbed by the dangling σ-bonds on the surface of the dopant-free DLC coating, producing a COF of 0.17. As the temperature increased to about 120 ºC, gaseous species desorbed from the surface, re-exposing the σ-bonds. The COF value then increased to 0.3 because interactions with the counter surface. At 300 ºC, adhesion occurred with large amounts of aluminum transfer, causing a high COF of 0.4 and high wear rates.

1.4.3.5 Tribological behaviour of metal doped DLC

The relevant literature showed that the surrounding environment governs the low COF of hydrogenated and dopant-free DLC. However, by adding dopants to the DLC, the chemistry and the tribological behaviour can be manipulated to achieve multi-functionality by tailoring the coating to the application. The addition of metal dopants also improves the adhesion of DLC coatings on substrates such as steel, which is commonly observed to be caused by high compressive stresses (>2GPa) [76], [77] and differences in elastic modulus, hardness, and coefficients of thermal expansion at the interface [58]. Strong interfacial adhesion can be attained between DLC and substrate by incorporating metals or refractory metals that form a carbide layer that can chemically react with the atoms of the substrate materials and thus insure strong bonding. These metals tend to form small nano-crystallites of metal or metal carbides in the DLC matrix [78], [79]. The addition of refractory metals, such as W, to DLC was found to generate a COF of 0.1 and almost 8 times less wear than TiN coating did [80]. They also found that the wear behaviour is governed by the W content and the least amount of wear was observed at 13 at% of W.

The addition of W to DLC (W-DLC) was found to increase hardness and provide a good compromise between mechanical and tribological properties for W-DLC coating with hardness ranging from 15-20 GPa and COF of ~ 0.2 at 40-45 at% of carbon as shown in Figure 1-24 [81]. Different W content was observed to generate different tribological regimes. El Mrabet et al. [82] showed that between 30-40 at% of C crystalline W_2C and WC_{1-x} phases exist with grain sizes of 5–10 nm. The coating had

high hardness ranging from 35–40 GPa with poor tribological properties caused by its brittle ceramic-like nature. Carbon content ranging from 40–65 at% exhibited hardness ranging from 21-23 GPa with high concentration of small hard WC_{1-x} crystals. These crystals generated abrasive debris particles that accelerated the degradation of the coating. At carbon contents higher than 65 at%, less abrasive WC_{1-x} crystals were observed and hardness ranged from 16–20 GPa, as shown in Figure 1-25. The coating generated a COF of 0.2, and the authors attributed the low COF to the formation of carbonaceous third-body material transfer.

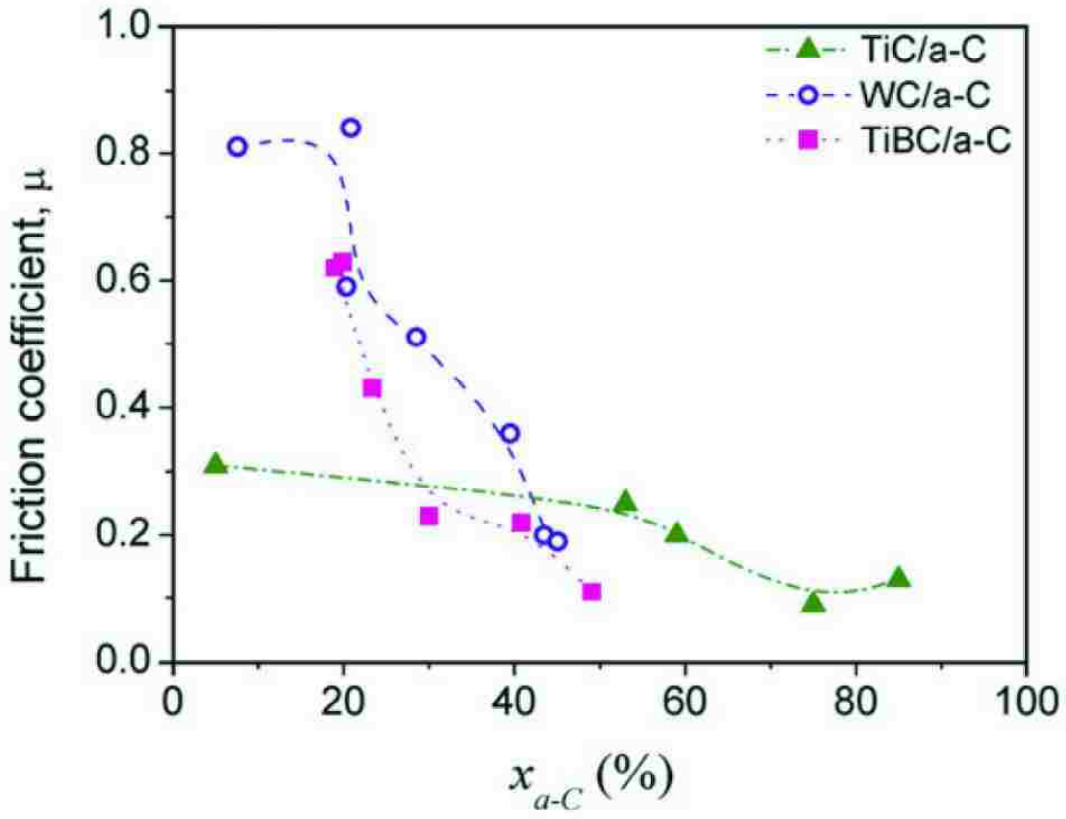

Figure 1-24: Coefficient of frication of W-DLC as a function of carbon content [81].

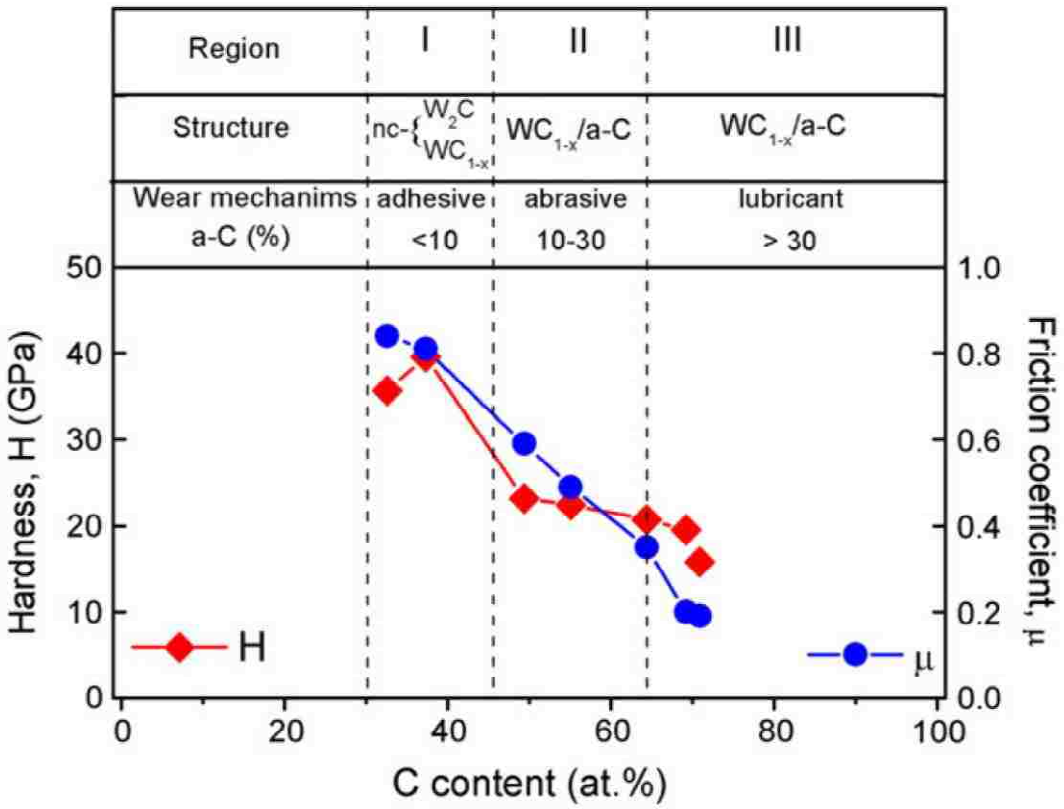

Figure 1-25: Coefficient of friction and hardness as a function of carbon content [82].

The effect of WC crystallinity on the tribological behaviour of W-DLC was investigated by Voevodin et al. [83]. In this study, WC crystallinity was altered by controlling the deposition temperature. At room temperature, near amorphous (na) WC crystals were formed in grain sizes of 1–3 nm with hardness of 15 GPa. Nanocrystaline (nc) WC was formed at 300 ºC deposition temperature in grain sizes of 5–10 nm with hardness of 26 GPa. The COF of both nc-W-DLC and na-W-DLC were found to decrease with increases in carbon content. When tested against steel in air (50 %RH) the COF of na-W-DLC was observed to drop from 0.5–0.4 to 0.15–0.10. The na-W-DLC was observed to generate slightly higher COF but followed the same trend. At carbon contents less than 60 at%, the COF ranged from 0.7 to 0.6, and at higher carbon contents the COF dropped to 0.4–0.3, as shown in Figure 1-26 (a). The same study also investigated the

effects of humidity and found that COF was dependent on the humidity in the surrounding atmosphere. When tested against steel in a nitrogen-rich atmosphere (0.5 %RH) the COF was higher than that observed at 50 %RH but had a similar trend, as shown in Figure 1-26 (b).

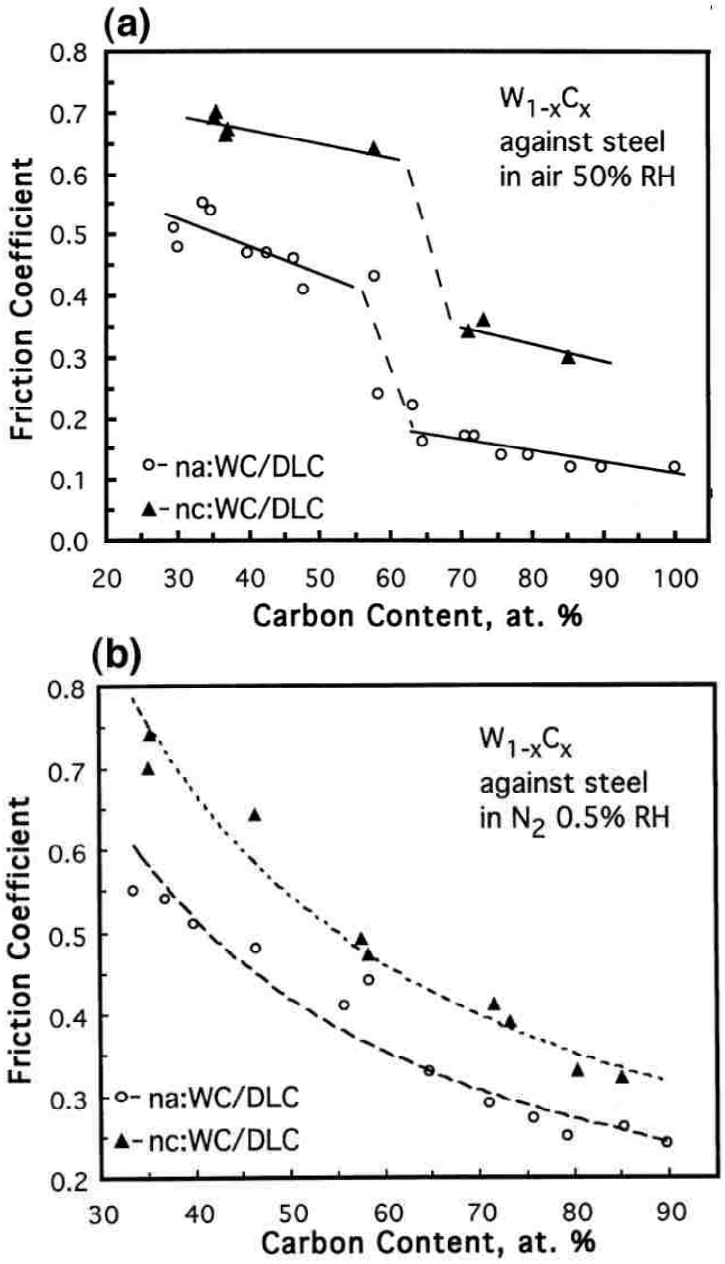

Figure 1-26: Coefficient of friction of W-DLC as a function of carbon content of na and nc W-DLC (a) air 50 %RH (b) nitrogen 0.5 %RH [83].

In summary, the tribological behaviour of carbon-based coatings and aluminum mitigation mechanism for DLC specifically was observed to be manipulated by the surrounding atmosphere and coating chemistry. Hydrogen was observed to reduce the COF in inert atmospheres. First principles and experimental results showed that low COF was caused by the formation of material transfer resulting in the hydrogen/hydrogen (van der Waals) type of interactions, thus reducing the COF.

The COF of dopant-free DLC was found to decrease with increases in humidity in the testing atmosphere. First principles and experimental analyses showed that the reduction in COF was attributed to the carbon surface passivation by H and OH molecules dissociated from the water molecules adsorbed or found on the sliding interface. Surface temperature was found to be detrimental to the low friction and wear behaviour of DLC. Surface analyses showed that increases in temperature typically desorbed water molecules from the sliding interface of hydrogen free DLC. Similarly, the hydrogen that passivated the carbon in hydrogenated DLC was observed to desorb as temperatures increased to 100–200 °C, causing coating oxidation and high friction and wear.

It is not however clear how the DLC would perform under these conditions and how the addition of metallic elements such as tungsten to the DLC would affect tribological behaviour. Thus, the purpose of this research project is to identify the friction and wear mechanisms to gain better understanding of the behaviour of carbon-based coatings at elevated temperatures and in humid and oxygen-rich environments. This work will be a fundamental study with the long-term objective of developing and laying a

foundation for the development of an ideal low-friction and low-wear surface coating to prevent aluminum adhesion.

1.5 Organization of dissertation

Chapter 2 investigates the effects of oxygen and humidity on the tribological behaviour of dopant-free DLC. Chapters 3 to 5 present experimental studies that investigate the tribological mechanisms of H-DLC and W-DLC at elevated temperatures and their mechanisms which reduce the tendency of aluminum adhesion to the surface. The friction and wear behaviour of dopant-free DLC (referred to as DLC from here on), H-DLC and W-DLC coatings at sub-zero temperatures are presented in Chapter 6. Chapter 7 focuses on the work of adhesion of the various coatings (H-DLC, dopant-free DLC, W-DLC) at elevated temperatures and how the work of adhesion relates to the friction. Finally, Chapter 8 summarizes the study and addresses the role of tungsten on the friction and wear mechanisms of DLC at elevated temperatures and the influence of the work of adhesion on the COF.

References

[1] A. Erdemir and C. Donnet, "Tribology of diamond-like carbon films: recent progress and future prospects", *Journal of Physics D: Applied Physics*, vol. 39, no. 18, pp. R311–R327, 2006.

[2] G. W. Stachowiak and A. W. Batchelor, "*Engineering Tribology*", 3rd edition. New York: Elsevier, 2005, p. 3.

[3] C. Taylor, "Automobile engine tribology--design considerations for efficiency and durability", *Wear*, vol. 221, pp. 1–8, 1998.

[4] S. C. Tung and M. L. McMillan, "Automotive tribology overview of current advances and challenges for the future", *Tribology International*, vol. 37, no. 7, pp. 517–536, 2004.

[5] H. Pierson, "Applications of Refractory Carbides and Nitrides", in *Handbook of Refractory Carbides and Nitrides*, New Jersey: Noyes Publications, 1996, pp. 309–325.

[6] B. J. Hamrock, S. R. Schmid, and B. O. Jacobson, "*Fundamentals of Fluid Film Lubrication*", 2nd edition. New York: CRC Press, 2004, pp. 4–10.

[7] S. M. Hsu and R. S. Gates, "Boundary lubricating films: formation and lubrication mechanism", *Tribology International*, vol. 38, no. 3, pp. 305–312, 2005.

[8] D. M. Mattox, "*Handbook of Physical Vapor Deposition (PVD) Processing*". Westwood, New Jersey, U.S.A.: Noyes publication, 1998, pp. 31–34.

[9] W. Jacob and A. Von Keudell, "Films Growth", in *Properties of amorphous carbon*, S. Ravi and P. Silva, Eds. London: The Institution of Electrical Engineers, 2003, pp. 279–287.

[10] S. V. Hainsworth and N. J. Uhure, "Diamond like carbon coatings for tribology: production techniques, characterisation methods and applications", *International Materials Reviews*, vol. 52, no. 3, pp. 153–174, 2007.

[11] A. Erdemir, I. Nilufer, O. Eryilmaz, M. Beschliesser, and G. Fenske, "Friction and wear performance of diamond-like carbon films grown in various source gas plasmas", *Surface and Coatings Technology*, vol. 120, pp. 589–593, 1999.

[12] A. Erdemir, "The role of hydrogen in tribological properties of diamond-like carbon films", *Surface and Coatings Technology*, vol. 146–147, no. 1, pp. 292–297, 2001.

[13] A. Erdemir, "Genesis of superlow friction and wear in diamondlike carbon films", *Tribology International*, vol. 37, no. 11–12, pp. 1005–1012, 2004.

[14] K. Holmberg and A. Matthews, "Coatings tribology — contact mechanisms and surface design", *Tribology International*, vol. 31, no. 98, pp. 107–120, 1998.

[15] K. Holmberg, "Tribology of thin coatings", *Ceramics International*, vol. 26, no. 7, pp. 787–795, 2000.

[16] Y. Qi and L. Hector, "Hydrogen effect on adhesion and adhesive transfer at aluminum/diamond interfaces", *Physical Review B*, vol. 68, no. 20, pp. 1–4, 2003.

[17] F. P. Bowden and L. Leben, "The nature of sliding and the analysis of friction", *Mathematical and Physical Sciences*, vol. 169, no. 938, pp. 371–391, 1939.

[18] Q. Zhang, Y. Qi, L. Hector, T. Cagin, and W. Goddard, "Origin of static friction and its relationship to adhesion at the atomic scale", *Physical Review B*, vol. 75, no. 14, pp. 1–7, 2007.

[19] D. Maugis, "Adhesion of Solids: Mechanical Aspects", in *Modern Handbook of Tribology*, B. Bhushan, Ed. New York: CRC Press, 2001, p. 165.

[20] M. W. Finnis, "The theory of metal - ceramic interfaces", *Journal of Physics: Condensed Matter*, vol. 8, no. 32, pp. 5811–5836, 1996.

[21] K. L. Johnson, "Adhesion and friction between a smooth elastic spherical asperity and a plane surface", *Proceedings of the Royal Society A: Mathematical, Physical and Engineering Sciences*, vol. 453, no. 1956, pp. 163–179, 1997.

[22] R. W. Carpick and M. Salmeron, "Scratching the surface: fundamental investigations of tribology with atomic force microscopy.", *Chemical reviews*, vol. 97, no. 4, pp. 1163–1194, 1997.

[23] J. S. McFarlane and D. Tabor, "Relation between friction and adhesion", *Mathematical and Physical Sciences*, vol. 202, no. 1069, pp. 244–253, 1950.

[24] J. S. McFarlane and D. Tabor, "Adhesion of solids and the effect of surface films", *Mathematical and Physical Sciences*, vol. 202, no. 1069, pp. 224–243, 1950.

[25] B. Bhushan, "Adhesion and stiction: Mechanisms, measurement techniques, and methods for reduction", *Journal of Vacuum Science & Technology B: Microelectronics and Nanometer Structures*, vol. 21, no. 6, pp. 2262–2296, 2003.

[26] X. Xiao, "Investigation of humidity-dependent capillary force", *Langmuir*, vol. 16, no. 21, pp. 8153–8158, 2000.

[27] L. Sirghi, R. Szoszkiewicz, and E. Riedo, "Volume of a nanoscale water bridge.", *Langmuir*, vol. 22, no. 3, pp. 1093–1098, 2006.

[28] T. Bouhacian, B. Desbat, J. P. Aime, T. Bouhacina, and J. P. Aim, "FTIR spectroscopy and nanotribological comparative studies: influence of the adsorbed water layers on the tribological behaviour", *Tribology Letters*, vol. 9, pp. 111–117, 2000.

[29] R. Neitola, H. Ruuska, and T. A. Pakkanen, "Ab initio studies on nanoscale friction between graphite layers: effect of model size and level of theory.", *The journal of physical chemistry. B*, vol. 109, no. 20, pp. 10348–10354, 2005.

[30] S. Snyder, W. Gerberich, and H. White, "Scanning-tunneling-microscopy study of tip-induced transitions of dislocation-network structures on the surface of highly oriented pyrolytic graphite", *Physical Review B*, vol. 47, no. 16, pp. 10823–10831, 1993.

[31] W. H. Bragg, "An Introduction to Crystal Analysis", in *An Introduction to Crystal Analysis*, London: G.Bell and Sons, 1928, p. 64.

[32] A. R. F. Deacon and J. F. Goodman, "Lubrication by lamellar solids", *Society*, vol. 243, no. 1235, pp. 464–482, 2009.

[33] Y. Dappe, M. Basanta, F. Flores, and J. Ortega, "Weak chemical interaction and van der Waals forces between graphene layers: A combined density functional and intermolecular perturbation theory approach", *Physical Review B*, vol. 74, no. 20, pp. 1–9, 2006.

[34] G. Rowe, "Some observations on the frictional behaviour of boron nitride and of graphite", *Wear*, vol. 3, no. 4, pp. 274–285, 1960.

[35] R. D. Arnell and D. G. Teer, "Lattice Parameters of Graphite in relation to Friction and Wear", *Nature*, vol. 218, no. 5147, pp. 1155–1156, 1968.

[36] B. K. Yen, B. E. Schwickert, and M. F. Toney, "Origin of low-friction behavior in graphite investigated by surface x-ray diffraction", *Applied Physics Letters*, vol. 84, no. 23, pp. 4702–4705, 2004.

[37] R. Savage, "Graphite lubrication", *Journal of applied physics*, vol. 19, no. 1, pp. 1–10, 1948.

[38] M. Kostov, E. Santiso, a. George, K. Gubbins, and M. Nardelli, "Dissociation of Water on Defective Carbon Substrates", *Physical Review Letters*, vol. 95, no. 13, pp. 1–4, 2005.

[39] J. K. Lancaster, "Instabilities in the frictional behaviour of carbons and graphites", *Wear*, vol. 3, pp. 275–290, 1975.

[40] L. Xiaowei, "Effect of temperature on graphite oxidation behavior", *Nuclear Engineering and Design*, vol. 227, no. 3, pp. 273–280, 2004.

[41] F. Bowden and J. Young, "Friction of diamond, graphite, and carbon and the influence of surface films", *Mathematical and Physical Science*, vol. 208, no. 1095, pp. 444–455, 1951.

[42] C. Muratore and A. Voevodin, "Chameleon Coatings: Adaptive Surfaces to Reduce Friction and Wear in Extreme Environments", *Annual Review of Materials Research*, vol. 39, no. 1, pp. 297–324, 2009.

[43] J. Martin, C. Donnet, and T. Le Mogne, "Superlubricity of molybdenum disulphide", *Physical Review B*, vol. 48, no. 14, pp. 10583–10586, 1993.

[44] W. E. Jamison and S. L. Cosgrove, "Friction Characteristics of Transition-Metal Disulfides and Diselenides", *A S L E Transactions*, vol. 14, no. 1, pp. 1–62, 1971.

[45] A. Erdemir and J.-M. Martin, Eds., "*Superlubricity*", First Edit. Amsterdam: Elsevier, 2007, p. 525.

[46] D. H. Buckley, "*Surface effects in adhesion, friction, wear, and lubrication*". New York: Elsevier, 1981, p. 643.

[47] T. Kubart, T. Polcar, L. Kopecký, R. Novák, and D. Nováková, "Temperature dependence of tribological properties of MoS2 and MoSe2 coatings", *Surface and Coatings Technology*, vol. 193, no. 1–3, pp. 230–233, 2005.

[48] M. A. Hamilton, L. A. Alvarez, N. A. Mauntler, N. Argibay, R. Colbert, D. L. Burris, C. Muratore, A. A. Voevodin, S. S. Perry, and W. G. Sawyer, "A Possible Link Between Macroscopic Wear and Temperature Dependent Friction Behaviors of MoS2 Coatings", *Tribology Letters*, vol. 32, no. 2, pp. 91–98, 2008.

[49] N. Ohmae, "Influence of atomic oxygen on space tribology in a low earth orbit", *Wear*, vol. 168, no. 1–2, pp. 99–103, 1993.

[50] N. M. U. Renevier, J. Hamphire, V. C. Fox, J. Witts, T. Allen, and D. G. Teer, "Advantages of using self-lubricating , hard , wear-resistant MoS 2 -based coatings", *Surface and Coatings Technology*, pp. 67–77, 2001.

[51] N. M. Renevier, H. Oosterling, U. König, H. Dautzenberg, B. J. Kim, L. Geppert, F. G. M. Koopmans, and J. Leopold, "Performance and limitations of MoS2/Ti composite coated inserts", *Surface and Coatings Technology*, vol. 172, no. 1, pp. 13–23, 2003.

[52] J. Robertson, "Diamond-like amorphous carbon", *Materials Science and Engineering: R: Reports*, vol. 37, no. 4–6, pp. 129–281, 2002.

[53] J. Robertson, "The deposition mechanism of diamond-like a-C and a-C: H", *Diamond and Related Materials*, vol. 3, no. 4–6, pp. 361–368, 1994.

[54] J. Vetter, W. Burgmer, and A. J. Perry, "Arc-enhanced glow discharge in vacuum arc machines", *Surface and Coatings Technology*, vol. 59, no. 1–3, pp. 152–155, 1993.

[55] H.-G. Fub and M. Frank, "Industrial production of DLC coatings", in *Tribology of Diamond-Like Carbon Films*, C. Donnet and A. Erdemir, Eds. New York, N.Y.: Springer, 2008, pp. 457–483.

[56] J. A. Thornton, "High rate thick film", *Annual Review of Materials Research*, vol. 7, pp. 239–260, 1977.

[57] C. P. O. Treutler, "Industrial use of plasma-deposited coatings for components of automotive fuel injection systems", *Surface and Coatings Technology*, vol. 200, no. 5–6, pp. 1969–1975, 2005.

[58] C. Donnet and A. Erdemir, "*Tribology of Diamond-Like Carbon Films*". Boston, MA: Springer US, 2008.

[59] C. Donnet, J. Fontaine, A. Grill, and T. Le Mogne, "The role of hydrogen on the friction mechanism of diamond-like carbon films", *Tribology Letters*, vol. 9, no. 3, pp. 137–142, 2001.

[60] K. Enke, H. Dimigen, and H. Hübsch, "Frictional properties of diamondlike carbon layers", *Applied Physics Letters*, vol. 36, no. 4, pp. 291–292, 1980.

[61] O. Eryilmaz and a Erdemir, "Surface analytical investigation of nearly-frictionless carbon films after tests in dry and humid nitrogen", *Surface and Coatings Technology*, vol. 201, no. 16–17, pp. 7401–7407, 2007.

[62] H. Li, T. Xu, C. Wang, J. Chen, H. Zhou, and H. Liu, "Tribochemical effects on the friction and wear behaviors of a-C:H and a-C films in different environment", *Tribology International*, vol. 40, no. 1, pp. 132–138, 2007.

[63] C. Donnet, T. Le Mogne, L. Ponsonnet, M. Belin, A. Grill, V. Patel, and C. Jahnes, "The respective role of oxygen and water vapor on the tribology of hydrogenated diamond-like carbon coatings", *Tribology Letters*, vol. 4, pp. 259–265, 1998.

[64] C. Donnet and A. Grill, "Friction control of diamond-like carbon coatings", *Surface and Coatings Technology*, vol. 94–95, pp. 456–462, 1997.

[65] E. Konca, Y.-T. Cheng, A. M. Weiner, J. M. Dasch, and A. T. Alpas, "The Role of Hydrogen Atmosphere on the Tribological Behavior of Non-Hydrogenated DLC Coatings against Aluminum", *Tribology Transactions*, vol. 50, no. 2, pp. 178–186, 2007.

[66] D. Tallant and J. Parmeter, "The thermal stability of diamond-like carbon", *Diamond and related …*, vol. 4, pp. 191–199, 1995.

[67] A. Vanhulsel, B. Blanpain, J.-P. Celis, J. Roos, E. Dekempeneer, and J. Smeets, "Study of the wear behaviour of diamond-like coatings at elevated temperatures", *Surface and Coatings Technology*, vol. 98, no. 1–3, pp. 1047–1052, 1998.

[68] S. Sattel, J. Robertson, H. Ehrhardt, and I. Introduction, "Effects of deposition temperature on the properties of hydrogenated tetrahedral amorphous carbon", *Journal of Applied Physics*, vol. 82, no. 9, pp. 4566–45778, 1997.

[69] S. Sattel, M. Weiler, J. Gerber, and T. Giessen, "Nucleation during deposition of hydrocarbon ions as a function of substrate temperature", *Diamond and Related Materials*, vol. 4, pp. 333–336, 1995.

[70] W. Ni, Y.-T. Cheng, A. M. Weiner, and T. A. Perry, "Tribological behavior of diamond-like-carbon (DLC) coatings against aluminum alloys at elevated temperatures", *Surface and Coatings Technology*, vol. 201, no. 6, pp. 3229–3234, 2006.

[71] E. Liu, Y. F. Ding, L. Li, B. Blanpain, and J.-P. Celis, "Influence of humidity on the friction of diamond and diamond-like carbon materials", *Tribology International*, vol. 40, no. 2, pp. 216–219, 2007.

[72] E. Konca, Y.-T. Cheng, A. M. Weiner, J. M. Dasch, and A. T. Alpas, "Effect of test atmosphere on the tribological behaviour of the non-hydrogenated diamond-like carbon coatings against 319 aluminum alloy and tungsten carbide", *Surface and Coatings Technology*, pp. 1783–1791, 2005.

[73] B. D. Strom, D. B. Bogy, C. S. Bhatia, and B. Bhushan, "Tribochemical Effects of Various Gases and Water Vapor on Thin Film Magnetic Disks With Carbon Overcoats", *Journal of Tribology*, vol. 113, no. 4, pp. 689–694, 1991.

[74] Y. Qi, E. Konca, and A. T. Alpas, "Atmospheric effects on the adhesion and friction between non-hydrogenated diamond-like carbon (DLC) coating and aluminum – A first principles investigation", *Surface Science*, vol. 600, no. 15, pp. 2955–2965, 2006.

[75] E. Konca, Y.-T. Cheng, A. M. Weiner, J. M. Dasch, and A. T. Alpas, "Elevated temperature tribological behavior of non-hydrogenated diamond-like carbon

coatings against 319 aluminum alloy", *Surface and Coatings Technology*, vol. 200, no. 12–13, pp. 3996–4005, 2006.

[76] G. Gille and B. Rau, "Buckling instability and adhesion of carbon layers", *Thin Solid Films*, vol. 120, no. 2, pp. 109–121, 1984.

[77] K. Enke, "Some new results on the fabrication of and the mechanical, electrical and optical properties of i-carbon layers", *Thin Solid Films*, vol. 80, no. 1–3, pp. 227–234, 1981.

[78] J. Jiang, "Structure and mechanics of W-DLC coated spur gears", *Surface and Coatings Technology*, vol. 176, no. 1, pp. 50–56, 2003.

[79] A. A. Voevodin, J. P. O'Neill, and J. S. Zabinski, "Nanocomposite tribological coatings for aerospace applications", *Surface and Coatings Technology*, vol. 116–119, pp. 36–45, 1999.

[80] H. Dimigen and C. Klages, "Microstructure and wear behavior of metal-containing diamond-like coatings", *Surface and Coatings Technology*, vol. 49, no. 1991, pp. 543–547, 1991.

[81] J. C. Sánchez-López, D. Martínez-Martínez, M. D. Abad, and A. Fernández, "Metal carbide/amorphous C-based nanocomposite coatings for tribological applications", *Surface and Coatings Technology*, vol. 204, no. 6–7, pp. 947–954, 2009.

[82] S. El Mrabet, M. D. Abad, and J. C. Sánchez-López, "Identification of the wear mechanism on WC/C nanostructured coatings", *Surface and Coatings Technology*, vol. 206, no. 7, pp. 1913–1920, 2011.

[83] A. Voevodin, "Tribological performance and tribochemistry of nanocrystalline WC/amorphous diamond-like carbon composites", *Thin Solid Films*, vol. 342, no. 1–2, pp. 194–200, 1999.

CHAPTER 2
ROLE OF OXYGEN AND HUMIDITY ON THE TRIBO-CHEMICAL BEHAVIOUR OF NON-HYDROGENATED DIAMOND-LIKE CARBON COATINGS

2.1 Introduction

Diamond-like carbon (DLC) is a metastable amorphous form of carbon, which has excellent tribological behaviour and for this reason DLC coatings are being used in applications ranging from medical devices to hard discs and automotive components [1], [2]. There have been several studies that contributed to the understanding of the tribological properties of DLC coatings under various test environments, including vacuum, inert, hydrogen atmospheres and high humidity environments [3]–[5]. The tribological behaviour of the hydrogenated and dopants free DLCs, were found to differ significantly under vacuum and inert (i.e. N_2 or Ar) atmospheres. Erdemir [6] tested hydrogenated and dopants free DLC coatings in a dry nitrogen atmosphere against a H13 steel disc using a 10 N load and a 0.3 m/s speed for a distance of 2-5 $x10^3$ m. The results have shown that the hydrogenated DLC generated a COF of 0.005, while the dopants free DLC produced a high COF of 0.75. The very low COF value was attributed to the elimination of π-π interactions and passivation of free σ-carbon bonds by the hydrogen atoms. Konca et al. [7] observed a high COF of 0.52 while testing a 319 Al alloy against a dopant free DLC, under vacuum at a load of 5 N and a sliding speed of 0.12 m/s. The same dopants free DLC produced a low COF of 0.16 when tested in ambient atmosphere, which was attributed to passivation of dangling carbon bonds by hydrogen (-H) and hydroxyl (-OH) groups, produced from the dissociation of water molecules in the

atmosphere. In a vacuum environment, dangling σ-carbon bonds at the dopant free DLC's surface interacted with the aluminum counterface, and promoted aluminum transfer to the dopant free DLC's wear track, leading to the observed high COF. Studies also explored the effect of hydrogen gas in the testing environment on the friction behaviour of DLC. Konca et al. [8] studied the role of hydrogen atmosphere on the frictional behaviour of dopants free DLC tested against 319 Al and found that COF was 0.01. The same test produced a COF of 0.74 when repeated in a pure He atmosphere, indicating that He did not play a role in the COF reduction and it was the H atoms that passivated the dangling carbon bonds at the contact surface.

The percentage of the relative humidity (% RH) in the test atmosphere has been found to be an important contributor to the changes in the COF of the DLC coatings. A pin-on-disk type sliding test conducted in order to investigate the effect humidity on the tribological behaviour of a dopants free DLC coating using 319 Al pin and WC ball with a 5 N load and a 0.12 m/s speed [9] revealed that the COF dropped to 0.08 in humid air (85% RH) from 0.50 measured in dry air (0% RH). Qi et al. [10] using first principles calculations, simulated the strength of the interfaces formed after the gas molecule adsorption of (111) diamond surfaces and calculated the resulting work of separation between diamond and aluminum interfaces. The simulation results showed that the dissociated -H and -OH radicals formed bonds with the surface carbon atoms. The calculated work of separation of two C-OH terminated surfaces was 0.02 J/m^2, much lower than the work must be done to separate an Al and a carbon surface with dangling bonds (4.5 J/m^2). In the case of an N_2 atmosphere, no dissociation occurred and hence, nitrogen atoms did not contribute to the passivation of carbon bonds. Liu et al. [11]

compared the frictional behaviour of diamond to hydrogenated and dopants free DLCs by conducting a reciprocating wear tests using an aluminum oxide ball at a 2 N load and 100 µm stroke with 8 Hz vibration frequency. The diamond's COF decreased from 0.09 to 0.03 as the RH increased from 10% to 85%. Similar behaviour was observed for the dopants free DLC, as the RH increased from 5% to 90%, for which the COF decreased from 0.10 to 0.04. The hydrogenated DLC showed an opposite trend, with the COF increasing from 0.07 to 0.13 with an increase of the RH from 5% to 85%.

Donnet et al. [12] explored the role of oxygen and water vapour on the hydrogenated DLC coatings sliding against a 52100 steel. The tribo-couple was tested in vacuum (10^{-8} Pa) and at an oxygen partial pressure up to 6 x 10^{3} Pa. The results showed that the increase in oxygen partial pressure had no significant effect on the COF value of 0.01. Other studies showed that the COF of dopants free DLC benefited from the presence of oxygen in the testing atmosphere. For instance, dopants free DLC sliding against Si_3N_4 in dry (5% RH) oxygen atmosphere produced a lower COF value (0.19) than in dry (5% RH) nitrogen atmosphere (0.40) [13]. Thermodynamic calculations by Guo et al. [14] predicted that would oxygen alter the surface bonds from partial C-H and C-OH terminations to full C-OH termination in the presence of water vapour, resulting in low friction and low adhesion to aluminum compared to an oxygen termination (C-O).

Despite the progress made on understanding the role of the environment on the tribological properties of DLC coatings as summarized above, the role of oxygen on the frictional behaviour of dopant free DLC coatings has yet to be explained. It is still not clear how oxygen would influence the COF in the presence of atmospheric humidity. The

use of dopants free DLC coatings have been shown to reduce friction forces during aluminum machining and shaping operations when these operations are performed using very small amounts of water spray as coolant [15]. Accordingly, this study investigated the frictional behaviour and tribochemical properties of dopants free DLC coatings sliding against a 319 Al counterface under a humid Ar atmosphere with 45% RH, a gas mixture of 50% O_2 + 50% Ar with 45% RH, and the same oxygen enriched gas mixture (50% O_2 + 50% Ar) under a dry atmosphere of 0% RH. Understanding of the tribo-chemical mechanisms responsible for the frictional behaviour of dopants free DLC coatings in wet oxygen enriched atmosphere is important in order to determine working conditions for improved tribological performance by achieving low friction and eliminating aluminum adhesion.

2.2 Experimental details

DLC coatings were deposited on AISI M2 grade tool steel substrates using an unbalanced magnetron sputtering system. The magnetron system consisted of one chromium target and two graphite targets. A 0.1 μm Cr interlayer was deposited on 25.1 mm diameter M2 discs to promote coating adhesion and then a 1.5 μm thick DLC coating was deposited on top. The hydrogen content was measured using elastic recoil detection (ERD) and the analysis revealed that the DLC coating contained less than 2 at% of hydrogen. The hardness and the elastic modulus of the coatings were calculated from the loading-unloading curves obtained by a Berkovich type nano-indenter penetrated to a maximum depth of 200 nm below the surface. Average hardness and elastic modulus values were 13.00 ± 1.10 GPa and 158.55 ± 6.82 GPa respectively. The DLC coated

coupons were tested against a 319 Al (Al 6 %Si 3.5 %Cu) pin with a rounded tip of 4 mm diameter.

Pin-on-disk type wear tests were performed using a CSM tribometer enclosed in an environmental chamber. The chamber was evacuated to 0.04 Pa (3.94×10^{-7} atm), and then purged with the desired working gas to create the following environmental conditions; (i) humid Ar with 45% RH, (ii) humid oxygen enriched gas mixture that consisted of 50% O_2 and 50% Ar with 45% RH and (iii) dry 50% O_2 and 50% Ar with 0% RH until the chamber pressure reached 101.33×10^3 Pa (1.0 atm) at the start of the sliding test. During the sliding experiments, a gas flow rate of 0.6 m^3/min was maintained, creating a positive pressure to prevent the surrounding laboratory atmosphere from contaminating the tribometer's environmental chamber. The humid environment of 45% RH was achieved by passing the working gases, Ar and/or O_2 through a flask filled with distilled water prior to admitting them into to the environmental chamber. Sliding tests were performed at a linear sliding speed of 0.10 mm/s and under the application of 5 N normal load for 1000 cycles. Additional short term pin-on-disk experiments were conducted to examine the effects of oxygen on the run-in period using humid Ar and humid 50% O_2 + 50% Ar gas mixtures. For this purpose, three separate tests with fresh 319 Al pins and coatings were conducted for 10, 40 and 80 sliding cycles for each environment. Following the sliding tests, the 319 Al pin contact surfaces were examined by a scanning electron microscope (SEM) and their compositions were analyzed using Fourier-Transformed Infrared (FTIR) spectroscopy. FTIR analyses were conducted using a Thermoelectron Nicolet 760 spectroscope in reflectance mode at two different spots using a 100 µm x 100 µm aperture.

2.3 Experimental desults

2.3.1 Steady-state COF

The variations of COF of the dopants free DLC coatings tested under an Ar atmosphere with 45% RH, (O_2 + Ar) gas mixture with 45% RH and an (O_2 + Ar) gas mixture with 0% RH atmospheres are shown in Figure 2-1 as a function of sliding distance. It is evident from the COF curves that the dry (O_2 + Ar) atmosphere with 0% RH produced the highest steady state COF of 0.35 ± 0.05. The Ar atmosphere with 45% RH, produced the lowest steady state COF of 0.09 ± 0.01. It was observed that humid (O_2 + Ar) atmosphere with 45% RH produced a low steady state COF of 0.12 ± 0.01, but higher than that of humid Ar with 45% RH. Thus, two conclusions can be drawn from these tests i) incorporation of moisture (45% RH) into a dry oxygen (O_2 + Ar) atmosphere, reduced the COF from 0.35 to 0.12; and ii) oxygen enrichment of the humid Ar atmosphere (with 45% RH) increased the COF from 0.09 to 0.12.

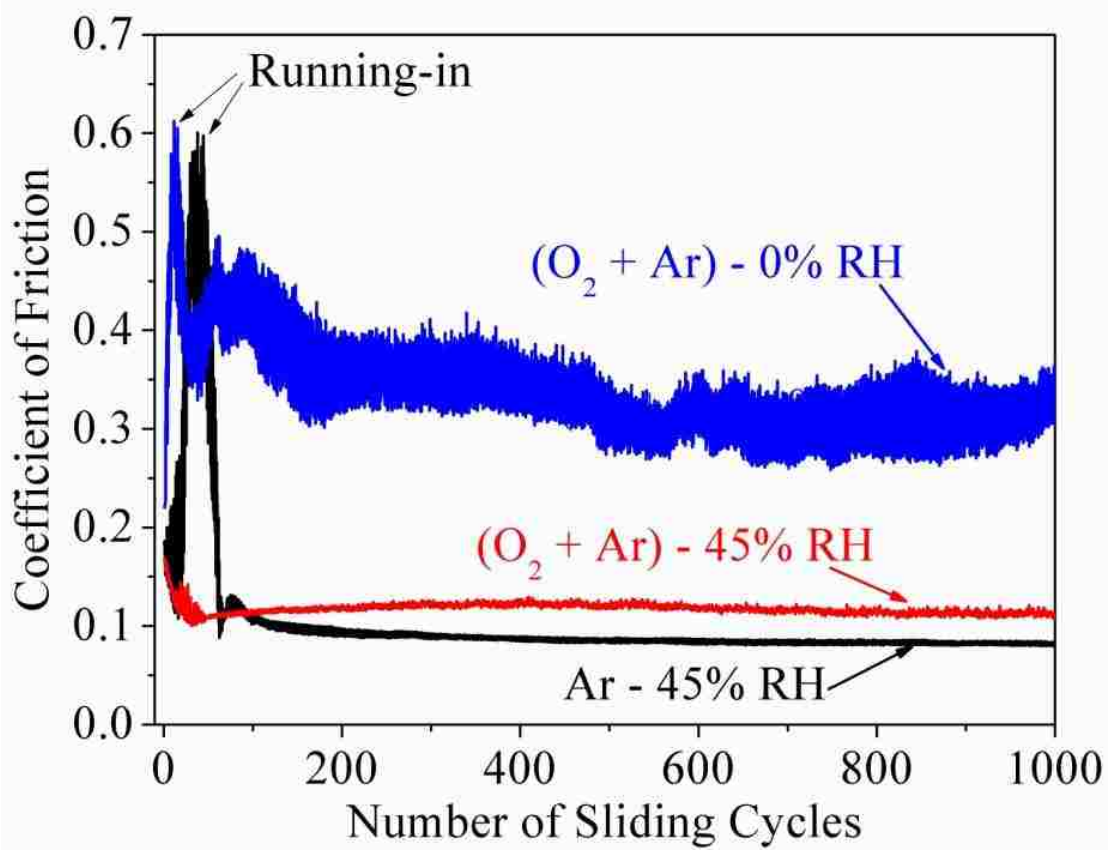

Figure 2-1: COF of dopants free DLC coating tested against 319 aluminum pins sliding for 1000 sliding cycles under humid Ar, humid and dry (O2 + Ar) at 5 N load and 0.1 m/s sliding speed.

The SEM micrographs of the 319 Al pins after the sliding tests for 1000 cycles showed that the contact surfaces were covered with a layer of carbonaceous material transferred from the DLC coating (Figure 2-2 (a, b and c)). FTIR analyses of the transferred material after testing each of the three environmental conditions (Figure 2-2 (d, e and f)) showed that the layers had different chemical compositions depending on the atmosphere under which the test was performed. The material transferred during the tests conducted under a humid Ar atmosphere (Figure 2-2 (a)) consisted of hydrocarbon compounds (Figure 2-2 (d)), where the bands attributed to (C-H) groups [16] could be

observed at 848 cm^{-1} and 1362 cm^{-1}. A broad band observed at 3458 cm^{-1} was attributed to the hydroxyl (O-H) groups. The CO_2 peaks at 2350 cm^{-1} observed in this and other FTIR spectra were due to contamination from the surrounding atmosphere [17], [18]. The material transfer layer formed in a humid (O_2 + Ar) gas mixture with 45% RH (Figure 2-2 (b)) had similar chemical composition; but in addition to a C-H band observed at 1000 cm^{-1} and a weak carbonyl (C=O) band observed at 1740 cm^{-1} (Figure 2-2 (e)) [16], [17]. The FTIR spectra of the transfer layer formed during sliding in a dry (O_2 + Ar) mixture with 0% RH (Figure 2-2 (c)) showed a C=C peak at 1500 cm^{-1} and oxidized carbon, as manifested by the presence of the strong C-O band at 1300 cm^{-1} (Figure 2-2 (f)) [17]–[19]. Consequently, FTIR analyses have shown that oxidation was more pronounced in the absence of humidity in the test atmosphere. Presence of atmospheric humidity inhibited surface oxidation and possibly promoted passivation of carbon atoms at the surface.

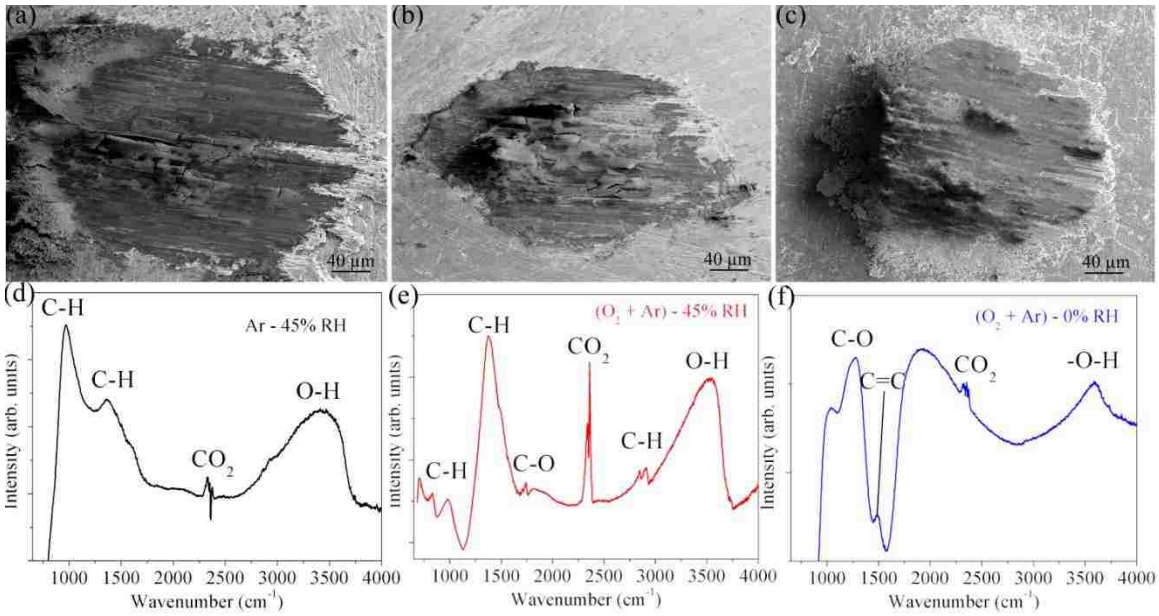

Figure 2-2: Secondary electron images of the material transfer layers observed on the 319 aluminum pins and their corresponding FTIR spectra after sliding in (a, d) humid Ar with 45 % RH; (b, e) humid (O_2 + Ar) atmosphere with 45% RH and; (c, f) dry (O_2 + Ar) atmosphere with 0% RH.

2.3.2 COF variation during running-in period

It was observed that during sliding under an Ar atmosphere with 45% RH (Figure 2-1) an initial running-in period occurred, where the COF reached a maximum value and then decreased to a lower steady state value within the first 80 sliding cycles. However, the COF curve generated under a humid O_2 + Ar atmosphere showed no evidence of a running-in period as illustrated in Figure 2-1. Thus, for better understanding of tribological events at various stages of the running-in period, separate pin-on-disk tests with fresh 319 Al pins were conducted for 10, 40 and 80 cycles under a humid argon (Figure 2-3 (a-c)) and a humid O_2 + Ar (Figure 2-3 (d-f)) atmospheres both with 45%

RH. The running-in period observed under a humid Ar atmosphere can be examined in three stages; for the first 20 cycles i.e., Stage (i) shown in Figure 2-3 (a), the COF started off at a relatively low value of about 0.15 for 20 sliding cycles. The COF then increased rapidly to a maximum COF value of 0.48 at 40 cycles (Stage (ii)) as shown in Figure 2-3 (b). Once a peak COF was reached it started to decrease rapidly to a steady-state COF of 0.12 after 80 cycles (Stage (iii)) shown in Figure 2-3 (c). In all three running-in stages experiments showed an initial COF of approximately 0.2, with the exception of humid (O_2 + Ar) atmosphere for 40 sliding cycles test (Figure 2-3 (e)) showed initial COF of 0.28 which could be due to initial surface roughness or slight misalignment in the contact, however the overall trend was the same, decreasing without COF peak during running-in.

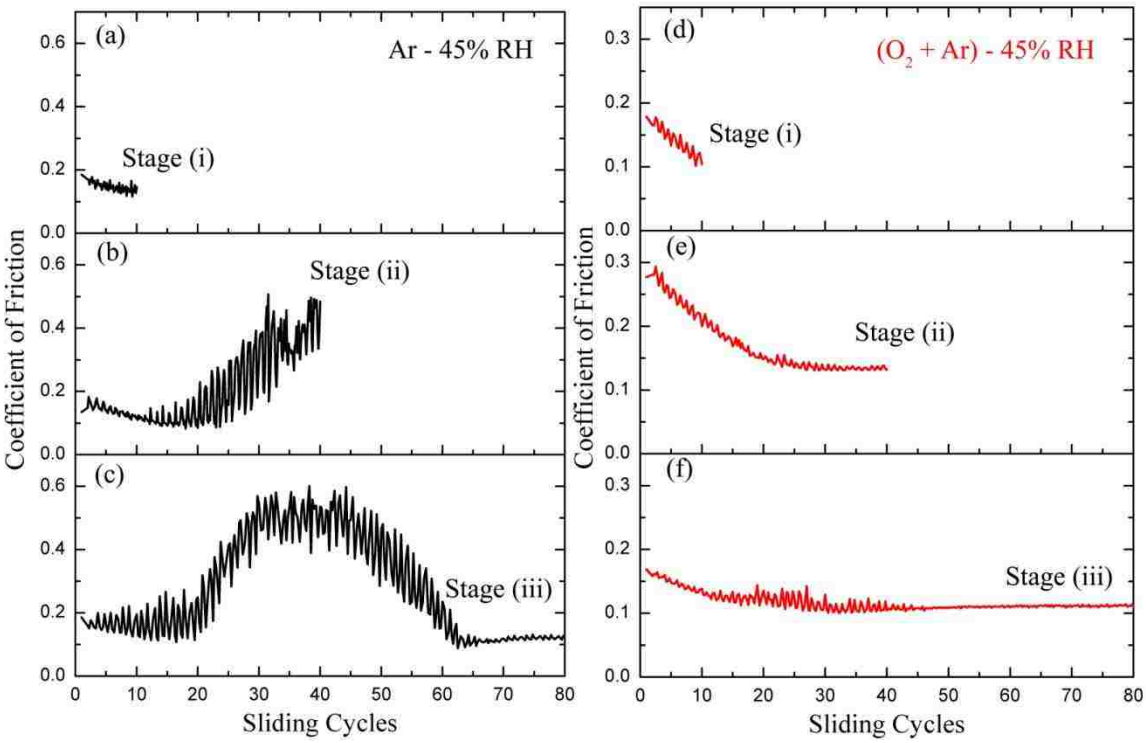

Figure 2-3: Running-in experiments of dopants free DLC coating against 319 aluminum pins sliding for 10 cycles, 40 cycles and 80 cycles under (a, b, c) humid Ar with 45% RH and (d, e, f) humid (O_2 + Ar) with 45% RH at 5 N load and 0.1 m/s sliding speed. Each curve represents a different test on a new sample.

The SEM micrographs of the pin surfaces taken after testing in humid Ar shown in Figure 2-4 (a, b, c), illustrate that during the initial 10 cycles the Al tip was subjected to plastic deformation and wear (Figure 2-4 (a)), with a trace of carbon around the edges as shown in the back scattered image in Figure 2-4 (d). After sliding for 40 cycles the pin continued to wear and the COF reached to its peak value of 0.48. The back scattered image of the wear scar reveal that carbon began to accumulate covered a portion of the worn surface. In the third stage (40-80 cycles) the carbon transfer layers covered most of the worn 319 Al tip surface as shown in Figure 2-4 (c) and the presence of carbon was confirmed by the back scattered image in Figure 2-4 (e). During the first 40 cycles where

the COF reached a maximum, aluminum adhesion was observed inside the wear tracks (Figure 2-5 (a, b)) and was confirmed by energy dispersive X-ray (EDX) analysis from inside the wear tracks. After approximately 60 sliding cycles the COF decreased to 0.12 and after 80 cycles no evidence of aluminum adhesion was detected inside the wear track as shown in Figure 2-5 (c).

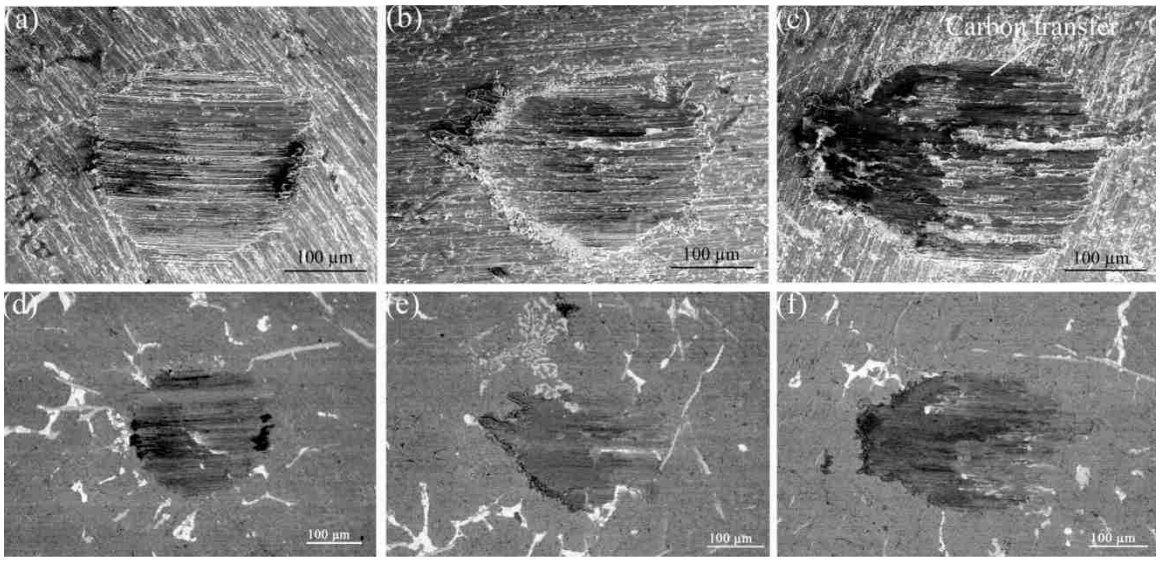

Figure 2-4: Secondary electron images of the 319 aluminum pins after sliding for (a) 10 cycles, (b) 40 cycles and (c) 80 cycles and their back scattered electron micrographs after sliding for (d) 10 cycles, (e) 40 cycles and (f) 80 cycles under a humid Ar atmosphere with 45% RH.

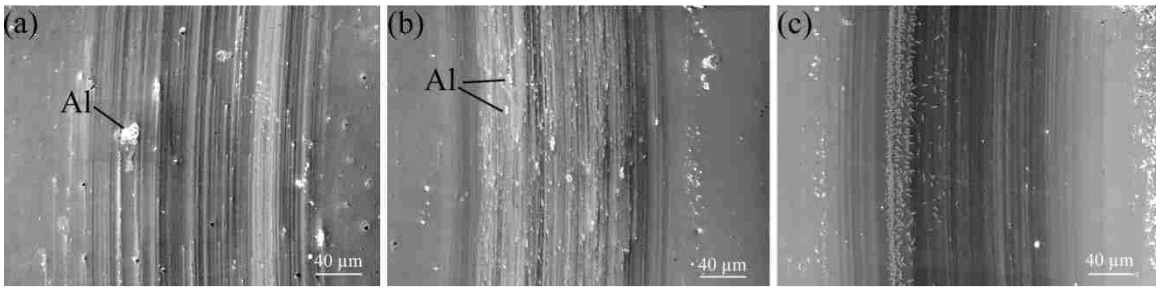

Figure 2-5: Secondary electron images of the dopants free DLC's wear tracks after sliding for (a) 10 cycles, (b) 40 cycles and (c) 80 cycles under a humid Ar atmosphere with 45% RH.

During the first 100 cycles in an (O_2 + Ar) atmosphere with 45% RH a carbon transfer layer was observed to cover the Al surface at a faster rate compared to sliding in a humid Ar atmosphere. SEM Micrographs of the Al pins after the running-in tests indicated that most of the wear occur in stage (i) within the first 10 sliding cycles. During stage (ii) between 10 and 40 cycles (Figure 2-6 (b)), a continuous carbon transfer layer observed to form on the tip of the 319 Al pin, covering almost the entire wear scar area. As the cycles increased to 80 (stage (iii)) carbon continued to build up on the previously formed carbon layers. Thus in humid Ar, carbon transfer layer begins to form at the third stage between 40 and 80 sliding cycles, while in humid (O_2 + Ar), the carbon transfer layer begins to form at an earlier stage of 10 and 40 sliding cycles.

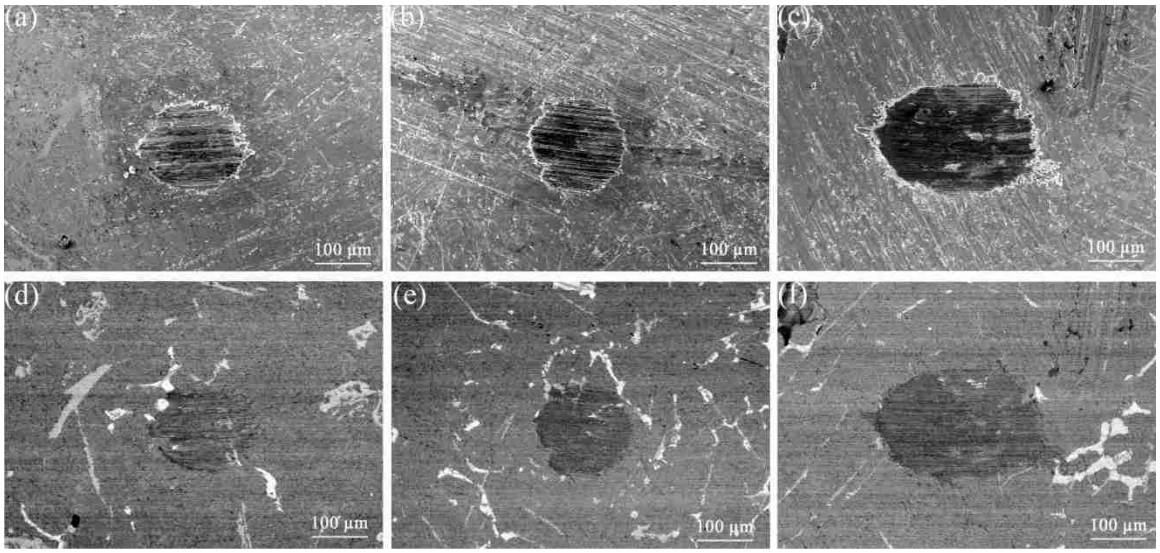

Figure 2-6: Secondary electron images of the 319 aluminum pins after sliding for (a) 10 cycles, (b) 40 cycles and (c) 80 cycles and their back scattered electron micrographs after sliding for (d) 10 cycles, (e) 40 cycles and (f) 80 cycles under humid (O_2 + Ar) atmosphere with 45% RH.

SEM micrographs of the DLC's wear tracks recorded after testing for 10, 40 and 80 sliding cycles under a humid (O_2 + Ar) atmosphere (Figure 2-7 (a, b, c)) did not show any evidence of aluminum adhesion and this was confirmed by the EDX analysis. However at 40 cycles, a small trace of particles observed in the middle of the wear track. EDX spectra show that these particles are carbonaceous debris and as the number of cycles increased to 80, more evidence of this carbon debris was seen inside the wear track.

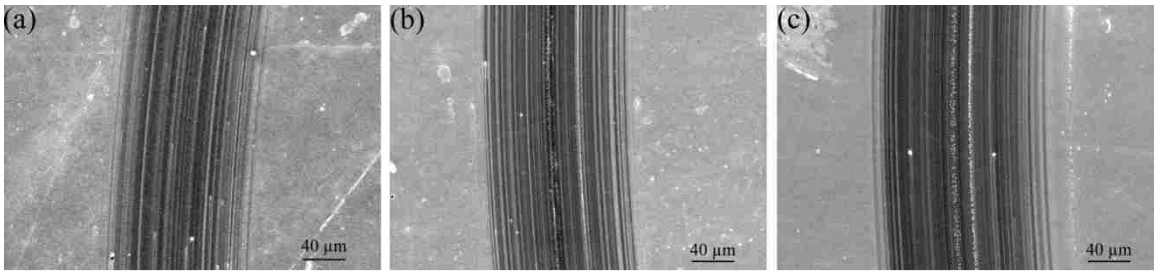

Figure 2-7: Secondary electron micrographs of the dopants free DLC's wear tracks after sliding for (a) 10 cycles, (b) 40 cycles and (c) 80 cycles under humid (O_2 + Ar) atmosphere with 45% RH.

2.4 Discussion

As shown in Figure 2-1 the incorporation of 45% RH into an (O_2 + Ar) gas mixture in the test environment, produced a lower steady-state COF of 0.12 for the dopants free DLC compared to the high COF of 0.35 observed under dry (O_2 + Ar) environment. In addition, results of the FTIR analyses shown in Figure 2-2 (d and f) indicated that in the presence of humidity, oxidation of the carbon transfer layers was inhibited. As shown in the schematic diagram of Figure 2-8 (a), in an (O_2 + Ar) environment with 0% RH, the dangling carbon atoms on DLC's surface are bonded to the oxygen atoms forming a C-O bond and hence the higher COF. On the contrary in an (O_2 + Ar) environment with 45% RH, the oxygen molecule may react with the hydrogen from the dissociated water molecule forming a hydroxyl surface termination as shown in Figure 2-8 (a). Thus, the possibility of surface oxidation (C-O), which was responsible of the high COF in case of dry oxygen enriched atmosphere, was suppressed. As indicated by the FTIR analysis, a much weaker C-O peak was observed for a humid (O_2 + Ar) environment (Figure 2-2 (d)) compared to that observed in dry (O_2 + Ar) environment (Figure 2-2 (f)). This observation is in agreement with the computer simulations by Guo

and Qi [14], who found that the incorporation of oxygen into a humid atmosphere would change the surface composition of diamond from a 50% -H and 50% -OH terminated surface to a fully -OH terminated surface. This can also explain the slightly higher COF of 0.12 in humid (O_2 + Ar) compared to the COF of 0.09 observed in humid Ar, since interfacial calculations have shown that C-OH/C-OH interface has a work of separation of 0.02 J/m^2, higher than 0.008 J/m^2 for C-H/C-H [10], [20]–[22].

The experiments performed to explore the running-in region (Figure 2-3 (a-c)) of the dopants free DLC tested in a humid Ar atmosphere with 45% RH exhibited the same trend. Starting off with relatively low COF of approximately 0.2 (Figure 2-3 (a)), after 40 cycles the COF reached a peaks at 0.48 (Figure 2-3 (b)) and then dropped to steady state COF of 0.12 after 80 sliding cycles. SEM micrographs of the 319 Al pin and DLC wear scars during the running-in period revealed evidence for two competing mechanisms, formation of a carbonaceous transfer layer on 319 Al surface and aluminum adhesion to DLC's. Aluminum would adhere to the carbon surface if i) the dangling carbon bonds on DLC surface were not passivated and ii) no carbonaceous transfer layer was formed. The Formation of a transfer layer sufficient to prevent adhesion but the layer must be passivated. In stage (i) shown in Figure 2-3 (a), some carbon transfer was observed to form along the edges of the wear 319 Al wear scar (Figure 2-4 (a, d)), meanwhile a few scattered aluminum adhered particles were found inside the wear track (Figure 2-5 (a)). The relatively low COF of 0.2 observed, could be attributed to the presence of native aluminum oxide layer on the 319 Al and other surface contaminates that prevent direct contact between aluminum and carbon. After approximately 20 cycles, i.e. in stage (ii), the COF increased rapidly reaching a COF maximum of 0.48 and fresh aluminum was

exposed and became adhered to the coating surface as shown in Figure 2-5 (b). Meanwhile a passivated carbon transfer layer formation started to occur simultaneously but has not been fully developed (Figure 2-4 (d, e)). Thus aluminum adhesion mechanism dominated during stage (ii). As the Al-Al decohesion energy (1.52 J/m^2) is lower than the Al-C decohesion energy (4.5 J/m^2) [10], it is conceivable that some aluminum would separate from the counterface and adhere to the DLC surface, hence the high COF. The high peak COF observed here was similar to the COF of 0.63 observed in the case of dopants free DLC tested in dry Ar atmosphere with 0% RH against pure Al, for which the COF remained at the same high level after prolonged sliding and never reached a low steady-state [23]. After approximately 60 cycles (stage (iii)) in humid Ar atmosphere, the effect of passivated carbon transfer to reduce the COF appeared to become dominant. As shown in Figure 2-4 (c, f) the transfer layer was well established, covering the 319 Al wear scar almost entirely and consequently the COF dropped to 0.12. The presence of passivated carbon transfer layer by -H and -OH (Figure 2-8 (b)) possibly dissociated from water in the atmosphere, served to eliminate interatomic interactions at the interface and hence a steady-state COF of 0.09 was reached.

The running-in period experiments under a humid (Ar + O_2) atmosphere with 45% RH shown in Figure 2-3 (d-f) were consistent with each other and exhibited the same decreasing trend. Unlike the humid Ar atmosphere experiments, an initial high COF was not observed, indicating that carbon transfer layer formation and surface passivation occurred in stage (i). This was confirmed by SEM micrographs shown in Figure 2-6, which revealed that the carbon transfer layer covered most of the pin surface only after sliding for 10 to 40 sliding cycles (Figure 2-6), faster than it would form under the humid

Ar atmosphere (Figure 2-4). Consequently it can be suggested that the presence of oxygen accelerated the dissociation water molecules and in turn caused a faster passivation (mostly by -OH, since the extra -H from water) of transfer layer formation at the counterface as shown in the schematic diagram of Figure 2-8 (b). This mechanism is supported by the first principle calculations of energies required for water dissociation and passivation at a diamond surface [14], according to which water by itself is not sufficient to passivate the diamond surface at room temperature except at very high water partial pressures ranging from 6×10^{11} Pa to 5×10^{14} Pa. Meanwhile, oxygen was observed to significantly reduce the partial pressure of water (3×10^{-13} Pa - 4×10^{-3} Pa) required for surface passivation through water dissociation, thus indicating that oxygen assisted water dissociation and promoted faster surface passivation. The lack of aluminum adhesion inside the wear tracks (Figure 2-7 (a, b and c)) even during the first 10 cycles of sliding in a humid Ar environment provide additional support for the view that oxygen promote faster surface passivation of transfer layers, eliminating the high COF during running-in period.

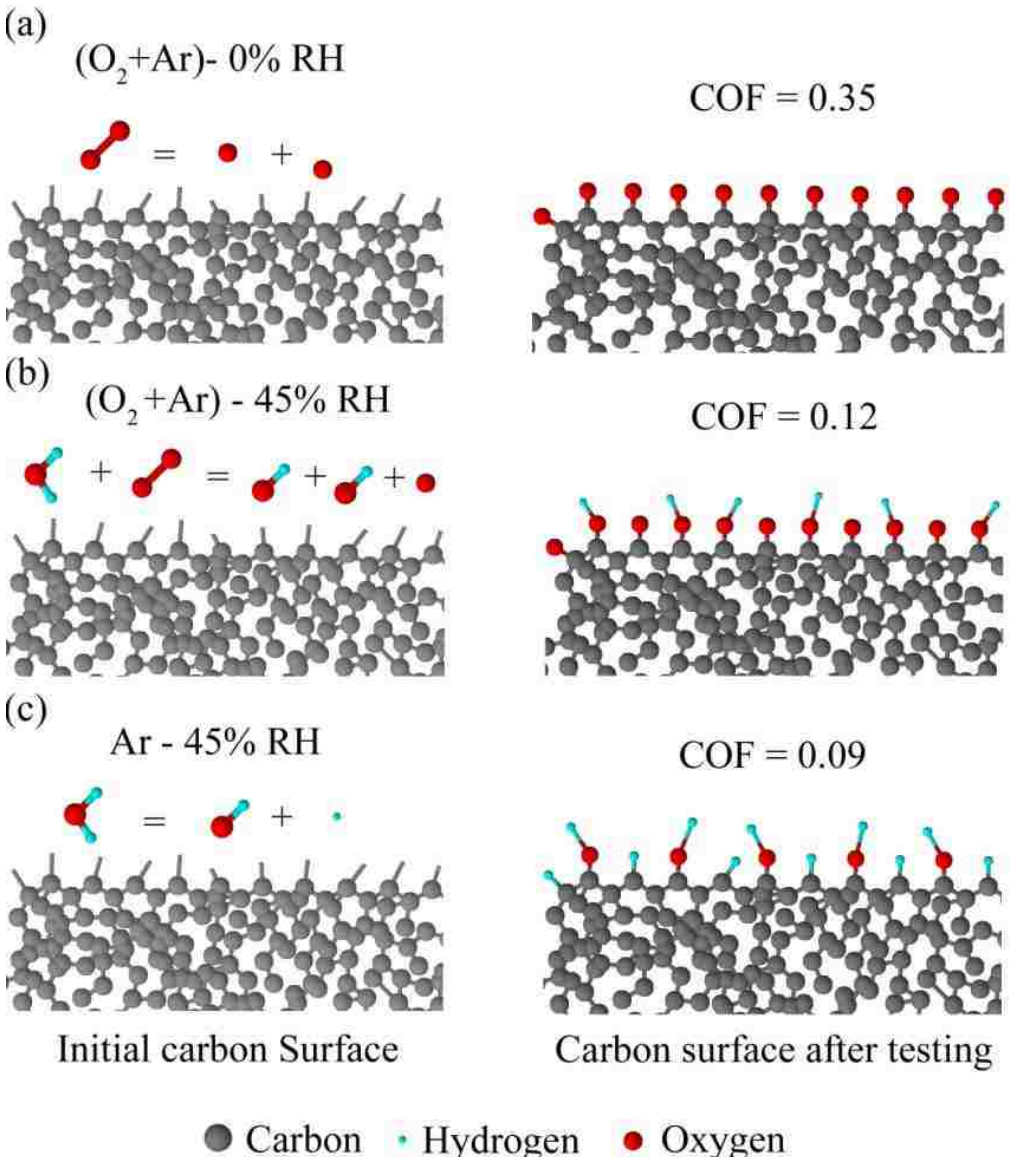

Figure 2-8: Schematic representation of the surface termination mechanisms in (a) humid $(O_2 + Ar)$ - 45% RH, (b) humid Ar - 45% RH and (c) dry $(O_2 + Ar)$ - 0% RH.

2.5 Conclusions

Dopant free DLC coating were subjected to sliding against 319 Al pins under an Ar atmosphere with 45% RH, O_2 +Ar atmosphere with 45% RH and dry O_2 + Ar atmosphere with 0% RH. Tests were repeated for shorter durations, 10, 40 and 80 sliding cycles to investigate the effects of an oxygen rich environment on the running-in period. FTIR and microscopical analyses of the wear tracks and counterface wear scars after each test lead to the following conclusions:

1. A high steady-state COF of 0.35 was observed when dopant free DLC was tested against 319 Al in dry oxygen rich atmosphere with 0% RH due to oxidation of carbon atoms at the sliding interface.
2. The increase in humidity (to 45% RH) of an oxygen rich atmosphere reduced the steady state COF of the dopant free DLC from 0.35 to 0.12 implying that the surface passivation by -H and -OH occurred as a result of dissociation of water molecules in the test atmosphere.
3. The initial high COF ranging from 0.5-0.6 observed during the running-in period of dopant free DLC tested in an Ar atmosphere with 45% RH could be attributed to a delay in carbon transfer layer formation, and aluminum adhesion to the DLC surface. Once the transfer layer was established and became passivated a low steady-state COF of 0.09 was reached.
4. The increase of oxygen in the test environment (50% O_2) resulted in elimination of the initial high COF by accelerating carbon transfer layer formation.

References

[1] S. C. Tung and M. L. McMillan, "Automotive tribology overview of current advances and challenges for the future", *Tribology International*, vol. 37, no. 7, pp. 517–536, 2004.

[2] R. Hauert, "An overview on the tribological behavior of diamond-like carbon in technical and medical applications", *Tribology International*, vol. 37, no. 11–12, pp. 991–1003, 2004.

[3] B. Bhushan, "Chemical, mechanical and tribological characterization of ultra-thin and hard amorphous carbon coatings as thin as 3.5 nm: recent developments", *Diamond and Related Materials*, vol. 8, no. 11, pp. 1985–2015, 1999.

[4] J. Robertson, "Diamond-like amorphous carbon", *Materials Science and Engineering: R: Reports*, vol. 37, no. 4–6, pp. 129–281, 2002.

[5] A. Erdemir and C. Donnet, "Tribology of diamond-like carbon films: recent progress and future prospects", *Journal of Physics D: Applied Physics*, vol. 39, no. 18, pp. R311–R327, 2006.

[6] A. Erdemir, "The role of hydrogen in tribological properties of diamond-like carbon films", *Surface and Coatings Technology*, vol. 146–147, no. 1, pp. 292–297, 2001.

[7] E. Konca, Y.-T. Cheng, A. M. Weiner, J. M. Dasch, and A. T. Alpas, "Vacuum tribological behavior of the non-hydrogenated diamond-like carbon coatings against aluminum: Effect of running-in in ambient air", *Wear*, vol. 259, no. 1–6, pp. 795–799, 2005.

[8] E. Konca, Y.-T. Cheng, A. M. Weiner, J. M. Dasch, and A. T. Alpas, "The Role of Hydrogen Atmosphere on the Tribological Behavior of Non-Hydrogenated DLC Coatings against Aluminum", *Tribology Transactions*, vol. 50, no. 2, pp. 178–186, 2007.

[9] E. Konca, Y.-T. Cheng, A. M. Weiner, J. M. Dasch, and A. T. Alpas, "Effect of test atmosphere on the tribological behaviour of the non-hydrogenated diamond-like carbon coatings against 319 aluminum alloy and tungsten carbide", *Surface and Coatings Technology*, pp. 1783–1791, 2005.

[10] Y. Qi, E. Konca, and A. T. Alpas, "Atmospheric effects on the adhesion and friction between non-hydrogenated diamond-like carbon (DLC) coating and aluminum – A first principles investigation", *Surface Science*, vol. 600, no. 15, pp. 2955–2965, 2006.

[11] E. Liu, Y. F. Ding, L. Li, B. Blanpain, and J.-P. Celis, "Influence of humidity on the friction of diamond and diamond-like carbon materials", *Tribology International*, vol. 40, no. 2, pp. 216–219, 2007.

[12] C. Donnet, T. Le Mogne, L. Ponsonnet, M. Belin, A. Grill, V. Patel, and C. Jahnes, "The respective role of oxygen and water vapor on the tribology of hydrogenated diamond-like carbon coatings", *Tribology Letters*, vol. 4, pp. 259–265, 1998.

[13] H. Li, T. Xu, C. Wang, J. Chen, H. Zhou, and H. Liu, "Tribochemical effects on the friction and wear behaviors of a-C:H and a-C films in different environment", *Tribology International*, vol. 40, no. 1, pp. 132–138, 2007.

[14] H. Guo and Y. Qi, "Environmental conditions to achieve low adhesion and low friction on diamond surfaces", *Modelling and Simulation in Materials Science and Engineering*, vol. 18, no. 3, p. 034008, 2010.

[15] S. Bhowmick and A. T. Alpas, "Minimum quantity lubrication drilling of aluminium–silicon alloys in water using diamond-like carbon coated drills", *International Journal of Machine Tools and Manufacture*, vol. 48, no. 12–13, pp. 1429–1443, 2008.

[16] J. Robertson, "Amorphour Carbon", *Advances in Physics*, vol. 35, pp. 317–374, 1986.

[17] C. E. Bell, D. F. Taber, and A. K. Clark, "*Infrared absorption spectroscopy, Organic Chemistry Laboratory: with Qualitative analysis: Standard and Microscale Experiments*", 3rd edition. Pacofic Grove, CA: Brooks/Cole Thomson Learning, 2001, p. 95.

[18] V. P. Tolstoy, I. V. Chernyshova, and V. A. Skryshevsky, "Infrared of Thin Layers in Silicon Microelectronics", in *Handbook of infrared spectroscopy of ultrathin films*, Hoboken, New Jeresey: John Wiley & Sons, 2003, p. 448.

[19] G. I. Dovbeshko, O. P. Gnatyuk, A. N. Nazarova, Y. I. Sementsov, and E. D. Obraztsova, "Vibrational Spectra of Carbonaceous Materials: A SEIRA Spectroscopy versus FTIR and Raman", *Fullerenes, Nanotubes and Carbon Nanostructures*, vol. 13, no. sup1, pp. 393–400, 2005.

[20] Y. Qi and L. Hector, "Adhesion and adhesive transfer at aluminum/diamond interfaces: A first-principles study", *Physical Review B*, vol. 69, no. 23, pp. 1–13, 2004.

[21] F. Bowden and J. Young, "Friction of diamond, graphite, and carbon and the influence of surface films", *Mathematical and Physical Science*, vol. 208, no. 1095, pp. 444–455, 1951.

[22] M. N. Gardos, "*Tribology and wear behavior of diamond, synthetic diamond*". New York: Electrochemical Society Series, 1994, pp. 419–504.

[23] E. Konca, Y.-T. Cheng, and A. T. Alpas, "Dry sliding behaviour of non-hydrogenated DLC coatings against Al, Cu and Ti in ambient air and argon", *Diamond and Related Materials*, vol. 15, no. 4–8, pp. 939–943, 2006.

CHAPTER 3
HIGH TEMPERATURE TRIBOLOGICAL BEHAVIOUR OF CARBON BASED (B_4C AND DLC) COATINGS IN SLIDING CONTACT WITH ALUMINUM

3.1 Introduction

Aluminum alloys are of a great interest for the transportation industry due to their high strength to mass ratio. However, aluminum adhesion to tools is a common obstacle in forming and machining of these alloys. The adhesion leads to aluminum built up on the tool which may lead to tool failure and also poor workpiece surface finish [1]. Thus, it is critical to introduce a low friction and non-sticking surface coating, with high thermal stability that can withstand hot forming temperatures and heat generated during aluminum machining.

Carbides are well known for their high temperature stability and one of the common carbides is boron carbide (B_4C), the third hardest material (25-29 GPa) [2] following diamond and cubic boron nitride. According to B-C phase diagram, the B_4C phase consists of 9-20 at% carbon with melting point of 2400 °C [2]. Thus, B_4C is considered to be a good candidate for high load and high temperature tribological applications such as metal forming, partly because it retains most of its hardness up to 1000 °C [3]. The coefficient of friction (COF) of hot pressed B_4C sliding against B_4C maintains a constant value of 0.4 up to 1000 °C in vacuum, as the temperature increased to 1800 °C, a lower COF of 0.2 was observed [4], [5]. In ambient air, the COF of B_4C

was 0.2 according to tests done at room temperature and decreased to 0.1 at 800 °C [6]. The low COF of 0.1 observed in air is attributed to the presence of boron oxide and hydroxides that began to form at 527 °C. At 827 °C, a continuous film of boron hydroxide was observed to cover the B_4C surface. Similar behaviour was observed for zirconia pins sliding against hot pressed B_4C under ambient atmosphere, which generated a COF of 0.3. After annealing the B_4C at 800 °C for an hour, zirconia and sapphire sliding against B_4C at room temperatures showed a significant drop in the COF to 0.05 [7], [8]. The observed very low COF is attributed to the presence of lubricious boron hydroxide film at the sliding interface.

Diamond like carbon (DLC) coatings combine a low COF and high hardness [9], [10]. Dopants free and hydrogenated grades of DLC coatings both produce a low COF of 0.1- 0.2 when sliding against aluminum at room temperature [11], [12]. The low friction of the dopants free DLC was attributed to the presence of water in the surrounding atmosphere as water dissociation to H and OH and passivate the carbon surface [13]. Consequently, the dissociated water molecule passivates carbon bonds on the surface [13] and hence reducing the friction and eliminating aluminum adhesion. The hydrogen inside the DLC coating mitigates strong carbon π-π interactions at the sliding interface, thus preventing counterface adhesion to the surface hydrogenated DLCs, which make them ideal for vacuum (space) applications [14]. Studies have shown that dopants free DLC coating sliding against aluminum loses its lubricous property at approximately 300 °C resulting in excessive aluminum adhesion [11]. It was reported that the hydrogenated DLC coating shows no sign of aluminum adhesion up to 240 °C [12]. The increase in

COF at elevated temperatures was attributed to the graphitization of carbon through the transformation of sp^3 (diamond-like) to sp^2 (graphite-like) hybridization a process that occurs at 250 °C [15]–[17]. For the hydrogenated DLC coatings loss of hydrogen begins at 450 °C [15]–[17].

In this study, we tested 319 aluminum sliding against two different carbon based coatings, B_4C and hydrogenated DLC coating supported with a WC layer to assess their tribological performance for aluminum applications up to 400 °C. The mechanisms of coating failure and adhesion during sliding at elevated temperatures are discussed in terms of coating microstructures and surface properties.

3.2 Experimental details

3.2.1 Coating deposition and properties

B_4C coating was deposited on M2 type tool steel substrates, using a physical vapour deposition (PVD) system equipped with three B_4C and one Cr targets. The substrates were plasma etched with Ar glow discharge and Cr layer was deposited on the steel substrate to promote adhesion of the B_4C coating. As will be described in detail in section 3.1 the B_4C coating had a columnar structure.

The DLC coating in fact consisted of two layers, a tungsten carbide (WC) layer on the M2 steel substrate and a (hydrogenated) DLC layer on the top. Initially, a relatively thick WC layer was deposited followed by a plasma assisted chemical vapour deposition (PACVD) of the DLC using methane as a reactive gas. The WC layer promotes adhesion and also was suggested to enhance the load carrying capacity of the

coating [18]. The WC layer had a columnar morphology, while the DLC had an amorphous structure (see section 3.2). The thickness of B_4C coating was 1.43 µm including a 0.1 µm Cr layer. The DLC coating was 1.71 µm thick over a 2.48 µm thick layer of WC. Elastic recoil detection (ERD) analysis at 2.0 MeV indicated that the DLC layer consisted of 69 at% carbon and 31 at% hydrogen.

The hardness and elastic moduli of the coatings were measured using Hysitron TI 900 Triboindenter equipped with a Berkovich nano-indenter. The indentation depth was limited to less than 150 nm, which was 10% of the total thickness of the coating. The hardness of the B_4C coating was 19.5 ± 4.5 GPa and the elastic modulus was 264.5 ± 31.5 GPa. The DLC coating had a hardness of 20.1 ± 2.9 GPa, and an elastic modulus of 166.5 ± 8.6 GPa.

3.2.2 Tribological tests and surface characterization

A CSM high temperature pin-on-disc tribometer was utilized to perform sliding tests on both coatings from room temperature to 400 °C at 0.1 m/s linear speed and under constant normal load of 5.0 N against 319 Al T6 pins with a radius of 2 mm rounded tip. The 319 Al alloy was chosen since it is one of the most common light weight alloys used for engine components. The COF was continuously recorded and the steady state values of COF averaged over a range of 1000 cycles were determined.

Camica SX-100 electron probe micro analysis (EPMA) was utilized to determine the amount of aluminum adhesion to the coatings' circular wear tracks. Measurements were obtained at four equally spaced locations to calculate the area percent covered by

aluminum on the B_4C. An optical surface profilometer (ZYGO NewView 7300) was employed to determine the amount of wear on the DLC coating by averaging depth profiles taken from four equidistant positions along the wear track. The wear rate was calculated by dividing the total volume loss to the sliding distance. Following the sliding experiments, FIB (Carl Zeiss NVision 40 CrossBeam) cross sections of the wear tracks were prepared to analyze the damage under the wear track. Cross sections were made perpendicular to the wear tracks sliding direction. A carbon layer was deposited prior to milling to avoid ion beam damage to the surface. Following the carbon deposition, trenches were milled with 13 nA ion current, for a smother surface finish a final mill was conducted at lower ion current (50 pA).

Raman spectra of wear tracks were obtained using a Dilor XY Micro Raman spectrometer with a 532 nm of an Ar^+ laser to analyze the structural evolution as a function of the testing temperature. In addition, the Al pins and any transfer layers were also analyzed using Thermoelectron Nicolet 760 Fourier-Transformed Infrared (FTIR) spectroscopy. The pins were analyzed after sliding in reflectance mode at two spots with an aperture of 100 µm x 100 µm.

3.3 Results

3.3.1 Boron carbide coating

The variation of the steady-state COF of 319 aluminum sliding against the B_4C coating as a function of the test temperature is shown in Figure 3-1. The steady state COF was 0.56 at 25 °C and maintained this value up to 250 °C. A decrease to 0.42 was noted

at 300 °C but at 350 °C a higher COF value of 0.65 was recorded, very similar to those at lower temperatures. COF values over the range of testing temperatures shown to vary between 0.42 and 0.65. Significant aluminum adhesion was observed on the B_4C surface at all temperatures.

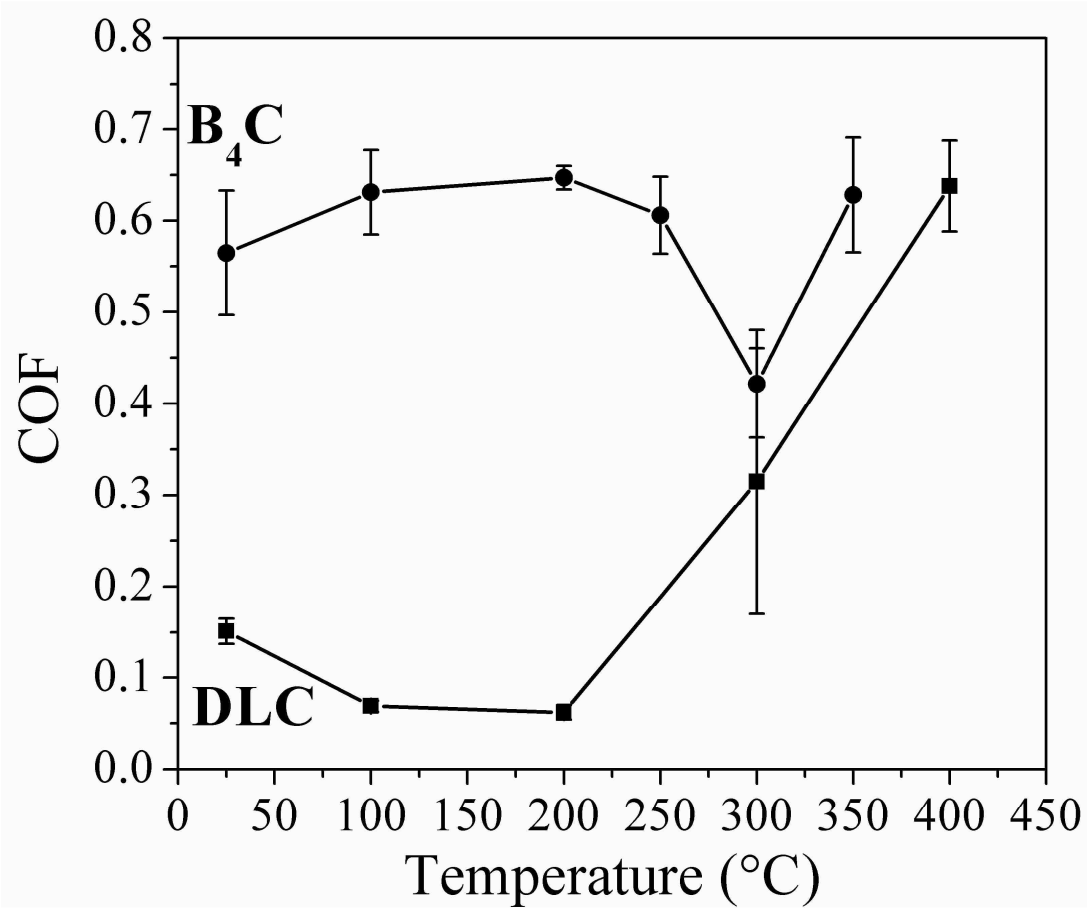

Figure 3-1: COF of 319 aluminum pins sliding for 1000 sliding cycles against the B_4C and DLC coating at temperatures ranging from 25 °C to 400 °C at 5 N load and 0.1 m/s sliding speed.

Figure 3-2 shows an increase in adhesion as temperature increased. At room temperature the percent area coverage of the adhered aluminum was 20 %. At 100 °C, the percent area coverage increased to 63 % and continued to increase, reaching a maximum

of 77 % at 350 °C. In addition, to significant aluminum adhesion, cohesive fracture of the coating as a result of fracture along the columnar grain boundaries was observed.

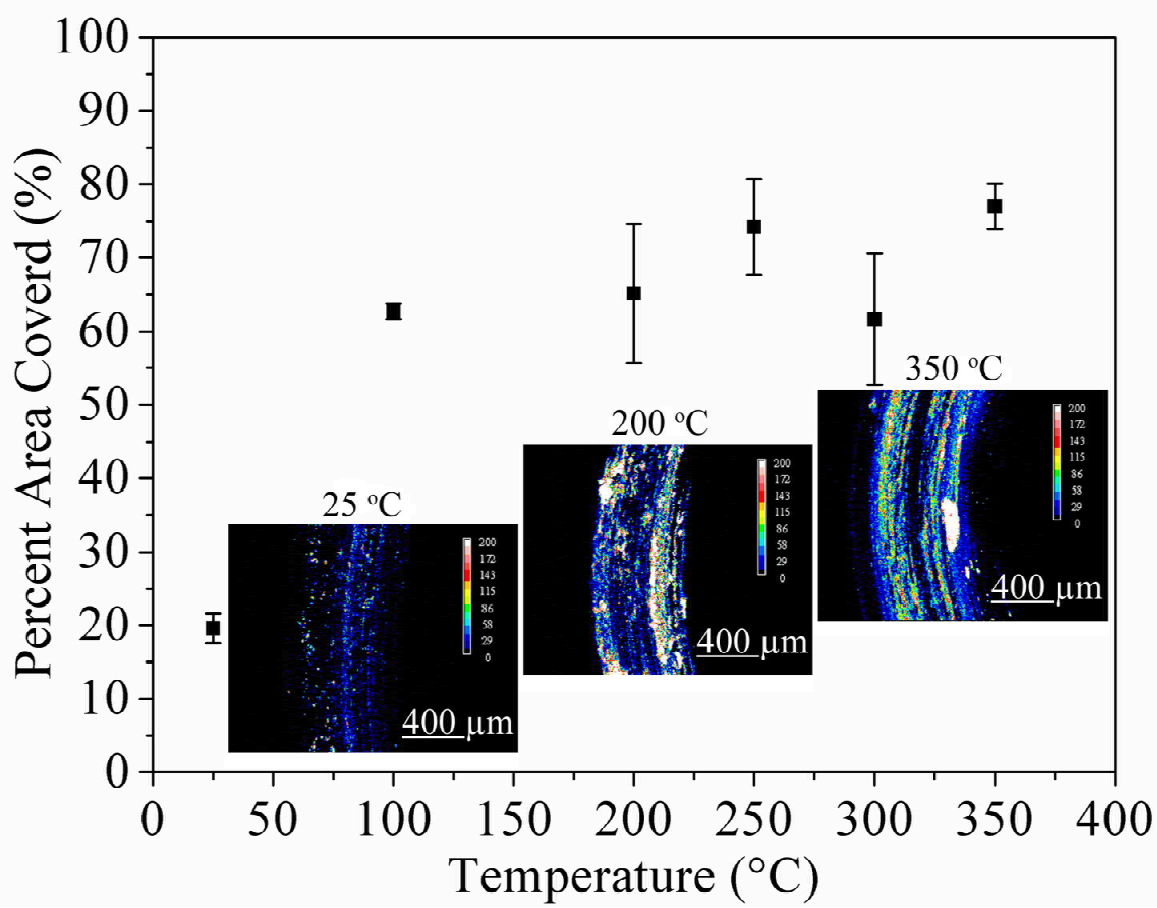

Figure 3-2: Percent area covered by aluminum inside the B_4C wear track, calculated from EPMA mapping of aluminum as a function of temperature.

FIB cross section of the wear track formed at 25 °C shown in Figure 3-3 (a) and 3-3 (b) illustrates shearing fracture along the columnar grains, which resulted in substrate damage. There was no notable wear on the contact surface according to SEM observations and as the FIB cross-section reveals the original thickness of the coating was maintained at 1.4 µm after the wear test. The cross sections of the wear track

produced at 300 °C (Figures 3-4 (a) and 3-4 (b)) also show the aluminum adhesion on the B_4C and cracking along the columnar structure of the coating, which led to the penetration of the fractured segments of the coating inside the steel substrate. In Figures 3-5 (a) and 3-5 (b), EDS mapping of aluminum, carbon, chromium and boron mapping of the cross section shown in Figure 3-4 (b), confirms the presence of aluminum adhesion on the coating surface.

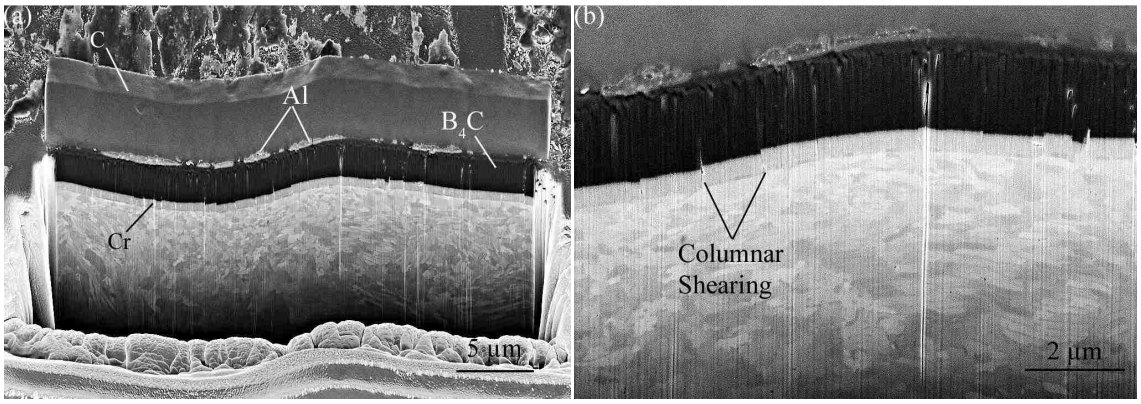

Figure 3-3: Micrographs of (a) B_4C wear track cross section produced at 25 °C by the aluminum counterface (b) coating fracture along the columnar grain boundaries

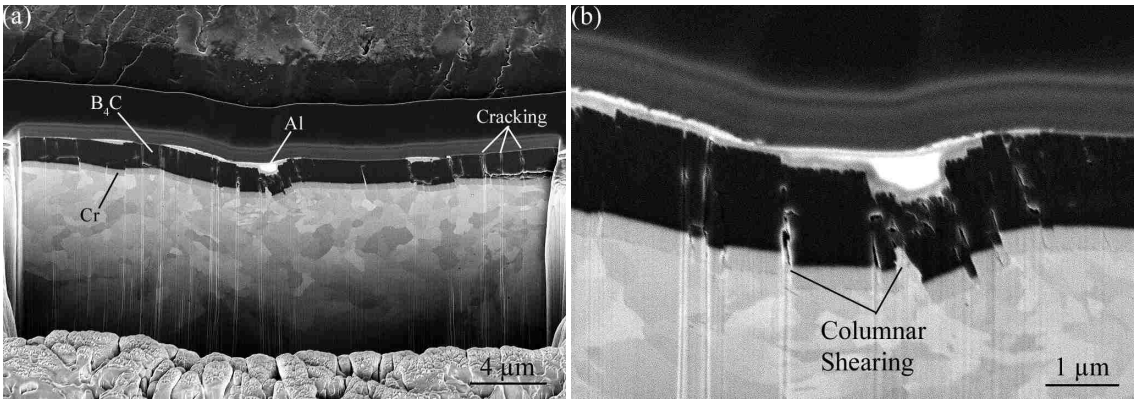

Figure 3-4: Micrographs of (a) B_4C wear track cross section wear track produced at 300 °C by the aluminum counterface (b) wear track damage due to sliding along the columnar grain boundaries inducing substrate deformation.

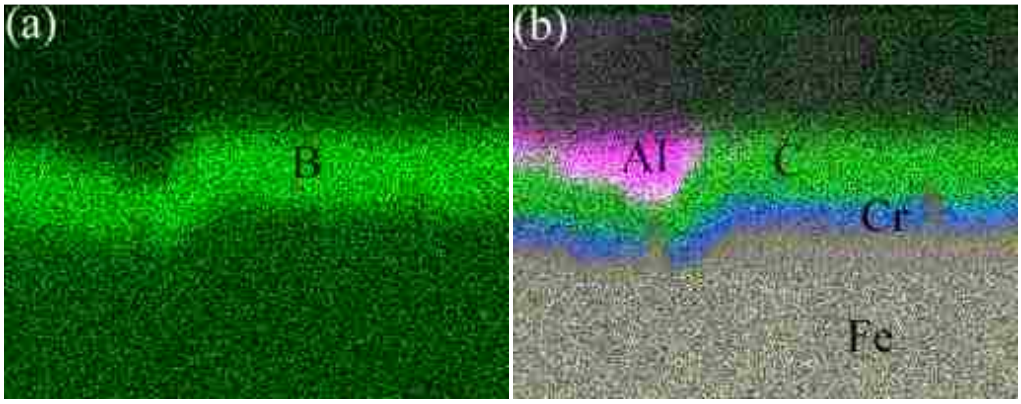

Figure 3-5: EDS Maping of (a) Boron and (b) Carbon, Aluminum, Chromium and Iron of the cross sectioned wear track, shown in Figure 4.

3.3.2 Diamond-like carbon coating

Steady state COF values of the DLC coating against 319 aluminum tested at different temperatures are presented in Figure 3-1. The COF at room temperature was 0.15, much lower than that observed with the B_4C coating. As the testing temperature increased to 200 °C, the COF decreased to 0.06. At higher temperatures, COF started to increase and at 400 °C it reached 0.64. The calculated wear rates for the DLC coating are presented in Figure 3-6 were observed to increase with testing temperature. At room temperature, the wear rate had the lowest value of 1.73×10^{-6} mm^3/Nm, as the temperature increased further, wear rate increased reaching a maximum of 3.29×10^{-5} mm^3/Nm at 400 °C. FIB cross section of the wear track at 400 °C (Figure 3-7 (a)), where the highest COF and wear were observed, illustrate that the coating was not completely worn. Micrographs of the wear tracks reveal that aluminum adhesion was observed only at

temperatures of 400 °C as shown in Figure 3-7 (b), where aluminum accumulated at locations where the coating has worn away or had spalled off.

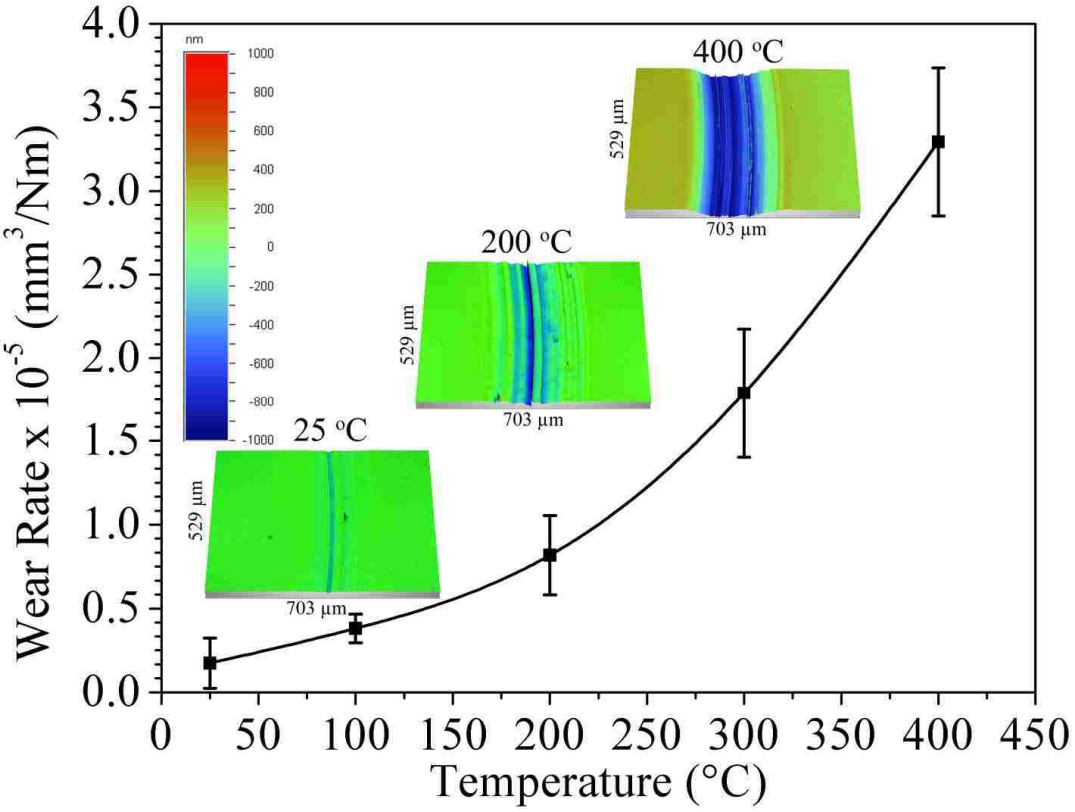

Figure 3-6: Wear rates of DLC as a function of temperature with inserts of surface profile images of the wear tracks at 25 °C, 200 °C and 400 °C

FTIR analyses of the carbonaceous material transferred from the DLC's wear tracks to 319 Al counterfaces at 200 °C and 400 °C have shown to have different organic molecules. In Figure 3-8 (a), the material transferred at 200 °C is shown to consist of hydrocarbon compounds, where bands attributed to (C-H) groups can be observed at 848 cm^{-1}, 2854 cm^{-1} and 2925 cm^{-1}. A carbon band was observed at 1600 cm^{-1} along with a broad band at 3458 cm^{-1} attributed to hydroxyl (O-H) groups. The material transfer layer formed at 400 °C (Figure 3-8b) is shown to have a modified chemical composition. In

addition to the hydrocarbon bands arising at 894 cm^{-1} and 2930 cm^{-1}; and the carbon band at 1666 cm^{-1}; a carbonyl band was observed at 1254 cm^{-1} as confirmed by literature [9], [19], [20].

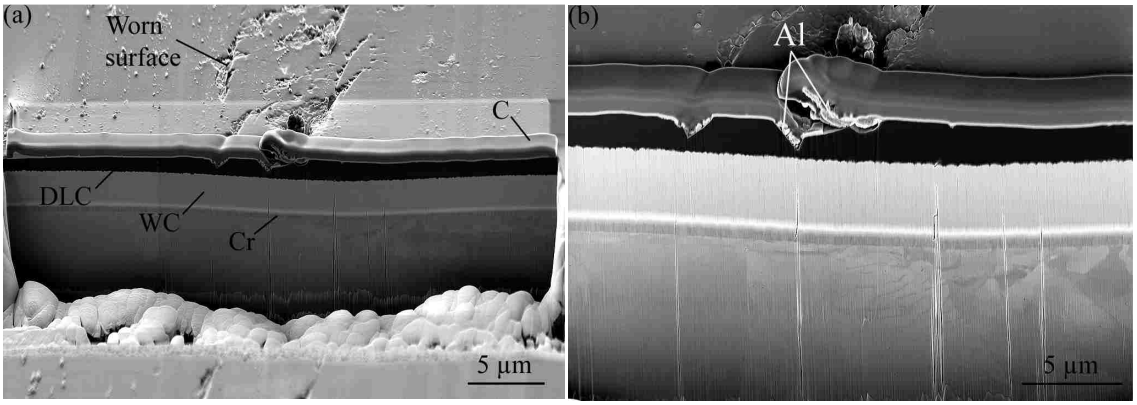

Figure 3-7: Micrographs of (a) the DLC wear track cross section (b) coating damage and aluminum adhesion inside the wear track at 400 °C.

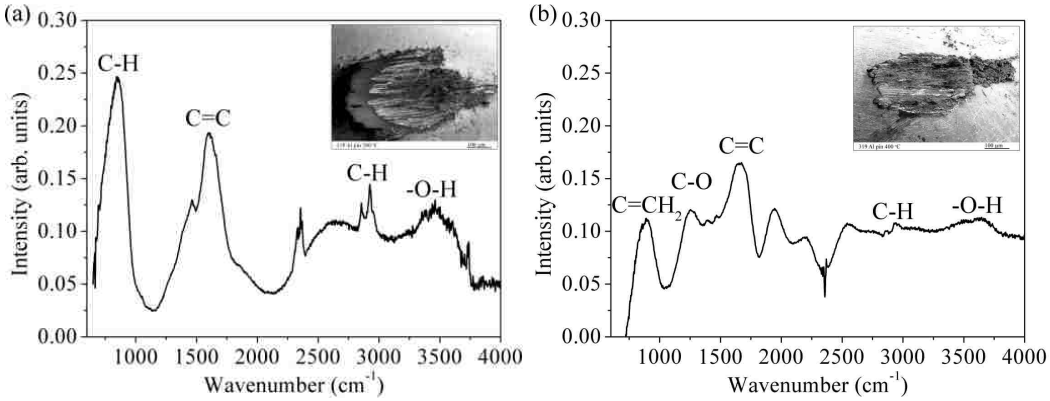

Figure 3-8: FTIR of the material transfer observed on the Al pins as shown in the micrograph inserts at (a) 25 °C and (b) 400 °C

3.4 Discussion

3.4.1 Intergranular coating fracture in B_4C

The COF of the B_4C maintained an almost constant mean value throughout the range of test temperatures at which the coating's sliding behaviour was studied (25-350 °C). Although sustaining a constant COF could be seen as an advantage, the recorded COF values were high and these high values were the result of aluminum adhesion to the coating surface during contact with 319 Al. The amount of adhesion increased with temperature but there was already a significant amount of aluminum adhesion documented at room temperature (Figure 3-2), which is sufficient to produce a high COF of 0.6. In addition to the surface damage due to aluminum adhesion, B_4C suffered from coating fracture along the columnar grain boundaries. The occurrence of intergranular fracture, which is demonstrated in Figures 3-3 and 3-4 can be attributed to the graphitization of the coating during sliding contact. Raman microspectroscopy investigations provided evidence for the graphitization of the material inside the wear tracks at different temperatures. The Raman spectra of the pristine B_4C coating shown in Figure 3-9 revealed a broad band between 900 cm^{-1} and 1200 cm^{-1}. The wear track formed at 25 °C exhibited the same features but with the exception of a weak shoulder that appeared at 1700 cm^{-1}. At 200 °C illustrated that the shoulder shifted to 1600 cm^{-1} and became sharper and broad peak observed in the pristine B_4C became weaker. At 300 °C, the broad peak completely disappeared and two strong peaks were observed at 1345 cm^{-1} and 1580 cm^{-1}, typical of the D and G graphite peaks as shown in Figure 3-9. Consequently, the Raman spectra acquired inside the wear tracks showed evidence of D

and G peaks commonly attributed to carbon graphitization or amorphization of carbon as reported in [21], [22]. Presence of graphite can be detrimental, especially if it is localized along the columnar boundaries; it would weaken the columnar grains and aid sliding under the applied contact stress. It was surprising to observe that the coating segment that were fractured penetrated into the substrate, inducing the plastic deformation of the steel underneath as seen in Figures 3-3 and 3-4.

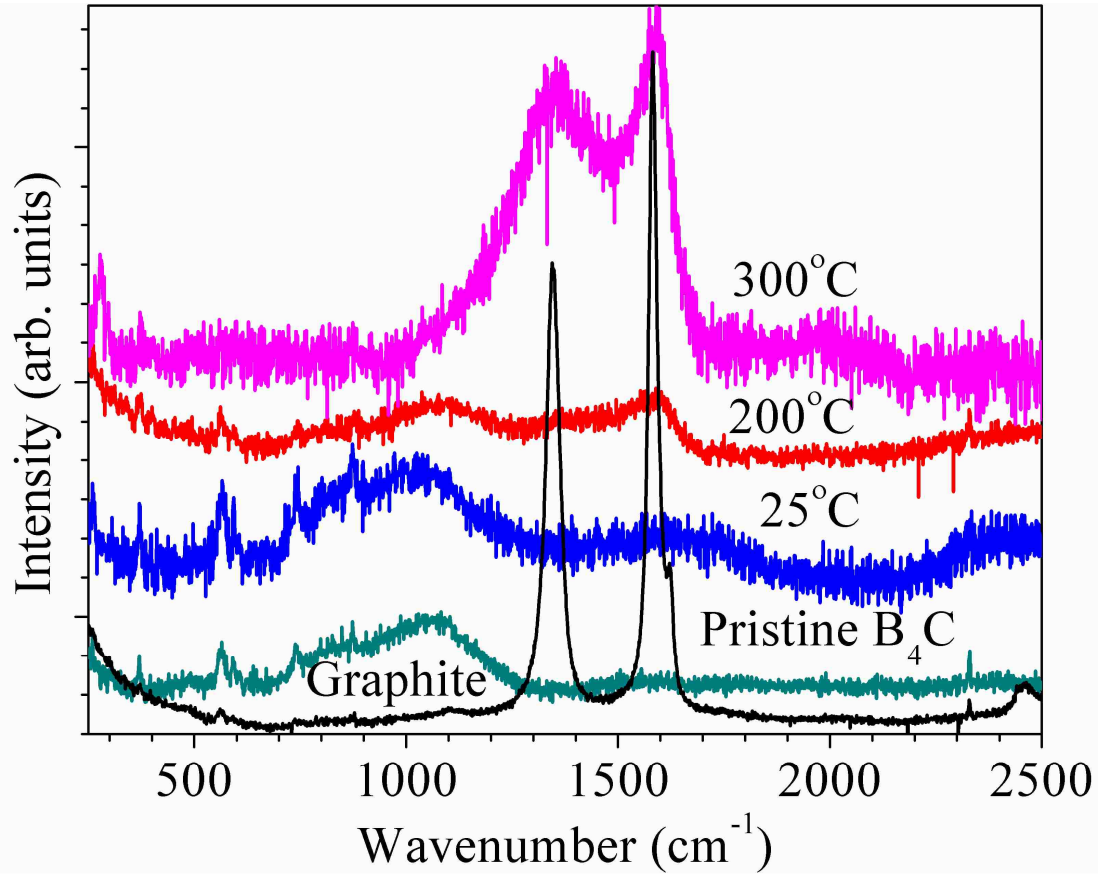

Figure 3-9: Raman spectra of the pristine B_4C, wear track after sliding in 25 °C, 200 °C and 300 ° C test conditions along with graphite spectra for reference.

3.4.2 Aluminum adhesion mitigation by DLC

The DLC coating incorporating 30 at% H exhibited a very low COF in the temperature range of 25 °C to 200 °C. In fact the room temperature COF of 0.20 decreased to 0.06 at 200 °C. The coating had excellent aluminum adhesion mitigating property in this temperature range. The coating was subjected to wear at all temperatures but the slope of wear curve increased when the tests were conducted at temperatures in the 200 °C - 400 °C range.

FTIR analysis of the material transferred on the 319 Al pin contact surface showed that at temperatures up to 200 °C a hydroxyl and hydrocarbon peaks were stronger than the C=C peak (Figure 3-8 (a)) inferring that a significant portion of the carbonaceous transferred material was terminated by either H or OH. Consequently, Al–C interactions at the sliding interface that lead to aluminum transfer to DLC surface are inhibited [13]. As the temperature increased to 400 °C, the strength of the C=C peak increased at the expense of the hydroxyl and hydrocarbon peaks indicating that the surface predominantly consisted of C=C. In addition, a carbonyl group was detected at 400 °C, suggestive of oxidation of carbon as shown in the FTIR spectra of Figure 8b. Hence, at temperatures above 200 °C, the rapid increase in COF and wear rates can be can be attributed oxidation of the coating. It was also suggested that the sp^3 to sp^2 transformation or graphitization that was reported to occur at 250 °C [17] could be a factor in rapid wear. Additionally, the evidence provided for aluminum transfer to the DLC surface at 400 °C as shown in Figure 3-8 can be attributed to the depletion of surface passivating groups in the light of the FTIR data.

3.5 Conclusions

1. B_4C coatings sliding against 319 Al produced an almost constant COF ranging between 0.42 and 0.61 in the temperature range of 25 °C - 350 °C. Aluminum adhesion to B_4C surface was a reason for the observed high COF. The amount of transferred aluminum increased with temperature making these coatings unsuitable for adhesion mitigating applications at elevated temperatures.
2. Fracture along the columnar grain boundaries, attributed to the weakening due to graphitization during sliding contact was another failure mechanism of the B_4C coatings.
3. Wear of DLC coating with 31 at% H occurred by transfer of carbon to aluminum counterface, no coating fracture was observed. The low COF of DLC coatings was attributed to the presence of hydrogen and hydroxyl groups terminating carbon bonds of the transfer layer on the 319 Al pin.
4. The DLC coating with 31 at% H produced the lowest friction of 0.06 at 200 °C against 319 Al with no signs of aluminum adhesion. The COF increased abruptly at higher temperatures. Thus, hydrogenated DLC coatings are considered to be suitable candidates to prevent aluminum adhesion for operating temperatures up to 200 °C.

References

[1] Q. Han and S. Viswanathan, "Analysis of the Mechanism of Die Soldering in Aluminum Die Casting", *Metallurgical and Materials transactions A*, vol. 34, no. January, pp. 139–146, 2003.

[2] F. Thvenot, E. Nationale, and S. Mines, "Boron Carbide", *Boron*, vol. 6, pp. 205–225, 1990.

[3] V. V. Dzhemelinskii, M. S. Kovalchenko, and G. N. Makarenko, "Indenter materials for high-temperature hardness measurement", *Boron*, vol. 2, no. 2, pp. 168–170, 1973.

[4] G. V. Samsonov, Y. G. Tkachenko, and A. G. Dobrovolskii, "Temperature depedance of the cofficient of friction of boron and silicon carbides in a vacuum", *Powder Metallurgy and Metal ceramics*, vol. 7, no. 7, pp. 79–81, 1970.

[5] Y. G. Tkachenko, B. L. Grabchuk, N. I. Bodnaruk, and V. V. Sychev, "Friction and wear of boron carbide at temperatures in the range 20-1500C", *Powder Metallurgy and Metal ceramics*, vol. 7, no. 7, pp. 541–543, 1977.

[6] Y. G. Tkachenko, D. Z. Yurchenko, V. K. Yulyugin, V. N. Molyar, L. M. Murzin, and E. S. Lugovskaya, "High temperature friction and some properties of hot pressed boron carbide", *Powder Metallurgy and Metal ceramics*, vol. 12, no. 12, pp. 41–43, 1985.

[7] C. Bindal and A. Erdemir, "Formation of ultralow friction surface films on boron carbide", *Applied physics letters*, vol. 68, no. November 1995, pp. 1995–1997, 1996.

[8] a. Erdemir, C. Bindal, C. Zuiker, and E. Savrun, "Tribology of naturally occurring boric acid films on boron carbide", *Surface and Coatings Technology*, vol. 86–87, pp. 507–510, 1996.

[9] J. Robertson, "Amorphour Carbon", *Advances in Physics*, vol. 35, pp. 317–374, 1986.

[10] J. Robertson, "Diamond-like amorphous carbon", *Materials Science and Engineering: R: Reports*, vol. 37, no. 4–6, pp. 129–281, 2002.

[11] E. Konca, Y.-T. Cheng, A. M. Weiner, J. M. Dasch, and A. T. Alpas, "Elevated temperature tribological behavior of non-hydrogenated diamond-like carbon coatings against 319 aluminum alloy", *Surface and Coatings Technology*, vol. 200, no. 12–13, pp. 3996–4005, 2006.

[12] W. Ni, Y.-T. Cheng, A. M. Weiner, and T. A. Perry, "Tribological behavior of diamond-like-carbon (DLC) coatings against aluminum alloys at elevated temperatures", *Surface and Coatings Technology*, vol. 201, no. 6, pp. 3229–3234, 2006.

[13] Y. Qi, E. Konca, and A. T. Alpas, "Atmospheric effects on the adhesion and friction between non-hydrogenated diamond-like carbon (DLC) coating and aluminum – A first principles investigation", *Surface Science*, vol. 600, no. 15, pp. 2955–2965, 2006.

[14] A. Erdemir, "Genesis of superlow friction and wear in diamondlike carbon films", *Tribology International*, vol. 37, no. 11–12, pp. 1005–1012, 2004.

[15] S. Sattel, M. Weiler, J. Gerber, and T. Giessen, "Nucleation during deposition of hydrocarbon ions as a function of substrate temperature", *Diamond and Related Materials*, vol. 4, pp. 333–336, 1995.

[16] S. Sattel, T. Gieben, H. Roth, M. Scheib, R. Samlenski, R. Brenn, H. Ehrhardt, and J. Robertson, "Temperature dependence of the formation of highly tetrahedral a-C:H", *Diamond and Related Materials*, vol. 5, no. 3–5, pp. 425–428, 1996.

[17] S. Sattel, J. Robertson, and H. Ehrhardt, "Effects of deposition temperature on the properties of hydrogenated tetrahedral amorphous carbon", *Journal of Applied Physics*, vol. 82, no. 9, pp. 4566–45778, 1997.

[18] H. Ronkainen, J. Koskinen, S. Varjus, and K. Holmberg, "Load-carrying capacity evaluation of coating / substrate systems for hydrogen-free and hydrogenated diamond-like carbon films", *Tribology Letters*, vol. 6, pp. 63–73, 1999.

[19] C. E. Bell, D. F. Taber, and A. K. Clark, "*Infrared absorption spectroscopy, Organic Chemistry Laboratory: with Qualitative analysis: Standard and Microscale Experiments*", 3rd edition. Pacofic Grove, CA: Brooks/Cole Thomson Learning, 2001, p. 95.

[20] V. P. Tolstoy, I. V. Chernyshova, and V. A. Skryshevsky, "Infrared of Thin Layers in Silicon Microelectronics", in *Handbook of infrared spectroscopy of ultrathin films*, Hoboken, New Jeresey: John Wiley & Sons, 2003, p. 448.

[21] X. Yan, Z. Tang, L. Zhang, J. Guo, C. Jin, Y. Zhang, T. Goto, J. McCauley, and M. Chen, "Depressurization Amorphization of Single-Crystal Boron Carbide", *Physical Review Letters*, vol. 102, no. 7, pp. 1–4, 2009.

[22] D. Ge, V. Domnich, T. Juliano, E. . Stach, and Y. Gogotsi, "Structural damage in boron carbide under contact loading", *Acta Materialia*, vol. 52, no. 13, pp. 3921–3927, 2004.

CHAPTER 4
HIGH TEMPERATURE TRIBOLOGICAL BEHAVIOUR OF W-DLC AGAINST ALUMINUM

4.1 Introduction

Diamond-like carbon (DLC) coatings have shown to be promising surface coatings for tribological components that can be found in forming, stamping operations and internal combustion engine due to their low friction and low wear rates, especially against aluminum alloys [1]. However, the main obstacle with DLC coatings is that they tend to lose their attractive low friction and low wear rate at elevated temperatures [2]–[6]. Thus research studies have been undertaken to explore new ways to modify the DLC coatings with acceptable high temperature performance. Studies have shown that one can improve the friction behaviour of the coatings by changing the metal to carbon ratio. Strondl et al. [7] deposited DLC coatings with different tungsten to carbon ratio using acetylene in an unbalanced magnetron sputtering system with two WC targets and two Cr targets to promote adhesion with the substrate. Results showed that as the acetylene flow increased from 25 sccm to 140 sccm, coefficient of friction (COF) decreased from 0.31 to 0.13 (measured against alumina at 5N load and 0.01m/s), but hardness decreased from 27 GPa to 8 GPa. The WC was distributed in the form of rich WC layers rather than WC crystallites, which was observed in another study that used pure W targets instead of WC [8]. Voevodin et al. [9] studied both nanocrystalline (nc) WC and nearly amorphous (na) WC embedded in a DLC matrix. The friction and wear rate of nc WC-DLC sliding against 440 C steel (0.98 N load and 1 m/s sliding speed in air with 50 %RH and in dry

nitrogen) were observed to decrease from 0.7 to 0.3 as the carbon content increased from 30 at% to 90 at%. Under the same testing conditions, na WC-DLC coating was observed to behave in a similar trend, but with a COF of 0.6-0.1, lower than the nc WC-DLC coating. Raman analysis of the transfer layer formed on 440C steel showed evidence of metal oxide, which was attributed to the relatively high COF compared to single phase DLC coatings. A recent study by Sanchez-Lopez et al. [10] studied the tribological behaviour of DLC doped with various carbides (TiC, TiBC, and WC). The three coatings were deposited on M2 steel substrates with graphite, Ti, TiC:$TiB_{2,}$ and WC targets. The coatings were tested against AISI 52100 steel in ambient air with 5 N load and 0.1 m/s sliding speed. For all three coatings it was observed that friction, wear rate, and hardness decreased with increase of carbon content. At 70 - 85 C at%, WC doped DLC had the lowest wear rate of $4.4x10^{-8}$ mm^3/Nm, and TiBC doped DLC was the hardest with 24.6 GPa, however, it had poor wear properties arising from its brittle nature. TiC doped DLC had the lowest COF of 0.13, but at the same time the softest coating with 8 GPa hardness. Thus it was concluded that WC doped DLC had the most balanced properties considering the hardness (15-20 GPa) and friction (COF = 0.2).

WC and WC/Co composites (cermets) have been widely used in high temperature applications due to their high melting point and their excellent wear and corrosion resistance. Particularly cermets are among the most common materials for drilling and mining tools. Their hardness ranges from 10 - 17 GPa with a high melting point of 2785 °C ± 10 °C [11]. WC can also be used in the form of coatings as explored by Fervel et al. [12]. Block-on-ring experiments were conducted with thermally sprayed WC17%Co

(WCCo) against Al_2O_3-13%TiO_2 (A13T) and Al_2O_3-40%TiO_2 (A40T). Tests were conducted in ambient air with 0.25 m/s linear speed for 1 hour or 900 m with 295 N load. Results show a COF of approximately 0.2 for both A13T and A40T counterfaces. The relatively low COF of 0.2 was attributed to the presence of thin WO_3 layer and some graphite on the surface, which was confirmed by X-ray photoelectron spectroscopic (XPS) analyses. Pure tungsten was observed to rapidly oxidize above 200 °C, and between 375 °C and 400 °C, a well adhered thin oxide layer begins to form on the tungsten surface, and above 500 °C the oxide layer begins to crack [11]. Other studies have shown that two oxide layers form between 700 °C and 1000 °C. The inner layer consists of a well adhered dense oxide that is dark-blue in colour and the outer layer that is porous, powdery, and yellow in colour [13]. WO_2 and WO_3 are two common forms of tungsten oxide, and WO_3 is the more stable of the two oxides that was found to form at temperatures below 500 °C [14].

The literature has shown that the combination of metals such as W with DLC can be an asset for improving high temperature mechanical and tribological properties. However, it is not clear how the W affects the tribological behaviour at elevated temperatures. Therefore, the current study investigates the effect of material transfer, tribo-layer, and their composition on the wear and friction behaviour of W containing DLC (W-DLC) with 319 Al counterface at elevated temperatures ($T < 500$ °C).

4.2 Experimental details

4.2.1 Coating properties

W-DLC coating was deposited on M2 steel coupons with 25.4 mm diameter for tribo tests and on 50.8 mm (100) Si wafers for microstructural analysis, using a physical vapour deposition (PVD) system. The M2 steel surfaces were first cleaned by Ar glow discharge, and then a Cr layer was deposited to promote adhesion of the DLC on the steel substrate.

The hardness and elastic modulus of the coating was measured using a Hysitron TI 900 Triboindenter equipped with a Berkovich nano-indenter. The hardness of the W-DLC coating was 8.7 ± 1.7 GPa, and the elastic modulus was 104.3 ± 18.8 GPa. The micrograph of W-DLC cross section coating deposited on Si shown in Figure 4-1 (a) indicates that the coating is 3 µm thick with a columnar morphology. In addition, EDS mapping shown in Figure 4-1 (b) and (c) indicates that the tungsten is integrated evenly throughout the DLC coating.

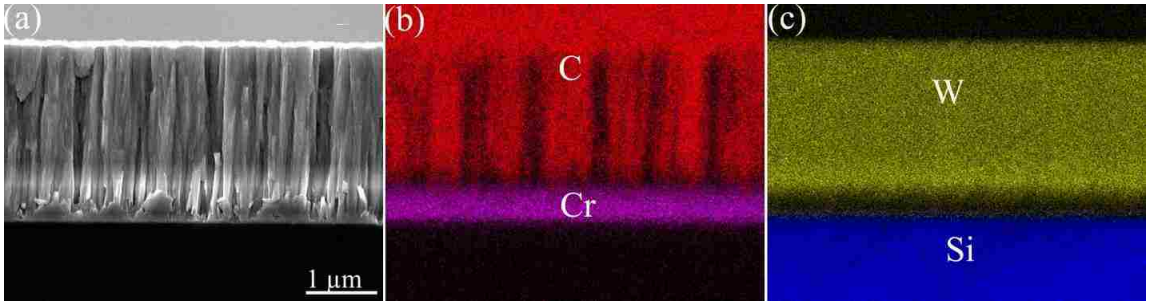

Figure 4-1: (a) Cross section of the W-DLC coating deposited on Si substrate and EDS Mapping of (b) Carbon, Chromium and (c) Tungsten and Silicon

4.2.2 Tribological tests and analyses

A high temperature pin-on-disk tribometer was utilized to measure the friction and wear rates of W-DLC coatings between 25 ºC and 500 ºC (25, 50, 80, 100, 200, 300, 400, and 500 °C) at 0.1 m/s linear speed and a constant normal load of 5.0 N for 1000 sliding cycles. A 319 Al pin with 4 mm rounded tip, generating a maximum Hertzian contact pressure of 0.5 GPa, was used as a sliding counterface. In addition, an optical surface profilometer (ZYGO NewView 7300) was employed to calculate the wear rate of the W-DLC coating by measuring the cross sectional area of each wear track at four different areas after each test and multiplying the area with the parameter of each track to get the volume loss. Then the wear rate was calculated from the known relationships between volume loss, sliding distance, and load.

Following the sliding experiments, focused ion beam (FIB) (Carl Zeiss NVision 40 CrossBeam) cross-sections of the wear tracks were prepared to analyze the damage under the wear track. Cross-sections were made perpendicular to the sliding direction of the wear tracks. A carbon layer was deposited prior to milling to avoid ion beam damage to the surface. Following the carbon deposition, trenches were milled with 13 nA ion current; for a smoother surface finish, a final milling was conducted at a lower ion current of 50 pA. Transmission electron microscopy (TEM) samples were prepared by FIB using the H-bar method. The sample was ion milled to a thickness of 100 nm for TEM (Jeol GEM 2100F) investigation. A tungsten needle was then brought in contact and welded to the milled sample using a thin layer of carbon. The sample was then lift-out by milling either side of the sample and was transported to the TEM chamber on a copper grid.

For chemical analysis, a PHI Quantera XPS with a monochromatoed Al-K_α (1486.5 eV) was utilized to investigate the carbon (C1s), tungsten (W4f), and oxygen (O1s) concentrations as a function of sputtering time of the as-received coating and of the coating after testing at 500 ºC. In addition, Raman spectra of the W-DLC coating as a function of annealing temperature were obtained using a Dilor XY Micro Raman spectrometer with a 532 nm of an Ar^+ laser to analyze the structural evolution as a function of temperature. A (100) Si wafer, 50.8 mm (2”) in diameter coated with W-DLC was cleaved into 10 mm x 10 mm samples. The samples were then annealed for 1 hour at 100, 200, 300, 400 and 500 °C; after annealing, the samples were air cooled and analysed with Raman.

4.3 Results

4.3.1 Pin-on-disk tests

Shown in Figure 4-2 (a) are COF values as a function of sliding cycles of W-DLC coating sliding against the 319 Al pins at different testing temperatures. In Figure 4-2 (b), average steady state (defined as the portion after the run-in period) is presented as a function of testing temperature. At room temperature, the COF was 0.20 ± 0.01, much lower than what was observed at intermediate temperatures, that is 100 °C, 200 °C, and 300 °C, which generated a COF average of 0.60 ± 0.10, 0.60 ± 0.11, and 0.60 ± 0.12 respectively. Mean while, when tested 400 °C, the COF average decreased, reaching 0.18 ± 0.07, slightly lower than that observed at room temperature, which was 0.2, and the COF average decreased even further to 0.12 ± 0.01 when tested at 500 ºC.

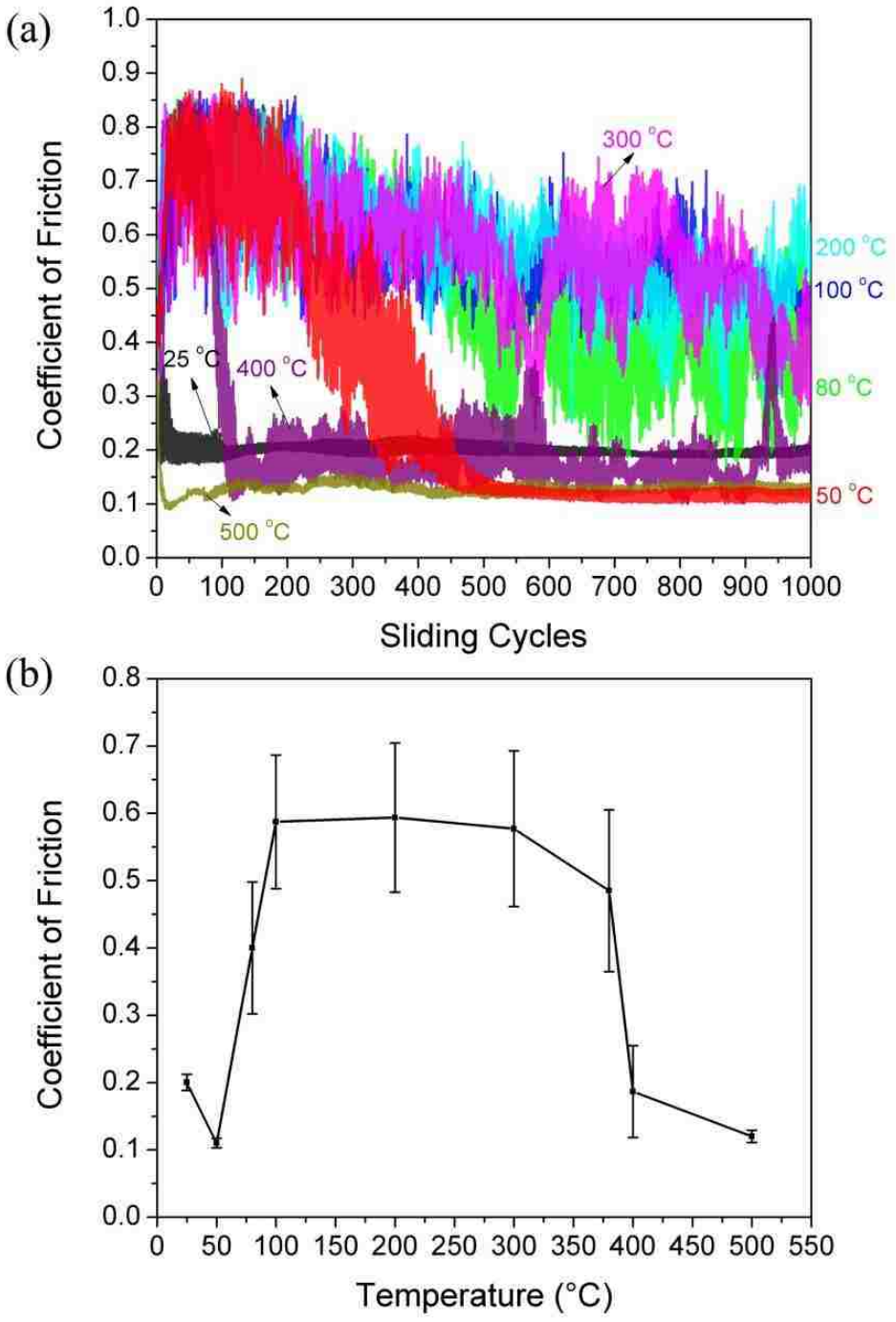

Figure 4-2: (a) COF as a function of sliding cycles at temperatures ranging from 25 °C to 400 °C (b) Steady-state COF as a function of temperature. Error bars are the standard deviations of the steady state values.

Secondary electron microscopy (SEM) images shown in Figure 4-3 did not show evidence of Al adhesion inside the wear track tested at room temperature (Figure 4-2 (a)). Images of the worn 319 Al pin shown in Figure 4-3 (b) illustrate that during sliding, a transfer layer was formed. However, analysis of the 100°C test shown in Figure 4-3 (c), Al adhesion was observed inside the wear track. In addition, Figure 4-3 (d) of the 319 Al wear scar after testing at 100 ºC shows scuffing marks along the sliding direction with no evidence of material transfer. Similar to the 100 ºC SEM observation, the coating tested at 300 °C showed Al adhesion again inside the wear track as presented in Figure 4-3 (e), however to a much lesser extent compared to what was seen at 100 °C. Furthermore, at 300 °C, it was observed that a transfer layer started to form once again but covered only a small portion of the 319 Al counterface, as shown in Figure 4-3 (f). At higher testing temperature of 400 °C, there was no evidence of adhered Al inside the wear track (Figure 4-3 (g)). Images of the 319 Al pin (Figure 4-3 (h)) revealed that a transfer layer was formed once again during sliding and covering the contact area of the 319 Al pin, similar to what was observed at room temperature.

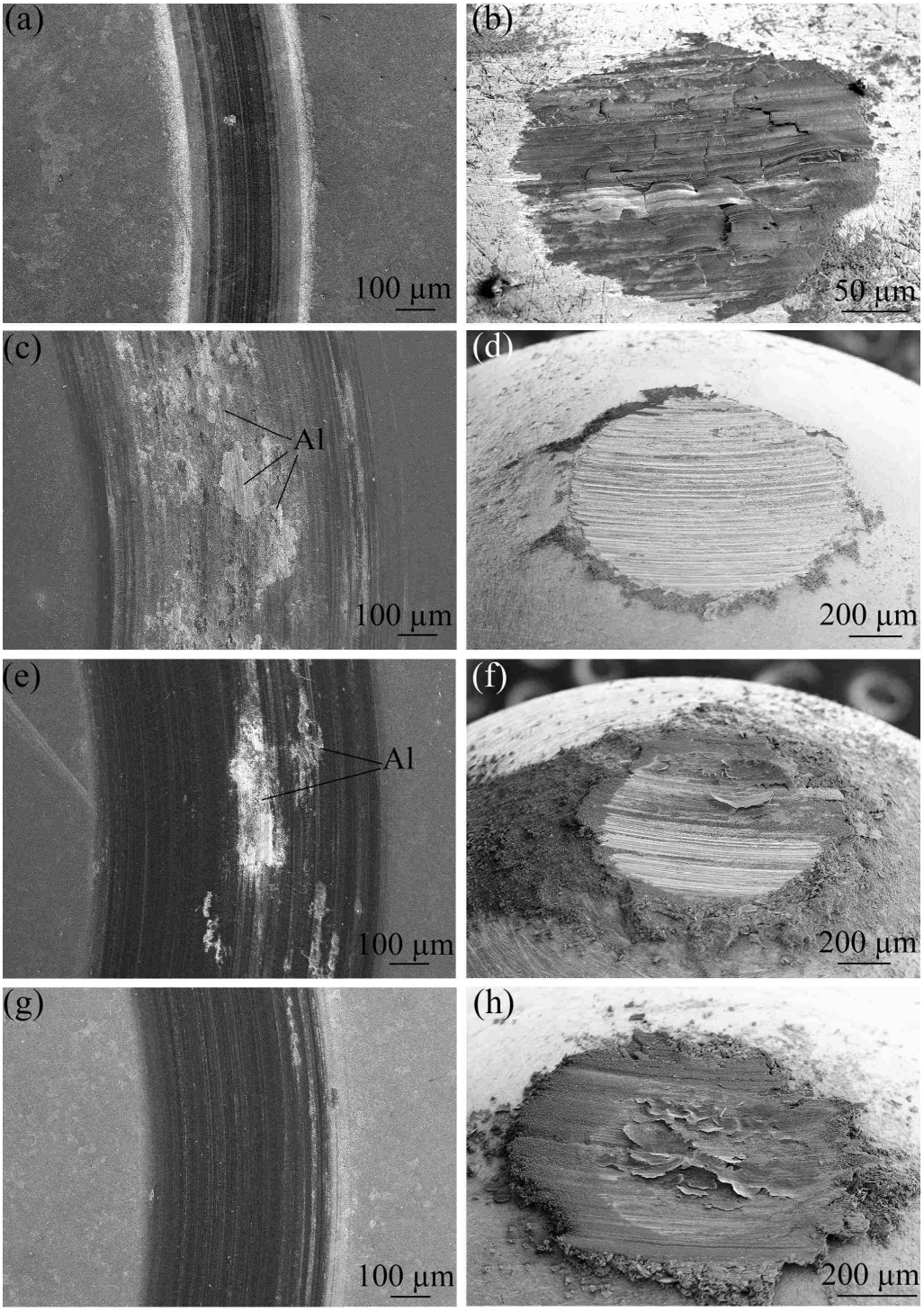

Figure 4-3: SEM image of W-DLC wear tracks and aluminum pins wear scar after testing at (a), (b) room temperature (b), (c) 100 °C, (e), (f) 300 °C and (g), (h) 400 °C

The wear rates of the W-DLC coatings followed a similar trend to that of the friction curve (Figure 6-4). At room temperature, the wear rate was the lowest at 9.42×10^{-7} mm^3/Nm. The wear rate then increased to 8.18×10^{-5} mm^3/Nm at 100 °C, and at higher temperatures of 200 °C and 300 °C, the wear rate decreased slightly to 7.14×10^{-5} and 6.58×10^{-5} mm^3/Nm respectively. Further decrease in wear rate was observed at 400 °C and 500 ºC, reaching 5.52×10^{-5} mm^3/Nm and 2.94×10^{-5} mm^3/Nm respectively.

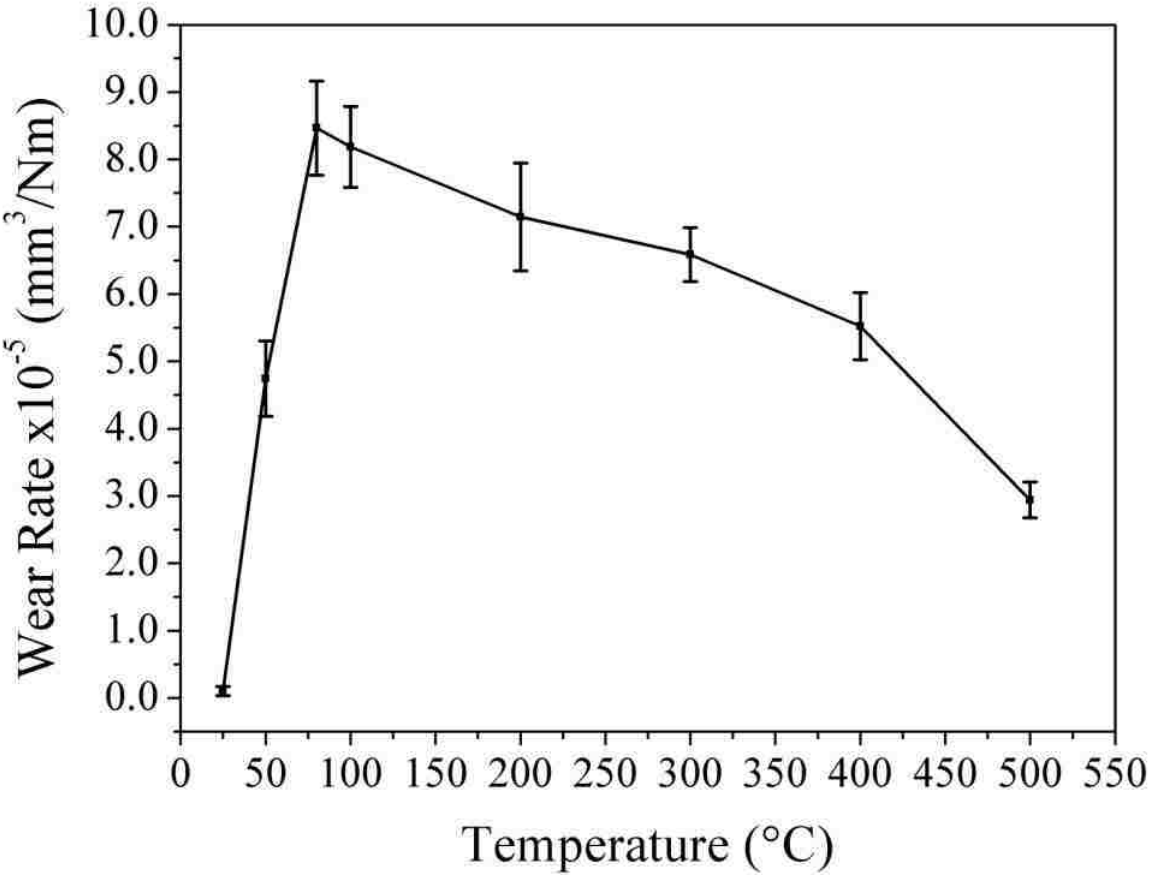

Figure 4-4: Wear rates of W-DLC as a function of temperature ranging from 25 °C to 400 °C. The error bars represent the standard deviation of four separate measurements.

4.3.2 Structural analysis

Adhesion and subsurface damage were studied using FIB milled cross-sections taken from inside the wear tracks at 100 °C and 400 °C. The cross-section of the wear track at 100 °C (Figure 4-5 (a)) revealed that the coating was completely worn in some parts of the wear track, which resulted in aluminum adhering to the substrate. This can explain the relatively high average COF of 0.6, mechanism details will be elaborated on in the discussion in section 4 below. In Figure 4-5 (b), a higher magnification of the interface between the aluminum and the substrate showing the severity of the coating damage observed after testing at 100 °C. The composition of the cross-section and the adhered material is confirmed by the EDS elemental mapping shown in Figure 4-5 (c). The observation suggests that the adhesion is of a mechanical nature rather than a result of making a chemical bonding with the iron surface. Cross-section of the wear track tested at 400 °C shown in Figure 4-6 (a), indicates that the coating was still intact after the test, and no sign of substrate damage was evident. In Figure 4-6 (b), the coating was observed to be slightly worn, but no evidence of aluminum adhesion or coating failure was found. The EDS elemental mapping of the cross section shown in Figure 4-6 (c) confirms that the coating was well adhered to the substrate at 400 °C.

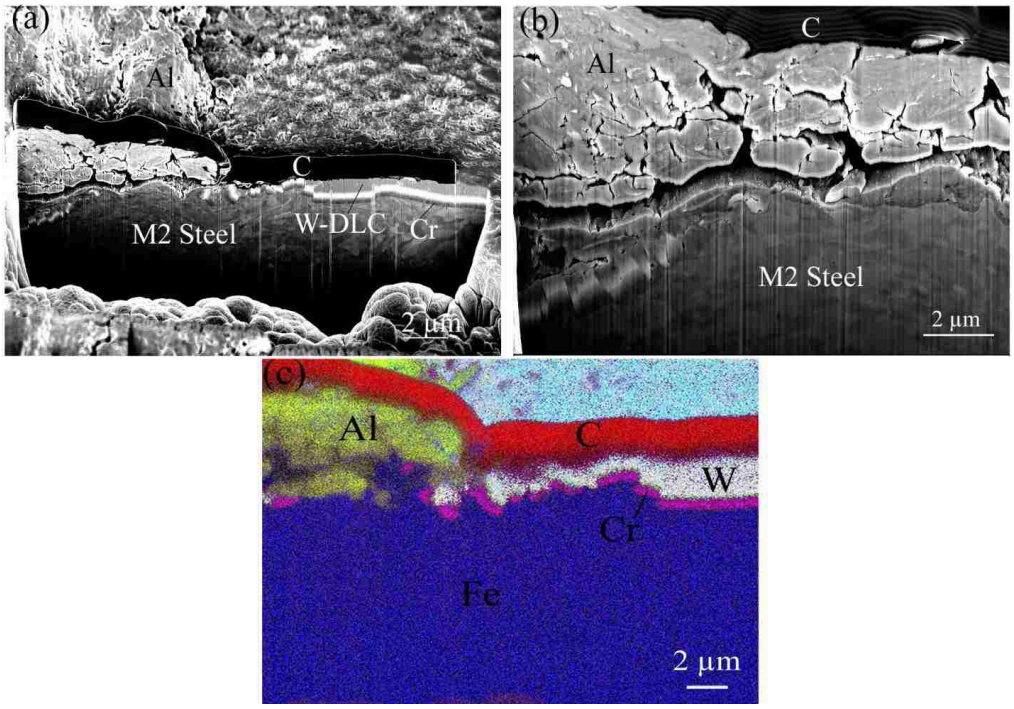

Figure 4-5: SEM of (a) the W-DLC wear track FIB cross-section (b) coating damage and aluminum adhesion inside the wear track at 100 °C (c) EDS elemental mapping of W in the DLC coating, Cr interlayer, Fe from the substrate and C deposited by the FIB prior to milling.

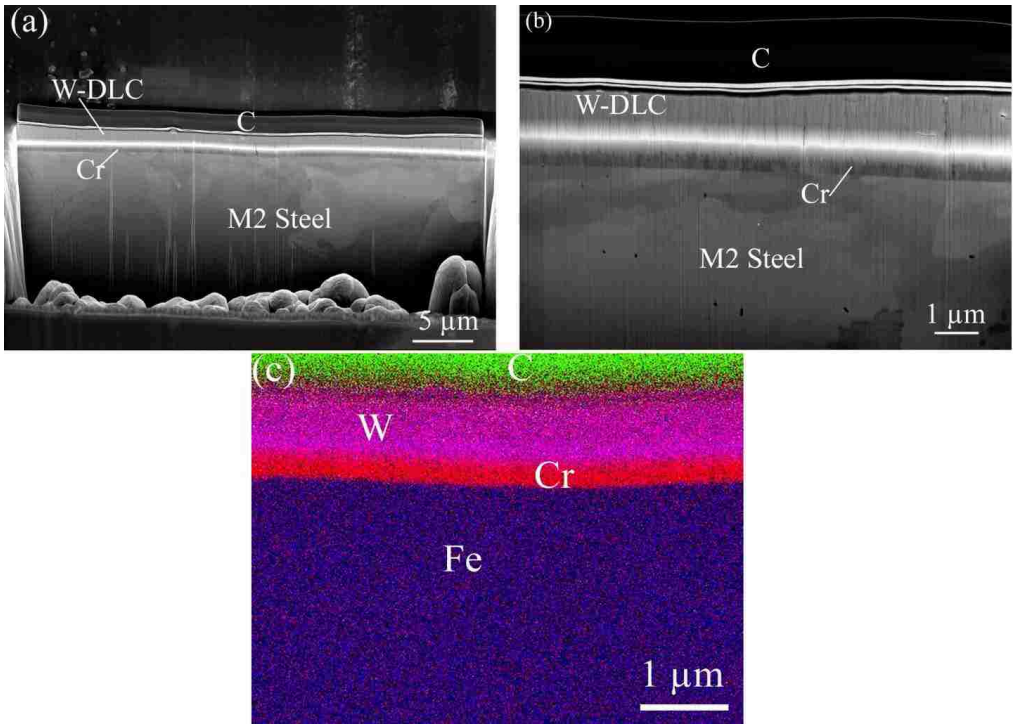

Figure 4-6: SEM of (a) the W-DLC wear track FIB cross-section (b) higher magnification of the cross section at 400 °C (c) EDS elemental mapping of W in the DLC coating, Cr interlayer, Fe from the substrate and C deposited by the FIB prior to milling.

TEM analyses revealed that at 400 ºC the coating preserved its structure (Figure 4-7(a)) but developed a top surface layer as indicated in Figure 4-7 (b). The layer was observed to be approximately 20 nm thick. High resolution image of the top surface layer formed, along with the selected area electron detraction pattern (SAED) as shown in Figure 4-7 (c) insert, revealed that the top layer has an amorphous structure, with a different composition than the rest of the coating, as will described in section 4.3.3.

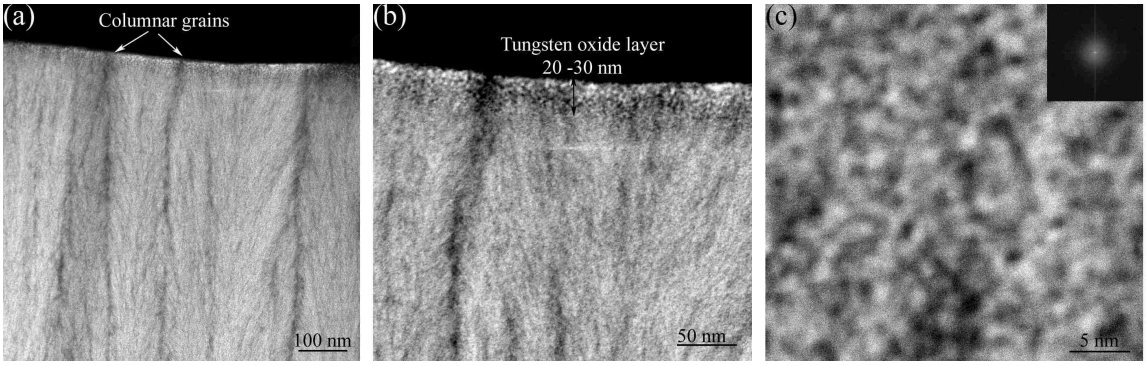

Figure 4-7: TEM images of W-DLC coating (a) columnar structure (b) top surface (c) high resolution of the top surface layer after testing at 400 ºC, with insert of SAED showing the diffraction of an amorphous structure.

4.3.3 Chemical Analysis

Surface and subsurface chemical composition of the as-received sample and the sample which was tested at 500 ºC were analyzed using XPS. The analyses of the as-received sample (Figure 4-8 (a)) showed that the C, W, and O were consistent throughout the sputtered depth, with average C concentration of 75.39 at%, W average concentration of 20.31 at%, and O average concentration of 2.18 at%.

However, in Figure 4-8 (b) the sample which was tested at 500 ºC showed different atomic concentration throughout the sputtered depth. After about 0.5 minute of sputtering, the C concentration began to increase from almost zero, reaching 75 at% at 12 minutes of sputtering time, while O decreased from 70 at% to 5 at% during the first 12 minutes of sputtering. On the other hand, W concentration was observed to increase from 20 at% to 35 at% within the first 3 minutes and then decreased to 20 at%, similar to the

typical values observed in the as-received sample. This may suggest that the carbon on the surface was sublimated, thus leaving a tungsten oxide rich layer on the coating surface.

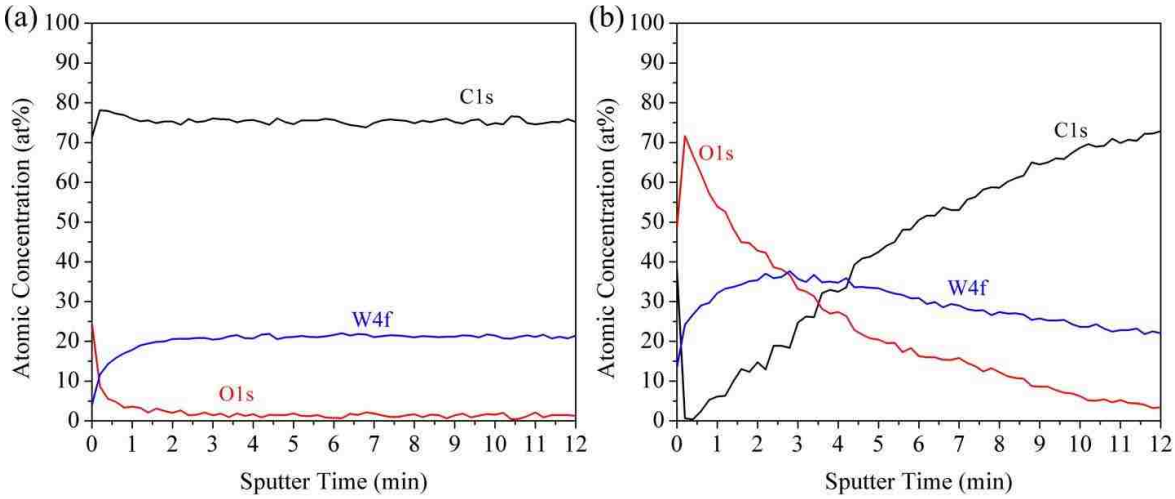

Figure 4-8: X-ray photoelectron spectroscopy of W-DLC coating (a) as-received (b) after testing at 500 ºC.

The micro-Raman spectra in Figure 4-9, is of the transfer material formed on the 319 Al pins after sliding at 25 °C and 400 °C observed in Figures 4-3 (b) and (h). The spectra reveal that both transfer layers consist of carbon, as indicated by the presence of D and G peaks at 1354 cm^{-1} and 1588 cm^{-1} respectively [15]–[17]. The transfer layer on the aluminum pin tested at 400 °C revealed evidence of tungsten oxide, which is indicated by the peaks observed at 257, 700, 806, and 886 cm^{-1} [18]–[20].

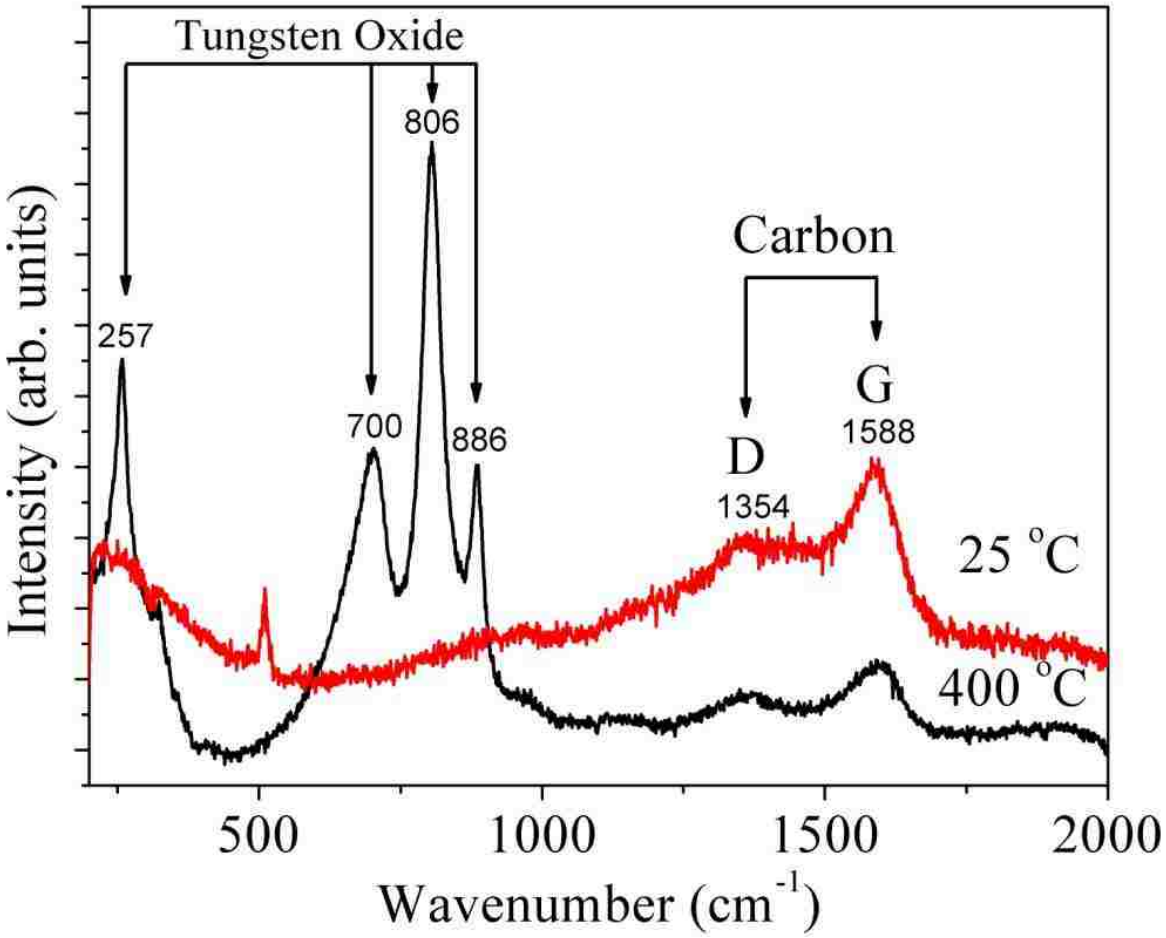

Figure 4-9: Micro-Raman spectra of material transfer formed on the 319 Al pins after sliding against W-DLC at 25 °C and 400 °C.

4.4 Discussion

The COF results of W-DLC sliding against 319 Al at temperatures ranging from 25 °C to 500 °C were observed to have three different regimes controlling the friction behaviour observed in Figure 4-2. At 25 °C a COF of 0.2 was generated, which is typical of DLC coatings tested at room temperature in ambient atmosphere [21]. The relatively low COF and wear rate observed under ambient conditions was attributed to the transfer

layers formed on the 319 Al during sliding, as shown in Figure 4-3 (b). These layers were found to be carbon rich as confirmed by the Raman spectra found in Figure 4-9. According to literature [1], [22], these layers were considered to be lubricious due to the presence of atmospheric humidity, which dissociates to H and OH and passivates the dangling carbon bonds and minimizes C/C interactions between the layers and the sliding interface.

Experiments conducted at intermediate temperatures (100 °C ≤ T ≤ 300 °C) led to a higher COF average of 0.6 that remained almost constant in this range. Also in the same temperature range, excessive coating wear and severe aluminum adhesion were observed (Figure 4-5 (a)). Severe coating damage observed in Figure 4-5 (b) was the typical feature of wear in this temperature range along with aluminum transferred from the counterface being transferred to the exposed steel substrate in many locations where the coating was spalled off. Here, moisture depletion due to water evaporation around the contact point resulted in lack of passivation, and consequently interfacial C/C or Al/C interactions occur, thus possibly preventing the formation of lubricous transfer layers on the aluminum counterface as shown in Figure 4-3 (d).

As for tests conducted at 400 °C and 500 °C, the COF average was 0.18 and 0.12 respectively, which was lower than for tests conducted at intermediate temperatures between 100 °C and 300 °C. Not only did the coating exhibit low COF at temperatures above 400 °C but it was observed that the coating had lower wear rate of 5.52×10^{-5} mm^3/Nm and 2.94×10^{-5} mm^3/Nm at 400 ºC and 500 ºC respectively. DLC coatings do not typically survive such temperatures, which was attributed to the graphitization process of

carbon through the transformation of sp^3 (diamond-like) to sp^2 (graphite-like) which occurs at 250 °C [4-6]. In addition, no evidence of aluminum adhesion on the coating surface was found (Figure 4-6) and coating damage was not as severe compared to 100 °C test. This improvement in tribological performance may be due to the formation of new transfer layers once again as observed in Figure 3 (h). The reason for saying new is because the transfer layers at 400 ºC were found to have different chemistry than the layers observed at room temperature. The transfer layers formed at 400 ºC consist of tungsten oxide, whereas those formed at 25 ºC consist mainly of carbon, as shown in (Figure 4-9). This also concurs with the thermo-chemical equilibrium calculations of tungsten oxide formation due to the reaction between Al_2O_3 and W in the presence of oxygen [23]. TEM observations as shown in Figure 4-7 (b) revealed that a 20-30 nm tungsten oxide layer was also observed to form at the coating surface which was tested at 500 ºC. XPS depth profile analysis shown in Figure 4-8 (b) revealed that the carbon at the surface was depleted. Thus suggesting that the formation of the tungsten oxide rich layer was due to carbon oxidation, which may have led to sublimation or the formation of carbon monoxide (CO) gas at 400 ºC and 500 ºC. Thus, W was exposed, which in turn was oxidized and formed a tungsten oxide rich layer, as observed from the TEM images in Figure 7 (b) and confirmed by Raman in Figure 4-10 discussed.

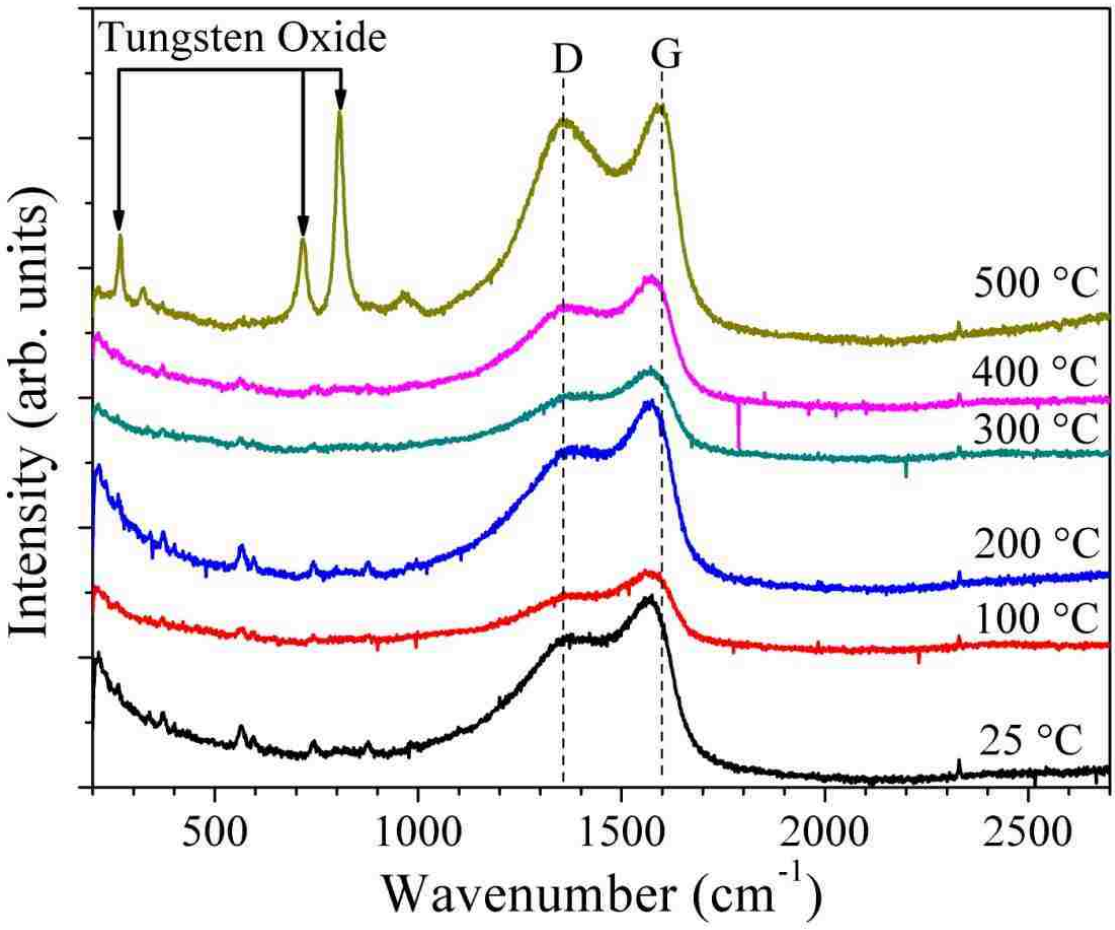

Figure 4-10: Micro-Raman spectra of W-DLC coating deposited on (100) Si wafer as received and annealed samples at 100, 200, 300, 400, and 500 °C.

The low friction property of tungsten oxide is in agreement with the literature, where it was found that the formation of crystalline WO_3 film reduces COF to 0.18 [24]. In addition, the Raman spectra of the annealed coatings presented in Figure 4-10 indicate that the formation of WO_3 started to occur at approximately 500 °C. It is shown in Figure 4-10, that up to 400 °C, two Raman peaks were observed at 1566 cm^{-1} and 1357 cm^{-1} commonly seen for DLC and labeled as G and D respectively [15]–[17]. At temperatures from 100 °C - 400 °C, no significant change in DLC spectra was observed compared to

the as-received coating; only a slight shift in the G peak from 1566 cm^{-1} of the as received to 1573 cm^{-1} was noted at 400 °C. Further shift of the G peak is observed after 1 hour of annealing at 500 °C to 1600 cm^{-1} and the D peak became sharper. In addition, peaks at 270, 715 and 808 cm^{-1} were observed. Such peaks are commonly attributed to tungsten trioxide (WO_3) [18]–[20]. The temperature dependence of WO_3 can then explain the observed COF drop to 0.18 after an initial high COF of 0.8 peak observed during run-in at 400 °C test (Figure 4-2 (a)). That is, at 400 °C as the COF reach peak value of 0.8, flash temperature at the sliding interface may exceed 500 °C, thus triggering the formation of this tungsten oxide rich layer. This amorphous tungsten oxide layer as observed to form on the coating surface as observed in the TEM analyses (Figure 4-7 (c)) and also form a transfer layer on the sliding counterface, which was found to reduce the COF from 0.6 observed at intermediate temperatures (100 ºC - 300 ºC), to 0.18 and 0.12 observed at 400 ºC and 500 ºC respectively. As a result, the presence of tungsten oxide layer act as a lubricous film, preventing Al/C interaction at the sliding interface in the absence of surface passivation agents such as H (present inside the coating) or OH (from moisture in the atmosphere), as observed to be ineffective at temperatures beyond 200 °C [2], [3], which is a critical factor in achieving a low COF [1], [22].

4.5 Summary and conclusions

In this study a W-DLC coating was tested against 319 Al at temperatures up to 500 °C in air using a pin-on-disk tribo-configuration. Results and analysis lead to the conclusion that three tribological regimes could be observed at temperatures ranging from 25 °C to 500 °C:

- At 25 °C aluminum does not adhere to the W-DLC coating and generates a low COF (0.2) and a low wear rate (9.42×10^{-7} mm^3/Nm), that can be attributed to the water passivation mechanism observed for dopants free DLC.
- For tests at intermediate temperatures, ranging from 100 °C to 300 °C, the COF was observed to be relatively high (0.6) with high wear rates (8.18×10^{-5} mm^3/Nm to 6.58×10^{-5} mm^3/Nm). Micrographs of the surface and cross-sections of the wear tracks formed at 100 °C revealed that the high COF was due to coating failure, which resulted in aluminum adhesion inside the wear track.
- At 400 °C and 500 °C, the coating was observed to behave in a similar way as was observed at 25 °C; the COF was 0.18 without any signs of coating failure or aluminum adhesion. In addition, the wear rate was 5.52×10^{-5} mm^3/Nm, relatively lower than what was observed for 100 °C - 300 °C tests.
- The relatively low COF and wear rate at 400 °C and 500 °C were attributed to the formation of a tungsten oxide layer on the coating surface and the sliding counterface. This film was seen to exhibit a lubricious behaviour at temperatures above 400 ºC.

References

[1] A. Erdemir and C. Donnet, "Tribology of diamond-like carbon films: recent progress and future prospects", *Journal of Physics D: Applied Physics*, vol. 39, no. 18, pp. R311–R327, 2006.

[2] A. A. Gharam, M. J. Lukitsch, M. P. Balogh, and A. T. Alpas, "High temperature tribological behaviour of carbon based (B4C and DLC) coatings in sliding contact with aluminum", *Thin Solid Films*, vol. 519, no. 5, pp. 1611–1617, 2010.

[3] E. Konca, Y.-T. Cheng, A. M. Weiner, J. M. Dasch, and A. T. Alpas, "Elevated temperature tribological behavior of non-hydrogenated diamond-like carbon coatings against 319 aluminum alloy", *Surface and Coatings Technology*, vol. 200, no. 12–13, pp. 3996–4005, 2006.

[4] S. Sattel, M. Weiler, J. Gerber, and T. Giessen, "Nucleation during deposition of hydrocarbon ions as a function of substrate temperature", *Diamond and Related Materials*, vol. 4, pp. 333–336, 1995.

[5] S. Sattel, T. Gieben, H. Roth, M. Scheib, R. Samlenski, R. Brenn, H. Ehrhardt, and J. Robertson, "Temperature dependence of the formation of highly tetrahedral a-C:H", *Diamond and Related Materials*, vol. 5, no. 3–5, pp. 425–428, 1996.

[6] S. Sattel, J. Robertson, and H. Ehrhardt, "Effects of deposition temperature on the properties of hydrogenated tetrahedral amorphous carbon", *Journal of Applied Physics*, vol. 82, no. 9, pp. 4566–45778, 1997.

[7] C. Strondl, "Investigation on the formation of tungsten carbide in tungsten-containing diamond like carbon coatings", *Surface and Coatings Technology*, vol. 162, no. 2–3, pp. 288–293, 2003.

[8] C. Strondl, G. J. van der Kolk, T. Hurkmans, W. Fleischer, T. Trinh, N. M. Carvalho, and J. T. M. de Hosson, "Properties and characterization of multilayers of carbides and diamond-like carbon", *Surface and Coatings Technology*, vol. 142–144, pp. 707–713, 2001.

[9] A. A. Voevodin, J. P. O. Neill, and J. S. Zabinski, "WC / DLC / WS 2 nanocomposite coatings for aerospace tribology", *Tribology Letters*, vol. 6, pp. 75–78, 1999.

[10] J. C. Sánchez-López, D. Martínez-Martínez, M. D. Abad, and A. Fernández, "Metal carbide/amorphous C-based nanocomposite coatings for tribological applications", *Surface and Coatings Technology*, vol. 204, no. 6–7, pp. 947–954, 2009.

[11] E. Lassner and W. Schubert, "*Tungsten: Properties, Chemistry, Technology of the Element, Alloys, and Chemical Compounds*". New York, N.Y.: Kluwer Academic / Plenum Publishers, 1998.

[12] V. Fervel, B. Normand, H. Liao, C. Coddet, E. Bêche, and R. Berjoan, "Friction and wear mechanisms of thermally sprayed ceramic and cermet coatings", *Surface and Coatings Technology*, vol. 111, no. 2–3, pp. 255–262, 1999.

[13] W. W. Webb, T. John, and C. Wagner, "Oxidation of Tungsten", *Journal of the electrochemical society*, vol. 103, no. 2, pp. 107–111, 1956.

[14] A. Warren, A. Nylund, and I. Olefjod, "Oxidation of Tungsten and Tungsten Carbide in Dry and Humid Atmospheres", *International Journal of Refractory Metals and Hard Materials*, vol. 14, pp. 345–353, 1996.

[15] T. W. Scharf and I. L. Singer, "Third Bodies and Tribochemistry of DLC Coatings", in *Tribology of Diamond-Like Carbon Films*, no. Dlc, C. Donnet and A. Erdemir, Eds. Springer, 2008, pp. 201–236.

[16] M. J. Pelletier, "*Analytical Applications of Raman Spectroscopy*". Blackwell Publishing, 1999.

[17] I. Pocsik, M. Hundhausen, M. Koos, L. Ley, and I. Pócsik, "Origin of the D peak in the Raman spectrum of microcrystalline graphite", *Journal of Non-Crystalline Solids*, vol. 227–230, pp. 1083–1086, 1998.

[18] J. A. Horsley, E. Wachs, J. M. Brown, G. H. Via, and F. D. Hardcastlex, "Structure of Surface Tungsten Oxide Species in the WO ,/ AI , O , Supported Oxide System from X-ray Absorption Near-Edge Spectroscopy and Raman Spectroscopy", *Journal of Physical Chemistry*, vol. 91, pp. 4014–4020, 1987.

[19] M. A. Vuurmant and I. E. Wachs, "I n Situ Raman Spectroscopy of Alumina-Supported Metal Oxide Catalysts", *Journal of Physical Chemistry*, vol. 96, pp. 5008–5016, 1992.

[20] K. Nonaka, A. Takase, and K. Miyakawa, "Raman Spectra of Sol-gel-derived tungsten oxides", *Journal of materials Science lett*, vol. 12, pp. 274–277, 1993.

[21] H. Ronkainen and K. Holmberg, "Environmental and Thermal Effects on the Tribological Performance of DLC Coatings", in *Tribology of Diamond-Like Carbon Films*, no. Dlc, C. Donnet and A. Erdemir, Eds. USA: Springer, 2008, pp. 155–198.

[22] Y. Qi, E. Konca, and A. T. Alpas, "Atmospheric effects on the adhesion and friction between non-hydrogenated diamond-like carbon (DLC) coating and

aluminum – A first principles investigation", *Surface Science*, vol. 600, no. 15, pp. 2955–2965, 2006.

[23] T. W. Scharf and I. L. Singer, "Role of the Transfer Film on the Friction and Wear of Metal Carbide Reinforced Amorphous Carbon Coatings During Run-in", *Tribology Letters*, vol. 36, no. 1, pp. 43–53, 2009.

[24] O. Greenwood, S. Moulzolf, and P. Blau, "The influence of microstructure on tribological properties of WO3 thin films", *Wear*, vol. 232, pp. 84–90, 1999.

CHAPTER 5
TRIBOLOGICAL BEHAVIOUR OF HEAT TREATED TUNGSTEN DOPED DIAMOND-LIKE CARBON COATING AT ELEVATED TEMPERATURES

5.1 Introduction

Diamond-like carbon (DLC) coatings are of a great interest to the manufacturing industry, as they prolong tool life and increase productivity due to their low coefficient of friction (COF) and low tendency to adhere to aluminum. However, in applications such as warm forming or machining, elevated operating temperatures can be challenging, as the COF of most DLC coatings increase abruptly with increase in temperature, which lead to limited service life at elevated temperatures. Studies have shown that hydrogen-free DLC coating sliding against aluminum loses its lubricous property at approximately 150 °C, resulting in high COF and excessive aluminum adhesion [1]. While hydrogenated DLC coating was observed to sustain a low COF of 0.08 up to 200 ºC [2], [3]. Further increase in temperature, lead to the release of hydrogen and loss low COF and wear resistance [4], [5]. The addition of dopants such as Mo, W and Si observed to promote higher percentage of the sp^3 bonded carbon, which stabilizes the structure at higher temperatures compared to pure DLC [6], [7].

In efforts to better understand the effects of dopants such as W on the high temperature tribological behaviour of DLC coatings, experiments were conducted at temperatures from 25 ºC to 500 ºC. The addition of W to DLC was found to reduce the COF to 0.12 at 400 ºC and 500 ºC [8]. Analysis showed that the low COF was attributed

to the formation of a lubricious oxide (LO) WO_3 which formed due to heating to 400 ºC and 500 ºC. Studies found in literature have demonstrated that several metal oxides were shown to provide low shear at the sliding interface with thermal stability at elevated temperatures [9]. For instance, tribo-oxidation of Ti alloys was observed to improve the tribological performance due to formation of Magneli TiO_2 [10]. Other studies have also shown that metal oxides with high ionic potentials and mixed oxides with large difference in the ionic potential such as NiO-WO_3 and PbO-B_2O_3 exhibit low shear strength which lead to low COF at elevated temperatures [11]–[13]. Consequently, this study investigates the W-DLC ability to form a LO by heat treatment and the effects on the tribological behaviour over testing temperatures ranging from 25 ºC to 400 ºC.

5.2 Experimental details

Tungsten doped DLC (W-DLC) coatings were deposited on M2 steel substrates for tribotesting and (100) Si wafers for microstructural and chemical analysis. 2 um thick coatings were deposited on the selected substrates using physical vapour deposition (PVD). Detailed structure, chemical and mechanical properties of the as deposited coating are provided in ref. [8]. One set of coatings were heat treated at 500 °C and the another was heat treated at 600 ºC for an hour each then air cooled.

Focused ion beam (FIB) was used to prepare the transmission electron microscopy (TEM) specimens by the H-bar method to investigate coating morphology. An X-ray photoelectron spectroscopy (XPS) with a monochromated Al-K_α (1486.5 eV) was utilized to investigate the tungsten (W4f) concentrations as a function of coating depth. In addition, X-ray diffraction (XRD) investigations of the as-deposited and heat

treated coatings were carried out with Cu Kα radiation (40 kV and 40 mA). Each scan was conducted using parallel beam mode with 2º incidence angle, 0.04 º/sec step size and 1 sec/step.

Tribological performance of the heat treated coatings was investigated using a high temperature tribometer. Pin-on-disk tests were conducted on each of the heat treated coatings with 5 N load, 0.1m/s linear sliding speed for 1000 sliding cycles at 25 ºC, 100 ºC, 200 ºC, 300 ºC and 400 ºC. All tests were conducted using 319 Al pins with tips rounded to 2 mm radius. The pins and the coatings wear tracks at each of the testing temperature were investigated using secondary electron microscopy (SEM).

5.3 Results

5.3.1 Structure and composition

TEM investigations of the coating heat treated at 500 ºC showed a surface layer approximately 60 nm (Figure 5-1 (a)). In an earlier study, this layer was shown to be rich in W [8]. The chemical state of the W(4f) was investigated and showed an evolution as a function of depth using XPS for the coating heat treated at 500 ºC (Figure 5-1 (b)). Near surface analyses showed peaks at 35.4 eV and 37.4 eV which correspond to WO_3 [14]. After approximately 8 seconds of Ar sputtering, the WO_3 peaks were observed to shift to lower energy values, reaching the electron spin states of W (31.2 eV and 33.4 eV). Consequently, the XPS analysis revealed that annealing of the W-DLC coating resulted in a WO_3 rich layer on the surface.

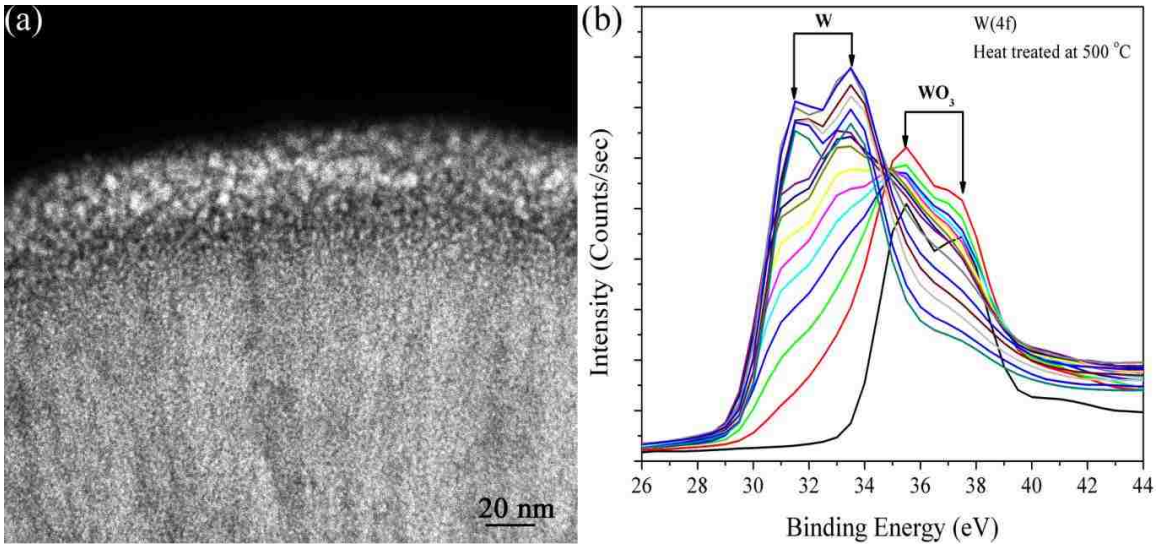

Figure 5-1: W-DLC heat treated at 500 °C (a) cross sectional TEM and (b) XPS depth profile

XRD analyses revealed that the as-deposited coating (Figure 5-2) consisted of one broad peak at 2θ of 32°; indicating that the coating was of an amorphous nature. Annealing at 500 ºC showed other peaks characteristics of monoclinic WO_3 (PDF 43-1035). The broad peak disappeared at both heat treated coatings and evidence of SiO_2 (PDF 01-075-3159) was observed when the coating was heat treated at 600 º C. The presence of SiO_2 is an indication of coating decay and exposure of the substrate.

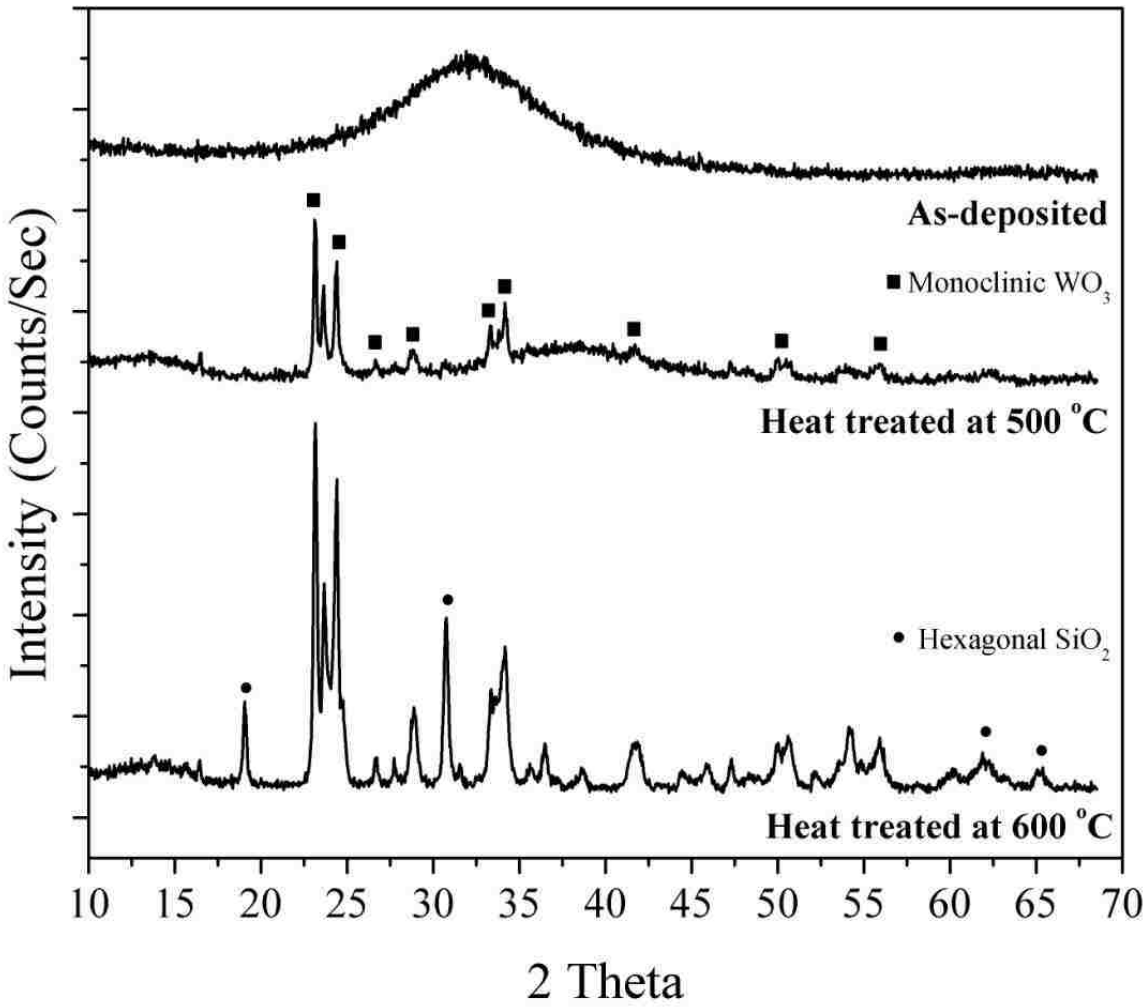

Figure 5-2: XRD of W-DLC coating deposited on (100) Si wafer as deposited and heat treated at 500 °C and 600 °C.

5.3.2 Tribological behaviour

Pin-on-disk results of 319 Al pins sliding against W-DLC heat treated at 500 ºC and 600 ºC are shown in Figure 5-3. The tribological performance of the coatings heat treated at 500 ºC was observed to be highly dependent on the testing temperature. At temperatures below 100 ºC, low average steady state COF of 0.17 at 25 ºC and 0.11 at 100 ºC were observed (Figure 5-3(a)). When tested at 200 ºC the COF was 0.12 for the

first 100 sliding cycles and increased to a steady state COF of 0.57.A similar trend of increasing COF occurs in the first 30 cycles of the test performed at 300 ºC however, the initial COF starts at 0.05 and increases to 0.11. After 100 cycles, the COF drastically increased to 0.68 and began to fluctuate between 0.2 and 0.6. Testing at 400 ºC, however, was shown to generate low COF of 0.02 immediately after the initial 16 sliding cycles. On the contrary, no low COF was observed for the 600 °C heat treated coating the COF curves as shown in Figure 3 (c) and (d) did not change with the testing temperature ranging from 25 ºC to 400 ºC with average COF of 0.5. The coating heat treated at 500 ºC exhibited a lower average COF as compared the as-deposited and heat treated at 600 ºC (Figure 5-4 (a)).

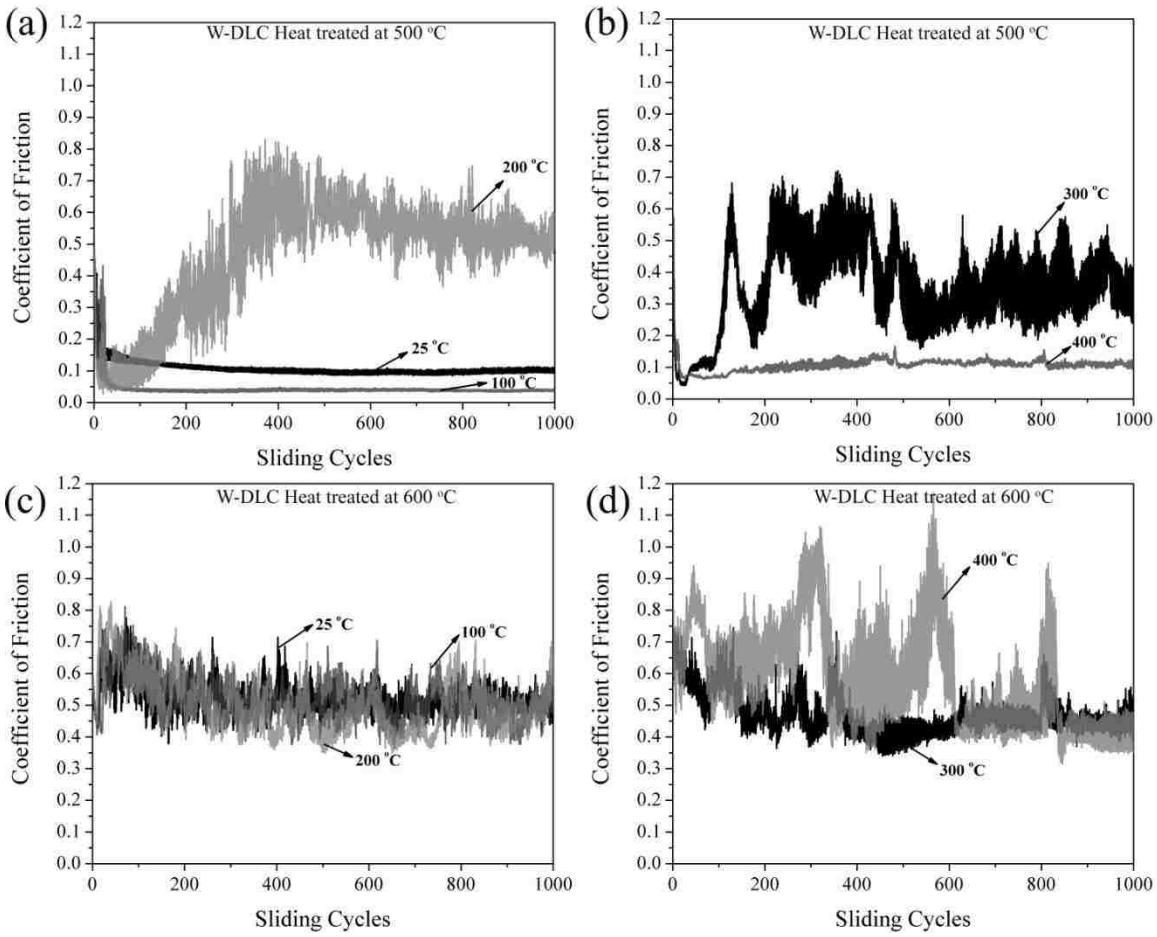

Figure 5-3: Coefficient of friction of W-DLC heat treated at 500 °C tested at (a) 25 °C, 100 °C, 200 °C and (b) 300 °C, 400 °C and W-DLC heat treated at 600 °C tested at (c) 25 °C, 100 °C, 200 °C, (d) 300 °C and 400 °C.

The average wear rate observed at each testing temperature presented in Figure 5-4 (b). The average wear rates showed similar trend to the COF. In Figure 5-4 (b), the wear rate at 25 ºC and 100 ºC were 2.5×10^{-6} mm^3/Nm and 8.3×10^{-6} mm^3/Nm respectively, for the 500 °C heat treated sample. At 200 ºC, the wear rate increased to 6.6×10^{-5} mm^3/Nm, which is 8 times higher than the 25 ºC and 100 ºC tests. The wear rate decreased to 5.2×10^{-5} mm^3/Nm and 2.6×10^{-6} mm^3/Nm at 300 ºC and 400 ºC testing temperatures respectively. In contrast the wear rate of the coating heat treated at 600 ºC

was invariant with testing temperature. An average wear rate of $8.5x10^{-5}$ mm^3/Nm was observed.

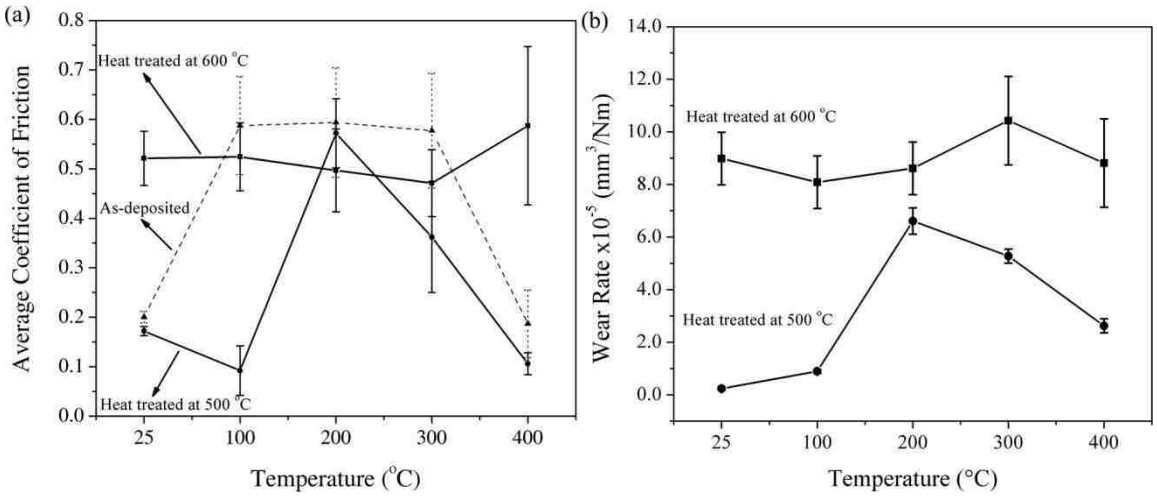

Figure 5-4: (a) Average COF of as-deposited and heat treated at 500 °C and 600 °C, (b) Wear rates of W-DLC as a function of temperature ranging from 25 °C to 400 °C.

5.3.3 SEM investigations

SEM analyses of the 319 Al pins and the wear tracks of the 500 °C heat treated sample are presented in Figure 5-5. Images of the aluminum pins after testing show that material transfer formed on almost all the pins except the pin tested at 200 ºC. The pins tested at 25 ºC and 100 ºC show a fully developed material transfer layer covering the area of the pin in contact with the coating. The coating wear tracks were observed to be smooth with no evidence of aluminum adhesion or coating failure.

SEM of the Al pin tested at 200 ºC showed no evidence of material transfer Figure 5-5 (e) while the SEM image of the wear track revealed a significant amount of aluminum transfer (Figure 5-5 (f)). This may explain the relatively high COF of 0.5

observed in the pin-on-disk test performed at 200 °C. In contrast material transfer was observed on the pin tested at 300 ºC as shown in Figure 5-5 (g). The transfer of material to the pin is not continuous and appears as clusters on the wear scar of the pin. The wear track showed no evidence of aluminum adhesion as presented in Figure 5-5 (h). For the test conducted at 400 ºC, the pin wear scar was completely covered by material transfer (Figure 5-5 (i)) and no evidence of aluminum adhesion was formed inside the wear track (Figure 5-5 (j)).

The pin wear scars and the coating wear tracks formed on the 600 °C heat treated samples are presented in Figure 5-6. At all testing temperatures (25 ºC to 400 ºC), wear scars on the pins show no evidence of material transfer, only severe wear and plowing marks along the sliding direction were observed. All wear tracks were observed to have similar characteristics, which were severe plowing along the sliding direction and clusters of smeared aluminum from the counterface.

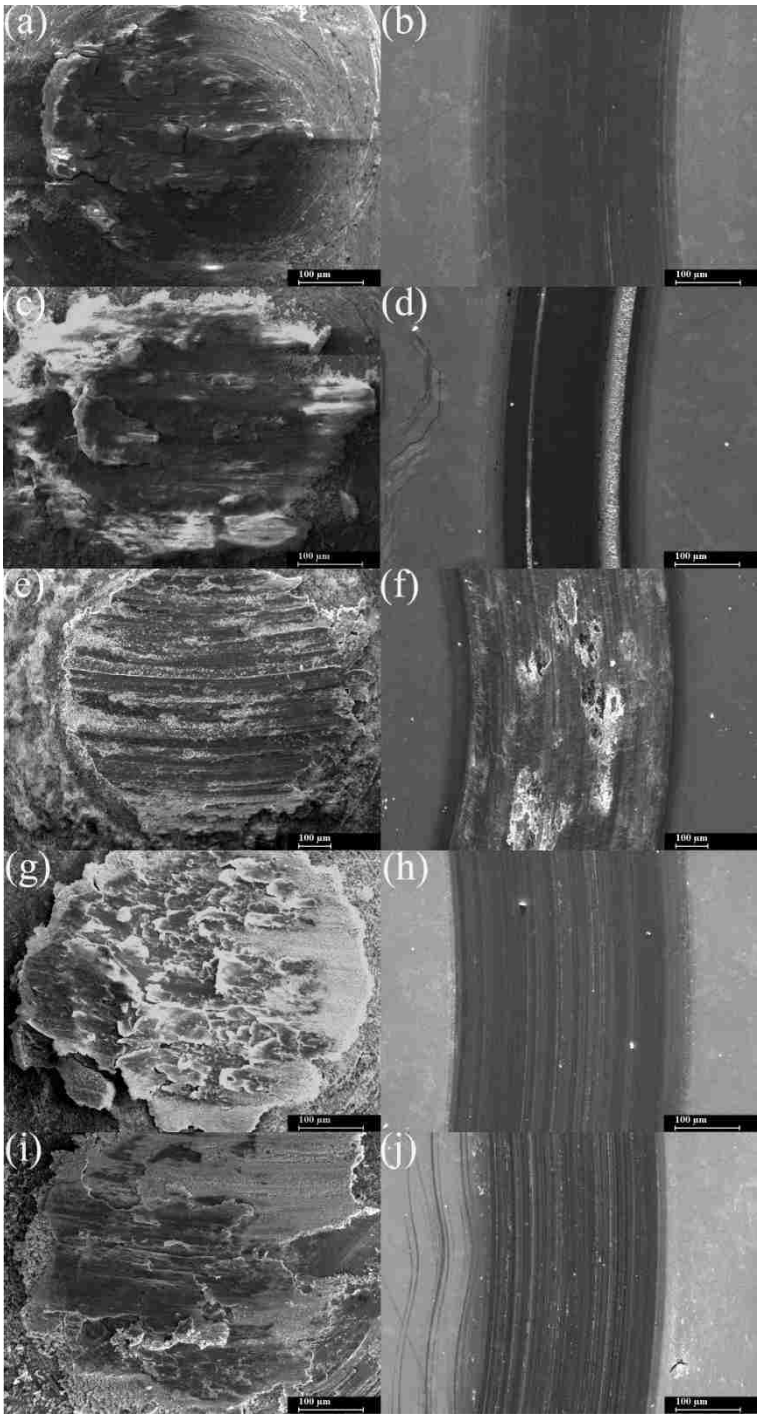

Figure 5-5: SEM image of W-DLC heat treated at 500 °C wear tracks and aluminum pins wear scar after testing at (a), (b) 25 °C, (c), (d) 100 °C, (e), (f) 200 °C, (g), (h) 300 °C and (i), (j) 400 °C.

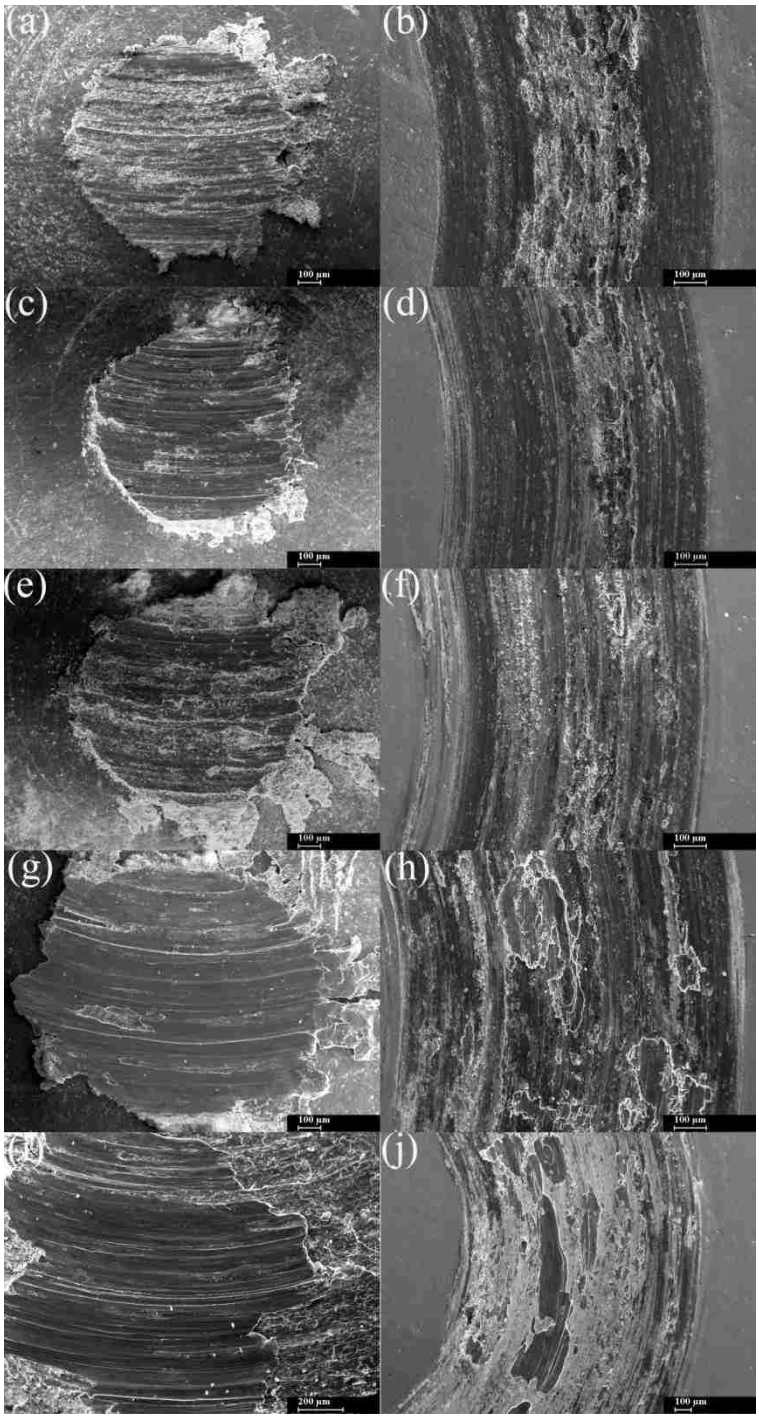

Figure 5-6: SEM image of W-DLC heat treated at 600 °C wear tracks and aluminum pins wear scar after testing at (a), (b) 25 °C, (c), (d) 100 °C, (e), (f) 200 °C, (g), (h) 300 °C and (i), (j) 400 °C.

5.4 Discussion

Heat treatment of the W-DLC coating led to the formation of WO_3 rich layer (Figures 5-1 and 5-2) and was observed to have a low COF and direct relation to material transfer. SEM observations of the counterface slid against the coating heat treated at 500 ºC showed material transfer to the Al pin tested at 25 ºC (Figure 5-5 (a)). The formation of material transfer from the coating to the pin is commonly observed for DLC and attributed to the low COF [15], [16]. A low average COF of 0.11 was also observed at 100 °C and SEM observations revealed material transferred on the counterface, unlike that observed in an earlier study [8].

The difference noted here can be attributed to the formation of an oxide rich layer on the surface as a result of heat treatment. The WO_3 acted as a protective sacrificial layer assisting the formation of material transfer on the Al pin which led to the low COF observed. At 200 ºC the WO_3 layer could not provide the protection or the sufficient aid needed to form the material transfer. This was evident from aluminum adhesion with significant coating wear observed in Figure 5-5 (e), (f). The COF curve in Figure 5-3 shows that the sliding started at a low COF value of 0.12 for the first 100 cycles. Thereafter, the COF gradually increased to 0.57 and the value remained steady for the rest of the test. This indicating that the WO_3 layer (formed due to annealing at 500 ºC) was consumed within the first 100 cycles and was not regenerated to sustain material transfer formation and the low COF. The material transfer was again observed on the Al pin tested at 300 ºC, yet the average COF was 0.36 as shown in Figure 5-4 (a). The COF curve (Figure 5-3 (b)), showed large fluctuations from 0.2 to 0.6 and aluminum adhesion was observed inside the wear track (Figure 5-5 (h)). In addition, material transfer

accumulated only in the form of patches that covered the pin surface (Figure 5-5 (g)), which left some areas of the pin exposed for interactions for higher levels of adhesion. The observations noted can be attributed to two competing mechanisms, (1) consumption rate of the material transfer during sliding; (2) material transfer formation rate, which was observed to consist primarily of W oxide in previous study [17], [18]. Further detailed investigation of the coating surface and material transfer chemistry is needed to better understand the mechanisms at 300 ºC. The test performed at 400 ºC on the heat treated sample at 500 ºC formed a material transfer that completely covered the counterface (Figure 5-5 (i)). Indicating that the material transfer is formed as it is being continuously replenished, thus forming a stable and protective material transfer on the Al pin which led to the low COF of 0.11.

The W-DLC coating heat treated at 600 ºC was found to have a negative effect on the coating's tribological behaviour. The COF was higher with values ranging from 0.5 to almost 1, in addition the wear rates were much higher (Figure 5-4 (a)) ranging from 8.01×10^{-5} mm^3/Nm to 1.42×10^{-4} mm^3/Nm. The high COF is attributed to absence of the protective and lubricious material transfer to the Al pin at all test temperatures. XRD of the coating heat treated at 600 ºC (Figure 5-2) showed evidence of severe oxidation resulted in SiO_2 the formation from the substrate.

5.5 Summary and Conclusions

- W-DLC coating heat treated at 500 °C have reduced the COF to as low as 0.05 at 100 ºC, where the as-deposited W-DLC tends to exhibit a higher COF.
- The low COF at 100 °C testing temperature, of the COF of coating heat treated at 500 °C attributed to the formation of material transfer, aided by the WO_3 layer.
- At 200 °C and 300 °C testing temperatures, the oxide layer was consumed within the first 100 sliding cycles, leading to high COF.
- Testing at 400 °C led to the regeneration of oxide layer as it was consumed, which stabilized and aided the material transfer formation.
- Annealing the W-DLC coating at 600 °C resulted in severe oxidation; coating wear and high COF were observed at testing temperatures ranging from 25 °C to 400 °C.

References

[1] E. Konca, Y.-T. Cheng, A. M. Weiner, J. M. Dasch, and A. T. Alpas, "Elevated temperature tribological behavior of non-hydrogenated diamond-like carbon coatings against 319 aluminum alloy", *Surface and Coatings Technology*, vol. 200, no. 12–13, pp. 3996–4005, 2006.

[2] A. A. Gharam, M. J. Lukitsch, M. P. Balogh, and A. T. Alpas, "High temperature tribological behaviour of carbon based (B4C and DLC) coatings in sliding contact with aluminum", *Thin Solid Films*, vol. 519, no. 5, pp. 1611–1617, 2010.

[3] W. Ni, Y.-T. Cheng, A. M. Weiner, and T. A. Perry, "Tribological behavior of diamond-like-carbon (DLC) coatings against aluminum alloys at elevated temperatures", *Surface and Coatings Technology*, vol. 201, no. 6, pp. 3229–3234, 2006.

[4] S. Sattel, J. Robertson, and H. Ehrhardt, "Effects of deposition temperature on the properties of hydrogenated tetrahedral amorphous carbon", *Journal of Applied Physics*, vol. 82, no. 9, pp. 4566–45778, 1997.

[5] T. Mikami, H. Nakazawa, M. Kudo, and M. Mashita, "Effects of hydrogen on film properties of diamond-like carbon films prepared by reactive radio-frequency magnetron sputtering using hydrogen gas", *Thin Solid Films*, vol. 488, no. 1–2, pp. 87–92, 2005.

[6] W.-J. Wu and M.-H. Hon, "Thermal stability of diamond-like carbon films with added silicon", *Surface and Coatings Technology*, vol. 111, no. 2–3, pp. 134–140, 1999.

[7] R. Fu, Y. Mei, M. Fu, X. Liu, and P. Chu, "Thermal stability of metal-doped diamond-like carbon fabricated by dual plasma deposition", *Diamond and Related Materials*, vol. 14, no. 9, pp. 1489–1493, 2005.

[8] A. A. Gharam, M. J. Lukitsch, M. P. Balogh, N. Irish, and A. T. Alpas, "High temperature tribological behavior of W-DLC against aluminum", *Surface and Coatings Technology*, vol. 206, no. 7, pp. 1905–1912, 2011.

[9] C. Muratore and A. Voevodin, "Chameleon Coatings: Adaptive Surfaces to Reduce Friction and Wear in Extreme Environments", *Annual Review of Materials Research*, vol. 39, no. 1, pp. 297–324, 2009.

[10] M. Woydt, A. Skopp, I. Dörfel, and K. Witke, "Wear engineering oxides/anti-wear oxides", *Wear*, vol. 218, no. 1, pp. 84–95, 1998.

[11] A. Erdemir, "A crystal-chemical approach to lubrication by solid oxides", *Tribology Letters*, vol. 8, pp. 97–102, 2000.

[12] M. B. Peterson, S. F. Murray, and J. J. Florek, "Consideration of Lubricants for Temperatures above 1000 F", *Tribology Transactions*, vol. 2, no. 2, pp. 225–234, 1959.

[13] I. Allam, "Solid lubricants for applications at elevated temperatures", *Journal of materials science*, vol. 26, pp. 3977–3984, 1991.

[14] S. Xu and L. Diao, "Study of tungsten oxidation in O[sub 2]/H[sub 2]/N[sub 2] downstream plasma", *Journal of Vacuum Science & Technology A*, vol. 26, no. 3, p. 360, 2008.

[15] F. G. Sen, Y. Qi, and A. T. Alpas, "Material transfer mechanisms between aluminum and fluorinated carbon interfaces", *Acta Materialia*, vol. 59, no. 7, pp. 2601–2614, 2011.

[16] A. Erdemir, C. Bindal, J. Pagan, and P. Wilbur, "Characterization of transfer layers on steel surfaces sliding against diamond-like hydrocarbon films in dry nitrogen", *Surface and Coatings Technology*, vol. 77, pp. 559–563, 1995.

[17] T. W. Scharf and I. L. Singer, "Third Bodies and Tribochemistry of DLC Coatings", in *Tribology of Diamond-Like Carbon Films*, no. Dlc, C. Donnet and A. Erdemir, Eds. Springer, 2008, pp. 201–236.

[18] O. Greenwood, S. Moulzolf, and P. Blau, "The influence of microstructure on tribological properties of WO_3 thin films", *Wear*, vol. 232, pp. 84–90, 1999.

CHAPTER 6
TEMPERATURE EFFECT ON THE TRIBOLOGICAL BEHAVIOUR OF W-DLC AND H-DLC

6.1 Introduction

Diamond-like carbon coatings have been studied with increasing interest for the past decade because of their low friction and wear behaviour, particularly against aluminum and its alloys. However, the term DLC includes a wide range of amorphous carbons with various chemical compositions and alloying elements that directly influence their tribological behaviour in different environments. Humidity and moisture was found to play a critical role in reducing the coefficient of friction (COF) of hydrogen-free DLC [1] [2] [3]. The findings were confirmed by first principle calculations, illustrating that as water molecules from the atmosphere approach the dangling carbon bond, the molecule dissociates to H and OH, passivating the dangling bonds, thus minimizing the interatomic interactions and reducing the COF [4]. However, humidity was found to have a negative effect on hydrogenated DLC (H-DLC). Other studies found that as relative humidity increased, the COF of H-DLC increases [5], [6], [7]. Several studies attributed this behaviour to physical adsorption of the water molecules, which might lead to an increase in interatomic interactions. However, the process proved reversible and no tribo-chemical interactions were observed [8], [9]. Others found that silicon containing DLC was insensitive to humidity, compared to pure non-doped DLC. This was attributed to the formation of SiO_2 at the sliding interface and the increase in sp^3 content caused by the incorporation of Si in DLC [10] [11].

Another common environmental effect on the friction and wear of DLC is temperature. H-DLC was found to withstand up to 200 ºC before hydrogen began to desorb, freeing dangling carbon bonds that interacted with the mating surface [12] [13] [14]. This study will investigate the effects of temperature (-10 ºC >T< 500 ºC) on the tribological behaviour of W-DLC and H-DLC sliding against 319 Al pins.

6.2 Experimental details

Coatings were deposited on M2 steel coupons at 25.4 mm. W-DLC was deposited using a physical vapour deposition (PVD) system. The M2 steel surfaces were first cleaned by Ar glow discharge, and then a Cr layer was deposited to promote adhesion of the DLC on the steel substrate. The W-DLC coating had a hardness of 20.1 ± 2.9 GPa, and an elastic modulus of 166.5 ± 8.6 GPa. The hardness of the W-DLC coating was 8.7 ± 1.7 GPa, and the elastic modulus was 104.3 ± 18.8 GPa. According to X-ray photoelectron spectroscopy (XPS) analysis, the W-DLC coating consisted of 20 at% of W and 80 at% of C.

H-DLC coating was deposited using a plasma-assisted chemical vapour deposition (PACVD) of the DLC, using methane as a reactive gas. The H-DLC coating had a hardness of 20.1 ± 2.9 GPa and an elastic modulus of 166.5 ± 8.6 GPa. Elastic recoil detection (ERD) analysis at 2.0 MeV indicated that the DLC layer consisted of 69 at% carbon and 31 at% hydrogen.

The high-temperature tribological behaviour of the DLC coatings against 319 Al was tested using a high temperature CSM tribometer. For sub-zero temperatures, testing

was conducted using a liquid cell fitted to the tribometer at which both the DLC coating and the 319 Al pin were submerged in liquid nitrogen throughout the testing duration. Thus, the contact was submerged and prevented water condensation that may have lubricated or interfered with the friction and wear results. All tests were conducted at 0.1 m/s with 5 N load for 1000 sliding cycles.

6.3 Results

6.3.1 Friction at elevated temperature

The friction of both W-DLC and H-DLC against 319 Al with 5 N load was shown to be highly dependent on the testing temperature. As shown in Figure 6-1, the COF of W-DLC at 25 ºC was at 0.35 and within 100 cycles, the COF decreased to a steady state value of 0.20. While at 200 ºC, the COF started at 0.55 and fluctuated between 0.6 and 0.7 for the duration of the test. However, at 400 ºC, the COF started with a very high running-in COF value of 0.8, but within 100 cycles the COF reached a steady state of 0.18 similar to that observed at 25 ºC.

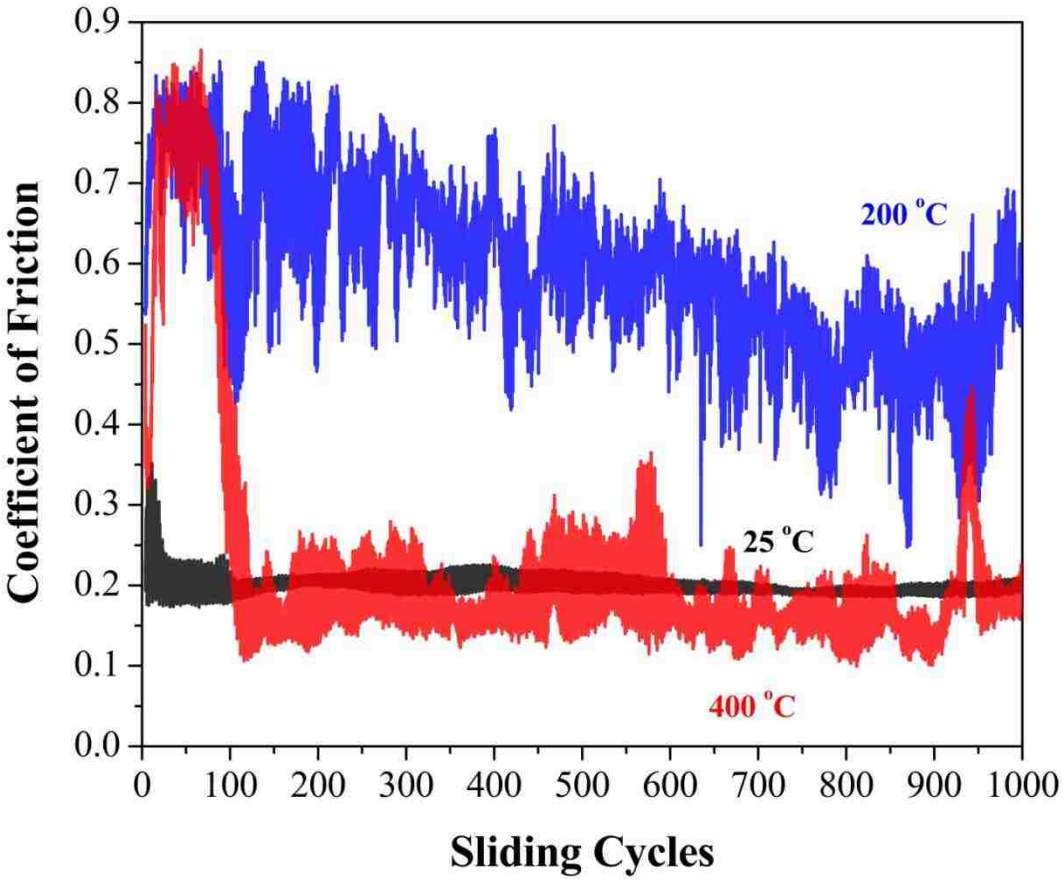

Figure 6-1: COF of W-DLC sliding against 319 Al at 25 °C, 200 °C and 400 °C.

The COF of H-DLC showed a different trend (Figure 6-2). The COF at room temperature was observed to have a high initial running-in period with a COF of 0.65, and it reached a steady state COF of 0.15 within the first 50 cycles. At 200 °C, the steady state of 0.06 was reached after a running-in period that lasted 100 cycles. The COF at 400 ºC had an initial running-in period for 200 cycles, and the COF started to increase to and average steady-state COF of 0.64.

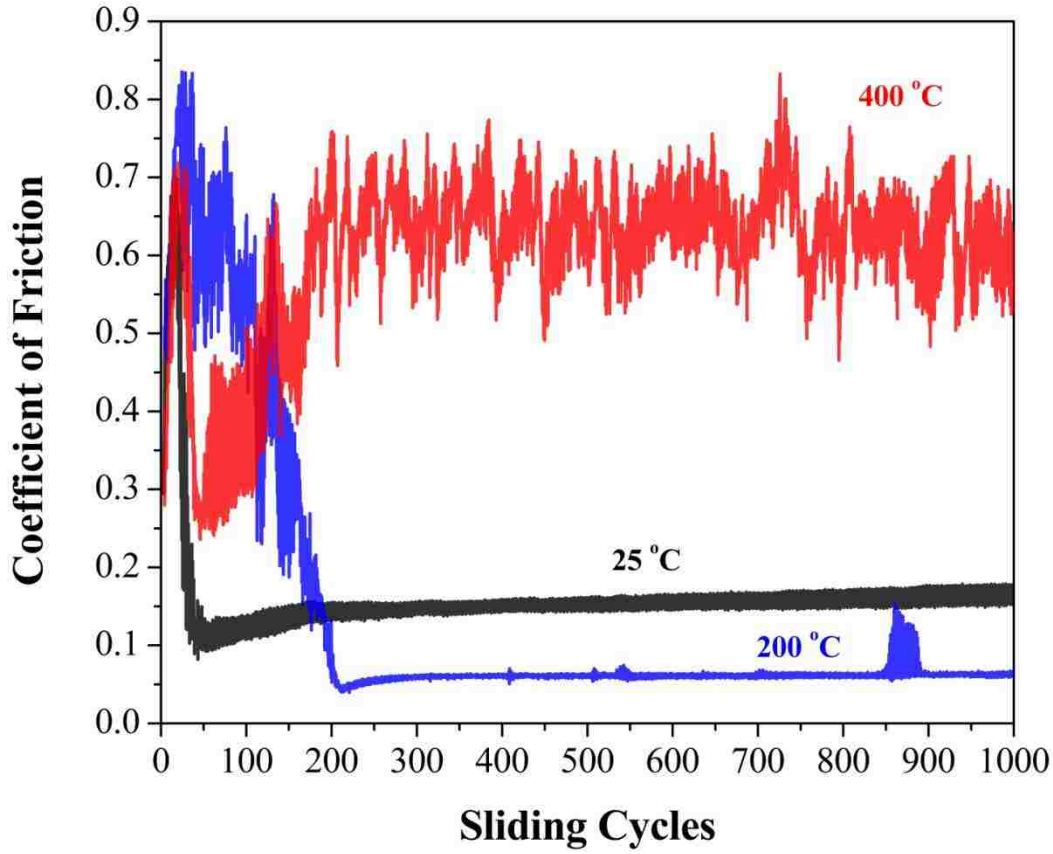

Figure 6-2: COF of H-DLC sliding against 319 Al at 25 °C, 200 °C and 400 °C.

6.3.2 Effects of subzero temperatures

The friction of the DLC coatings was also investigated at sub-zero temperatures. For these experiments, liquid nitrogen was used to cool the counterparts and the surrounding atmosphere to mimic cold or freezing operating temperatures. Liquid nitrogen was poured into the liquid cell and maintained a level above the point of contact throughout the test duration to eliminate the effects of water and condensation on friction and wear behaviour. A temperature-reading thermocouple located below the coupon during testing indicated beyond the detection limit of -10 ºC. As shown in Figure 6-3, both DLC coatings generated COFs lower than the uncoated 52100 steel reference. 319 Al against uncoated 52100 Steel was found to start at a COF of 0.20 followed by 100

cycle running-in period with COF as high as 0.65. The COF for the testing duration fluctuated at an average of 0.50. The W-DLC coating had a steady state COF of 0.18. However, steady state was reached after 300 cycles of running-in period with COF as high as 0.85. In H-DLC, the steady state COF of 0.18 was reached after a much shorter running-in period of only 50 sliding cycles with COF as high as 0.50.

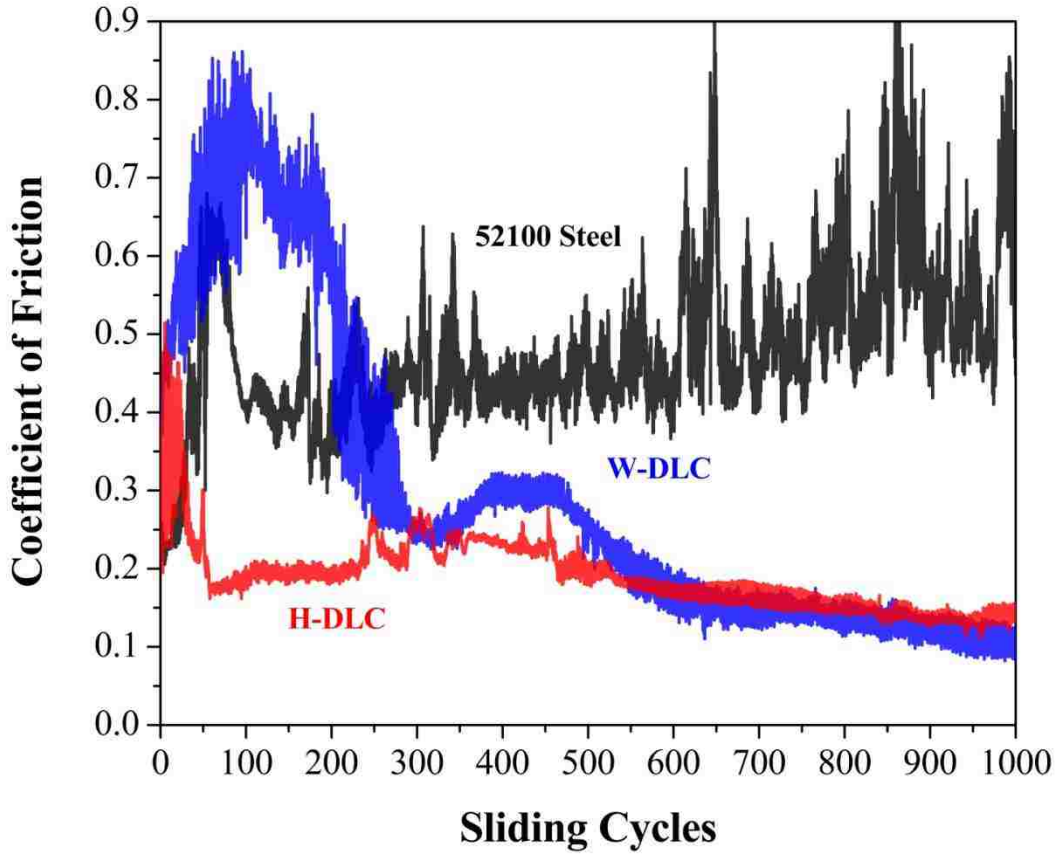

Figure 6-3: COF of H-DLC, W-DLC and uncoated 52100 steel sliding against 319 Al at below freezing temperature in liquid nitrogen.

Despite the low COF of W-DLC, the coating had the highest wear rate of 9.11 x 10^{-6} mm^3/Nm, and H-DLC had the lowest wear rate of 1.64 x 10^{-6} mm^3/Nm, as shown in

Figure 6-4. Uncoated 52100 steel fell somewhere in between, with a wear rate of 4.33 x 10^{-6} mm^3/Nm. Conversely, as shown in Figure 6-4, the pin-wear rates of both H-DLC and W-DLC were 2.22 x 10^{-7} mm^3/Nm and 4.22 x 10^{-7} mm^3/Nm, respectively, which were lower than the uncoated 52100 steel with the wear rate of 6.7x10^{-6} mm^3/Nm.

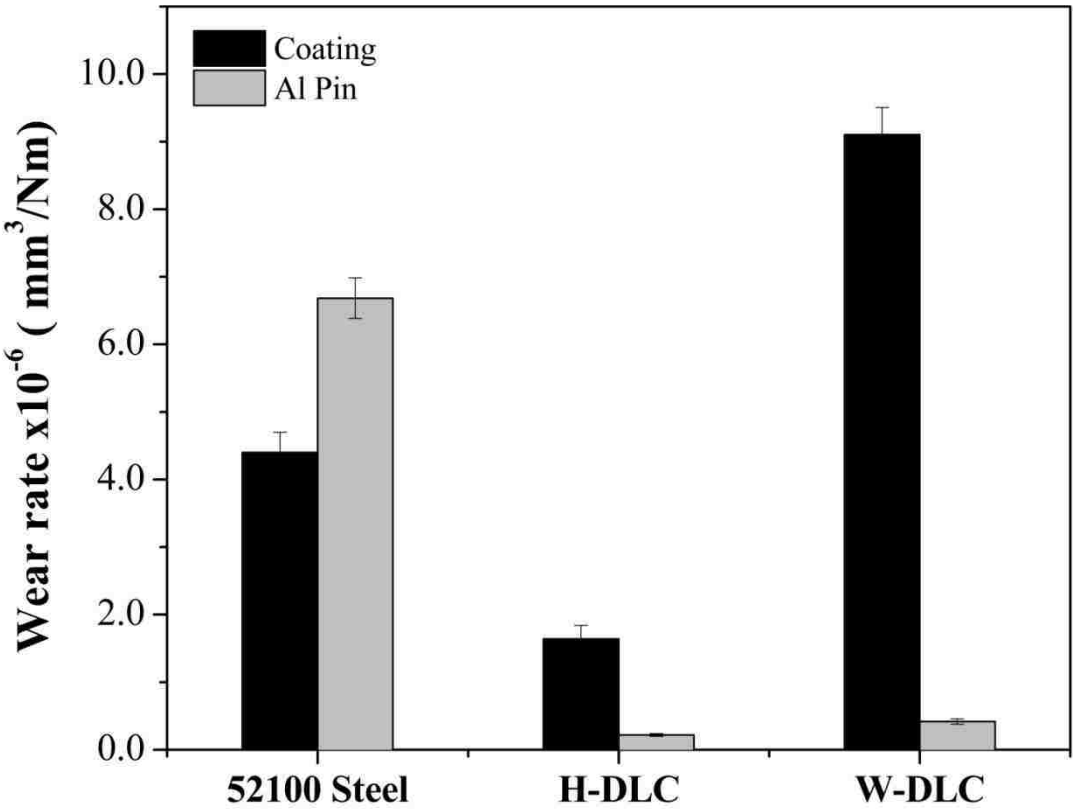

Figure 6-4: Wear rates of H-DLC, W-DLC, uncoated 52100 steel and 319 Al pins after testing at subzero temperatures.

SEM images of the uncoated steel show significant amounts of aluminum adhesion and debris along the sides of the wear track (Figure 6-5 (a)). Both DLC wear tracks shown in Figure 6-5 (b) and (c) are much narrower than that of uncoated 52100 steel. Indeed, the H-DLC wear track is barely visible (Figure 6-5 (c)). As shown in Figure

6-5 (d)-(f), the 319 Al wear scars after the sliding experiments against H-DLC and W-DLC showed no signs of material transfer, which is commonly observed to be a major contributor to the low COF of DLC coatings.

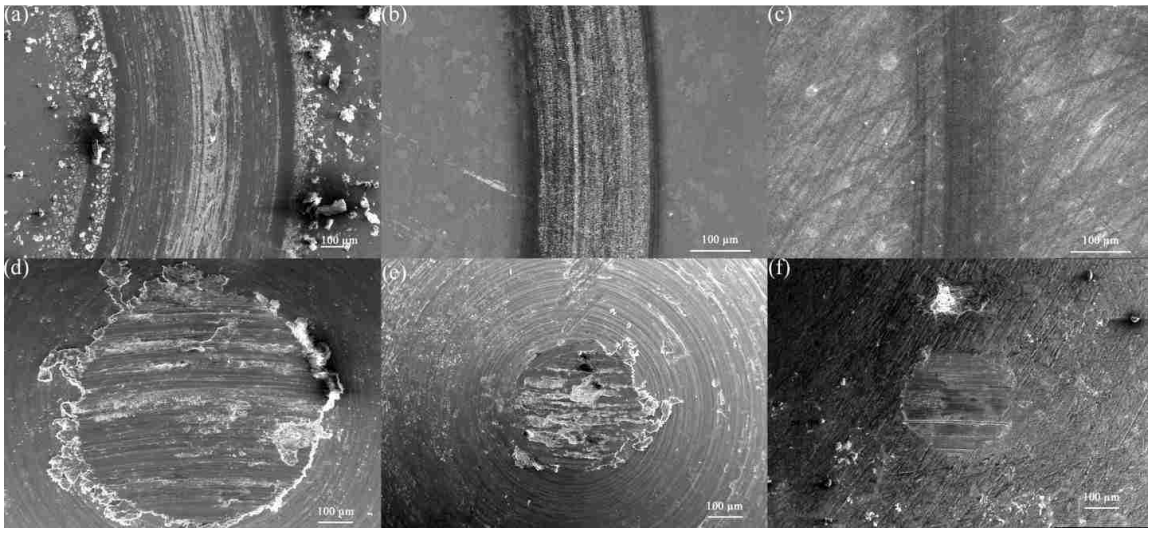

Figure 6-5: SEM of (a) Uncoated 52100 steel, (b) W-DLC, (c) H-DLC wear tracks and 319 aluminum pins wear scar after testing at subzero temperature against (d) Uncoated 52100 steel, (e) W-DLC, (f) H-DLC.

6.4 Discussion

At sub-zero temperatures (T < -10 ºC), both DLC coatings generated a low COF of 0.18. H-DLC, however, had the least amount of wear (1.64 x 10^{-6} mm^3/Nm) compared to W-DLC and uncoated 52100 steel against 319 Al. Pin wear was also the lowest against H-DLC (2.20 x 10^{-7} mm^3/Nm) compared W-DLC and uncoated 52100 steel. The investigations of pin surface showed no evidence of material transfer when tested against both DLC coatings at T < -10 ºC, which typically forms when low COF is observed for

DLC [15]–[17]. Thus, the results showed that at sub-zero temperatures, material transfer may not be as critical as that observed for ambient atmosphere or elevated temperatures.

At elevated temperatures, the incorporation of tungsten and hydrogen in the DLC coatings influenced the friction and wear differently (Figure 6-6). H-DLC coating was found to lose its low COF property beyond 200 ºC. This was attributed to the loss of hydrogen at elevated temperatures, exposing dangling carbon bonds, which caused coating/counterface interactions leading to the observed high COF [14]. On the other hand, W-DLC was observed to reduce the COF to 0.1 at 400 ºC and 500 ºC, as shown in Figure 6-6. The low COF at elevated temperatures was attributed to the formation of passive tungsten oxide-rich material that was transferred from the coating to the aluminum counterface, thus minimizing carbon aluminum interactions at the sliding interface [18].

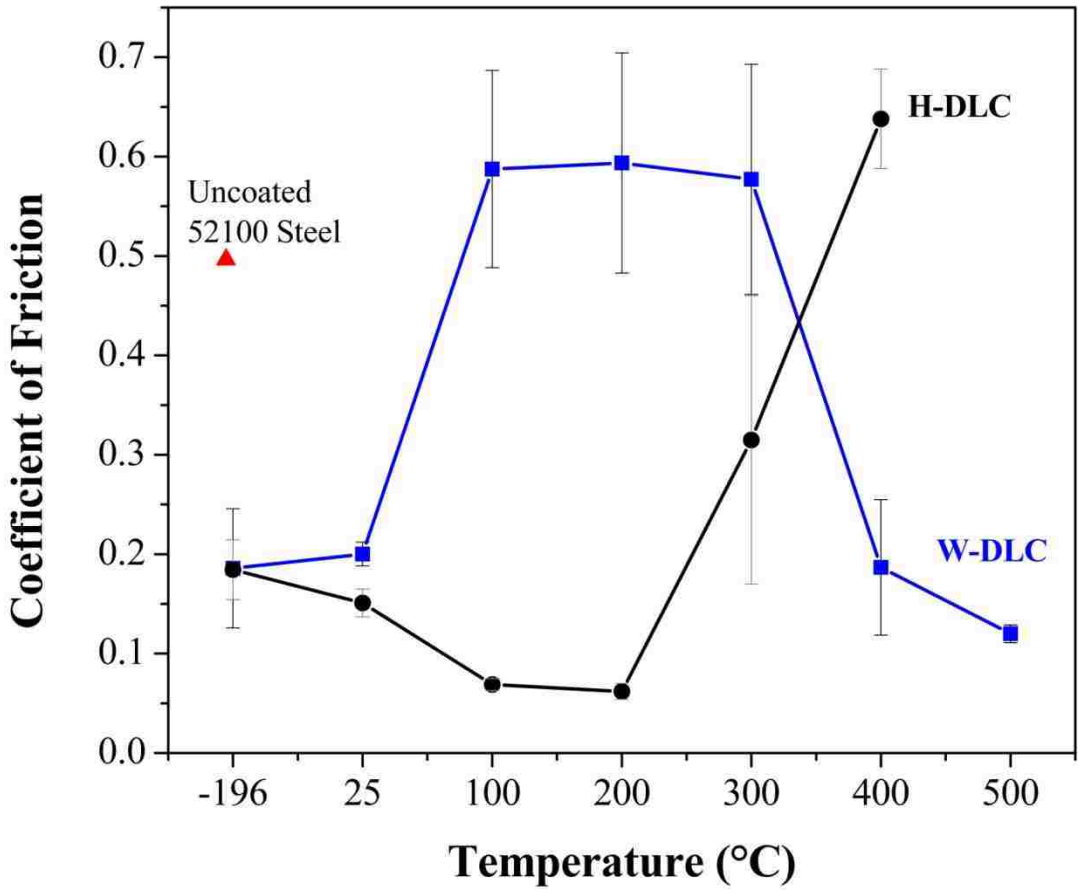

Figure 6-6: Average COF of W-DLC and H-DLC coatings as a function of temperatures ranging from -196 °C to 500 °C.

Both tungsten and hydrogen induce attractive low COF properties but seem activated at different temperature ranges. These mechanisms may provide insight into creating a chameleon coating by combining both elements in the DLC to activate low COF over a wider range of temperatures. By adding hydrogen, DLC would generate low COF of 0.09 up to 200 ºC. The presence of tungsten would generate WO_3 and reduce the COF to 0.1 at 400 ºC and 500 ºC. However, it is not clear how the addition of hydrogen and tungsten would affect the tribological behaviour at 300 ºC. Thus, further

investigation is needed to confirm this theory and show how the tribological behaviour of multi element-doped DLC differs from that of single element-doped DLC.

6.5 Conclusions

1) At elevated temperatures, both W-DLC and H-DLC were observed to generate low COF against 319 Al at different temperature ranges:
   a) W-DLC generated low COF at 400 ºC and 500 ºC.
   b) H-DLC generated low COF from 25 ºC up to 200 ºC.
2) Both W-DLC and H-DLC generated low COF of 0.18 at sub-zero temperatures below -10 ºC.
3) At sub-zero testing temperatures, it was observed that material transfer was required to generate low COF at temperatures less than -10 ºC.

References

[1] Y. Özmen, "The effect of humidity on the tribological behavior of diamond-like carbon (DLC) film coated on WC-Co by physical vapor deposition method", *Surface and Coatings Technology*, vol. 133–134, no. 1, pp. 455–459, 2000.

[2] E. Konca, Y.-T. Cheng, A. M. Weiner, J. M. Dasch, and A. T. Alpas, "Effect of test atmosphere on the tribological behaviour of the non-hydrogenated diamond-like carbon coatings against 319 aluminum alloy and tungsten carbide", *Surface and Coatings Technology*, pp. 1783–1791, 2005.

[3] A. Abou Gharam, M. J. Lukitsch, Y. Qi, and A. T. Alpas, "Role of oxygen and humidity on the tribo-chemical behaviour of non-hydrogenated diamond-like carbon coatings", *Wear*, vol. 271, no. 9–10, pp. 2157–2163, 2011.

[4] Y. Qi, E. Konca, and A. T. Alpas, "Atmospheric effects on the adhesion and friction between non-hydrogenated diamond-like carbon (DLC) coating and aluminum – A first principles investigation", *Surface Science*, vol. 600, no. 15, pp. 2955–2965, 2006.

[5] H. I. Kim, J. R. Lince, O. L. Eryilmaz, and A. Erdemir, "Environmental effects on the friction of hydrogenated DLC films", *Tribology Letters*, vol. 21, no. 1, pp. 51–56, 2006.

[6] H. Li, T. Xu, C. Wang, J. Chen, H. Zhou, and H. Liu, "Tribochemical effects on the friction and wear behaviors of a-C:H and a-C films in different environment", *Tribology International*, vol. 40, no. 1, pp. 132–138, 2007.

[7] C. Donnet, T. Le Mogne, L. Ponsonnet, M. Belin, A. Grill, V. Patel, and C. Jahnes, "The respective role of oxygen and water vapor on the tribology of hydrogenated diamond-like carbon coatings", *Tribology Letters*, vol. 4, pp. 259–265, 1998.

[8] A. Laikhtman, A. Lafosse, A., Le Coat, Y., Azria, R., Hoffman, "Interaction of water vapor with bare and hydrogenated diamond film surfaces", *Surface Science*, vol. 551, no. 1–2, pp. 99–105, 2004.

[9] H. Ronkainen and K. Holmberg, "Environmental and Thermal Effects on the Tribological Performance of DLC Coatings", in *Tribology of Diamond-Like Carbon Films*, no. Dlc, C. Donnet and A. Erdemir, Eds. USA: Springer, 2008, pp. 155–198.

[10] S. V. Hainsworth and N. J. Uhure, "Diamond like carbon coatings for tribology: production techniques, characterisation methods and applications", *International Materials Reviews*, vol. 52, no. 3, pp. 153–174, 2007.

[11] Š. Meškinis and A. Tamulevičienė, "Structure , Properties and Applications of Diamond Like Nanocomposite (SiO x Containing DLC) Films : A Review", *Materials Science*, vol. 17, no. 4, pp. 44–46, 2011.

[12] H. Ito, K. Yamamoto, and M. Masuko, "Thermal stability of UBM sputtered DLC coatings with various hydrogen contents", *Thin Solid Films*, vol. 517, no. 3, pp. 1115–1119, 2008.

[13] W. Ni, Y.-T. Cheng, A. M. Weiner, and T. A. Perry, "Tribological behavior of diamond-like-carbon (DLC) coatings against aluminum alloys at elevated temperatures", *Surface and Coatings Technology*, vol. 201, no. 6, pp. 3229–3234, 2006.

[14] A. A. Gharam, M. J. Lukitsch, M. P. Balogh, and A. T. Alpas, "High temperature tribological behaviour of carbon based (B4C and DLC) coatings in sliding contact with aluminum", *Thin Solid Films*, vol. 519, no. 5, pp. 1611–1617, 2010.

[15] T. W. Scharf and I. L. Singer, "Role of the Transfer Film on the Friction and Wear of Metal Carbide Reinforced Amorphous Carbon Coatings During Run-in", *Tribology Letters*, vol. 36, no. 1, pp. 43–53, 2009.

[16] A. Erdemir, C. Bindal, and J. Pagan, "Characterization of transfer layers on steel surfaces sliding against diamond-like hydrocarbon films in dry nitrogen", *Surface and Coatings Technology*, vol. 77, pp. 559–563, 1995.

[17] F. G. Sen, Y. Qi, and A. T. Alpas, "Material transfer mechanisms between aluminum and fluorinated carbon interfaces", *Acta Materialia*, vol. 59, no. 7, pp. 2601–2614, 2011.

[18] A. A. Gharam, M. J. Lukitsch, M. P. Balogh, N. Irish, and A. T. Alpas, "High temperature tribological behavior of W-DLC against aluminum", *Surface and Coatings Technology*, vol. 206, no. 7, pp. 1905–1912, 2011.

CHAPTER 7
EXPERIMENTAL INVESTIGATIONS OF WORK OF ADHESION BETWEEN DLC AND SINGLE CRYSTAL (111) ALUMINUM

7.1 Introduction

In Chapters 2 to 6, the friction of DLC was observed to be dependent on the testing condition. In tribological systems, friction and wear are greatly influenced by the chemical and mechanical interactions that occur between the sliding asperities. Earlier studies found that interfacial interactions and chemistry at the asperity level can greatly influence friction. It was observed that the friction increased significantly when the surface oxides were removed [1]. In 1939, Bowden and Hughes defined friction as minute adhesion that occurs at the real contact or between the asperity junctions [2].

Recently, molecular dynamic simulations were utilized to quantify the interatomic interactions between solids by calculating the work of adhesion (W_{ad}), which is the energy required to break interfacial bonds. This can be calculated using *ab initio* calculation, in other words, first principle calculation. W_{ad} for Al/Al and Al_2O_3/Al_2O_3 interfaces were investigated in vacuum [3]. The results showed that Al/Al had a W_{ad} of 0.45 J/m^2, which was much higher than the Al_2O_3/Al_2O_3 that exhibited a W_{ad} value of 0.18 J/m^2. Another study investigated the interfacial interactions between Al and ceramics (WC, VC, CrN, TiN, VN, and two types of Al_2O_3, one where the Al was oriented at the surface ($Al_2O_3^{Al}$), and the other where O was oriented at the surface ($Al_2O_3^{O}$)) [4]. The calculations showed that $Al/Al_2O_3^{Al}$ was the lowest (W_{ad} = 1.06 J/m^2), whereas $Al/Al_2O_3^{O}$ had the highest W_{ad} of 9.73 J/m^2. This result can be attributed to the

high surface energy of the $Al_2O_3^O$, which ranged from 4.45- 10.83 J/m^2 compared to 1.59 J/m^2 of the $Al_2O_3^{Al}$ surface. Various work of the adhesion values attained through first principle calculations in the literature are presented in Table 7-1.

The calculated W_{ad} showed that $Al/Al_2O_3^O$ Al/WC^W Al/WC^C configurations exhibited the highest W_{ad}, ranging from 4.08–9.73 J/m^2, which was attributed to the polar nature of the interfacial orientation. Consequently, from this calculation, Al will tend to adhere to these materials because the Al will separate from the bulk at only 1.52 J/m^2, whereas non-polar nitride ceramics exhibit the smallest values, ranging from 1.47-1.73 J/m^2. Further investigations showed that the Al surface has a low tendency of adhesion towards carbon, particularly when terminated with hydrogen, which creates a Van der Waals type of interactions at the interface, generating a W_{ad} ranging from 0.33–0.008 J/m^2 [5] [6] [7].

Table 7-1: Work of adhesion literature for various interfaces.

Interface	**Orientation**	**W_{ad} (J/m^2)**	**Ref.**
$Al/Al_2O_3^{Al}$	(111)[110]Al || (0001)[1010]Al_2O_3	1.06	[4]
$Al/Al_2O_3^{O}$	(111)[110]Al || (0001)[1010]Al_2O_3	9.73	[4]
Al/WC^{W}	(111)[110]Al || (0001)[1120]WC	4.08	[4]
Al/WC^{C}	(111)[110]Al || (0001)[1120]WC	6.01	[4]
Al/WC	(110)[110]Al || (1120)[0001]WC	3.14	[4]
Al/VC	(100)[001]Al || (100)[001]VC	2.14	[4]
Al/VN	(100)[001]Al || (100)[001]VN	1.73	[4]
Al/CrN	(100)[001]Al || (100)[001]CrN	1.45	[4]
Al/TiN	(100)[001]Al || (100)[001]TiN	1.52	[4]
Al/Al	Al(111) || (111)Al	1.52	[5]
Al/C (Diamond)	(111)Al || (111)C - 1x1	4.08	[5]
Al/C (Diamond)	(111)Al || (111)C - 2x1	0.33	[5]
Al/C (Graphite)	(111) [112]Al || (0001) [1010]C	0.11	[6]
Al/C:H	(111)Al || (111)C - 1x1:H	0.02	[5]
Al/C:OH	(111)Al || (111)C - 1x1:OH	0.2	[5]
C:H/C:H	(111)C - 1x1:H l || (111)C - 1x1:H	0.008	[7]
C:OH/C:OH	(111)C - 1x1:OH l || (111)C - 1x1:OH	0.02	[7]

Recently, the adhesion forces between solids were measured using an atomic force microscope (AFM). Y. Li and D. Li [8] investigated the adhesion between 3d transition metals (Ti, V, Cr, Mn, Fe, Co, Ni, Cu and Zn) and Si_3N_4 AFM tip in ambient air (22–45% RH). The adhesion between the silicon nitride tip and the tested surface was

evaluated by measuring the vertical deflection of the cantilever when the tip approached and when it left the sample surface. Ti and Mn were observed to have the highest adhesive force of 9 nN, while V, Co, and Ni had the lowest adhesive force of 4.5 nN. Studies also showed that the adhesive force was dependent on humidity in the atmosphere [9]. Studies of pull-off force using an AFM Si_3N_4 tip against silicon oxide was observed to first increase up to 75 nN at 70 %RH and then decrease with further increases in humidity [10]. Other studies showed that the capillary forces caused by moisture decreased with temperature. AFM measurements of pull-off as a function of temperature [11] showed that the adhesive force decreased from 1 N/m at room temperature to 0.6 N/m at 160 ºC. An investigation of FTIR confirmed that the liquid film was evaporated at high temperatures.

In this study, the work of adhesion was investigated using the nano-indentation technique equipped with a Berkovich diamond nano indenter and a high temperature stage. The study compares different DLC coatings (hydrogenated DLC, dopant-free DLC, and W-doped DLC) and their adhesion mitigation mechanisms at temperatures up to 200 °C. By understanding the adhesion mechanisms, engineers and designers will be able to tailor a coating chemistry that can be controlled and monitored by altering the recipe for the application.

7.2 Experimental details

The pull-off adhesion measurements were carried out using a calibrated nano-indentor (TI 950 TriboIndenter) equipped with a Berkovich diamond tip and a high temperature stage. The indentation experiments were carried out in depth control mode

with 5 sec loading time to 300 nm depth (h_{max}) to penetrate the surface oxide layer on the aluminum sample, followed by a 2 s. pause and a 20 s. unloading segment (Figure 7-1). Indentations were conducted on hydrogenated DLC (H-DLC), dopant-free DLC (DLC), tungsten-doped DLC (W-DLC) coatings, and (111) Al single crystal (SC Al) at 25 °C, 100 °C and 200 °C. SC Al was chosen to avoid measurement inconsistencies due to indenter falling on grain boundaries or other phases which may exist in other aluminum alloys. Prior to the elevated temperature experiments, each sample was heated to the desired temperature for 1 to 2 hours, and then the tip was held in contact with the heated surface for 10 to 20 min to insure that the tip reached the surface temperature and thermal drift was minimized. For each specimen, 9 indents were conducted at each temperature (shown in Appendix A), and between indents the tip was cleaned using a cotton swab and acetone. In this study, W_{ad} was calculated by integrating the area under the curve (Figure 7-1) and normalized by the final tip area, as described in Appendix A. The final tip area was calculated from the calibrated tip area function using the final depth (h_f).

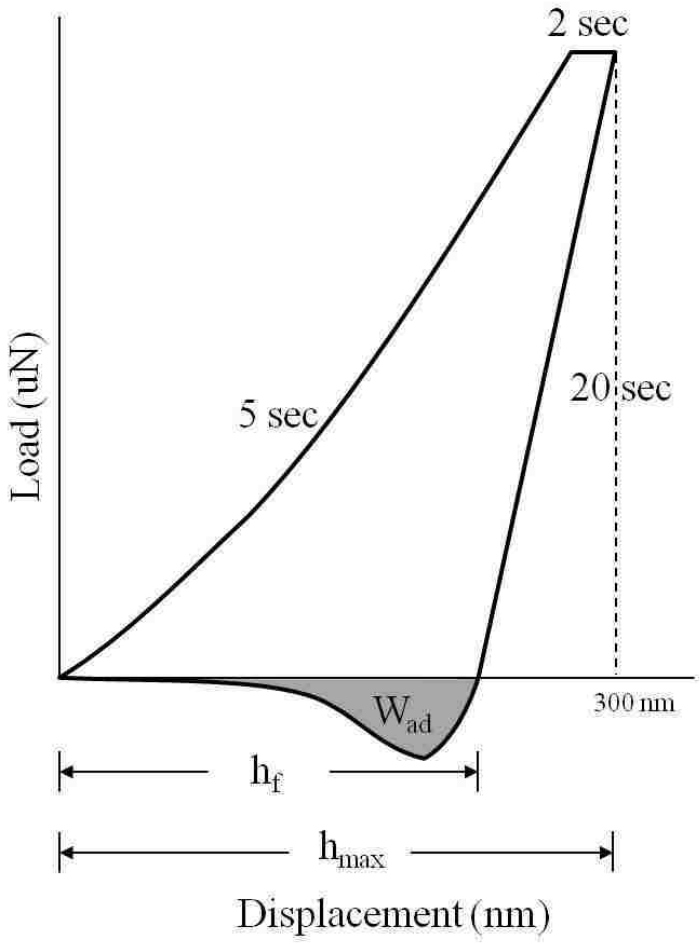

Figure 7-1: Loading-unloading schematic

7.3 Results

The three types of DLC coatings showed that the W_{ad} against diamond decreased with increase in temperature. The loading and unloading curves (Figure 7-2) of the H-DLC showed increases in displacement as the temperature increased from 25 ºC to 200 ºC, whereas the pull-off force decreased with increases in temperature, thus equating to W_{ad} of 0.15 J/m^2 at 25 ºC. As the temperature increased to 100 ºC and 200 ºC, the W_{ad} at both temperatures decreased to 0.011 J/m^2, as shown in Figure 7-6.

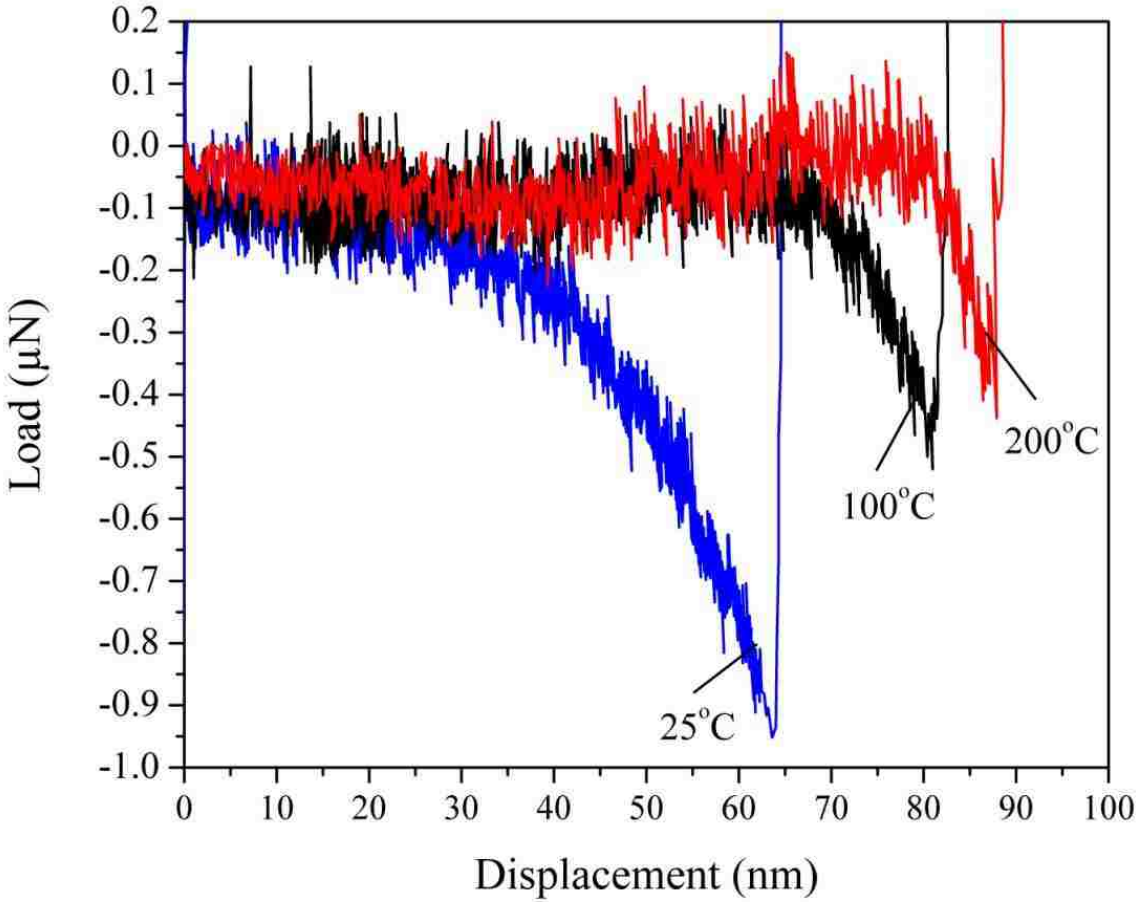

Figure 7-2: Typical load displacement curve of H-DLC as a function of testing temperature.

Dopant-free DLC and W-DLC showed trends similar to H-DLC with increases in displacement as the temperature increased and decreases in the pull-off force with increases in temperature, as shown in Figure 7-3 and Figure 7-4. However, the W_{ad} values of both dopant-free DLC and W-DLC had higher values compared to H-DLC. The calculated W_{ad} of the dopant-free DLC coating was 0.20 J/m^2 at 25 ºC. Similar to H-DLC, the W_{ad} decreased to 0.08 J/m^2 at 100 ºC and 0.069 J/m^2 at 200 ºC. The W-DLC had similar values to those observed for the dopant-free DLC. W_{ad} at 25 ºC was 0.19

J/m^2, and the values decreased to 0.063 J/m^2 at 100 ºC and 0.055 J/m^2 at 200 ºC, as presented in Figure 7-6.

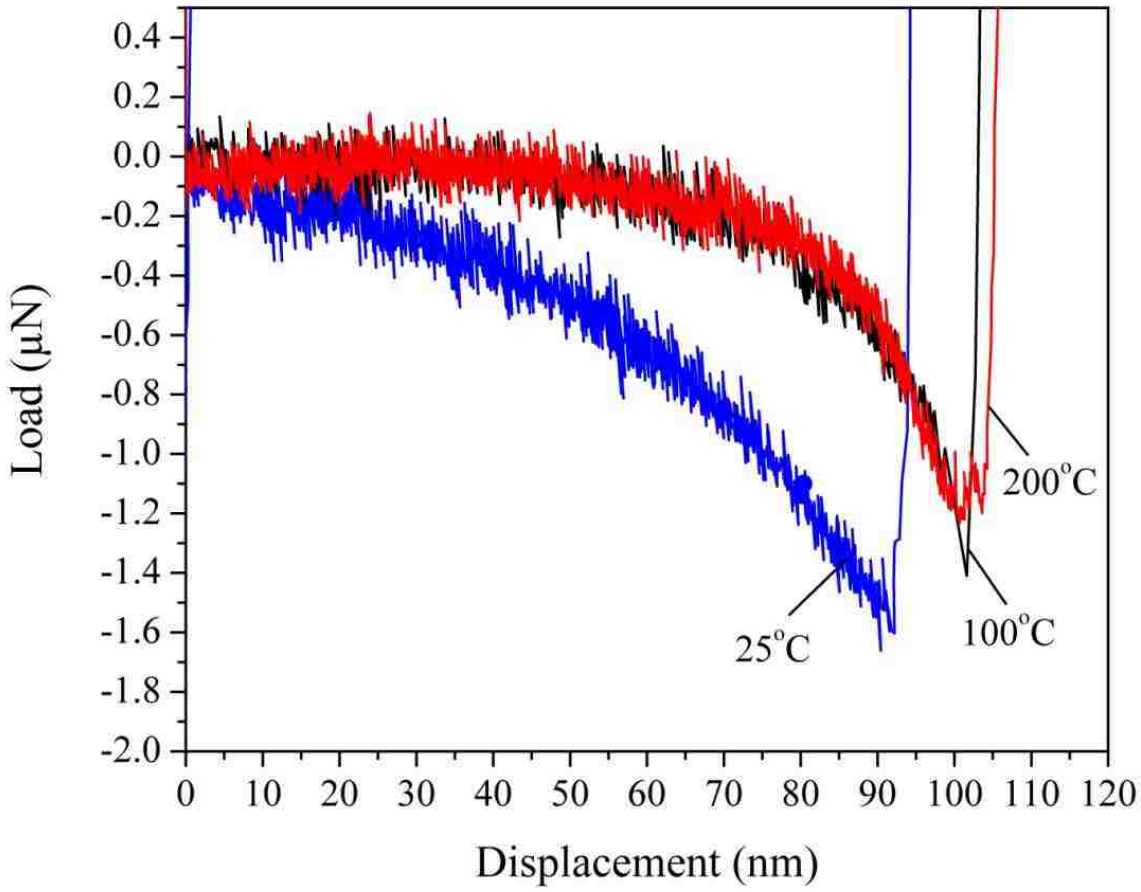

Figure 7-3: Typical load displacement curve of dopants free DLC as a function of testing temperature.

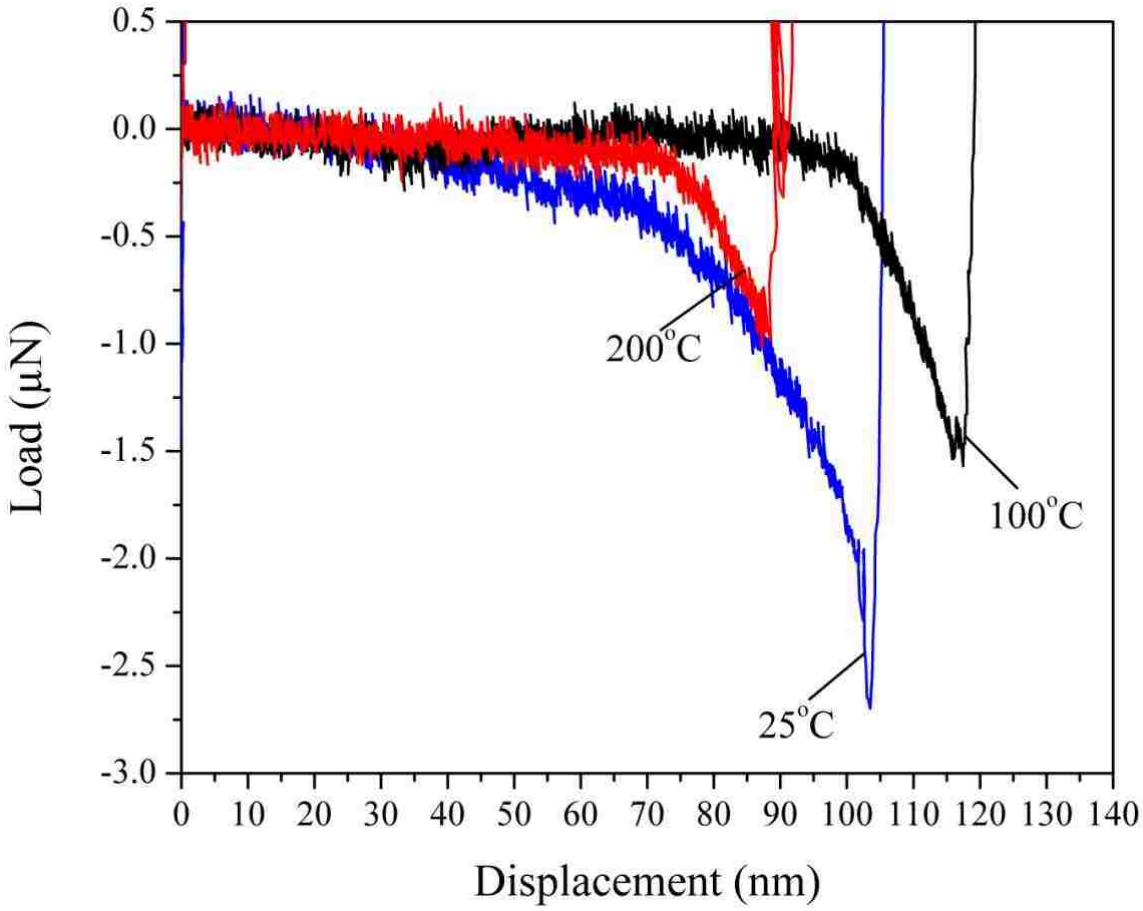

Figure 7-4: Typical load displacement curve of W-DLC as a function of testing temperature.

The W_{ad} of the SC Al was high compared to the three types of DLC coatings (Figure 7-7). However, the general trend of decreasing W_{ad} as temperature increased was observed. At 25 ºC, the calculated W_{ad} was 0.35 J/m^2, which decreased to 0.32 J/m^2 at 100 ºC and to 0.25 J/m^2 at 200 ºC.

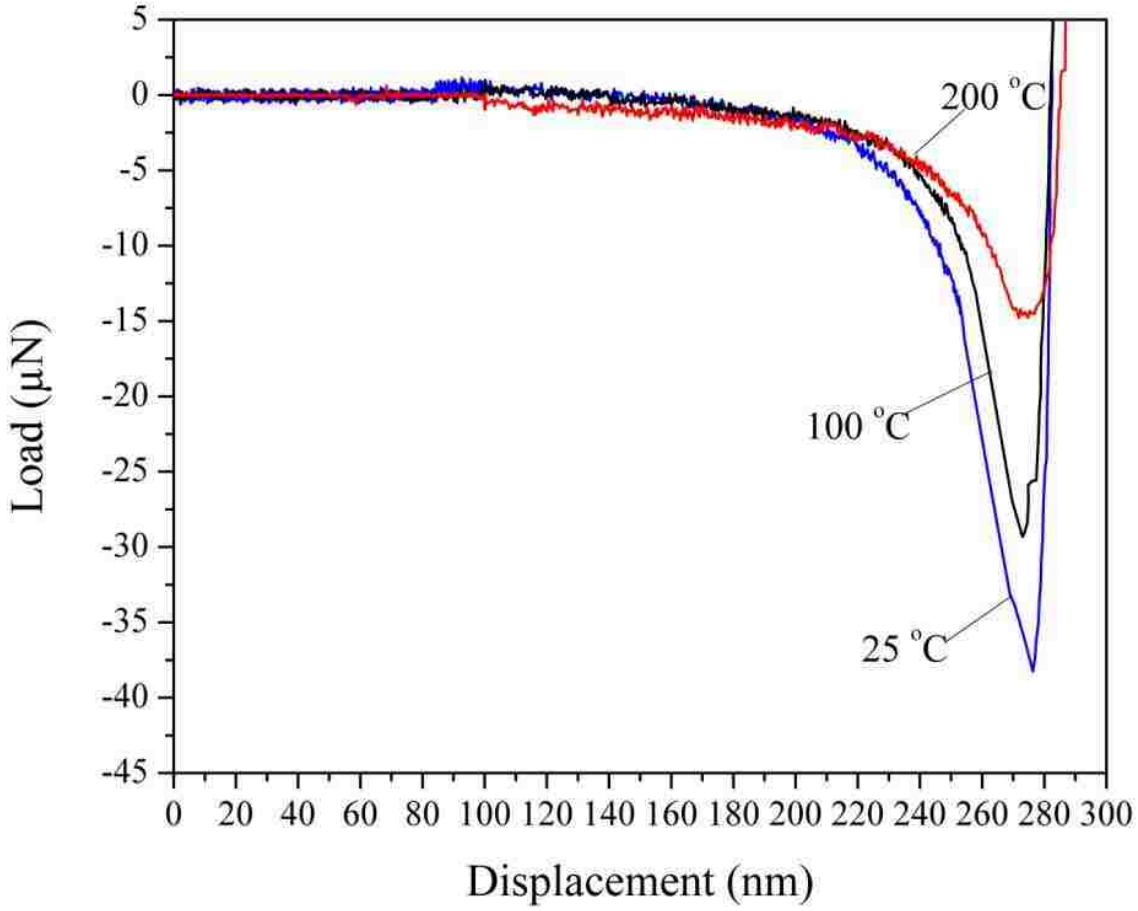

Figure 7-5: Typical load displacement curve of single crystal Aluminum (SC Al) as a function of testing temperature.

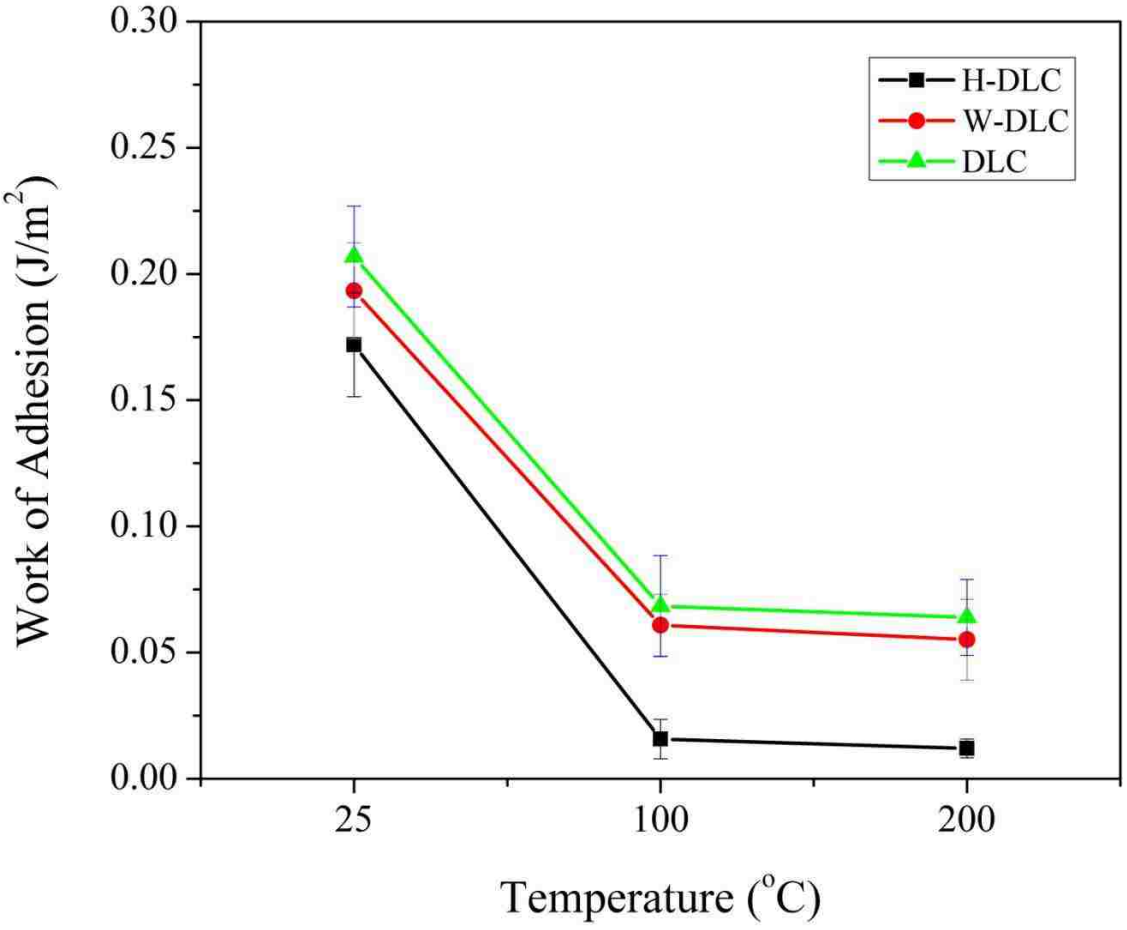

Figure 7-6: W_{ad} of hydrogen doped DLC (H-DLC), dopants free DLC (DLC) and Tungsten doped DLC (W-DLC) as a function of temperature.

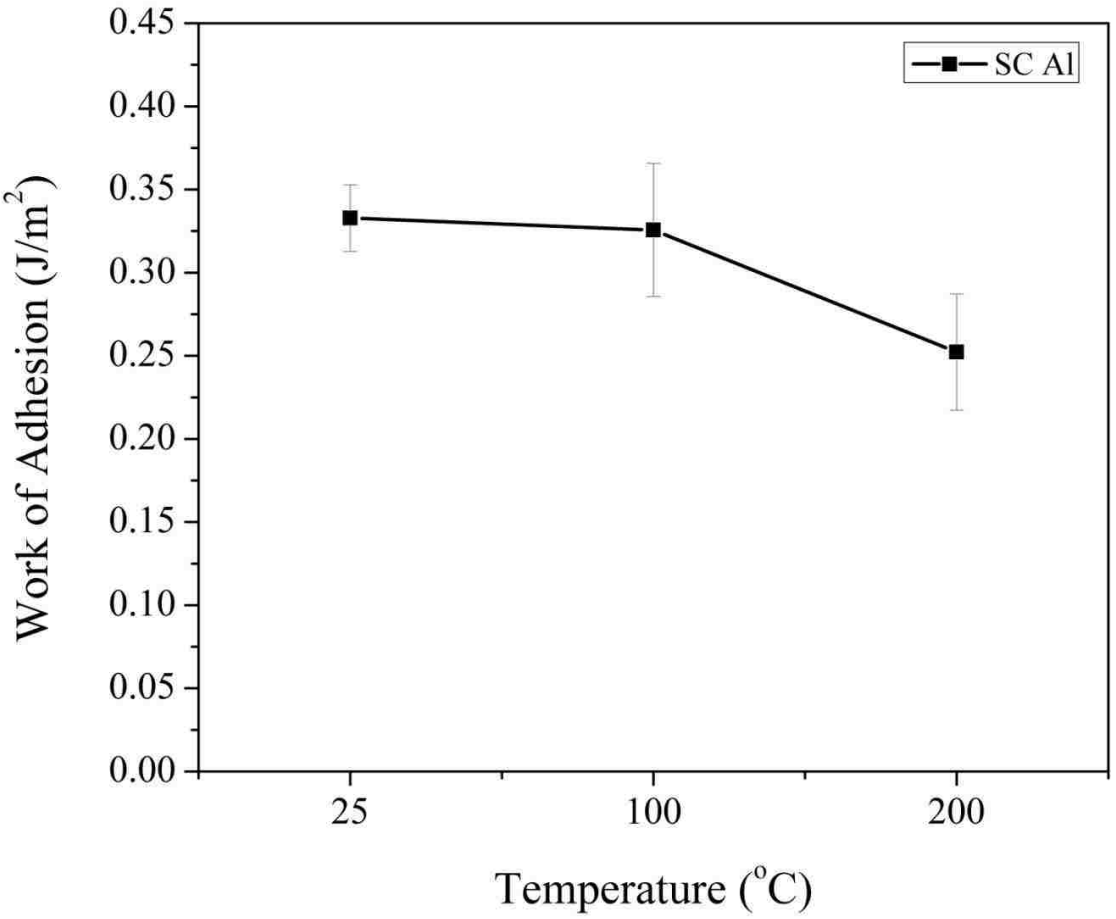

Figure 7-7: W_{ad} of SC Al as a function of temperature.

7.4 Discussion

The W_{ad} for all four samples was observed to decrease with temperature (Figure 7-9). This observation can be attributed to the presence of water molecules on the surface, as commonly observed in previous AFM studies [9]. In ambient air, the surface is usually covered with water molecules, which were observed to form a water bridge (meniscus) between the AFM tip and the sample surface [12]. When the contact surfaces were separated, the capillary water bridges formed at the contacts stretched until a certain distance of separation. The water bridge exerted a negative force on the tip, thus

contributing to the pull-off force of the adhesion [13]. These forces increased the adhesion force from approximately 30 nN at 10% RH to 70 nN at 70% RH, accounting for more than 50% of the adhesion force as observed in the Si_3N_4 AFM tip engaged with silica (SiO_2) [10], [14]. In this study, the decrease in W_{ad} can also be attributed to the meniscus forces caused by the presence of water molecules between the surface and the diamond indenter at 25 ºC, as shown in Figure 7-8.

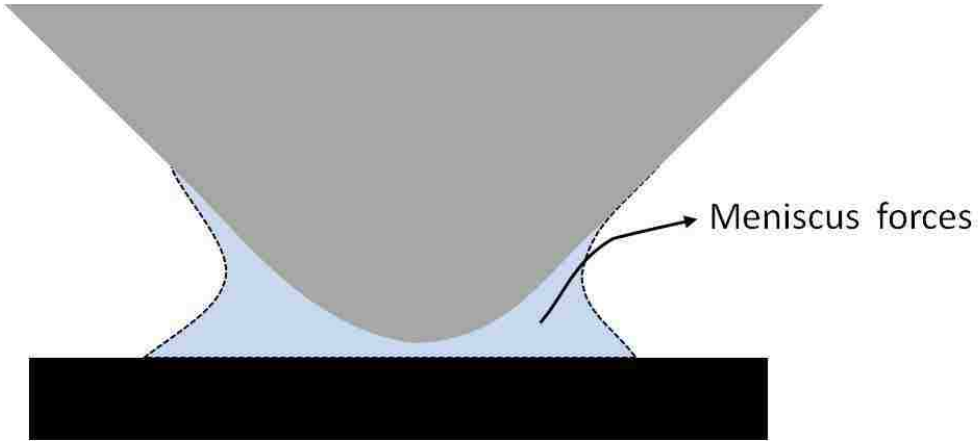

Figure 7-8: Schematic of meniscus forces due to presence of water molecules between the nano indenter tip and the specimen surface.

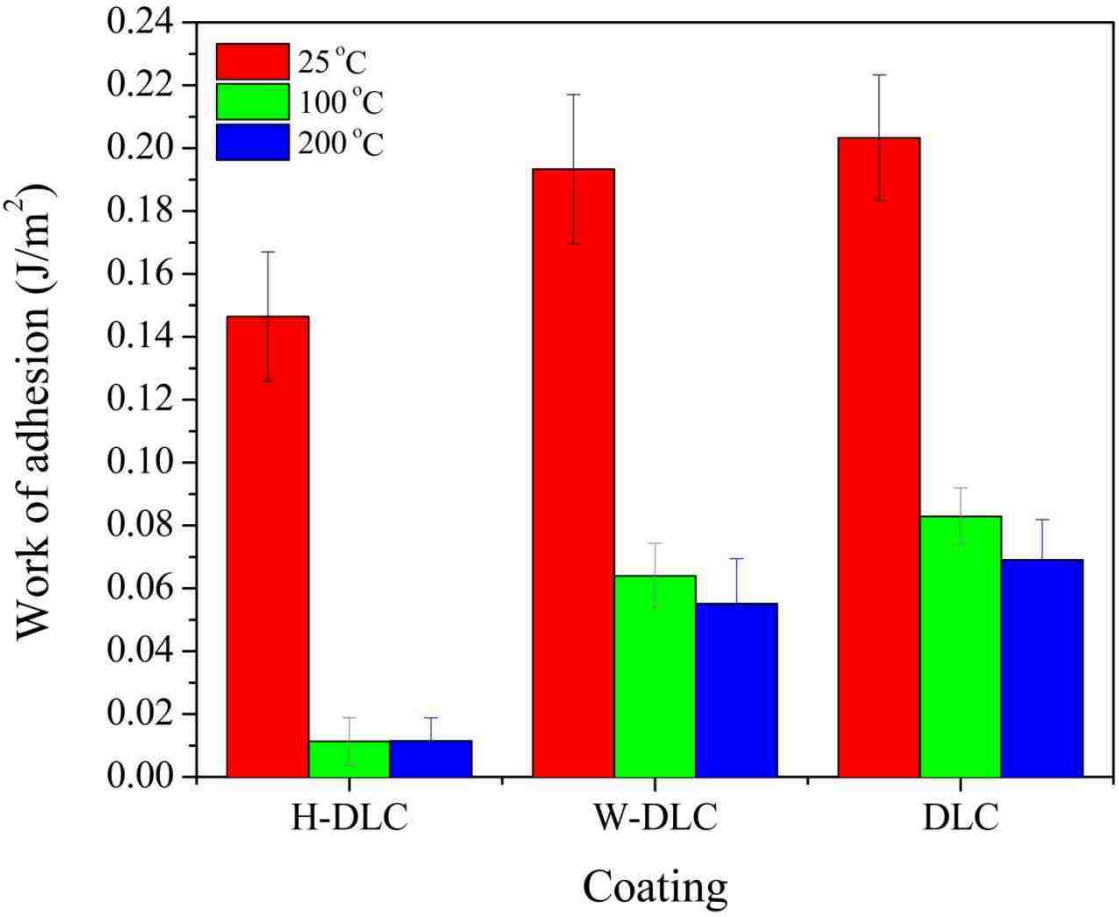

Figure 7-9: W_{ad} of H-DLC, dopants free DLC, W-DLC and SC Al as a function of temperature.

The H-DLC coating had the lowest W_{ad} at all testing temperatures, as shown in Figure 7-9. The observation can be attributed to the presence of hydrogen in the DLC, which mitigated atomic interactions with the diamond tip. In addition, the diamond surface was most likely terminated with OH, as observed by first principle investigations. Guo and Qi showed that in ambient conditions, water vapour passivates the diamond (111) and (100) surfaces forming an OH-terminated surface [3], [15]. Consequently, diamond/H-DLC represents the C-OH/C-H configuration of interactions at the atomistic

level. Thus, at elevated temperatures (100 ºC and 200 ºC) the water molecules evaporate, and hydrogen/hydrogen (Figure 7-10) interactions govern the adhesion mechanism between the diamond tip and the H-DLC, thereby generating a W_{ad} value of 0.01 J/m^2. This value is very close to the value of 0.008 J/m^2 reported in the literature as found for two hydrogen-terminated diamond surfaces [16]–[19].

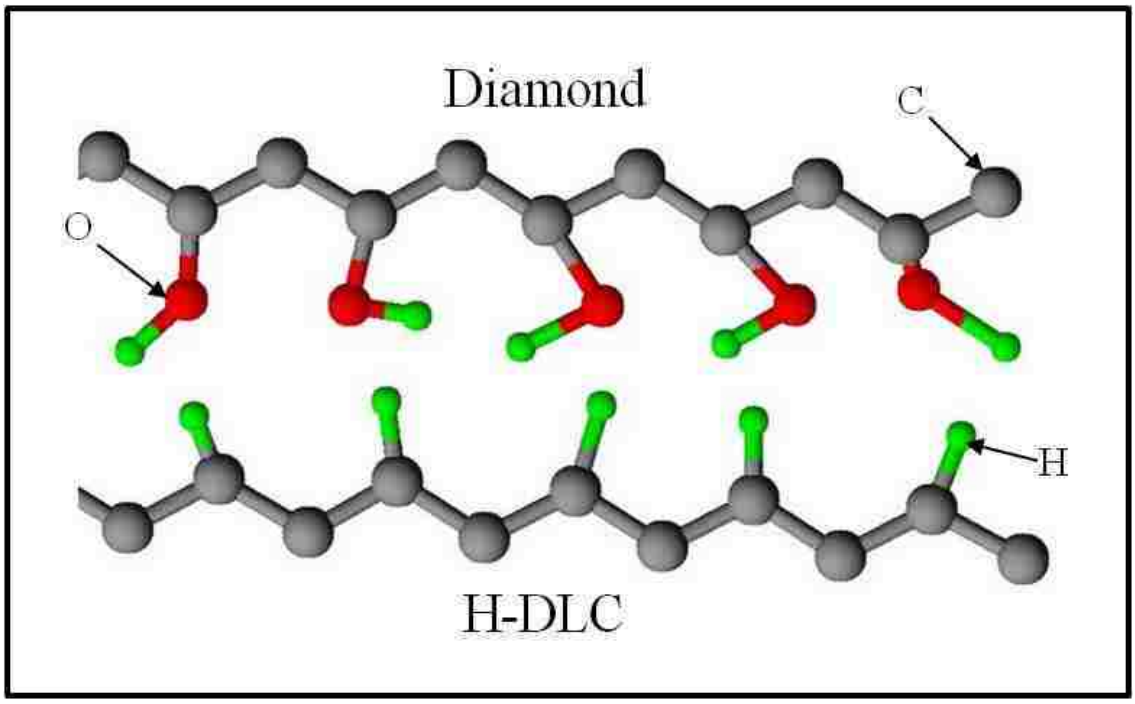

Figure 7-10: Schematic of the diamond / H-DLC interface

Dopant-free DLC and W-DLC coatings showed the same W_{ad} decreasing trend with increases in temperature. The decrease can also be attributed to the presence of water adsorption on the surface [20], inducing meniscus-attractive forces between the tip and the specimens. The calculated W_{ad} of both coatings were higher than the H-DLC (0.01 J/m^2), ranging from 0.05–0.06 J/m^2 at both 100 ºC and 200 ºC (Figure 7-9). This result is attributed to the interactions between hydrogen and the freshly cleaved dangling

carbon bonds (C-OH/C-) caused by diamond penetration into the dopant-free DLC and W-DLC coatings, as illustrated in Figure 7-11. Thus, the results showed that measurements should be conducted above 100 ºC to eliminate the effects of moisture or humidity and to generate results that are more accurate than those of numerical calculations are.

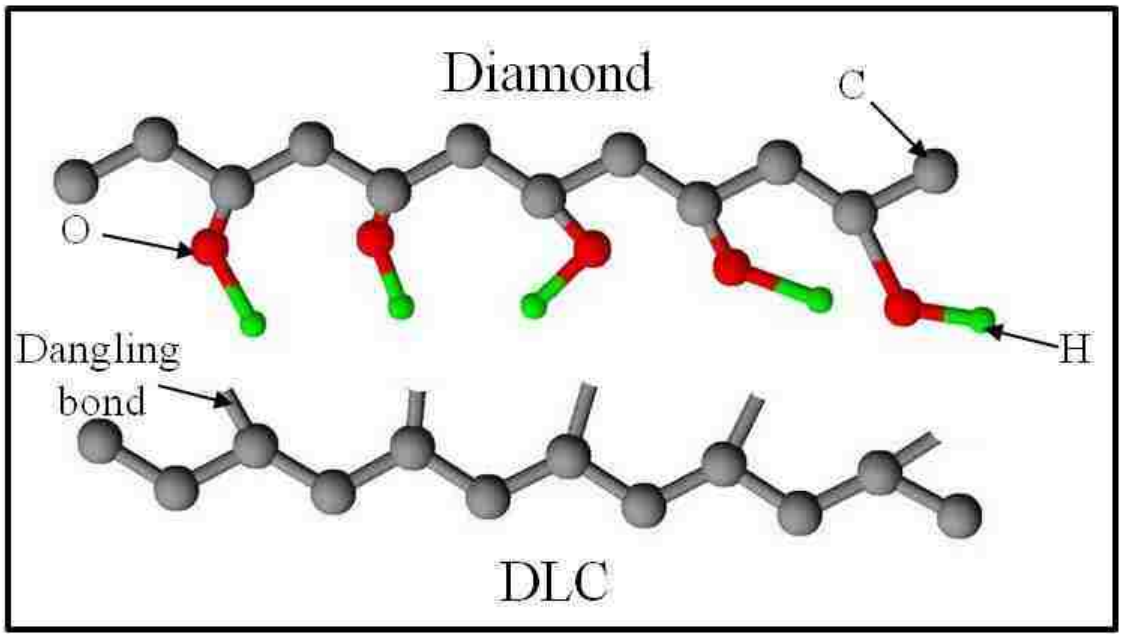

Figure 7-11: Schematic of the diamond / dopants free DLC interface and diamond / W-DLC interface

SC Al had the highest W_{ad} compared to the coatings against diamond (Figure 7-9). At elevated temperatures, once the adsorbed water molecules evaporated, direct contact between the diamond surface and freshly formed aluminum was established as the tip penetrated the few nanometers of aluminum oxide on the surface [21], [22]. The W_{ad} ranged between 0.25 and 0.30 J/m^2, which was consistent with values of 0.2 J/m^2

found in the literature [7]. These values were lower than the Al/Al W_{ad} of 0.75 J/m^2 and the Al/C W_{ad} of 1.60 J/m^2 [16], thus indicating no aluminum adhesion or transfer onto the diamond tip at any of the testing temperatures. This result can be attributed to the presence of OH termination on the diamond surface, which mitigated interatomic interactions at the contact interface (Figure 7-12).

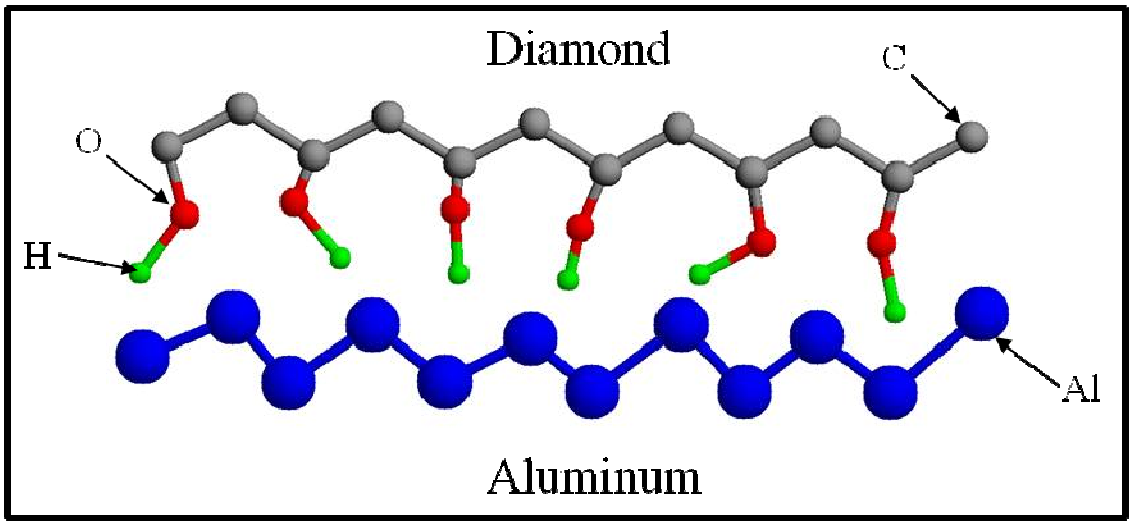

Figure 7-12: Schematic of the diamond / Al interface

7.5 Conclusions

The study showed that W_{ad} can be estimated using the nano-indentation technique. The results were very accurate and in line with theoretical studies. The experimental values provide insight into the tribological behaviour of surface coatings and could be a valuable step in the development of coating for tribological application. The values found in this study could be used to provide insight into which materials and elements are compatible and which are not. In this study, the experimental evaluations of W_{ad} led to the following conclusions:

1. The work of adhesion in all four specimens (H-DLC, dopant-free DLC, W-DLC, and SC Al) was observed to decrease with increased temperature, which can be attributed to the presence of meniscus forces caused by adsorbed water molecules on the specimen surface.
2. The presence of hydrogen on the DLC coating mitigated interatomic interactions and reduced the work of adhesion to as low as 0.01 $J/m^{2.}$
3. Dopant-free DLC and W-DLC were observed to have slightly higher work of adhesion at 0.06–0.05 J/m^2, which was attributed to the interactions of dangling carbon bonds with the hydrogenated diamond surface.
4. SC Al had a W_{ad} ranging from 0.30 to 0.25 J/m^2 , which was higher than the three types of DLC coatings, because of Al/C-H interactions. This results conforms with the first-principle calculation values reported in the literature [7].

References

[1] J. S. McFarlane and D. Tabor, "Relation between friction and adhesion", *Mathematical and Physical Sciences*, vol. 202, no. 1069, pp. 244–253, 1950.

[2] T. R. Society, R. Society, and P. Sciences, "The mechanism of sliding on ice and snow", vol. 172, no. 949, pp. 280–298, 2013.

[3] Q. Zhang, Y. Qi, L. Hector, T. Cagin, and W. Goddard, "Origin of static friction and its relationship to adhesion at the atomic scale", *Physical Review B*, vol. 75, no. 14, pp. 1–7, 2007.

[4] D. Siegel, L. Hector, and J. Adams, "Ab initio study of Al-ceramic interfacial adhesion", *Physical Review B*, vol. 67, no. 9, pp. 1–4, 2003.

[5] Y. Qi and L. Hector, "Adhesion and adhesive transfer at aluminum/diamond interfaces: A first-principles study", *Physical Review B*, vol. 69, no. 23, pp. 1–13, 2004.

[6] Y. Qi, L. G. Hector, N. Ooi, and J. B. Adams, "A first principles study of adhesion and adhesive transfer at Al(111)/graphite(0001)", *Surface Science*, vol. 581, no. 2–3, pp. 155–168, 2005.

[7] Y. Qi, E. Konca, and A. T. Alpas, "Atmospheric effects on the adhesion and friction between non-hydrogenated diamond-like carbon (DLC) coating and aluminum – A first principles investigation", *Surface Science*, vol. 600, no. 15, pp. 2955–2965, 2006.

[8] Y. Li, "Experimental studies on relationships between the electron work function, adhesion, and friction for 3d transition metals", *Journal of applied physics*, vol. 95, no. 12, pp. 7961–7967, 2004.

[9] Y. Gan, "Atomic and subnanometer resolution in ambient conditions by atomic force microscopy", *Surface Science Reports*, vol. 64, no. 3, pp. 99–121, 2009.

[10] X. Xiao, "Investigation of humidity-dependent capillary force", *Langmuir*, vol. 16, no. 21, pp. 8153–8158, 2000.

[11] T. Bouhacian, B. Desbat, and J. P. Aime, "FTIR spectroscopy and nanotribological comparative studies: influence of the adsorbed water layers on the tribological behaviour", *Tribology Letters*, vol. 9, pp. 111–117, 2000.

[12] M. Calleja, M. Tello, and R. García, "Size determination of field-induced water menisci in noncontact atomic force microscopy", *Journal of Applied Physics*, vol. 92, no. 9, pp. 5539–5544, 2002.

[13] L. Sirghi, R. Szoszkiewicz, and E. Riedo, "Volume of a nanoscale water bridge.", *Langmuir*, vol. 22, no. 3, pp. 1093–1098, 2006.

[14] O. H. Pakarinen, a S. Foster, M. Paajanen, T. Kalinainen, J. Katainen, I. Makkonen, J. Lahtinen, and R. M. Nieminen, "Towards an accurate description of the capillary force in nanoparticle-surface interactions", *Modelling and Simulation in Materials Science and Engineering*, vol. 13, no. 7, pp. 1175–1186, 2005.

[15] H. Guo and Y. Qi, "Environmental conditions to achieve low adhesion and low friction on diamond surfaces", *Modelling and Simulation in Materials Science and Engineering*, vol. 18, no. 3, pp. 1–17, 2010.

[16] Y. Qi and L. Hector, "Hydrogen effect on adhesion and adhesive transfer at aluminum/diamond interfaces", *Physical Review B*, vol. 68, no. 20, pp. 1–4, 2003.

[17] M. N. Gardos and B. L. Soriano, "The effect of environment on the tribological properties of polycrystalline diamond films", vol. 90245, no. March, pp. 2599–2609, 1990.

[18] W. G. Goddard III, "Theoretical chemistry comes alive", *Engineering and Science*, pp. 1–8, 1985.

[19] A. Erdemir and C. Donnet, "Tribology of diamond-like carbon films: recent progress and future prospects", *Journal of Physics D: Applied Physics*, vol. 39, no. 18, pp. R311–R327, 2006.

[20] M. Henderson, "The interaction of water with solid surfaces: fundamental aspects revisited", *Surface Science Reports*, vol. 46, pp. 1–308, 2002.

[21] W. . Krueger and S. R. Pollack, "The initial oxidation of aluminum temperature thin films at room", *Surface Science*, vol. 30, pp. 263–279, 1972.

[22] L. P. H. Jeurgens, W. G. Sloof, F. D. Tichelaar, and E. J. Mittemeijer, "Growth kinetics and mechanisms of aluminum-oxide films formed by thermal oxidation of aluminum", *Journal of Applied Physics*, vol. 92, no. 3, pp. 1649–1656, 2002.

CHAPTER 8
GENERAL DISCUSSION AND CONCLUSIONS

8.1 Summary and general discussion

The tribological behaviour (friction, wear and aluminum adhesion mitigation properties) of DLC coatings is governed by the formation of a material transfer layer that is dictated by the DLC chemistry, the temperature and the surrounding atmosphere. The study aimed to identify the low-friction mechanisms in oxygen-rich environments to understand how oxygen in ambient atmosphere contributes to the friction and wear of DLC. The tribological behaviour at elevated and sub-zero temperatures were also investigated to understand how DLC could benefit applications, such as DLC-coated drill bits for dry machining and DLC-coated piston rings to eliminate cold scuffing during cold starts of internal combustion engines. For this purpose the tribological behaviour of dopant-free DLC, H-DLC and W-DLC were investigated using pin-on-disc configuration against a 319 Al counterface. In addition, the amounts of adhesion that occur at the sliding interface were investigated and quantified by determining the work of adhesion (W_{ad}), which was carried-out from pull-off force measurements obtained by nano-indentation. Identification of these mechanisms will provide guidelines in coating design to create a robust low-friction DLC with low tendency of adhesion to aluminum for a wide range of environments.

Chapter 2 showed that the friction and wear of dopant-free (i.e. non-hydrogenated) DLC sliding against 319 Al was reduced to a very low COF of 0.09 in the presence of humidity (45%, relative humidity, RH) in an Ar atmosphere. This was

attributed to the formation of material transfer layers and the surface passivation of carbon (both on transfer layers and coated surface) by the H and OH groups from moisture or water molecules in the atmosphere. The presence of dry (0% RH) oxygen led to a higher COF of 0.35, which was caused by the oxidation of carbon atoms at the sliding interface, as observed by FTIR analyses of the carbon transfer layers formed on aluminum.

The results showed that the increase in oxygen in the test environment (50% O_2) in the presence of humidity eliminated the initial high COF by accelerating the formation of the carbon transfer layer and possibly the surface passivation by the H and OH groups. SEM analyses indicated that a long running-in period of DLC was caused by the delay in the formation of a carbon transfer layer and aluminum adhesion to the DLC surface. As tested on dopant-free DLC proved that submerging this coating in water or increasing the relative humidity will reduce the COF to less than 0.1 as shown in the summary Figure 8-1. Thus DLC coating qualifies as a good candidate for water pumps shafts that require low COF to eliminate friction losses during operation.

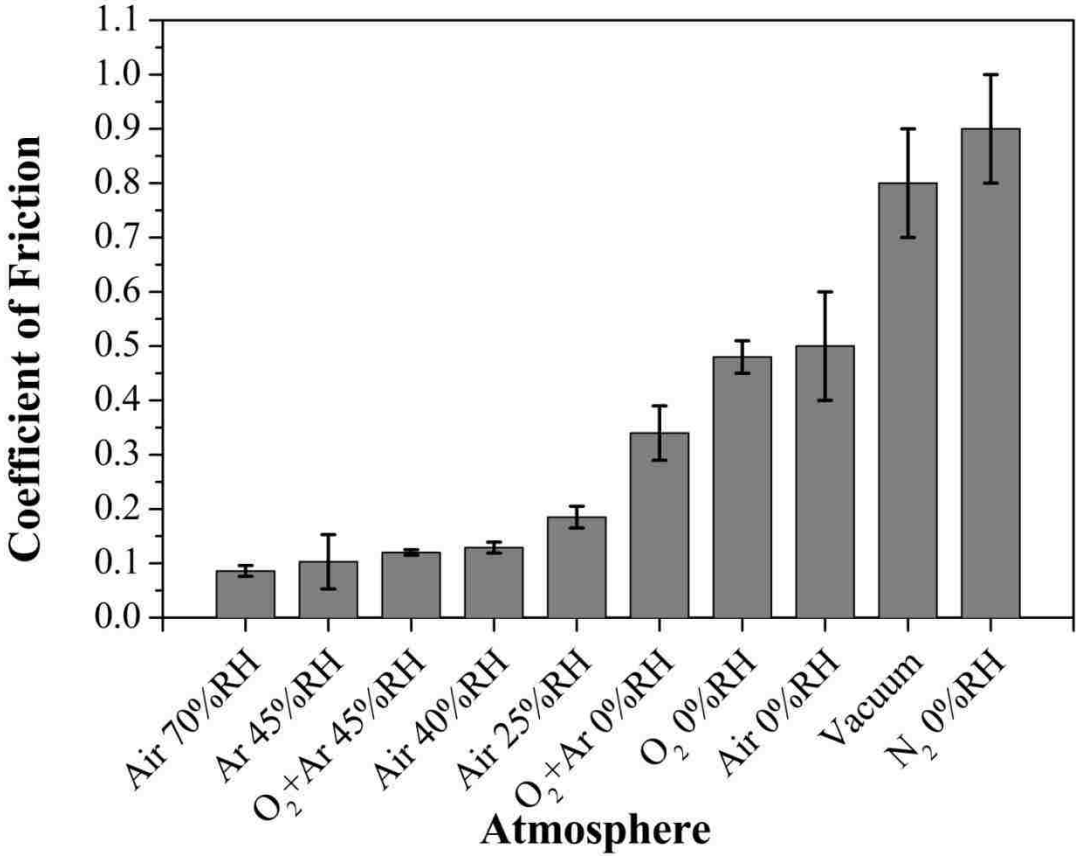

Figure 8-1: Average COF obtained by pin-on-disc of 319 Al sliding against dopant-free DLC at various environments

Chapters 3, 4 and 5 investigated the elevated temperature tribological behaviour of H-DLC and W-DLC at temperatures up to 500 ºC, under controlled atmosphere including vacuum. H-DLC was observed to generate low COF in vacuum because of the presence of hydrogen that passivated the sliding interface as observed from the FTIR analyses. It was observed that hydrogen in the coating can withstand temperatures up to 200 ºC. At this temperature, the 319 Al / H-DLC interface was observed to retain low COF of 0.06 and the carbon transfer layers were still present. However, the hydrogen was observed to desorb from the sliding interface (as shown by FTIR), promoting an increase

in carbon dangling bond interactions (C-/C-) and leading to a high COF of 0.6 at 400 ºC. Consequently, the formation of carbon transfer layers and surface passivation were not sufficient to generate low COF and reduce aluminum adhesion.

Tribological behaviour of B_4C was investigated for comparison because of its high hardness and wear resistance against steel properties. B_4C generated a high COF of 0.6 against 319 Al throughout the temperature range of 25-400 ºC. B_4C was observed to graphitize, causing the collapse of the columnar structure. Graphitization of the B_4C coating was observed to be accelerated at higher temperatures, as shown by micro Raman spectroscopy. It might be thought that graphitization would be beneficial to reduce friction and wear. However, graphitization without proper surface passivation is insufficient to reduce friction. The presence of carbon transfer layers without surface passivation, led to interactions between carbon dangling bonds at the sliding interface and hence the high friction of 0.6, which was similar to that observed for H-DLC at 300 ºC was observed.

In Chapter 4, W-DLC coating properties was investigated in a manner similar to the investigations of H-DLC and B_4C in Chapter 3. Similar to H-DLC, W-DLC was observed to form carbon-rich material transfer on the Al pin and to generate the low COF of 0.1, which was attributed to the effect of the humidity in the atmosphere to passivate these carbon-dangling bonds similar to what was described above for dopant-free DLC. However, as the temperature increased, the material transfer and passivation mechanism was not sustained causing a rapid increase in COF. Not until 300 ºC did the W began to

oxidize, forming a new mechanism that reduced COF at elevated temperatures. TEM, XPS and Raman analysis of the coating tested at 400 ºC and 500 ºC revealed that the top surface had a tungsten oxide layer of 20 nm. The W oxide on W-DLC then took over and formed a transfer layer on the Al pin, causing a drop in the COF back down to 0.1 at 500 ºC and eliminating aluminum adhesion. Thus, W-DLC formed carbon-rich material transfer layers with W oxide, which possibly acted as a solid lubricant and mitigated aluminum adhesion.

Chapter 5 builds on the idea of utilizing the beneficial properties of the tungsten oxide layer by heat treating the coating at 500 ºC in order to generate the oxide layer. The heat-treated W-DLC was observed to form transfer layers up to 100 ºC which eliminated aluminum adhesion and generate the low COF of 0.05. As the temperature increased to 200 ºC and 300 ºC, the tungsten oxide was consumed but not regenerated. Carbon transfer layer on the Al pin began to regenerate again at 400 ºC leading to a low COF. Heat treatment at temperatures higher than 500 ºC did not sustain material transfer and caused severe oxidation, wear, as well as high COF of 0.55. The practical value of these observations is that this coating can be used in hot-forming of Al sheets.

In Chapter 6, low temperature dependance tribo-mechanisms were investigated in more details. H-DLC, W-DLC and AISI 52100 were tested against 319 Al pins at -196 ºC (liquid nitrogen). Both DLC coatings were observed to generate a COF of 0.18, which was lower than the COF of uncoated steel (0.4). Unlike the elevated temperature mechanisms of DLC, the low friction was not accompanied by material transfer on the Al

pin or Al adhesion on the DLC coating, which indicated that the formation of the transfer layer favoured ambient temperatures and higher, as observed in the previous chapters.

The addition of H and W should be considered in designing a carbon-based coating for elevated-temperature, low-friction and applications, such as drill bits for aluminum machining and piston rings in an aluminum internal combustion engine. Hydrogen would support the coating and generate low friction from below 0 ºC up to 300 ºC by passivating the carbon transfer layer on the mating surface and thus mitigate aluminum adhesion. Tungsten would carry low friction behaviour from 300 ºC up to 500 ºC through the formation of a tungsten oxide-rich transfer layer, reducing aluminum adhesion and friction up to 500 ºC.

However, it is not clear how adhesive transfer to the mating surface. In Chapter 7, the work of adhesion was calculated by measuring the adhesion force using the pull-off method with the nano-indentation technique. The pull-off force measurements quantified the interactions at the interface, which then yielded insight into the adhesion of material transfer mechanisms at the Al sliding interface and also into the friction and adhesion between the carbon transfer layers.

From the unloading portion, the energy required to separate the diamond indenter from the surface was the area under the curve W_{ad} was calculated. W_{ad} was normalized by by the contact area of the diamond tip. The W_{ad} values of all four specimens (H-DLC, dopant-free DLC, W-DLC and SC Al) are observed to decrease with an increase in

temperature and could be discussed in terms of the presence of meniscus forces caused by adsorbed water molecules on the specimen surface. As temperatures increased, the adsorbed water evaporated, resulting in clean contact between the diamond and the samples.

At elevated temperatures, the W_{ad} calculations revealed that the interactions between the diamond tip and DLC coatings were governed by a van der Waals type of interaction, ranging from 0.06 J/m^2 to 0.01 J/m^2, because of the OH termination commonly found on the diamond surface. H-DLC generated the lowest W_{ad}, which was attributed to the presence of hydrogen in the coating, inducing hydrogen interactions once the adsorbed water molecules evaporated at 100 ºC and 200 ºC. The results concurred with the findings of the tribological tests performed in Chapter 3, which showed a decrease in COF from 0.12 at 25 ºC to 0.06 at 200 ºC. Dopant-free DLC and W-DLC were observed to have slightly higher W_{ad} of 0.06–0.05 J/m^2, which was attributed to the interactions of cleaved dangling carbon bonds (caused by penetration of the tip into the coating) with the hydroxyl-terminated diamond surface (HO-C/-C).

Single crystal (SC) Al had W_{ad} ranging from 0.30–0.25 J/m^2, which was higher than the DLC coatings, because of the Al/C-H interactions. The relatively higher W_{ad} could be correlated to the high COF observed during the running-in, as observed in H-DLC sliding against 319 Al. As shown in Chapter 2, these high running-in COFs were observed prior to the formation of material transfer, which caused Al/H-C interactions. The relatively high W_{ad} also could explain the adhesion of the carbon transfer layer to the

Al sliding interface. As the near surface carbon atoms graphitized due to thermo-mechanical process as described above, the carbon atoms and molecules adhered to the Al interface, thus forming a lubricous transfer layer.

In conclusion, it was shown that the COF is closely related to the formation of material transfer and the surface passivation of the dangling carbon bonds which eliminate aluminum adhesion. The nano-indentation technique was shown to give a viable, quick indication of material transfer layer formation, which could be easily performed to calculate work of adhesion while measuring coating hardness. In all, three mechanisms were observed: dopant-free DLC reduced friction by reacting with water molecules and oxygen in the atmosphere to form an OH passivated layer that eliminated atomic interactions. H-DLC was proven to out-perform dopant-free DLC and W-DLC because of the presence of a stable hydrogen-terminated surface up to 200 ºC. W-DLC had the lowest COF at 400 ºC and 500 ºC because of the presence of layer rich in WO_3. Consequently, the coatings for the desired applications could be designed with consideration of these mechanisms. For instance, by adding hydrogen and tungsten to DLC, low aluminum adhesion and COF may be achieved in a temperature range from 25 ºC to 500 ºC.

8.2 A summary of original conclusions of this work

The mechanisms identified in this dissertation as described below should act as guidelines for DLC coating design and selection to mitigate aluminum adhesion and reduce friction.

1. Oxygen in the environment eliminates the initial high COF by accelerating carbon transfer layer formation and reduces aluminum / carbon interactions and adhesion. Thus oxygen may be introduced to the surrounding atmosphere (e.g. by forced air) during machining, drilling or tapping of aluminum with DLC machining tools.

2. H-DLC produced the lowest COF of 0.06 at 200 °C against 319 Al with no sign of aluminum adhesion. The COF increased abruptly at higher temperatures. Thus, hydrogenated DLC coatings are considered to be suitable candidates to prevent aluminum adhesion for operating temperatures up to 200 °C in components such as water pumps, tappets and cam follower.

3. W-DLC forms a tungsten oxide layer on the coating surface when heated; thus mitigating aluminum adhesion. This film exhibits a lubricious behaviour up to 500 ºC. Thus, the use of W-DLC can be of interest in hot forming and machining tool applications for aluminum.

4. H-DLC and W-DLC coatings was shown to still function as a low friction coating at subzero temperatures. Hence, these coatings can be utilized in piston ring applications to prevent or mitigate cold scuffing type of damage to the bore.

5. A nano indentation technique can be used as a practical way to determine and calculate the work of adhesion which gives insight to coating adhesion with mating surfaces.

APPENDIX A

Work of adhesion was calculated from the load vs displacement curve generated by nano indentation. As the diamond tip penetrates the specimen, diamond is exposed to freshly cleaved active surface, which result in adhesion between diamond and the specimen material. This force can be detected by slowing down the unloading cycle in order for the data acquisitions to record it. The measurement will result in a negative force as the tip is being pulled down by the adhered material or adhesion forces between diamond and the specimen as shown in Figure below.

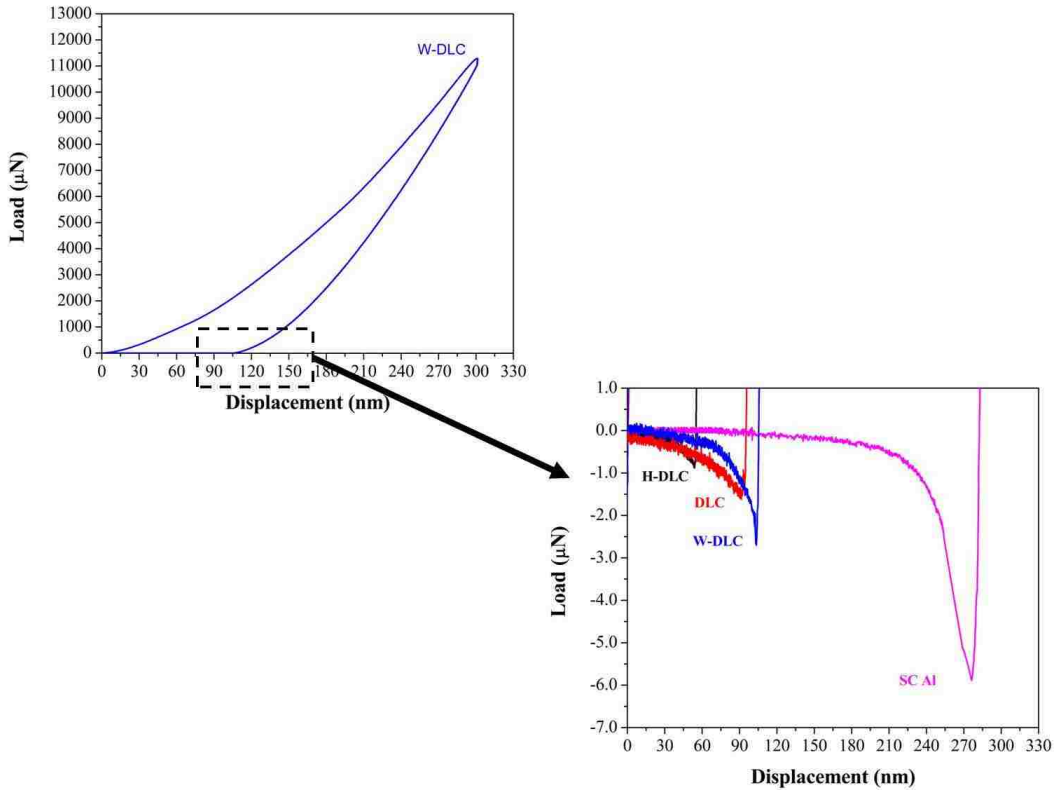

Figure A-1: Load vs Displacement curve of single crystal aluminum, hydrogenated DLC (H-DLC), dopant free DLC (DLC) and tungsten doped DLC (W-DLC) at room temperature.

The area below the zero force represents the energy requires to separate tip from the specimen. Thus work of adhesion can be calculated by dividing the negative force area by the tip area, which is calculated from the penetration depth as shown in figure below.

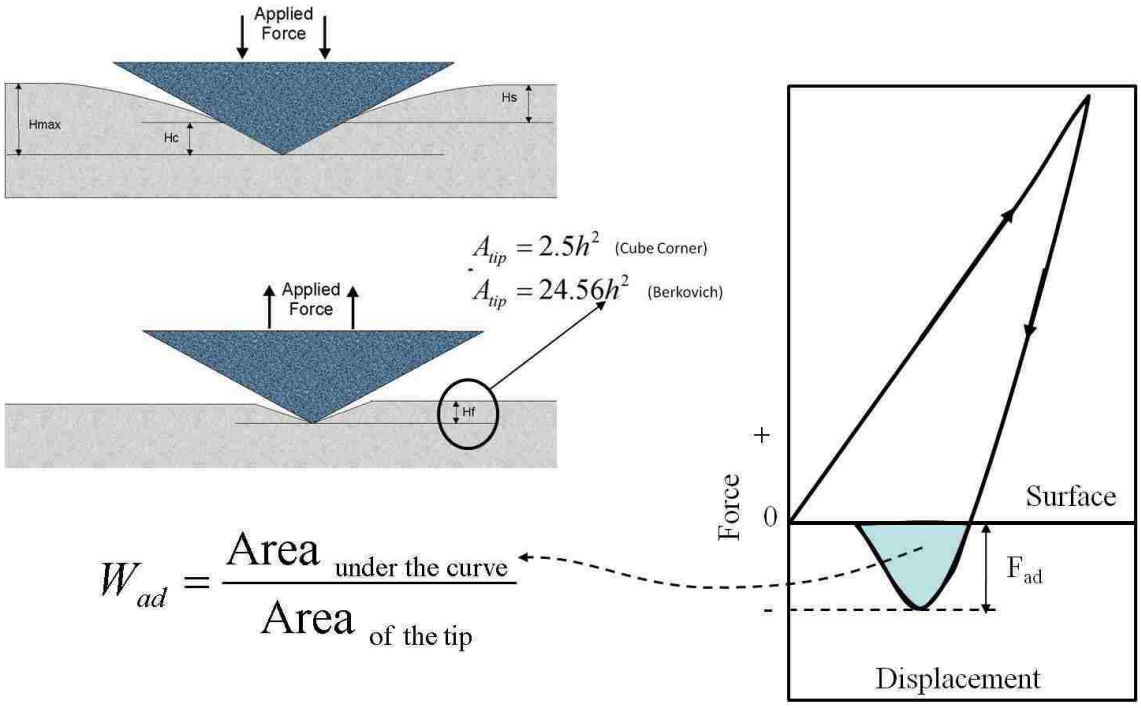

Figure A-2: Schematics of work of adhesion calculation

Experimental results of 9 indents at each temperature for each specimen are presented in table below.

Table A-8-1: Work of adhesion calculation of H-DLC

	25 °C			100 °C			200 °C		
H-DLC	**Hf (nm)**	**Curve Area (J)**	**W ad (J/m^2)**	**Hf (nm)**	**Curve Area (J)**	**W ad (J/m^2)**	**Hf (nm)**	**Curve Area (J)**	**W ad (J/m^2)**
1	63.90	18.39	0.18	54.15	0.00	0.00	93.01	10.19	0.05
2	78.67	11.69	0.08	78.46	8.41	0.06	91.58	2.34	0.01
3	59.92	16.23	0.18	66.38	5.43	0.05	85.67	1.52	0.01
4	59.28	15.51	0.18	101.31	4.21	0.02	97.63	0.00	0.00
5	61.02	14.29	0.16	76.85	2.71	0.02	92.16	2.80	0.01
6	62.27	15.05	0.16	88.22	1.19	0.01	75.65	2.97	0.02
7	64.16	18.72	0.19	104.74	3.18	0.01	92.21	1.27	0.01
8	52.74	13.36	0.20	97.33	1.40	0.01	99.46	2.15	0.01
9	67.51	9.27	0.08	99.97	4.89	0.02	106.30	6.09	0.02
Average			0.16			0.02			0.02
STDV			0.05			0.02			0.01

Table A-8-2: Work of adhesion calculation of W-DLC

	25 °C			100 °C			200 °C		
W-DLC	**Hf (nm)**	**Curve Area (J)**	**W ad (J/m^2)**	**Hf (nm)**	**Curve Area (J)**	**W ad (J/m^2)**	**Hf (nm)**	**Curve Area (J)**	**W ad (J/m^2)**
1	53.21	11.72	0.17	112.46	18.58	0.06	102.46	12.04	0.05
2	52.65	10.26	0.15	127.64	20.40	0.05	107.64	10.25	0.04
3	51.43	11.32	0.17	127.37	21.43	0.05	107.37	13.25	0.05
4	50.34	12.20	0.20	123.64	18.74	0.05	103.64	11.92	0.05
5	46.89	12.20	0.23	110.35	15.28	0.05	100.35	13.50	0.05
6	47.43	10.50	0.19	124.67	26.13	0.07	104.67	15.80	0.06
7	50.76	12.61	0.20	116.56	20.98	0.06	106.56	12.35	0.04
8	53.89	14.27	0.20	126.25	23.21	0.06	106.25	11.44	0.04
9	46.42	11.19	0.21	122.48	27.28	0.07	102.48	19.15	0.07
Average			0.19			0.06			0.05
STDV			0.02			0.01			0.01

Table A-8-3: Work of adhesion calculation of dopant free DLC

	25 °C			100 °C			200 °C		
DLC	**Hf (nm)**	**Curve Area (J)**	**W ad (J/m^2)**	**Hf (nm)**	**Curve Area (J)**	**W ad (J/m^2)**	**Hf (nm)**	**Curve Area (J)**	**W ad (J/m^2)**
1	92.56	60.87	0.29	98.44	18.29	0.08	100.44	17.82	0.07
2	90.54	10.15	0.05	102.64	20.54	0.08	101.35	16.42	0.07
3	93.90	36.80	0.17	98.38	17.81	0.08	99.10	14.98	0.06
4	91.08	11.30	0.06	99.64	18.38	0.08	100.87	16.39	0.07
5	90.05	50.80	0.26	100.35	17.90	0.07	97.10	13.85	0.06
6	90.46	53.08	0.26	99.66	20.22	0.08	102.65	15.67	0.06
7	89.52	44.63	0.23	102.45	20.49	0.08	98.54	17.69	0.07
8	88.76	47.17	0.24	101.25	22.80	0.09	103.19	22.40	0.09
9	90.21	55.74	0.28	102.48	22.89	0.09	104.10	19.15	0.07
Average			0.20			0.08			0.07
STDV			0.09			0.01			0.01

Table A-8-4: Work of adhesion calculation of single crystal Al

	25 °C			100 °C			200 °C		
SC Al	**Hf (nm)**	**Curve Area (J)**	**W ad (J/m^2)**	**Hf (nm)**	**Curve Area (J)**	**W ad (J/m^2)**	**Hf (nm)**	**Curve Area (J)**	**W ad (J/m^2)**
1	286.98	700.20	0.35	289.29	637.40	0.31	300.44	610.11	0.28
2	289.67	700.13	0.34	290.87	598.60	0.29	301.35	590.65	0.27
3	292.20	685.55	0.33	290.62	656.00	0.32	309.10	623.33	0.27
4	290.87	800.80	0.39	298.10	761.00	0.35	300.87	562.92	0.25
5	288.40	705.36	0.35	297.82	838.50	0.39	297.10	552.27	0.26
6	293.21	670.67	0.32	292.83	804.00	0.38	310.65	615.83	0.26
7	290.75	655.23	0.32	295.71	649.00	0.30	298.54	580.22	0.27
8	291.05	800.12	0.39	295.48	765.90	0.36	303.19	576.70	0.26
9	289.17	702.51	0.34	289.28	613.80	0.30	304.10	500.10	0.22
Average			0.35			0.33			0.26
STDV			0.03			0.04			0.02

APPENDIX B

Chapter 2:

Supplier:	Elsevier Limited The Boulevard, Langford Lane Kidlington, Oxford, OX5 1GB, UK
Registered Company Number:	1982084
Customer name:	Ahmed Abou Gharam
License number:	3296040798565
License date:	Dec 25, 2013
Licensed content publisher:	Elsevier
Licensed content publication:	Wear
Licensed content title:	Role of oxygen and humidity on the tribo-chemical behaviour of non-hydrogenated diamond-like carbon coatings
Licensed content author:	A. Abou Gharam, M.J. Lukitsch, Y. Qi, A.T. Alpas
Licensed content date:	29 July 2011
Licensed content volume number:	271
Licensed content issue number:	9–10
Number of pages:	7
Start Page:	2157
End Page:	2163
Type of Use:	reuse in a thesis/dissertation
Intended publisher of new work:	other
Portion:	full article
Format:	both print and electronic
Will you be translating?	No
Title of your thesis/dissertation:	Tribological Behaviour of H- and W-DLC Coatings: Effects of Environment and Temperature on Adhesion
Expected completion date:	Dec 2013

Chapter 3:

Supplier:	Elsevier Limited The Boulevard, Langford Lane Kidlington, Oxford, OX5 1GB, UK
Registered Company Number:	1982084
Customer name:	Ahmed Abou Gharam
License number:	3296040893584
License date:	Dec 25, 2013
Licensed content publisher:	Elsevier
Licensed content publication:	Thin Solid Films
Licensed content title:	High temperature tribological behaviour of carbon based (B_4C and DLC) coatings in sliding contact with aluminum
Licensed content author:	A. Abou Gharam, M.J. Lukitsch, M.P. Balogh, A.T. Alpas
Licensed content date:	30 December 2010
Licensed content volume number:	519
Licensed content issue number:	5
Number of pages:	7
Start Page:	1611
End Page:	1617
Type of Use:	reuse in a thesis/dissertation
Intended publisher of new work:	other
Portion:	full article
Format:	both print and electronic
Will you be translating?	No
Title of your thesis/dissertation:	Tribological Behaviour of H- and W-DLC Coatings: Effects of Environment and Temperature on Adhesion
Expected completion date:	Dec 2013

Chapter 4:

Supplier:	Elsevier Limited The Boulevard, Langford Lane Kidlington, Oxford, OX5 1GB, UK
Registered Company Number:	1982084
Customer name:	Ahmed Abou Gharam
License number:	3296040592615
License date:	Dec 25, 2013
Licensed content publisher:	Elsevier
Licensed content publication:	Surface and Coatings Technology
Licensed content title:	High temperature tribological behavior of W-DLC against aluminum
Licensed content author:	A. Abou Gharam, M.J. Lukitsch, M.P. Balogh, N. Irish, A.T. Alpas
Licensed content date:	25 December 2011
Licensed content volume number:	206
Licensed content issue number:	7
Number of pages:	8
Start Page:	1905
End Page:	1912
Type of Use:	reuse in a thesis/dissertation
Portion:	full article
Format:	both print and electronic
Will you be translating?	No
Title of your thesis/dissertation:	Tribological Behaviour of H- and W-DLC Coatings: Effects of Environment and Temperature on Adhesion
Expected completion date:	Dec 2013

Chapter 5:

COPYRIGHT PERMISSION FORM

Date: 6/21/2013

FROM:

The Society of Vacuum Coaters
71 Pinon Hill Place, NE
Albuquerque, NM 87122

TO:

Ahmed Abou Gharam
University of Windsor
Engineering Materials Graduate Program
Windsor, Ontario N9B 3P4
E-mail: abougha@uwindsor.ca

You have requested usage of material from the work:

A. Abou Gharam, A.T. Alpas, and M.J. Lukitsch, "Tribological Behaviour of Heat Treated Tungsten Doped Diamond-Like Carbon Coating at Elevated Temperatures," 55th Annual Technical Conference Proceedings of the Society of Vacuum Coaters, 2012, pp. 623-629

published by the Society of Vacuum Coaters (SVC) (2012). SVC confirms ownership of the publishing rights to this material, and does not infringe upon the copyright or other rights of anyone.

The Society of Vacuum Coaters grants permission to use the above-titled material in a manner compliant with applicable Copyright Laws, ensuring proper acknowledgement of all referenced material in your publication; quoting the text and publication title of the original material, including the words "Reproduced by permission of the Society of Vacuum Coaters." Use the reference style listed above when referencing in this material in your publication.

This material will be used in the following work, entitled:

Used as a chapter in author's dissertation (print and digital)

Authored by:

Ahmed Abou Gharam

Society of Vacuum Coaters

Signed: Beth Strong Digitally signed by Beth Strong DN: cn=Beth Strong, o=Society of Vacuum Coaters, ou, email=bethstrong@svc.org, c=US Date: 2013.06.21 09:34:23 -07'00'

Date: 6/21/2013

PUBLICATIONS

- A. Abou Gharam, M.J. Lukitsch, A.T. Alpas, "Tribological Behaviour of Heat Treated Tungsten Doped Diamond-Like Carbon Coating at Elevated Temperatures" *55th SVC Annual Proceedings,* T14

- A. Abou Gharam, M.J. Lukitsch, M.P. Balogh, N. Irish, A.T. Alpas, "High temperature tribological behavior of W-DLC against aluminum" *Surface and Coatings Technology*, 206, 2011, 1905-1912.

- A. Abou Gharam, M.J. Lukitsch, M.P. Balogh, Y. Qi, A.T. Alpas, "Role of Oxygen and Humidity on the Tribochemical Behaviour of Non-Hydrogenated Diamond-Like Carbon Coatings" *Wear*, 271, 2011, 2157-2163.

- A. Abou Gharam, M.J. Lukitsch, M.P. Balogh, A.T. Alpas "High Temperature Tribological Behaviour of Carbon Based (B_4C and WC-DLC) Coatings against Aluminum" *Thin Solid Films*, 519, 2010, 1611-1617.

VITA AUCTORIS

Ahmed Abou Gharam was born in 1985 in Cairo, Egypt. In May 2006 he earned a B.A.Sc. degree in Material Science and Engineering from McMaster University in Hamilton, Ontario. Then Mr. Abou Gharam moved to Windsor, Ontario in September 2006 to pursue his graduate studies at the University of Windsor. Upon graduation in August 2008 with a M.A.Sc. degree, he continued his graduate studies with his supervisor and mentor Dr. Alpas in Engineering Materials at the University of Windsor and hopes to graduate with a Ph.D degree in December 2013.